Master Thesis, Department of Geosciences

Reservoir characterization of the Tertiary Balder field in the Norwegian North Sea

Fahad Ashraf

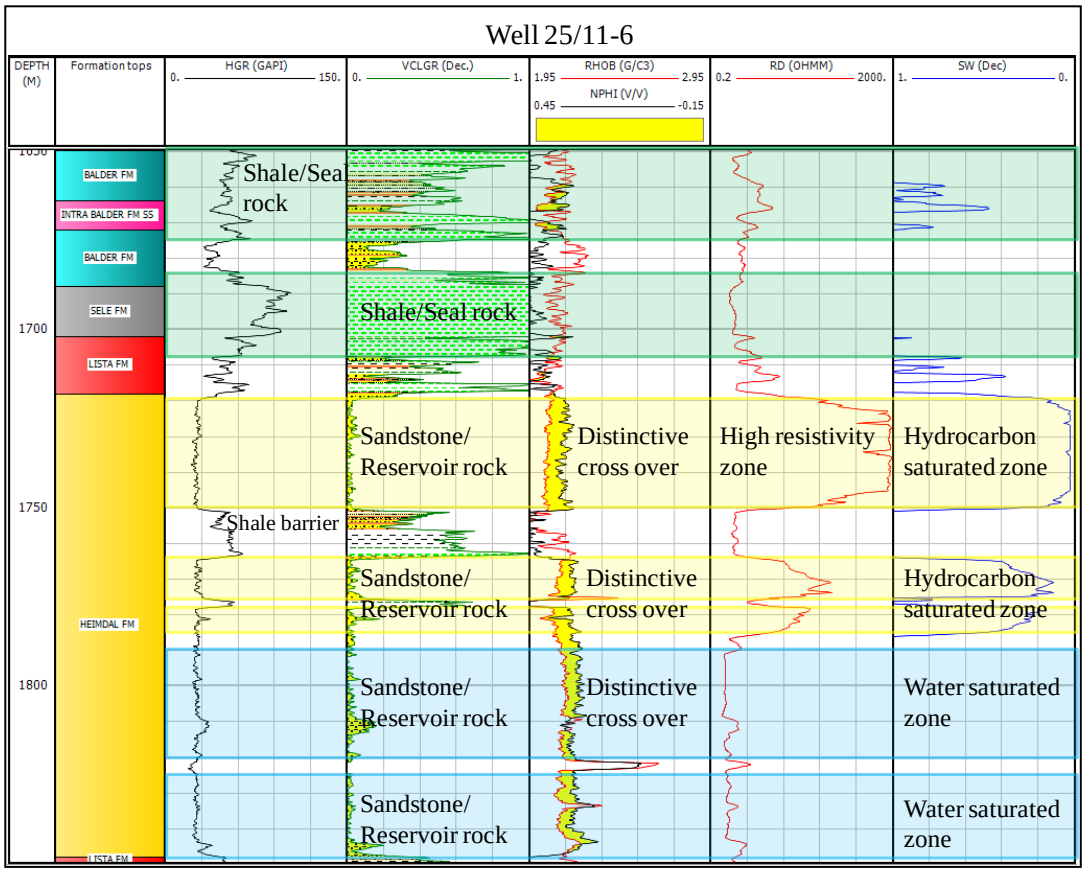

UNIVERSITY OF OSLO

FACULTY OF MATHEMATICS AND NATURAL SCIENCES

Reservoir characterization of the Tertiary Balder field in the Norwegian North Sea

Fahad Ashraf

Master Thesis in Geosciences

Discipline: Geology

Department of Geosciences

Faculty of Mathematics and Natural Sciences

University of Oslo

29.05.2013

Preface

This thesis is a part of the 'BarRock' (Barents Sea Rock Properties) project and is submitted to the Department of Geosciences, University of Oslo (UiO) in candidacy of the M.Sc. degree in Geology.

This research has been performed at the Department of Geosciences, University of Oslo during the period of August 2012 to May 2013 under the supervision of Dr. Nazmul Haque Mondol, Associate Professor, Department of Geosciences, UiO.

Acknowledgement

I would like to take this opportunity to thank my supervisor, Dr. Nazmul Haque Mondol, Associate Professor, Department of Geosciences, University of Oslo, for his encouragement and intellectual thoughts throughout of this study. I like to mention here that, when I first met him last year, he introduced this reservoir characterization project. Since than, his continuous motivation, feedback, supervision and regular meetings, has enabled to develop the skills from scratch and keep me on the track to make this study possible. I don't have enough words to thank him for the guidance and his time.

I would like to thank Michael Heermans and IT staff at Department of Geosciences for their technical support during this research. I am also obliged to the academic and administrative members of the Department of Geosciences for their cooperation during this work.

I would like to thank Mohammad Koochak Zadeh, Sirikarn Narongsirikul and Vladimiro Rago for their constructive input for this study. I would also like to thank master students, especially Arif Butt, Omer Saeed and Shahzeb Haider for their team spirit in achieving this goal. I would also like to thank my fellow students for their companionship to make university, a fun place as well.

In the end, I would like to convey my special gratitude to my parents, for their continous support and encouragement during my study and stay in Norway.

F.Ashraf

Abstract

Reservoir characterization is one of the most important step in exploration and development phases of any prospect. It combines the results of different analyses to reduce the risk and uncertainties and to enhance understanding of reservoirs. In this study an integrated approach; petrophysical analysis, compaction study and rock physics diagnostics is applied to characterize the reservoirs of the Balder field using log data from nine exploration and sixteen appraisal wells.

The Balder field is located in the Norwegian sector of the North Sea.The field was discovered in 1967. It compromises reservoir sands in three stratigraphic horizons of the Balder, Hermod and Heimdal Formations of Paleocene to Eocene age. The reservoir intervals are of turbidite systems which pinch out against the Utsira High. These reservoir rocks are unconsolidated to poorly cemented intervals of sands and sandstones (a post-rift petroleum play) interbedded with overpressure shales that acting as seal/cap rocks. These reservoir sands contain commercial quantities of hydrocarbons (mostly oil) which are being produced since 1999. The exploration and production gap of more than thirty years is due to the complex stratigraphy and structure of the reservoirs.

Parameters like porosity, shale volume and water saturation are calculated under petrophysical analyses using Interactive Petrophysics software. In addition, facies analysis as well as net-to-gross ratio estimation are performed by the Interactive Petrophysics. However, the compaction study helps to identify mechanical and checmical compaction regimes as well as transition zone between mechanical and chemical compactions. It also helps to understand the compaction behavior of the source, reservoir and cap rocks comparing the field data to model results. Finally the rock physics diagnostics are carried out to characterize the reservoir sands using a combination of different softwares (Excel, Petrel and Interactive Petrophysics). In this part cementation and hydrocarbon effect on the rock properties are carefully investigated.

An average, all the reservoir sand intervals possess a high porosity values (34%). These are moderately to well sorted sands contain a minor amount of clay, with a high net-to-gross ratio (90%). The Balder Formation is mostly mechanically compacted, the high temperature regime, where quartz cementation initiated put it in the transition zone of mechanical and chemical compactions. The Hermod and Heimdal formations are also in transition zone but still possess high porosity values. Rock physics diagnostics reveal that some reservoir intervals may contain a small amount of cement in the pores which, however may not be enough to derive the sediments more stiffen. Rock physics templates illustrate that rock properties in the reservoir intervals are influnced primarily by the depositional processes rather than the depth-related diagenetic trends.

In conclusion, it can be stated that the integration of petrophysical analysis, compaction study and rock physics diagnostics helps to understand and to characterize the reservoirs much better compared to any other single technique. This approach is useful especially when core data are not available. This integrated study give quick results and can help geophysicists, geologists and reservoir engineers to identify the risks and to enhance the opportunity. It can dramatically increase the geological models, reduce risks and improve process efficiency during the development, production and management phases.

Nomenclature

AI/Ip: Acoustic Impedance/P-Impedance

API: American Petroleum Institute

AVO: Amplitude Versus Offset

BHT: Bottom Hole Temperature

BSF: Below Sea Floor

CC: Chemical Compaction

Frac.: Fraction

Hc: Hydrocarbon

I_{GR}: Gamma Ray Index

IP: Interactive Petrophysics

Is: Shear Impedance/S-Impedance

Km: Kilometer

LMR: Lambda-Mu-Rho

MC: Mechanical Compaction

MFS: Maximum Flooding Surface

MD: Measured Depth

N/A: Not Applicable; Not Available

N/G: Net-to-Gross Ratio

NPD: Norwegian Petroleum Directorate

RKB: Relative to Kelly Bushing

RPT: Rock Physics Template

R^2: Correlation Coefficient

S_{hc}: Hydrocarbon Saturation

Sw: Water Saturation

TVD: Total Vertical Depth

Vp: P-wave Velocity

Vsh/V-Shale: Volume of Shale

Vs: S-wave Velocity

Φ: Porosity

Table of Contents

List of Figures

Chapter 1

Chapter 2

Chapter 3

Chapter 4

Chapter 5

Chapter 6

List of Tables

Chapter 1

Chapter 2

Chapter 3

Chapter 4

Chapter 5

Chapter 1: Introduction

1.1 Background and motivation

This study is conducted to analyze reservoir properties of the Balder field, Norwegian North Sea (Fig. 1.1). The Balder field was discovered in 1967, but production started 32 years later in 1999 (ExxonMobil, 2013; NPD, 2013). The reason behind this exploration and development gap is due to the complexity of the reservoirs developed by high-density deep marine gravity flows as well as possible fluid escape in the Balder field area. Over these years, several authors (Bergslien, 2002; Briedis et al., 2007; Jenssen et al., 1993; Sarg and Skjold, 1982) have proposed different geological models for the field. Full scale development of the field has been difficult until advent of new technologies in 1990s, such as high resolution 3D seismic. The Balder field has three main reservoir intervals in Paleocene and Early Eocene sands (Briedis et al., 2007). Each sand unit is interbedded with shale, which act as local seal and restricts the direct communication within the reservoir units (Briedis et al., 2007; Sarg and Skjold, 1982). Sand injection acts as migration path within the different units of the reservoirs (Jenssen et al., 1993). This study characterizes three reservoir sands of the Balder field for better understanding of the reservoir dynamics by integrating cross-disciplines of petrophysics, compaction study and rock physics.

1.2 Research objectives

The main objective of the research is to characterize the complex Paleocene and Eocene reservoir sands of Balder, Hermod and Heimdal Formations in the field area. In addition, a detail compaction study is performed to get better understanding of compaction and rock property evolution of the sedimentary packages penetrated by the 25 studied wells. To fullfill the objectives, the following analytical procedures are considered:

- Analysis the geological evolution, structure and tectonic and stratigraphy of the Balder field by reviewing the existing literatures.
- Estimate reservoir properties such as porosity, shale volume, water saturation and net-to-gross by utilizing petrophysical analysis.
- Analysis of the compaction trends (e.g velocity-depth, density-depth, velocity-density) within the Balder field and their effect on the reservoir quality.
- Use rock physics diagnostics to characterize the reservoir sands in the field.

Moreover, the following issues also investigated:

- To identify and to analyze the petroleum system (source, reservoir, cap rocks).
- To investigate the compaction behaviour of the overburden and underburden rocks.

1.3 Study area

The Balder field is located in the Norwegian sector of the North Sea (Fig. 1.1). It is about 190 km west of the Stavanger on northwestern flank of the Utsira High (a basement high along

the eastern flank of the Viking Graben) (Bergslien, 2002; Sarg and Skjold, 1982; NPD, 2013; Wang et al., 2003). The water depth in the area is about 125 metres. The field is a cluster of small hydrocarbon accumulations which have common fluid contacts across the field and adjacent areas (Bergslien, 2002; NPD, 2013; Wang et al., 2003). The first Production licence PL 001 was awarded on Block 25/11 in 1965 to ExxonMobil Exploration and Production Norway AS (NPD, 2013). ExxonMobil Exploration and Production Norway AS is the present operator of the field (Bergslien, 2002; NPD, 2013). The Balder field production operation includes 12 production wells, 3 water injection wells, 1 gas injection well and 1 water source well (ExxonMobil, 2013; NPD, 2013).

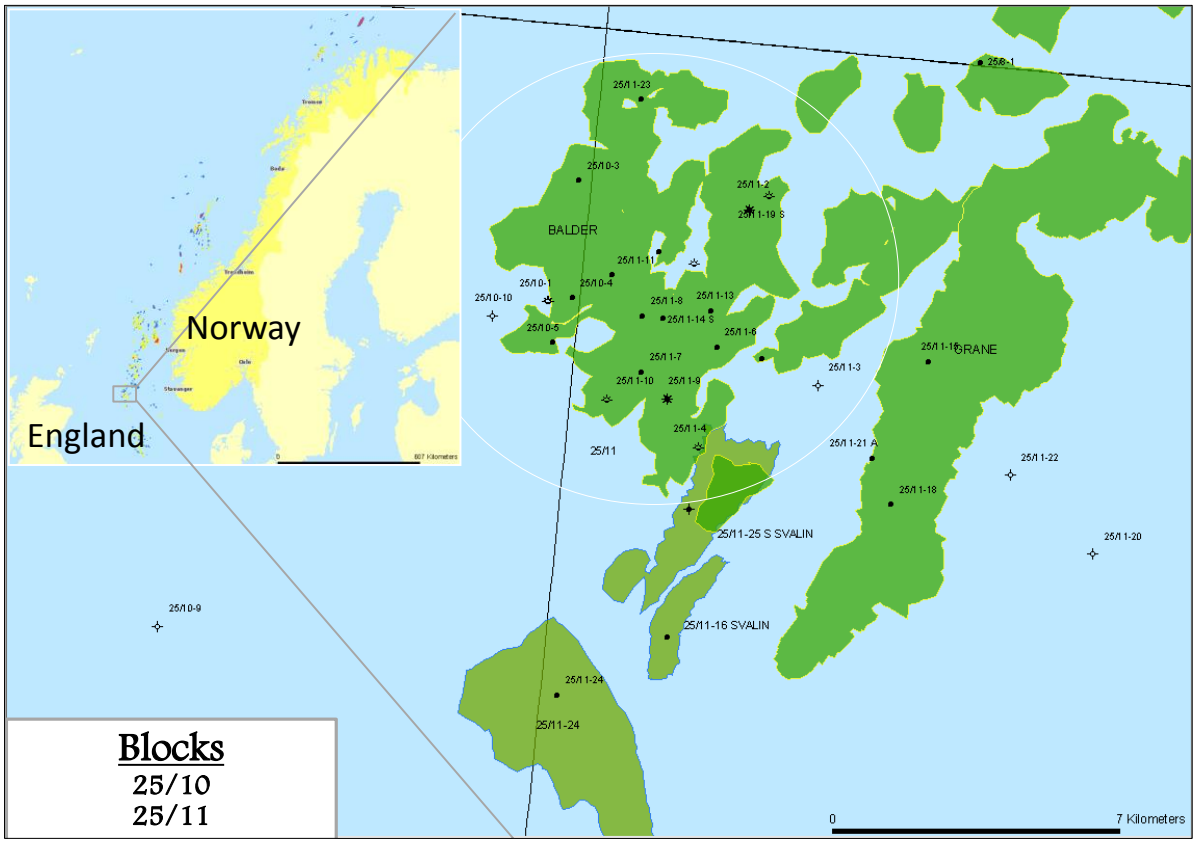

Figure 1.1 Location of the Balder field (white circle) in the blocks 25/10 and 25/11. Other adjacent Oil and Gas fields are also shown (modified from NPD, 2013).

The first well 25/11-1 was drilled in the area in 1967, and brought to surface the first oil samples discovered from the Norwegian Continental Shelf. Discovery well 25/11-5 however was drilled seven years later, as a 7th exploration well in the area (Bergslien, 2002; Wang et al., 2003). The field produce primarily by natural aquifer drive however few water injection wells are utilized for pressure support. The Balder field consists of a Floating Production, Storage, and Offloading (FPSO) vessel and several subsea production systems. The oil is transported by the tankers while excess gas is routed to Jotun field for gas export (Bergslien, 2002; Briedis et al., 2007; Exxonmobil, 2013; NPD, 2013). The main reservoir parameters and production history are given in Table 1.1.

Table 1.1 Reservoir parameters of the Balder field (Data source: ExxonMobil, 2013; NPD, 2013).

Recoverable oil reserves	Oil : 71.3 million Sm^3 ; Gas: 1.6 billion Sm^3
Remaining reserves as of end 2011	Oil: 17.3 million Sm^3 ; Gas: 0.3 billion Sm^3
Estimated production in 2012	Oil: 42000 barrels/day ; Gas: 0.05 billion Sm^3
Oil	Moderately biodegraded
API	23.78
Viscosity	2.4 cp.
OWC	1760 m subsea
GOC	1695 m subsea
Oil column	10-65m gross
OW transition zone above OWC	18–25m
Water depth	125 m
Porosity	31-36 %
Permeability (D)	1-10+
Oil saturation	80-90+ %

1.4 Database

A total twenty five wells from the Balder field area are used in this study (Table 1.2). Most of these wells are from block 25/11 planned as appraisal and wildcat (Fig. 1.1). Only three wells are dry while six wells show hydrocarbons traces. The remianing sixteen wells were determined to have good potential for oil and gas Table 1.2. The year of drilling is also mentioned (Table 1.2) as the wells from 1970s and 1980s, do not have good quality and complete suite of the data.

Due to lack of 3D seismic data during the earliest exploration phase in the Northern North Sea, many wildcat wells were needed to establish startigraphic correlations and geological models of the field. Similarly appraisal wells were utilized to estimate the commercial quantity of hydrocarbons. Further detail of quality and availabilty of well logs in the study area are discussed in the chapter 3 under the heading “Log editing and quality check”.

Table 1.2 Detail information of all wells considered in this study (Data source: NPD, 2013).

Name	Year	Water depth (m)	Purpose-planned	Status	Content	Pay Zone (Formation)
25/10-1	1969	124	WILDCAT	SUSP	Shows	
25/10-2	1970	121	WILDCAT	SUSP	Shows	
25/10-3	1970	126	APPRAISAL	P&A	Oil	BALDER FM
25/10-4	1981	126	APPRAISAL	SUSP	Oil	BALDER FM, HEIMDAL FM
25/10-5	1981	125	APPRAISAL	P&A	Oil	BALDER FM
25/10-8	1997	115	WILDCAT	P&A	Oil/Gas	DRAUPNE FM
25/11-1	1967	125	WILDCAT	P&A	Oil	BALDER FM
25/11-2	1970	130	APPRAISAL	P&A	Shows	
25/11-3	1970	127	APPRAISAL	P&A	Dry	
25/11-4	1970	127	APPRAISAL	P&A	Shows	
25/11-5	1976	124	WILDCAT	P&A	Oil	BALDER FM, HERMOD FM
25/11-6	1978	125.7	APPRAISAL	P&A	Oil	BALDER FM, HEIMDAL FM
25/11-7	1978	124	APPRAISAL	P&A	Oil	BALDER FM, HEIMDAL FM
25/11-8	1979	124	APPRAISAL	P&A	Oil	BALDER FM, HEIMDAL FM
25/11-9	1980	126	APPRAISAL	P&A	Oil/Gas	BALDER FM, HERMOD FM
25/11-10	1981	124	APPRAISAL	P&A	Shows	
25/11-11	1981	126	APPRAISAL	P&A	Oil	BALDER FM, HEIMDAL
25/11-12	1981	127	APPRAISAL	P&A	Shows	
25/11-13	1981	127	APPRAISAL	P&A	Oil	BALDER FM, HEIMDAL FM
25/11-15	1991	127	WILDCAT	P&A	Oil	HEIMDAL FM
25/11-16	1992	120	WILDCAT	SUSP	Oil	HEIMDAL FM
25/11-17	1993	124	WILDCAT	P&A	Dry	
25/11-18	1994	128	APPRAISAL	P&A	Oil	HEIMDAL FM
25/11-20	1995	122	WILDCAT	P&A	Dry	
25/11-23	1999	127	APPRAISAL	P&A	Oil	BALDER FM

1.5 Limitations and future works

As this study is focused exclusively on well logs data and is conducted in a limited time frame and resources, the detailed sedimentological and stratigraphical analyses are not included. The lack of petrographical study (thin section of core or cutting samples) also put the limitation on the quantitative understanding of the reservoir properties like porosity, permeability and cement volume estimation. Furthermore, clay volume and water saturation cannot be calculated accurately due to the lack of core analysis. Similarly the absence of paleontological study also put limits on the understanding of depositional environments of the source and reservoir rocks.

Since no geochemical analysis is available, the understanding of the chemical compaction is of limited reliability. The whole geometry of the reservoir rocks with structural influence is not included due to the lack of seismic data. Shear wave velocity (Vs) is only available in one well (25/11-16) but the data quality is poor over the entire reservoir interval. Therefore predicted values of the Vs from Vp can also add significant errors in rock physics diagnostics.

Though the study has several limitations, still the analytical procedures (petrophysicals, compaction and rock physical analyses) provide useful information that could be utilized in future for quantitative seismic interpretation, AVO modelling and petrographical analysis.

1.6 Chapter descriptions

This study is organized in seven chapters. The first chapter is focused on a general introduction of the study area along with research motivation and an overview of well logs database used in this study.

The aim of the second chapter is to understand the geological evolution of the study area. The petroleum system and the reservoir geometry of the Balder field are also discussed based on existing literature.

The third chapter covers the theoretical background and research methodologies, used in this study. A brief explanation of theoretical background for petrophysical, compaction and rock physics diagnostic techniques are provided with additional description of data sets in this chapter.

Chapter four focuses on the evaluation of the petrophysical properties of the Balder field. The fourth chapter also covers the correlation of the reservoir rocks along with estimation of net-to-gross thickness and facies analysis of reservoir intervals.

Chapter five covers the compaction analysis within the study area. The transition zone is marked to differentiate the mechanical and chemical compacted zones, as this can affect the reservoir quality. Geothermal gradient map of the area also generated to analyze the temperature variations and its effect across the field. This chapter also covers the compaction of the petroleum system.

Chapter six emphasises on rock physis diagnostics for a better characterization of the reservoir sand.

Finally, the last chapter (chapter seven) includes a summary of this work along with conclusions of major findings in this study.

Chapter 2: Geology of the study area

This chapter focuses on the geological settings of the study area, by reviewing the published literatures. It covers four parts under the four major headings a) Regional tectonic and geologic evolution, b) structural elements, c) stratigraphy and d) petroleum systems in and around the Balder field.

2.1 Regional tectonic and geologic evolution

The study area is in the Norwegian sector of the North Sea (Figs. 2.1 and 2.4), which categorized as extensional/rift basin. Several authors (Badley et al., 1988; Færseth, 1996; Kjennerud et al., 2001; Nøttvedt et al., 1995; Ziegler, 1990; Ziegler and Hoorn, 1989) have documented that the two major phases of extension/rifting shape the basin as following: The pre-rift deposits belong to Devonian, Carboniferous and Permian age, and the syn-rift deposits relate to the Mesozoic. The Cenzoic deposits characterize as post-rift sediments.

The crystalline basement rocks in the North Sea is of Late Precambiran basment complex, which consolidated during the Caledonian orogenic cycle. These rocks also formed the part of the Fennoscadian Shield (Badley et al., 1988; Færseth et al., 1996; Hospers and Ediriweera, 1991; Nøttvedt et al., 1995; Ziegler and Hoorn, 1989). North Atlantic Caledonides collapsed during the Devonian time, which are part of the Scottish-Norwegian Caledonides of the northern North Sea (Fig. 2.1a) (Fjeldskaar et al., 2004; Ziegler and Hoorn, 1989). In Late Devonian time, the Greenland and Scandinavia were centered around the equator latitudes (Fig. 2.1a) (Torsvik et al., 2002; Ziegler and Hoorn, 1989).

The North Sea was thermally destabilized due to the Permian and Carboniferous volcanonism. This destabilization lead the wrench fault systems and subsidence of highly volcanic Oslo Graben basins. The Oslo region experience several episodes of peak magmatic activities associated with the rifting (Fig. 2.1b) (Torsvik et al., 2002; Ziegler and Hoorn, 1989). During the Saxonian, the wrench fault seized and the Northern and Southern Permian basins began to subside, both basins are separated by the Mid North Sea Ringkøbing-Fyn (Fig. 2.1c) (Ziegler and Hoorn, 1989). In Late Permian Mid Norway was located at around 35^0 N, while the North Sea was in subtropic region. The North Sea experienced the arid environment during this age (Torsvik et al., 2002). The Zechstein Sea advances which flooded the basins and deposited the highly orgainc rich thin Kupferschiefer group. Repeated glacio-eustatic cycles and continued northward movement change the environment from warm and arid to more temprate and humid (Torsvik et al., 2002). This variation lead to deposition of the Zechstein carbonate, sulfate and halite series in the basin (Fig. 2.4) (Torsvik et al., 2002; Ziegler and Hoorn, 1989).

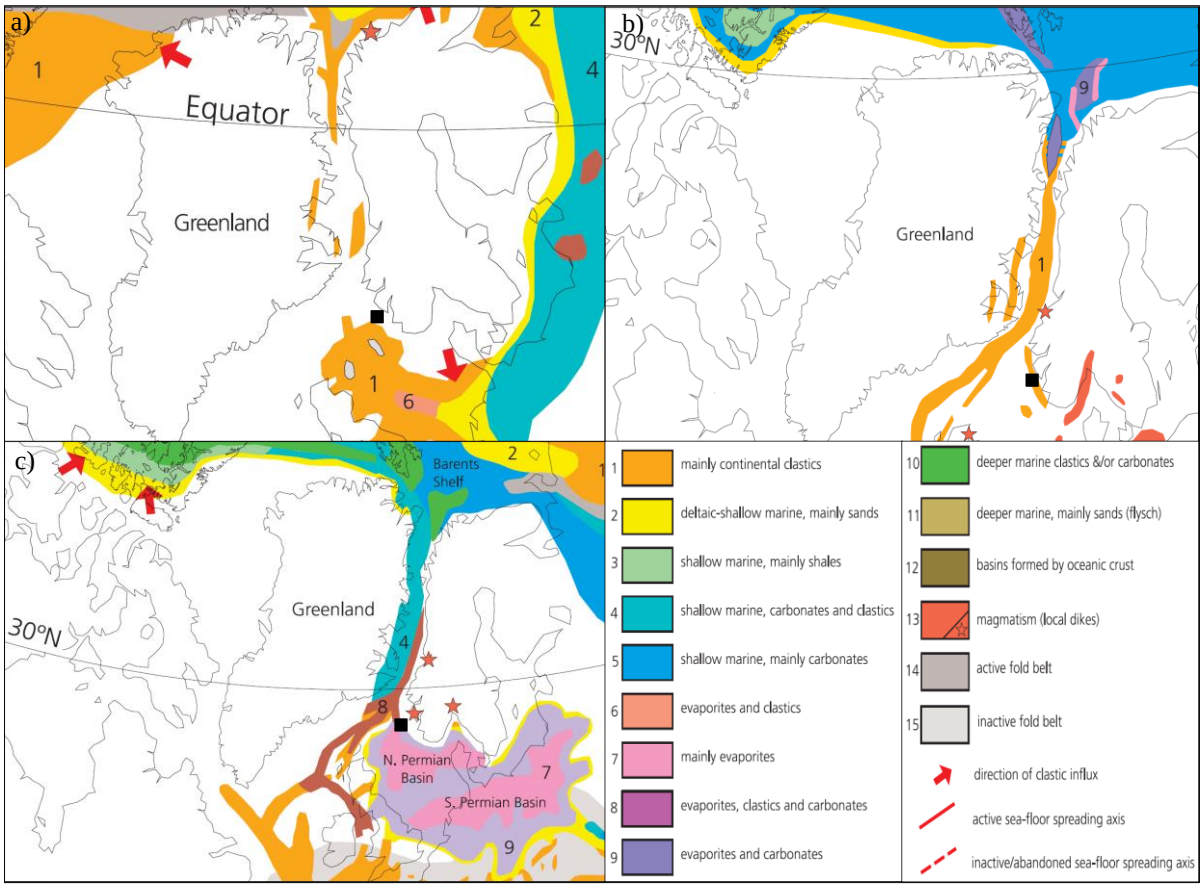

Figure 2.1 a) Regional tectonic and geologic evolution in L. Devonian (360 Ma), b) L. Carboniferous-E. Permian (290 Ma) and c) L. Permian (250 Ma) time. The Legend is shown in the right-bottom corner. The legend is also valid for the Figures 2.1, 2.2 and 2.3). The approximate location of the study area is marked as the black rectangle (modified from Torsvik et al., 2002).

In L. Triassic time, the Mid Norway was located around 45^{O} N (Fig. 2.2 a). The North Sea basin was the site for deposition of continental deposits, but the marine transgression from southeast by Tethys Ocean, also deposited the minor halites and anhydrites (Fig. 2.4) (Torsvik et al., 2002; Ziegler and Hoorn, 1989). The South Viking Graben evolved from several episodes of crustal extention, have been marked in the Mesozoic, which cross cut the Caledonian basement rocks (Badley et al., 1988; Faleide et al., 2002; Færseth et al., 1996; Fichler and Hospers, 1990; Fjeldskaar et al., 2004; Jackson et al., 2010; Odinsen et al., 2000; Voorde et al., 2000; Wang et al., 2003; Wild and Briedis, 2010). First phase of the rifting is marked in the Permian-Triassic time (Fig. 2.2a). In Permian-Triassic transition, rifting accelerated in the Norwegian-Greenland Sea area. In E. Triassic time, the rifting causes subsidence, which set complex multidirectional graben and troughs (Fig. 2.2a) (Badley et al., 1988; Bergslien, 2002; Fjeldskaar et al., 2004; Goff, 1983; Heritier et al., 1979; Odinsen et al., 2000; Sarg and Skjold, 1982; Steel and Ryseth, 1990; Voorde et al., 2000; Ziegler and Hoorn, 1989). This rifting causes the reactivation of the Permian-Carboniferous fracture system, which lead the localization of the Triassic graben such as the North Danish basin, but the Viking and Central Grabens were new features (Figs. 2.2a and 2.4) (Ziegler, 1982; Ziegler, 1988; Ziegler and Hoorn, 1989). The rifting occur along the Viking Graben area that flooded the Permian Basins from the North (Torsvik et al., 2002). During E. to M. Jurassic, the central North Sea was uplifted as broad arch (Fig. 2.2b) (Ziegler and Hoorn, 1989). Large

volcanic complex are associated with this dome in the North Sea (Fig. 2.2b). This uplifted domal struture was site of erosion and deposited as the deltaic deposits in surrounding areas, such as Brent Group in the Viking Graben (Fig 2.4) (Goff, 1983; Graue et al., 1987; Torsvik et al., 2002; Voorde et al., 2000; Ziegler and Hoorn, 1989).

During the M. Jurassic and E. Cretaceous, the second major rifting occurred as the rate of crustal extention increases in the North Sea rift system. During this period further collapse of the basement causes subsidence in the South Viking Graben area (Fig. 2.2 c and d) (Badley et al., 1988; Faleide et al., 2002; Færseth, 1996; Fichler and Hospers, 1990; Goff, 1983; Odinsen et al., 2000; Szarawarska et al., 2010; Wild and Briedis, 2010; Ziegler, 1982; Ziegler and Hoorn, 1989). In this period depositional environment varies from shallow marine to coastal plain on the platforms of Viking Graben, while deep marine environment in the Central Graben area (Fig. 2.4) (Goff, 1983; Ziegler and Hoorn, 1989). During this time, the shelf mudstone of Heather Formation and the deep marine mudstone of Draupne Formation (potential source rock) were deposited (Badley et al., 1988; Goff, 1983; Jackson et al., 2010).

Each of the rifting phase is followed by the post-rift cooling and subsidence interval (Badley et al., 1988; Færseth, 1996; Faleide et al., 2002; Fichler and Hospers, 1990; Goff, 1983; Nøttvedt et al., 1995; Odinsen et al., 2000; Szarawarska et al., 2010; Wild and Briedis,2010; Ziegler, 1982; Ziegler and Hoorn, 1989). Cenozoic Era marked as post-rift deposits in the Viking Graben area (Nøttvedt et al., 1995). In the late Cretaceous, rifitng reduces in the North Sea, while Norwegian-Greenland Sea was still active, which causes crustal sepration later in the Paleocene-Eocene time (Fig. 2.2d) (Bukovics and Ziegler, 1985; Duindam and Hoorn, 1987; Ziegler and Hoorn, 1989).

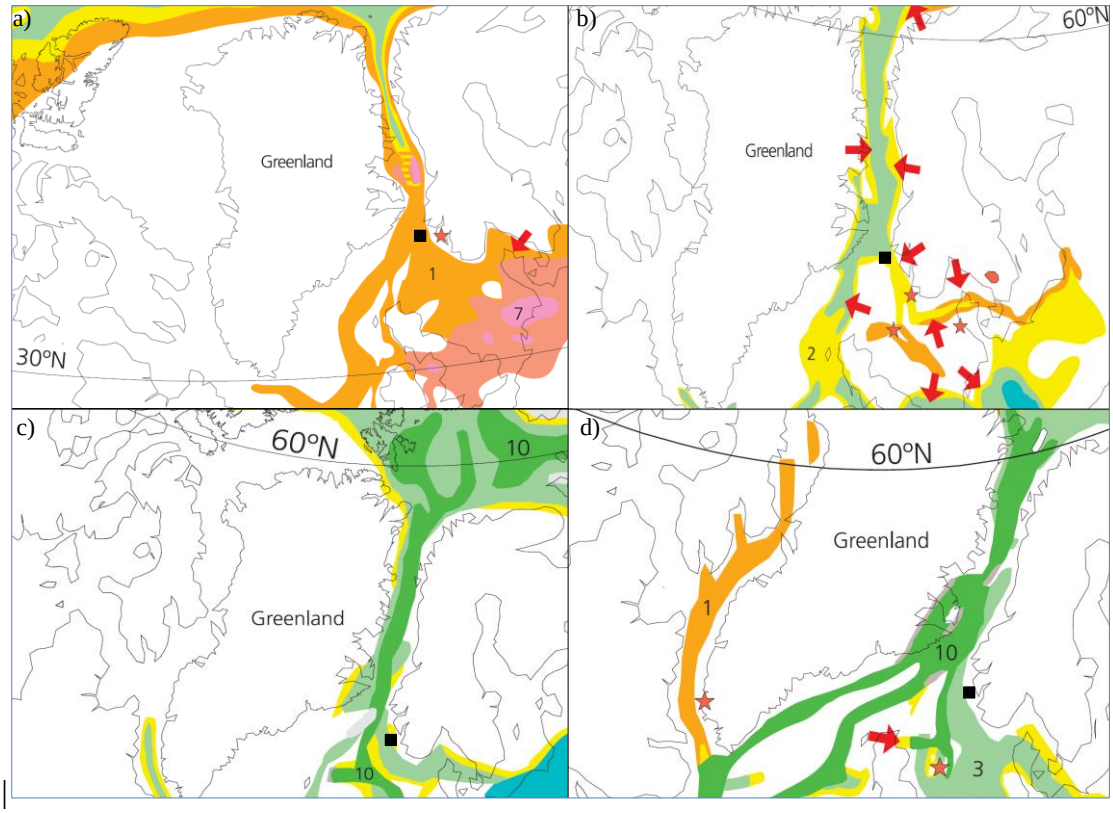

Figure 2.2 Regional tectonic evolution in a) Triassic (220 Ma) b) Middle Jurassic (170 Ma) c) L. Jurassic (150 Ma) and d) Early Cretaceous (130 Ma). The approximate location of the study area marked as the black box (modified from Torsvik et al., 2002).

In the L. Cretaceous, Atlantic rift propagated northwards (Fig. 2.3a). In the North Sea clear water condition prevailed and pelagic chalk deposited in the L. Cretaceous, as clastic inputs were decreased in the basin (Fig. 2.3 a) (Goff, 1983; Torsvik et al., 2002: Ziegler and Hoorn, 1989).

After opening of the northern North Atlantic and Norwegian-Greenland Sea, the North Sea become tectonically stable and most of the evolution is now due to the thermal relaxation of the lithosphere, as there is no evidence of reactivation of the North Sea graben system in Paleo-Eocene time (Ziegler and Hoorn, 1989). In the North Sea, local subsidence and Permian salts movement control the further evolution of the post rift sediments (Rattey and Hayward, 1993; Ziegler and Hoorn, 1989). In this period reservoir rocks of the study area deposited as deep marine gravity sands (Fig. 2.3 b) (Bergslien, 2002; Briedis et al., 2007; Jenssen et al., 1993). Regional uplift associated to Icelandic plume that lead the anoxic condition in the North Sea basin, as it cuts the circulation with the ocean. This upliftment also leads the erosion of flanks which bring clastic sediments into the basin (Fig. 2.3 b) (Jackson et al., 2010; Torsvik et al., 2002). In the Late Oiligocene (25 ma) (Fig. 2.3 c), the Mid Norway drifted to 60-65 ^{O}N. The clay deposited as the pelagic sediments, while the sands deposited as the deltaic sheets deposit, sourced from the uplifted flanks (Torsvik et al., 2002). In Miocene (20 Ma) (Fig. 2.3 d), the Mid Norway was located around 65 ^{O}N. The sea level flactuation cause the complex sedimentary sequences. The sedimentation rates increase compared to the subsidence, which results in thick clastic accumulation in the Viking Graben area (Torsvik et al., 2002).

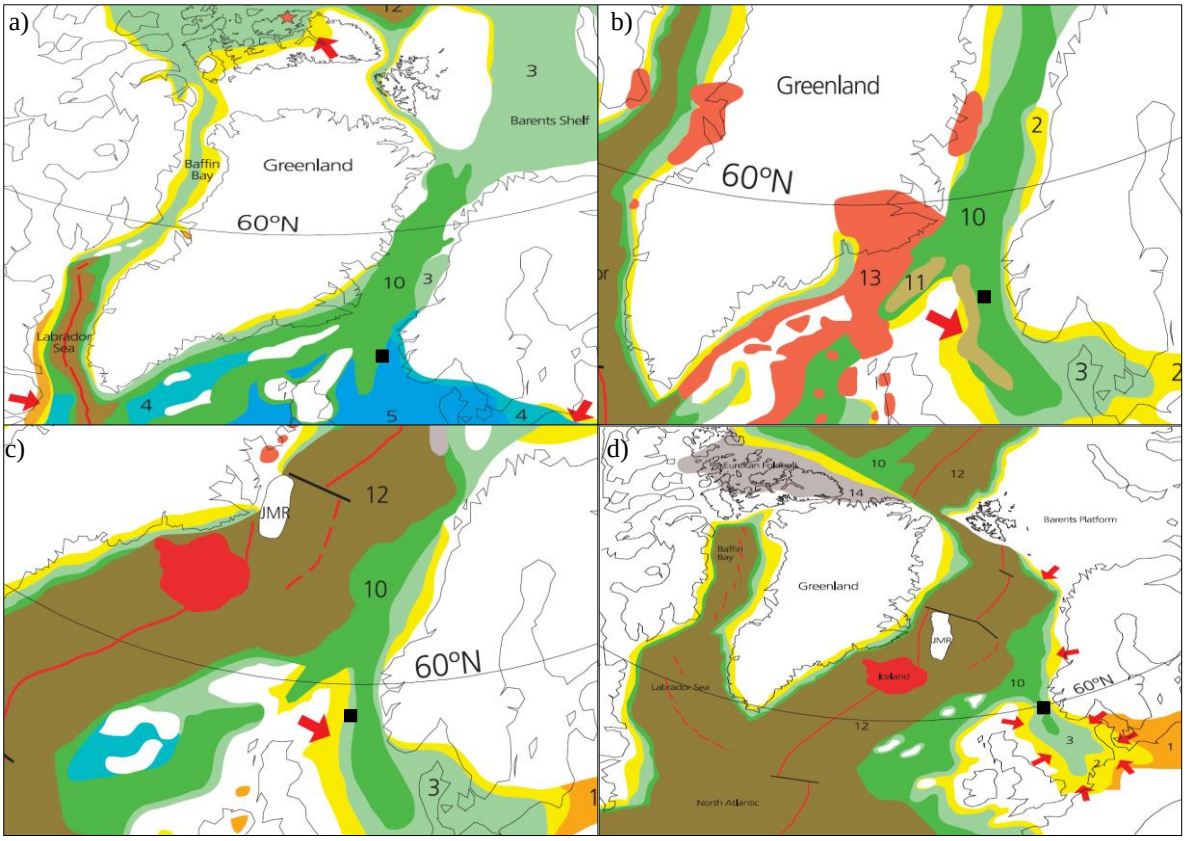

Figure 2.3 a) Regional tectonic and geologic evaluation of the study area in different geologic time a) L. Cretaceous (80 Ma) b) Early Tertiary (60 Ma) c) Mid-Tertiary (25 Ma) and d) Late Tertiary (15 Ma).The approximate location of the study area is marked by the black rectangle (modified from Torsvik et al., 2002).

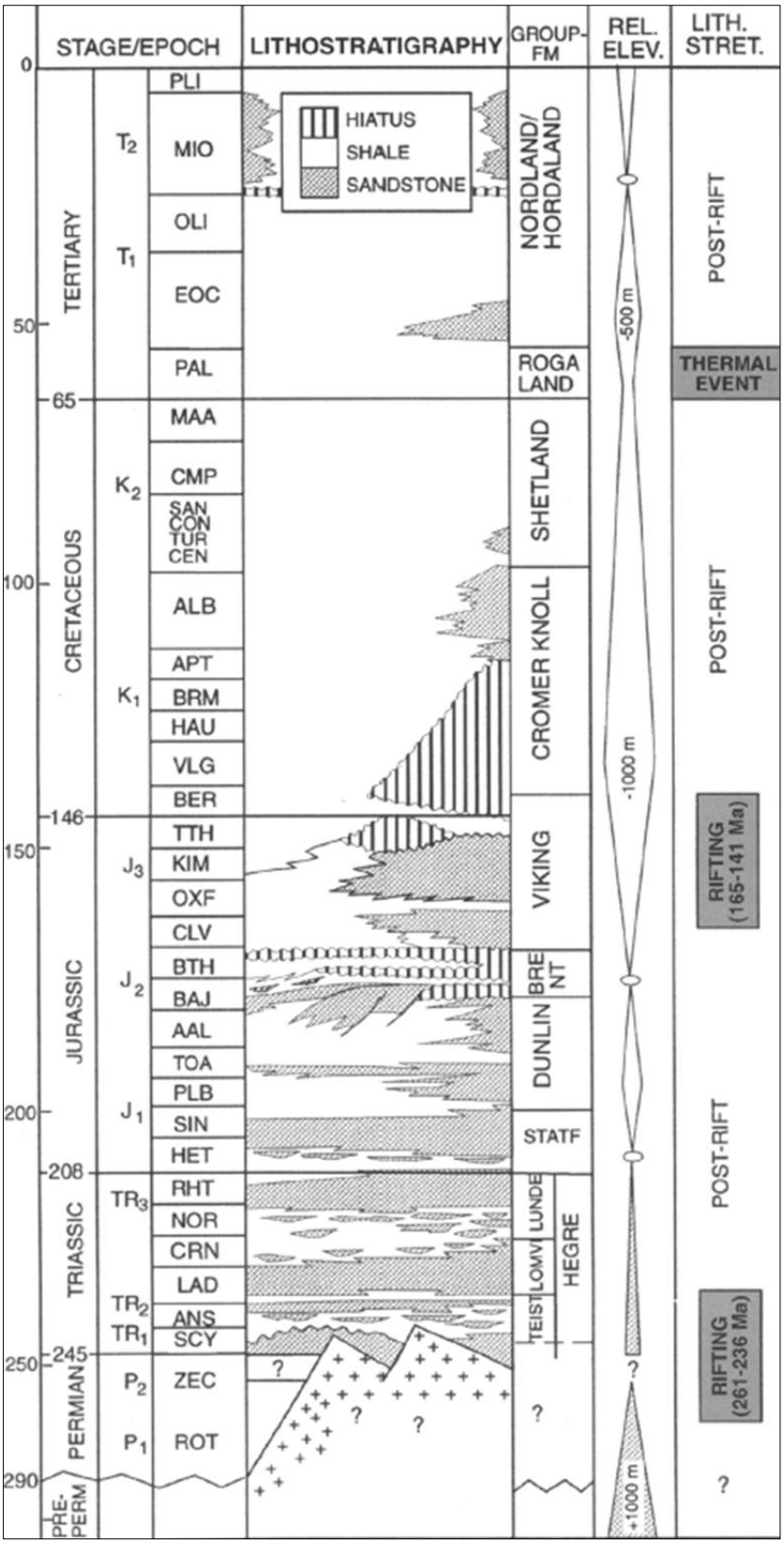

Figure 2.4 Tectonic-sedimentological events in the northern North Sea (Source: Odinsen et al., 2000; modified from Gabrielsen et al., 1990; Nøttvedt et al., 1995; Time scale from Harland et al., 1990).

2.2 Structural elements

The Balder field lies on northwestern flank of the Utsira High, at the eastern margin of South Viking Graben in the North Sea (Fig. 2.5) (Briedis et al., 2007; Bergslien, 2002; Jenssen et al., 1993). The South Viking Graben is 170-200 km wide zone in most parts of the North Sea, in west it is bounded by the Shetland Platform while in east it is bounded by the Norwegian mainland (Bergslien, 2002; Fichler and Hospers, 1990; Fjeldskaar et al., 2004; Nøttvedt et al., 1995; Sarg and Skjold, 1982) (Fig. 2.5). The South Viking Graben developed in Permian as a elongated narrow rift basin, by the several episodes of crustal extensions through the Mesozoic (Cockings et al., 1992; Fjeldskaar et al., 2004; Jackson and Larsen, 2009; Jenssen et al., 1993; Platt and Catwright, 1998).

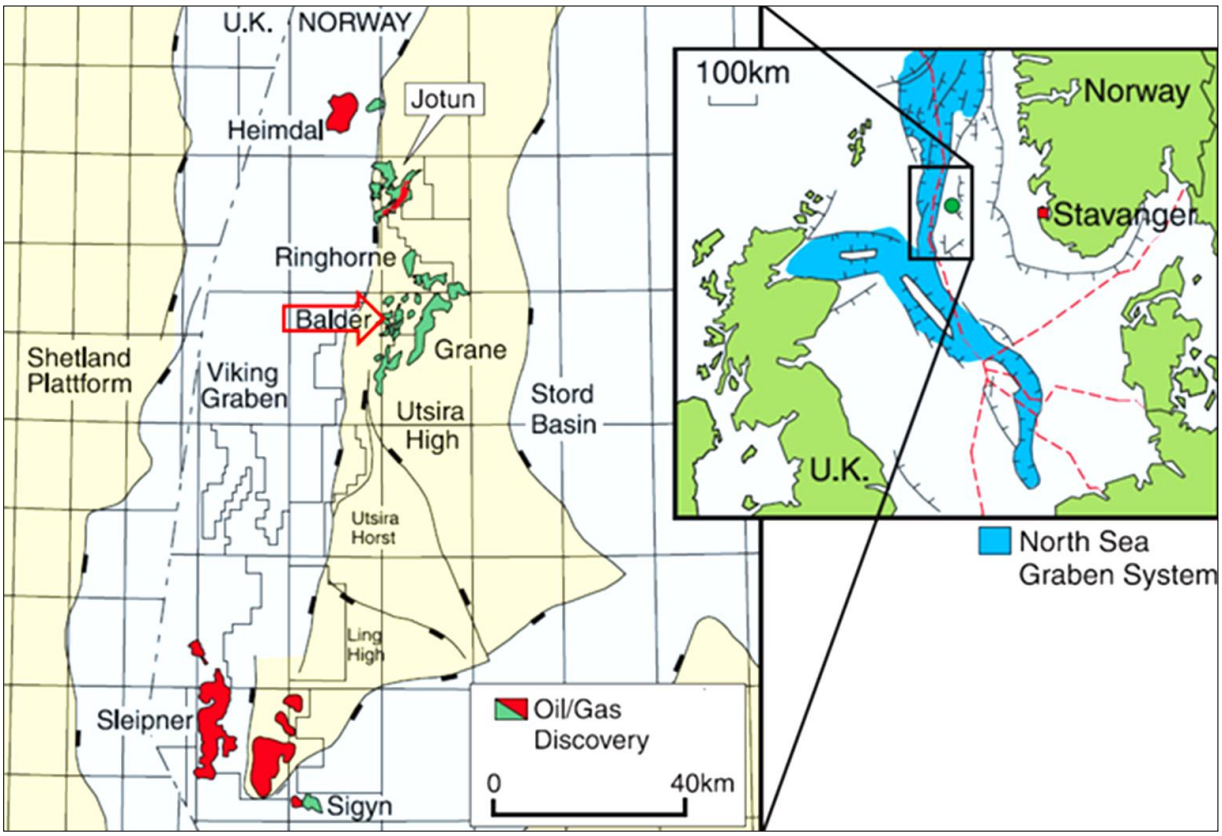

Figure 2.5 The present day structural elements of the study area, the red arrow shows the Balder field (modified from Bergslien, 2002).

The East Shetland Platform classed as structural highs and has very less thin Mesozoic-Cenozoic sedimentary cover (Platt and Catwright, 1998). Reservoir and seal rocks of the study area are sourced from the East Shetland Platform (Timbrell, 1993). The Utsira High is positive feature along the eastern margin of the Viking Graben (Cockings et al., 1992). It has trending in the N-S direction. The Utsira High is 45 km wide and 250 km long (Fig. 2.5) (Gabrielsen et al., 2001). The structural crest of the Utsira High migrated from west to east during Cretaceous and Eocene time. This movement controls the deposition pattern of the Paleocene sediments (Jenssen et al., 1993). The Utsira High buried by the Late Cretaceous and Cenozoic sediments, and their thickness decreases easterly (Bergslien et al., 2005; Jenssen et al., 1993; Cockings et al., 1992). Further in the east, the Stord Basin is prominent feature, which was more wider than the Viking Graben system in E. Cretaceous (Gabrielsen et al., 2001).

2.3 General Stratigraphy

The Balder field comprises of different stratigraphic layers (Figs. 2.6 and 2.7). The Paleocene intervals contain 25-60% of sands with thickness ranges from 80 to 240 m (Fig. 2.7) (NPD, 2013; Sarg and Skjold, 1982). The source rocks belonged to Upper Jurassic age, while the reservoir rocks belonged to Paleocene to Late Eocene age (Fig. 2.7) (Isaksen and Ledje, 2001). The hydrocarbon migrated from the Jurassic source rocks to the Tertiary reservoir rocks (Isaksen and Ledje, 2001; Schlakker et al., 2012). The reservoir units: Balder, Hermod and Heimdal sands deposited during lowstand periods, while the seal/cap rocks of Sele and Lista formations shales deposited during transgressive and highstand (Fig. 2.6) (Briedis et al., 2007). The hemipelagic shale of Sele Formation and Lista Formation draped over the entire suprafan complex, which serves as the seal rocks (Fig. 2.6) (Briedis et al., 2007; Sarg and Skjold, 1982).

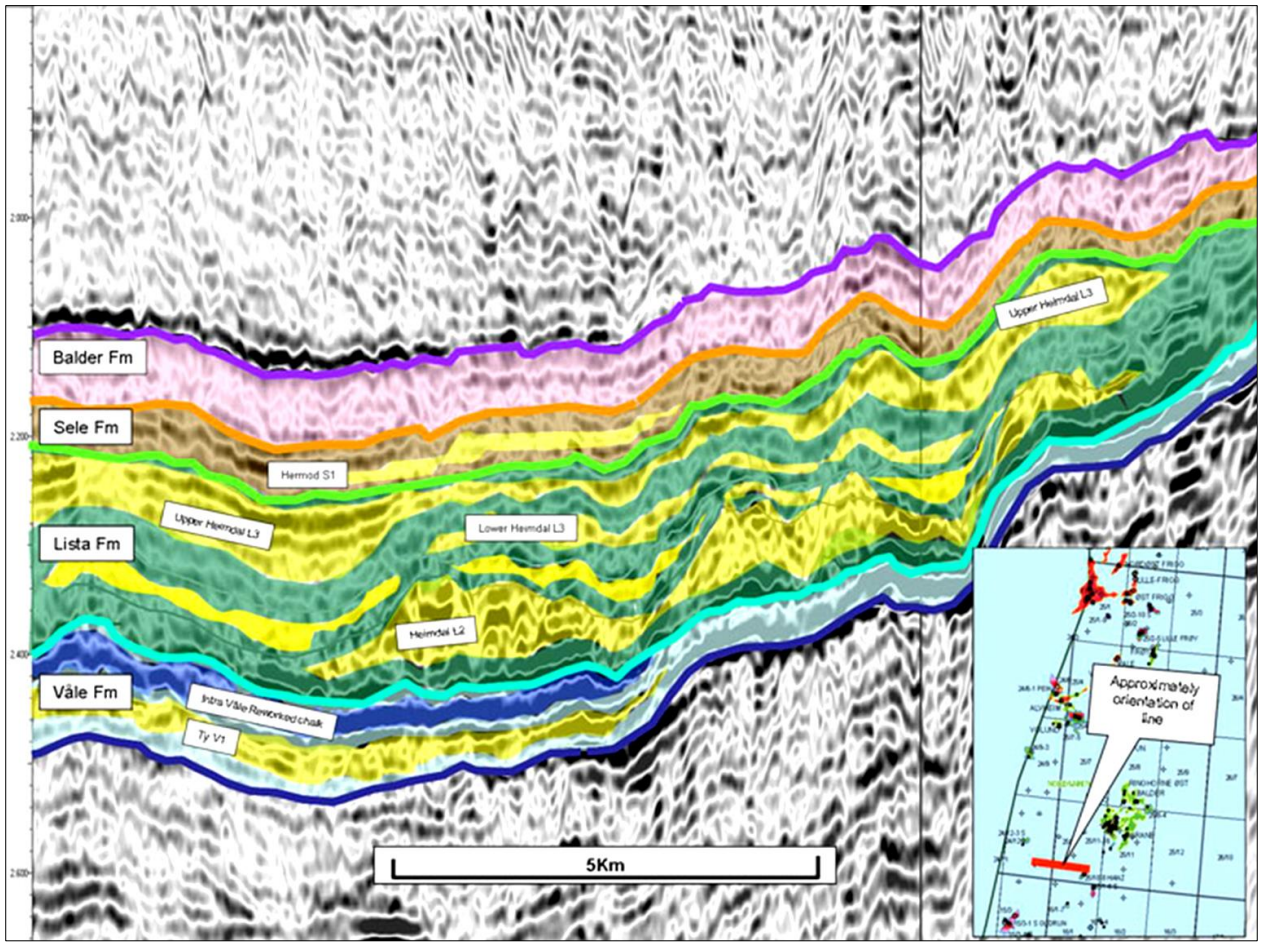

Figure 2.6 Example of seismic character of sandy facies of the Rogaland Group. The seismic section seen from EW section through southern parts of block 25/10 (Source: Norlex, 2013).

In the Balder field the deepest well is drilled till basement rocks of Pre Devonian (NPD, 2013). From the Table 2.1, it can be seen that the basement rocks, which encounter in the well 25/10-2 are much deeper as compare to the basement rocks encounter in the well 25/11-17. The further analysis on correlation of the stratigraphy and affect of the geothermal gradient, due to shallow basement rocks in southern part of the Balder field are discussed in the Chapter 5.

Table 2.1 Wells with oldest unit of penetration in the study area (Data source: NPD, 2013).

Well no.	Depth (m) RKB	TVD (m) RKB	Oldest unit	Age
25/10-1	2092	2092	Sele Fm	Paleocene
25/10-2	3181	3181	Basement	Pre-Devonian
25/10-3	1921	1921	Ekofisk Fm	Paleocene
25/10-4	2550	2550	Zechstein Gp	Late Permian
25/10-5	2011	2011	Viking Gp	Late Jurassic
25/10-8	2653	2653	Rotliegend Gp	Early Permian
25/11-1	2459	2459	Basement	Pre-Devonian
25/11-2	1824	1824	Sele Fm	Paleocene
25/11-3	1858	1858	Ekofisk Fm	Paleocene
25/11-4	1896	1896	Ekofisk Fm	Paleocene
25/11-5	2164	2464	No group defined	Triassic
25/11-6	1948	1948	Cromer knoll Gp	Early Cretaceous
25/11-7	1944	1944	Tor Fm	Late Cretaceous
25/11-8	1950	1950	Ekofisk Fm	Paleocene
25/11-9	1910	1910	Tor Fm	Late Cretaceous
25/11-10	1988	1988	Ekofisk Fm	Paleocene
25/11-11	1960	1960	Ekofisk Fm	Paleocene
25/11-12	1918	1918	Ekofisk Fm	Paleocene
25/11-13	1932	1932	Tor Fm	Late Cretaceous
25/11-15	2035	2035	Statfjord Fm	Early Jurassic
25/11-16	1945	1945	Hod Fm	Late Cretaceous
25/11-17	2256	2255	Basement	Pre-Devonian
25/11-18	1875	1874	Hod Fm	Late Cretaceous
25/11-20	1828	1828	Tor Fm	Late Cretaceous
25/11-23	2014	2010	Statfjord Fm	Early Jurassic

The general startigraphy of the Balder field area with marked source, reservoir and seal/overburden rocks briefly explained below (Fig. 2.7). The detail review on the source, reservoir and seal rocks is given in the section “2.4 Petroleum systems” in this chapter. Only those groups/formations are discussed here that penetrated by the studied wells (Table 2.1).

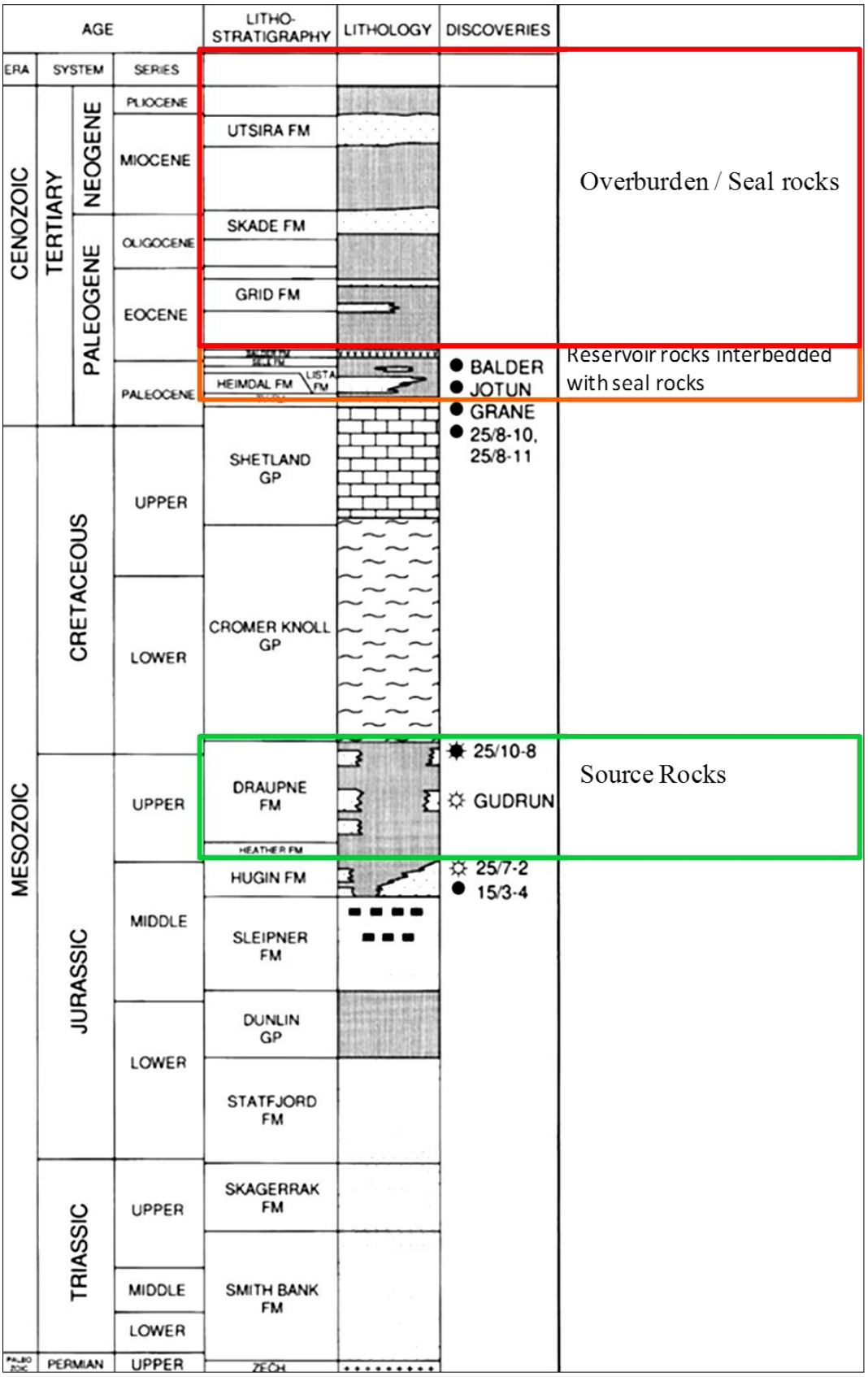

Figure 2.7 General Stratigraphic succession of the Balder area, Utsira High (modified after: Isaksen and Ledje, 2001).

2.3.1 Basement rocks

The metamorphic rocks of Pre-Devonian age are underlying in the study area. It is dark grayish red in color. Three wells out of twenty-five wells are penetrated the basement rocks. The depth of penetration varies in each well from 29 to 68 m (source: NPD, 2013).

2.3.2 Rotliegend Group

The Rotliegend Group is of Early Permian age. It is composed of clay, shales, sandstones and conglomerates. These sequences mostly belong to the continental environments. In Norwegian sector, no further subdivisions are recognized (NPD, 2013; Purvis, 1992). Only two wells out of twenty-five wells penetrated the Rotliegend Group. The thickness of this group varies from 52 to 138 m.

2.3.3 Zechstein Group

The Zechstein Group is of Late Permian age (Fig. 2.7). It is mainly composed of evaporates and carbonates rocks. These deposits belong to the marine environment (NPD, 2013; Purvis, 1992). Only four wells out of twenty-five wells penetrated the Zechstein Group. The thickness of this group varies from 17 to 87 m in these wells. In Norwegian sector, the group is further divided into Kupferschiefer Formation.

2.3.4 Viking Group

The Viking Group is of Upper Jurassic age (Fig. 2.7). It is mainly composed of mudstones, claystones, and shales, with minor intrusion of carbonates and sandstones. The deposits mostly belong to marine environment (Isaksen and Ledje, 2001; NPD, 2013). Only five wells out of twenty-five wells penetrated the Viking Group. The thickness of these groups varies from 5 to 57 m within these wells. Further, this group is sub categorized into several formations. In study area, following formations are encounter within the wells.

2.3.4.1 Heather Formation

The Heather Formation is of Upper Jurassic age (Fig. 2.7) (Isaksen and Ledje, 2001). The Heather Formation of the Viking Group (Schlakker et al., 2012) is secondary source rock in the Utsira High area, which shows poor to fair potential to generate oil (Isaksen and Ledje, 2001). The Heather Formation characterized as syn-rift deposits. It was deposited in an open marine environment during the stretching of the North Sea in Bathonian to Kimmeridgian age (Goff, 1983; Cited in Justwan and Dahl, 2005, Source: Isaksen and Tonstad, 1989; Vollset and Dore´, 1984). The Heather Formation is composed of grey silty mudstone (Isaksen and Tonstad, 1989; Justwan and Dahl, 2005). Only one well (25/10-4) is penetrated the formation in the Balder area out of the twenty-five wells (Table 2.1). In this well, the total thickness is 18 m.

2.3.4.2 Draupne Formation

The Draupne Formation is of Upper Jurassic age (Fig. 2.7) (Isaksen and Ledje, 2001). The Draupne Formation of the Viking Group (Schlakker et al., 2012) is primary oil-prone source rock in the Utsira High area (Isaksen and Ledje, 2001). The Draupne Formation is subdivided into lower and upper part, the lower part deposited as syn-rift deposits while the upper part deposited as post rift deposits (Justwan and Dahl, 2005). This formation deposited as marine shale during the marine transgression in the Viking Graben area in Early Collovian age

(Isaksen and Ledje, 2001). The shale is oil prone kerogen, which dominates by algal bodies and lipid-rich amorphous material (Isaksen and Ledje, 2001). The Draupne Formation penetrated by five wells out of twenty-five studied wells (Table 2.1). The total thickness varies from 8 to 70 m.

2.3.5 Cromer Knoll Group

The Cromer Knoll Group is of Lower Cretaceous age (Fig. 2.7) (Isaksen and Ledje, 2001). The Cromer Knoll Group composed of marlstones, siltstones, chalky claystones, mica, pyrite and gluconite (Norlex, 2013). These deposits belong to the open marine calm environment (Norlex, 2013). The Cromer knoll Group is further subdivide into six formation namely Åsgard, Tuxen (Jenssen et al., 1986), Mime, Sola (Hamar and Hesjedal, 1983; Jenssen et al., 1986), Rødby and Agat (Norlex, 2013; NPD-Bulletin No.5). This group thickness varies from 15 to 60 m in different studied wells (Table 2.1).

2.3.6 Shetland Group

The Shetland Group is of Upper Cretaceouse age (Fig. 2.7) (Isaksen and Ledje, 2001). The group is developed in the Central and Northern North Sea. The central part is dominated by chalk facies, while siliciclastic facies is dominated in the northern part (NPD Bulletin-5). The chalk is composed of limestones, marls and calcareous shale, while silicicalstic facies consists of mudstones interbedded with shale (NPD Bulletin-5). The thickness varies from 11 to 55 m in the studied wells penetrated the group (Table 2.1).

2.3.7 Rogaland Group

The Rogaland group is of Paleocene-Early Eocene age (Fig. 2.7). It is composed of sandstones interbedded with shales deposits. These deposits belong to deep marine environments and mostly characterized as submarine fan deposits in the study area (Norlex, 2013; NPD, 2013). The group penetrated by all wells, which are under consideration. The thickness of this group varies from 115 to 431 m in different studied wells. This group divided into several formations. In the study area, following formations are encounter within the wells.

2.3.7.1 Ty Formation

The Ty Formation is of Early Paleocene age (Fig. 2.7) (Isaksen and Ledje, 2001). It is belonged to the Rogaland Group (Bergslien, 2002). It is composed of clean sandstone of light grey color (NPD Bulletin-5). The Ty Formation deposited as deep marine deposits with interbedded shales (Norlex, 2013; NPD Bulletin-5). Its thickness varies from 20 to 33 m in the studied wells (Table 2.1).

2.3.7.2 Lista Formation

The Lista Formation is of Late Paleocene age (Fig. 2.7) (O'Connor and Walker, 1993; Isaksen and Ledje, 2001; Mudge and Bujak, 1996). The Lista Formation is composed of brown shales with small intrusions of limestones, dolomite and pyrites, which deposited in calm deep marine environment (O'Connor and Walker, 1993; Mudge and Bujak, 1996; NPD Bulletin-5). The Lista Formation interbedded with the Heimdal Formation and act as seal rock (Jenssen et al., 1993). Its thickness varies from 10-40 m in the studied wells (Table 2.1).

2.3.7.3 Heimdal Formation

The Heimdal Formation is of Late Paleocene age (Fig. 2.7) (Isaksen and Ledje, 2001). It is belonged to the Rogaland Group (Bergslien, 2002). In recent years, the Heimdal Formation name changed to Heimdal Member, as it is documented within the Lista Formation (Norlex, 2013). But in this study, the Heimdal Formation is used, as the Norwegian Petroleum Directorate still maintain the old name and status (NPD, 2013). The Heimdal Formation is composed of poorly cemented and sorted, fine to coarse sandstone with interbedded grey to black shales (O'Connor and Walker, 1993; Norlex, 2013; NPD Bulletin-5). The Heimdal Formation is deposited in high energy shallow marine environment on the western side (East Shetland), while in the Viking Graben area it deposited as submarine fans (Norlex, 2013; NPD Bulletin-5). The Heimdal Formation interbedded with Lista Formation and act as reservoir rock (Jenssen et al., 1993). Its thickness varies within the studied wells (Table 2.1), the minimum thickness encounter in the well 25/11-3 is 1 m while the maximum thickness is in the well 25/10-4 is 114 m. Further discussion of deposional pattern of Heimdal Formation is discussed under the heading "2.4.2 Reservoir rocks". The thickness variation discussed under the heading of "2.4.3 Reservoir geometry and stratigraphic correlation of the reservoir units" in later part of this chapter.

2.3.7.4 Sele Formation

The Sele Formation is of Late Paleocene age (Fig. 2.7) (Isaksen and Ledje, 2001). It is belonged to the Rogaland Group (Bergslien, 2002). The Sele Formation is composed of tuffaceous shales and siltstones, grey to greenish grey in color, deposited in deep marine environment (O'Connor and Walker, 1993; Norlex, 2013; NPD Bulletin-5). The Sele Formation interbedded with Hermod Formation and act as seal rock (Jenssen et al., 1993). Its thickness varies within the studied wells (Table 2.1), the minimum thickness encounter in the well 25/11-23 is 2 m while the maximum thickness in the well 25/10-4 is 75 m.

2.3.7.5 Hermod Formation

The Hermod Formation is of Late Paleocene-Early Eocene age (Fig. 2.7) (Isaksen and Ledje, 2001). It is belonged to the Rogaland Group (Bergslien, 2002). In recent years, the Hermod Formation name changed to Hermod Member, as it is documented within the Sele Formation (Norlex, 2013). But in this study, the Hermod Formation is used, as the Norwegian Petroleum Directorate still maintain the old name and status (NPD, 2013). It is composed of well-sorted sandstone, interbedded with claystones, deposited as submarine fan (Norlex, 2013; NPD Bulletin-5). It inter-bedded with the Sele Formation and act as reservoir rock (Jenssen et al., 1993). The thickness varies within the studied wells (Table 2.1), the minimum thickness encounter in the well 25/11-9 is 1 m while the maximum thickness in the well 25/11-23 is 56 m. Further, discussion of the depositional pattern of Hermod Formation is discussed under the heading "2.4.2 Reservoir rocks". The thickness variation is discussed under the heading "2.4.3 Reservoir geometry stratigraphic correlation of different reservoir units" in this chapter.

2.3.7.6 Balder Formation

The Balder Formation is of Paleocene-Early Eocene age (Early Ypresian) (Fig. 2.7) (Isaksen and Ledje, 2001; Mudge and Bujak, 1996; Timbrell, 1993). It is belonged to the Rogaland Group (Bergslien, 2002). The Balder formation is dominantly composed of thick sandstone with laminated shales and mudstone, which are interbedded with volcanic tuff. These

sequences deposited in deep marine environment as turbidite currents (Norlex, 2013; NPD Bulletin-5; Sarg and Skjold, 1982). The Balder Formation is present in all studied wells. The formation acts as regional seismic marker in the North Sea due to its gamma ray values. The Balder formation thickness varies from 12 to 100 m within the studied wells (Table 2.1).

The Balder Formation contains two following sandstone intervals:

1) Odin Member

2) Radøy Member

Odin Member

The Odin Member sandstone is distributed in western part of the Norwegian North Sea. It is composed of moderately sorted sandstone. This member is locally present within the Balder field. It is deposited as mass flow or sub marine fans, sourced from the East Shetland Platform but few sandstones bodies are interpretated as injections (Norlex, 2013).

Radøy Member

The Radøy Member sandstone is distributed in north-eastern part of the Norwegian North Sea. It is composed of clear-white to yellow, non calcareous sandstone. It is deposited as submarine channels and sub marine fans (Norlex, 2013).

2.3.8 Hordaland Group

The Hordaland Group is of Eocene to Early Miocene age. It is mainly composed of claystones with minor sandstones sequences. The deposits belong to the deep marine environment (Norlex, 2013; NPD Bulletin-5). It is pentrated by all the studied wells. The thickness varies from 690 to 1180 m in the study area.

2.3.8.1 Grid Formation

The Grid Formation is of Middle to Late Eocene age (Fig. 2.7) (Isaksen and Ledje, 2001). It belonged to the Hordaland Group (Bergslien, 2002). The Grid Formation dominantly composed of sandstone with interbedded claystones and siltstones, which deposited in the open marine environment during the eustatic sea level fall (Haq et al., 1987; Norlex, 2013). Its thickness varies from 11 - 70 m in different studied wells (Table 2.1).

2.3.8.2 Skade Formation

The Skade Formation is of Late Oligocene age (Fig. 2.7) (Isaksen and Tonstad, 1989). It is belonged to the Hordaland Group (Bergslien, 2002). The Skade Formation dominantly composed of clean sandstones interbedded with claystones, which deposited in the open marine environment during the eustatic sea level fall (Haq et al., 1987; NPD Bulletin-5). Its thickness varies from 100 to 300 m in different studied wells (Table 2.1).

2.3.9 Nordland Group

The Nordland Group is of Middle Miocene to Recent age in the study area. The group age varies in Norwegian continental shelf. It is mainly composed of marine claystones deposits, while sandy deposits in lower part of the group. These sequence deposited in the open marine

environment, while glacial deposits belongs to the upper part of the group (Bergslien, 2002; NPD, 2013; NPD Bulletin-5). It is penetrated by all wells which are under considerations. Its thickness varies from 690 to 950 m in the study area.

2.3.9.1 Utsira Formation

The Utsira Formation is of Middle to Late Miocene age (Fig. 2.7) (Isaksen and Ledje, 2001). It belonged to the Nordaland Group (Bergslien, 2002). The Utsira Formation dominantly composed of marine sandstone and claystones which are deposited as the shollow marine shelf deposits (NPD Bulletin-5). Its thickness varies from 100 to 300 m in different studied wells (Table 2.1).

2.4 Petroleum systems

Petroleum system is the natural geological system, which has once active source rock and all essential geological elements and processes to hold the hydrocarbons (Magoon and Dow, 1994). As further, explain by Magoon and Dow, 1994, these essential geological elements include following:

- Source Rock
- Reservoir Rock
- Seal and overburden Rock

Processes, which are essential for holding the hydrocarbons, define by (Magoon and Dow, 1994) are

1) Trap formation

2) Generation-Migration-Accumulation of hydrocarbons

In order to hold the hydrocarbons these geological elements and processes have to occur in specific space and time (Magoon and Dow, 1994).

Figure 2.8 shows different petroleum system event with relation to the geological time in the study area, if one of these geological elements or processes is missing, petroleum system is incomplete.

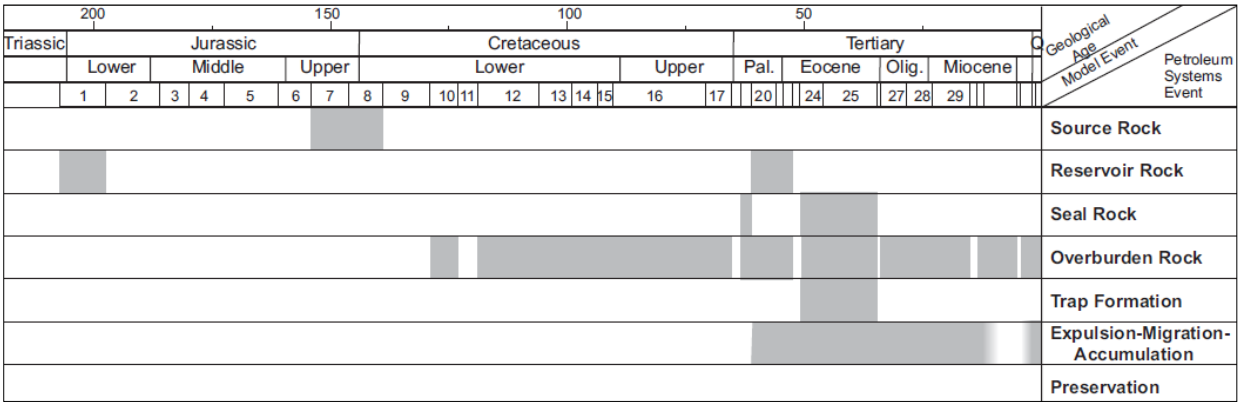

Figure 2.8 Petroleum system event chart for kimmeridge equivalent of the Draupne and Heather Formation in the Balder field area (Source: Justwan et al., 2006).

As from the Figure 2.8, it can be seen that the potential source rocks are deposited in the Jurassic Age, while the reservoir rocks are formed as early as in Triassic. The Balder field reservoirs belong to the Paleocene-Eocene age. It is more likely that these reservoirs are filled by the Jurassic source rocks (Schlakker et al., 2012). Further explanation of migration is discussed under the heading 2.4.4 in this chapter. These reservoirs are sealed by the same age cap/seal rocks (Fig. 2.8) (Justwan et al., 2006).

2.4.1 Source rocks

The Draupne and Heather formations are two potential source rocks in the study area (Cooper et al., 1995; Cornford, 1998; Justwan and Dahl, 2005). The Draupne Formation is dominated source rock for oil, whereas, the Heather Formation shows fair to good gas potential (Justwan and Dahl, 2005). The Heather Formation deposited as syn-rift deposits during the interval of Bathonian to Kimmeridgian age that mark the stretching phase in the North Sea (Justwan and Dahl, 2005; Vollset and Dore´, 1984). On the other hand, the Draupne Formation deposited during Late Oxfordian age, which mark the transgressive phase (Justwan and Dahl, 2005; Rawson and Riley, 1982). The Lower Draupne Formation characterized as syn-rift deposits while the Upper Draupne Formation characterized as post-rift deposits (Justwan and Dahl, 2005).

Quality of source rock

The Heather Formation has low values of TOC (3%). It is mostly dominated by the Type-III/IV kerogen with negligible presence of type-II because of more influence of the terrestrial input (Justwan and Dahl, 2005). It decreases eastern part of the basin as well as vertically (Fig. 2.9) (Cooper et al., 1995; Justwan and Dahl, 2005). On the other hand, the Draupne Formation is a mixture of Type-II and Type-III organic matter. During the transgression on the Utsira High, more organic matter preserve which has more TOC compared to the graben area to Utsira High (Fig. 2.9) (Justwan and Dahl, 2005).

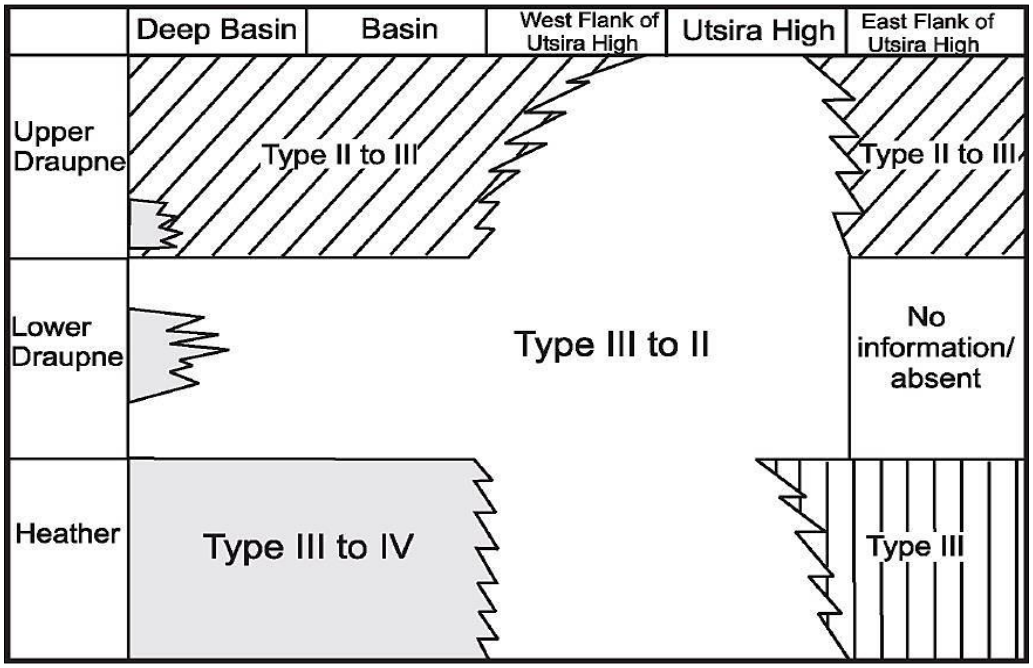

Figure 2.9 Type, quality and distribution of the Draupne and Heather formations (Source: Justwan and Dahl, 2005).

As in study by Dahl et al., (1987), Isaksen et al., (1998b) and Thomas et al., (1985) that expulsion and migration of these source rock started in Late Cretaceous to present day (cited in: Isaksen and Ledje, 2001).

Regional stratigraphic correlation of the source rocks

The Oxfordian to Ryazanian Kimmeridge Clay equivalent, the Draupne Formation diachronously overlies on the Heather Formation (Fig. 2.10) (Justwan and Dahl, 2005; Vollset and Dore´, 1984). In the Draupne Formation, a series of basin-ward thinning and fining sandy wedges of Kimmeridgian to Volgian are present in the South Viking Graben (Isaksen and Ledje, 2001; Justwan and Dahl, 2005; Partington et al., 1993; Underhill, 1998). These 'Intra-Draupne deposits' (encounter in one well 25/10-4) are sourced from the Utsira High and the East Shetland Platform. These deposits are significant in forming reservoirs in the South Viking Graben and inter-finger with the shales of the Draupne Formation having higher amounts of organic matter (Isaksen and Ledje, 2001; Justwan and Dahl, 2005; Underhill, 1998). During the rifting and subsidence episode in Kimmeridgian to Mid-Volgian times deep-water fan system were common (Fraser et al., 2003).

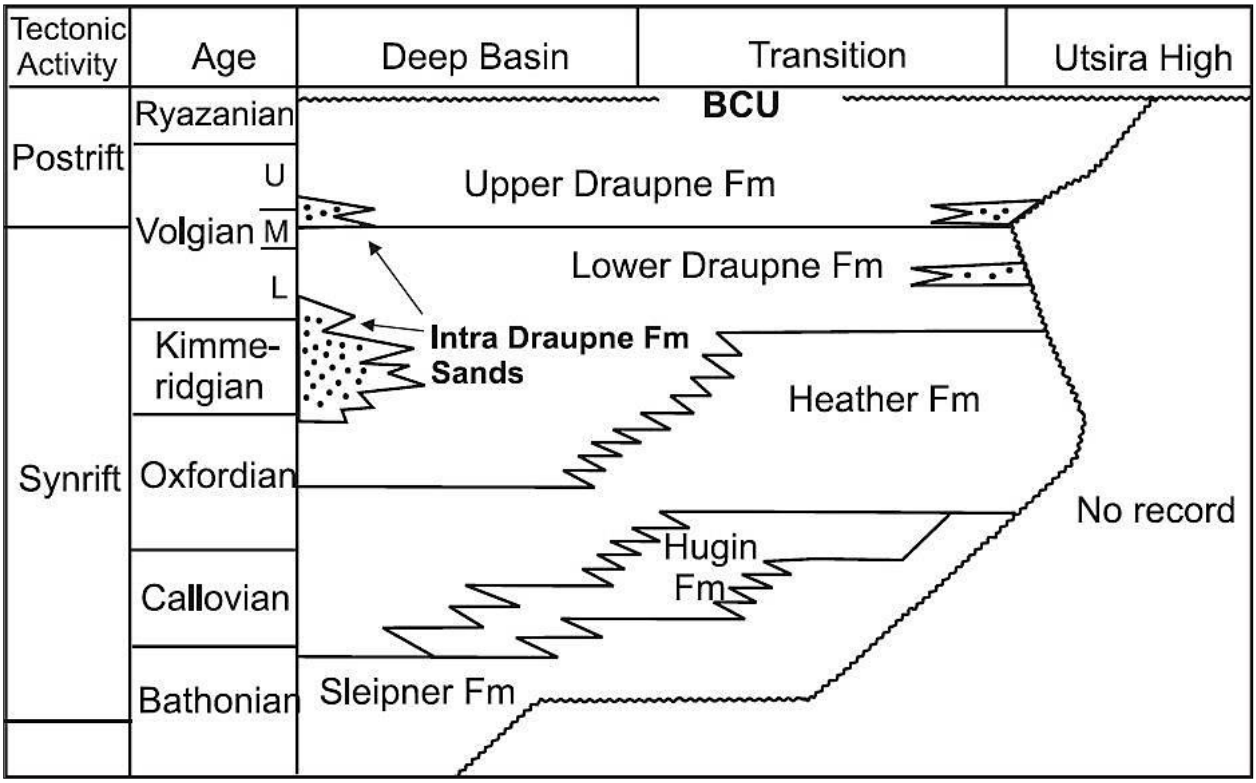

Figure 2.10 Stratigraphic range and occurrence of the Draupne and Heather formations (Source: Justwan and Dahl, 2005).

Source rocks correlation across the Balder field

In the Balder field, the Draupne Formation has thickness of 150 meters in western part (well 25/10-4) (Fig. 2.11), whereas it ranges above 1200 m in the center of the Viking Graben and the average TOC values in the Balder field area reaches 4 wt.% (Justwan and Dahl, 2005). Only five wells out of twenty-five wells, which are under consideration, penetrated the source rocks. The thickness of the source rocks decreases from west to east (Fig. 2.11).

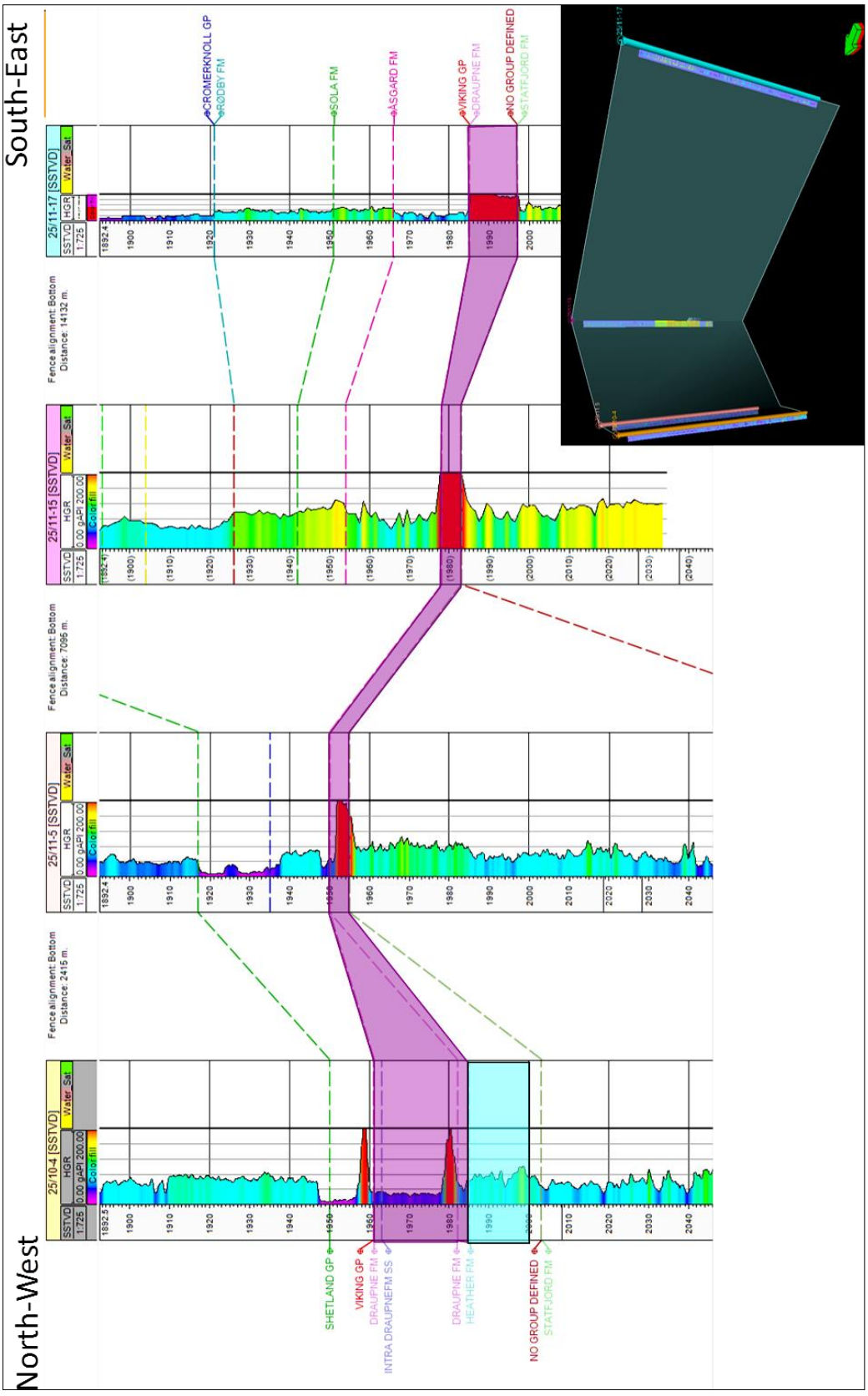

Figure 2.11 Stratigraphic cross-sectional view across the Balder field for source rocks, marked by the purple polygon for the Draupne Formation and light blue for the Heather Formation.

2.4.2 Reservoir rocks

Three main reservoir units in the Balder field namely Balder Sands, Hermod Sands and Heimdal Sands (Fig. 2.12) (Briedis et al., 2007) are present. These three sand units are of Paleocene-Early Eocene age and interbedded with shale (Fig. 2.12) (Jenssen et al., 1993).

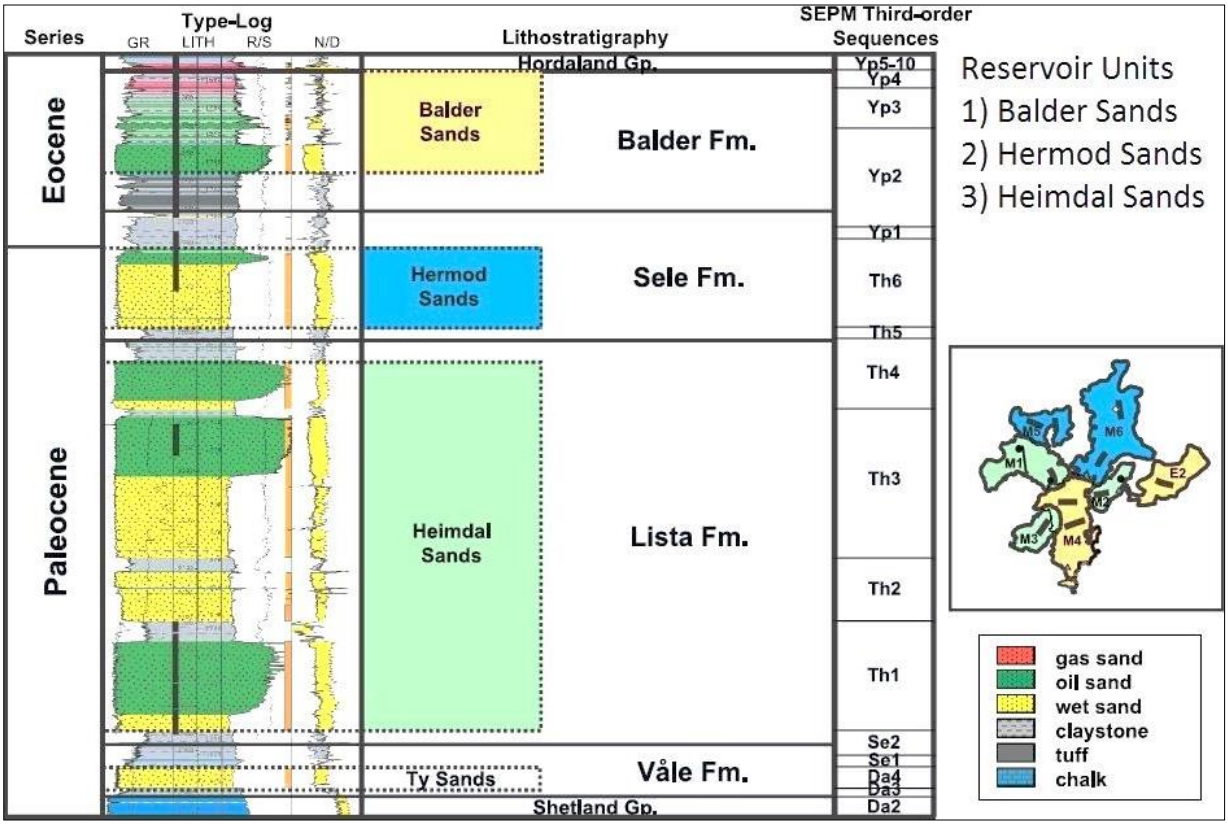

Figure 2.12 The Balder field's composite log and stratigraphic column (modified after: Briedis et al., 2007).

Jenssen et al., (1993) name these three sand units as IB, II, and III for Heimdal Sands, Hermod Sands, and Balder Sands respectively as shown in the Figure 2.12.

The Heimdal Formation of Paleocene age is main sandstone reservoir unit in the Balder field with thickness up to 125 m encounter in few wells, which is interbedded with shale of the Lista Formation. With the help of gamma ray log and density-neutron log cross over, Zone IB could be marked as the Heimdal Formation (Fig. 2.13) (Jenssen et al., 1993).

The Hermod Formation is another Paleocene sandstone reservoir unit in the Balder field with thickness up to 50 m in few wells, which interbedded with shale of Sele Formation. With help of gamma ray log and density-neutron log cross over, Zone II mark as the Hermod Formation (Fig. 2.13) (Jenssen et al., 1993).

The Balder Formation of lower Eocene is another sandstone reservoir interval in the Balder field with thickness ranges from 40-100 m in most of wells. The sandstone is interbedded with tuffaceous siltstones and shales. With the help of gamma ray and density-neutron log cross over, Zone III can be easily distinguished as the Balder sand body (Fig. 2.13) (Jenssen et al., 1993; Sarg and Skjold, 1982).

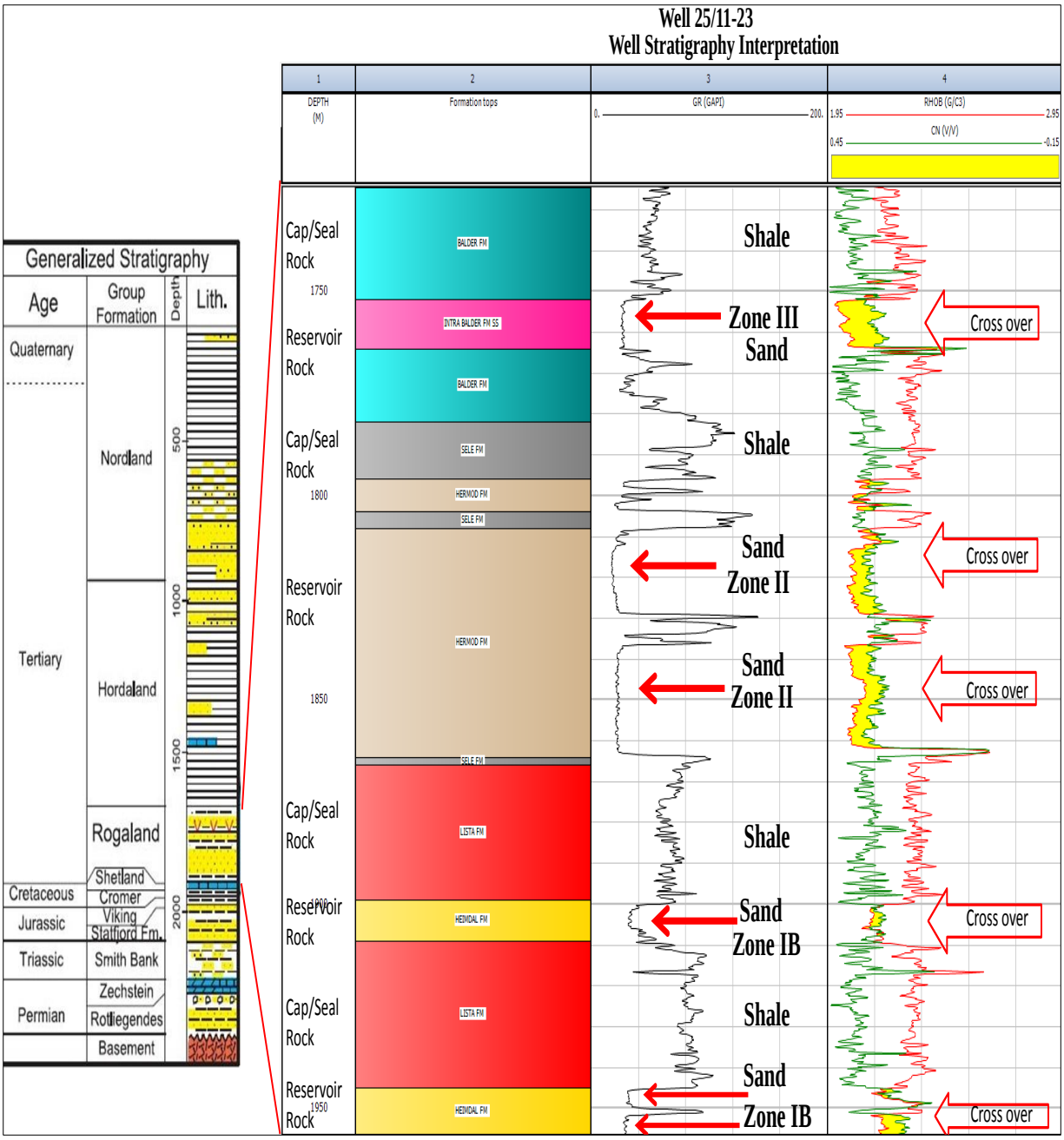

Figure 2.13 Well stratigraphic columns with interpretation of different zones (modified after: Bergslien, 2002)

The Heimdal Formation (Zone IB) and the Hermod Formation (Zone II) may contain oil (narrow cross over) (Fig. 2.13), while Balder Formation contains both oil and gas (wide cross over) (Fig. 2.13) (Bergslien, 2002). The average porosity of the Balder field ranges from 31 to 36 %, while permeability ranges from 1-10 Darcy (Briedis et al., 2007).

In the Balder field, the sedimentary structures are consistent with high-density, deep-water gravity-flow deposition and fluid escape (Briedis et al., 2007). Figures 2.14 and 2.15 show photograph of cores recovered from the Balder field. The Figure 2.14 shows typical deep-water massive sands, with fluid escape structures “a” and “b”, trough cross-bedding and gravel lag “c”, trough cross-bedding with floating pebbles “d”, and parallel lamination “e” (Briedis et al., 2007). The deep-water hemipelagic shales and volcanic tuffs of the Balder

field is shown in the Figure 2.15, oxygenated shale of the Lista Formation “a”, the anoxic shale of the Sele Formation “b”, anoxic shale of the Balder Formation and interbedded volcanic tuffs “c” and oxygenated shale of the Hordaland group “d” (Briedis et al., 2007).

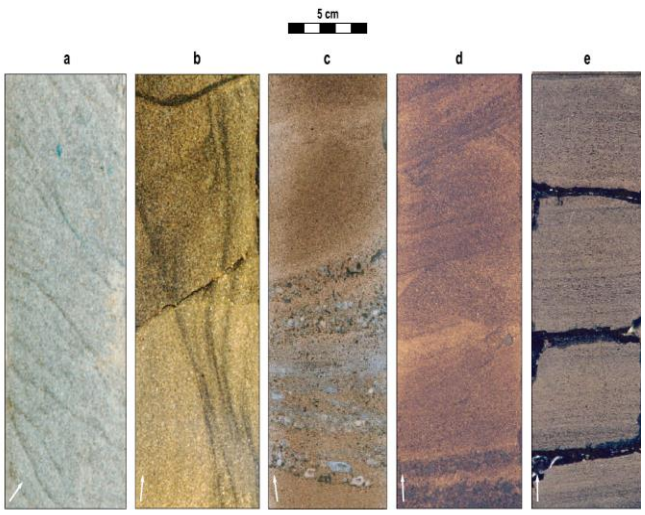

Figure 2.14 The Balder field’s deep-water gravity-flow deposited reservoirs. Some wells are deviated, arrows indicated stratigraphic up direction, scale 5cm (modified after: Briedis et al., 2007).

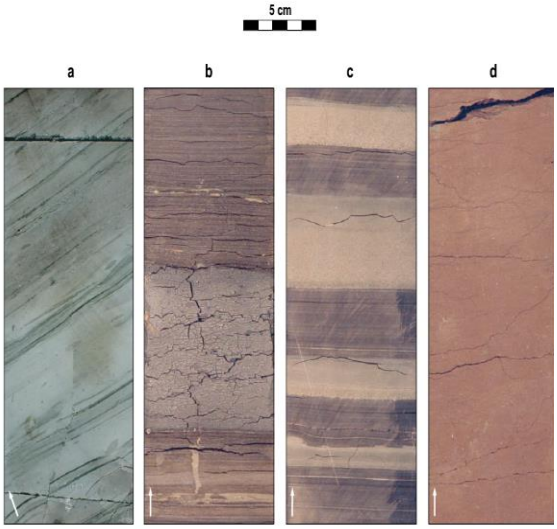

Figure 2.15 The Balder field’s deep-water hemipelagic shales and volcanic tuffs Some wells are deviated, arrows indicated stratigraphic up direction, scale 5cm (modified after: Briedis et al., 2007).

2.4.3 Reservoir geometry and stratigraphic correlation of different reservoir units

Several stratigraphic correlations and geological models have been presented by different authors Sarg and Skjold, 1982, proposed the erosional submarine fan produce the mounded topography, while Hanslien, 1987 proposed that mounds are deposited as it is and enhanced by the compaction (Jenssen et al., 1993).

Jenssen et al., (1993) proposed the geological model of the Balder field as shown in Figure 2.16 a. This geological model discussed further by many authors like (Bergslien, 2002 and Briedis et al., 2007). The Ty formation (Zone IA2) are the first sand deposits in the area (Bergslien, 2002), which are deposited by high-density turbidity currents onlapping the graben margin to the west of the Balder field (Fig. 2.16 a) (Jenssen et al., 1993; Sarg and Skjold, 1982). As shown in Figure 2.16 a, the Ty Formation (Zone-IA2) is absence from the central part of the basin, which can be interpreted as the turbidity currents follow the low elevation on the chalk surface. The sand present in the eastern part could have local transport direction from north (Jenssen et al., 1993).

The Heimdal Formation (Zone-IB) composed of sandstone and shale deposited in submarine-fan environment (Jenssen et al., 1993; Sarg and Skjold, 1982). It is recognized by the massive sandstones stacked pattern in the area (Fig. 2.16 b), which partly filled the lows on the chalk topography and produces the mounded sand deposits (Bergslien, 2002; Jenssen et al., 1993; Wild and Briedis, 2010). The Heimdal Formation (Zone-IB) down-laps the Ty Formation (Zone-IA2) at the margin of basin and it on laps the Ty Formation (Zone-IA2) and chalk at center (Jenssen et al., 1993; Sarg and Skjold; 1982).

The Hermod Formation (Zone-II) deposition generally control by the previously deposited Heimdal Formation (Zone-IB) (Jenssen et al., 1993). The Hermod Formation (Zone-II) down-laps against the Heimdal Formation (Zone-IB) and is characterized by sand-prone submarine fan complex (Sarg and Skjold, 1982). The Hermod Formation (Zone-II) depositional time marked as less sand input from source as accommodation space increases on the Shetland Platform (Jenssen et al., 1993). Due to this reason, most of the sand deposits are 20-40 m thick in northern and eastern part of the basin as shown in the Figure 2.16 b (Jenssen et al., 1993).

The Balder Formation (Zone-III) is youngest sequence of Eocene, covers the Hermod Formation (Zone-II) and Heimdal Formation (Zone-IB) (2.16 c). It consists of inter-bedded sandstone and tuffaceous silt deposits (Sarg and Skjold, 1982). In Early Eocene period due to reactivation of faults, the subsidence occurs along the Viking Graben (Figs. 2.16 c and 2.17), causes westward tilting in the Balder field (Bergslien, 2002; Jenssen et al., 1993). Due to this sliding, slumping and sand remobilization enhances the topography of the Paleocene mounds (Figs. 2.16 c and 2.17) (Bergslien, 2002; Jenssen et al., 1993). These Paleocene mounds provided the low relief area, where the Balder Formation (Zone-III) irregularly deposits in these lows area as shown in the Figure 2.17 (Bergslien, 2002; Jenssen et al., 1993; Wild and Briedis, 2010).

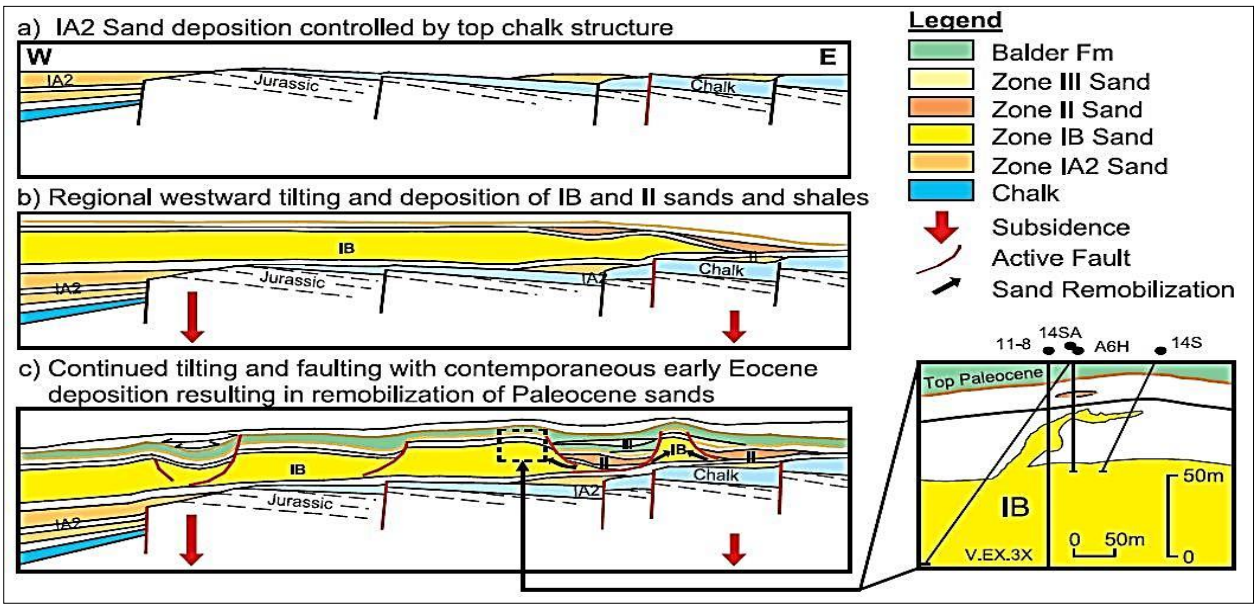

Figure 2.16 Geological model of the Balder field (Source: Bergslien, 2002)

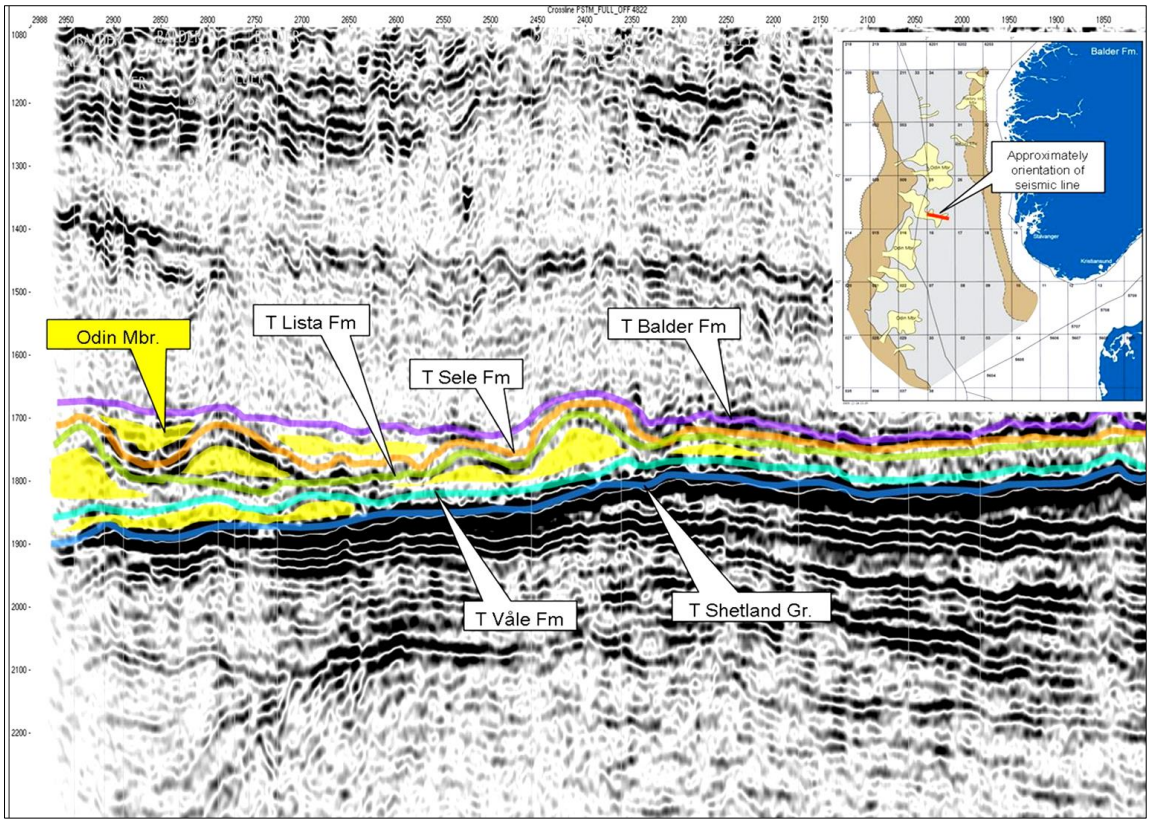

Figure 2.17 West-East seismic cross-section, through the study area between the northern Balder and Grane discoveries. Blocks 25/10 and 25/11 (Source: Norlex, 2013).

Mounds shown in the Figure 2.17 are most likely formed by the slump, slides, sand remobilization and sand evacuation (Bergslien, 2002; Jenssen et al., 1993). These mounds are penetrated by the wells 25/11-5, 25/11-8 and 25/11-16 in the study area shown in the Figure 2.18. The low relief area between these mounds are site for deposition of the Balder Formation (Wild and Briedis, 2010). These low relief area are penetrated by the wells 25/11-23 and 25/11-9 (Fig. 2.18). The reservoir units from Heimdal, Hermod and Balder formations are start pinching out in the south eastern wells (Figs. 2.17 and 2.18). The further analysis of reservoir correlation is included in the chapter 4.

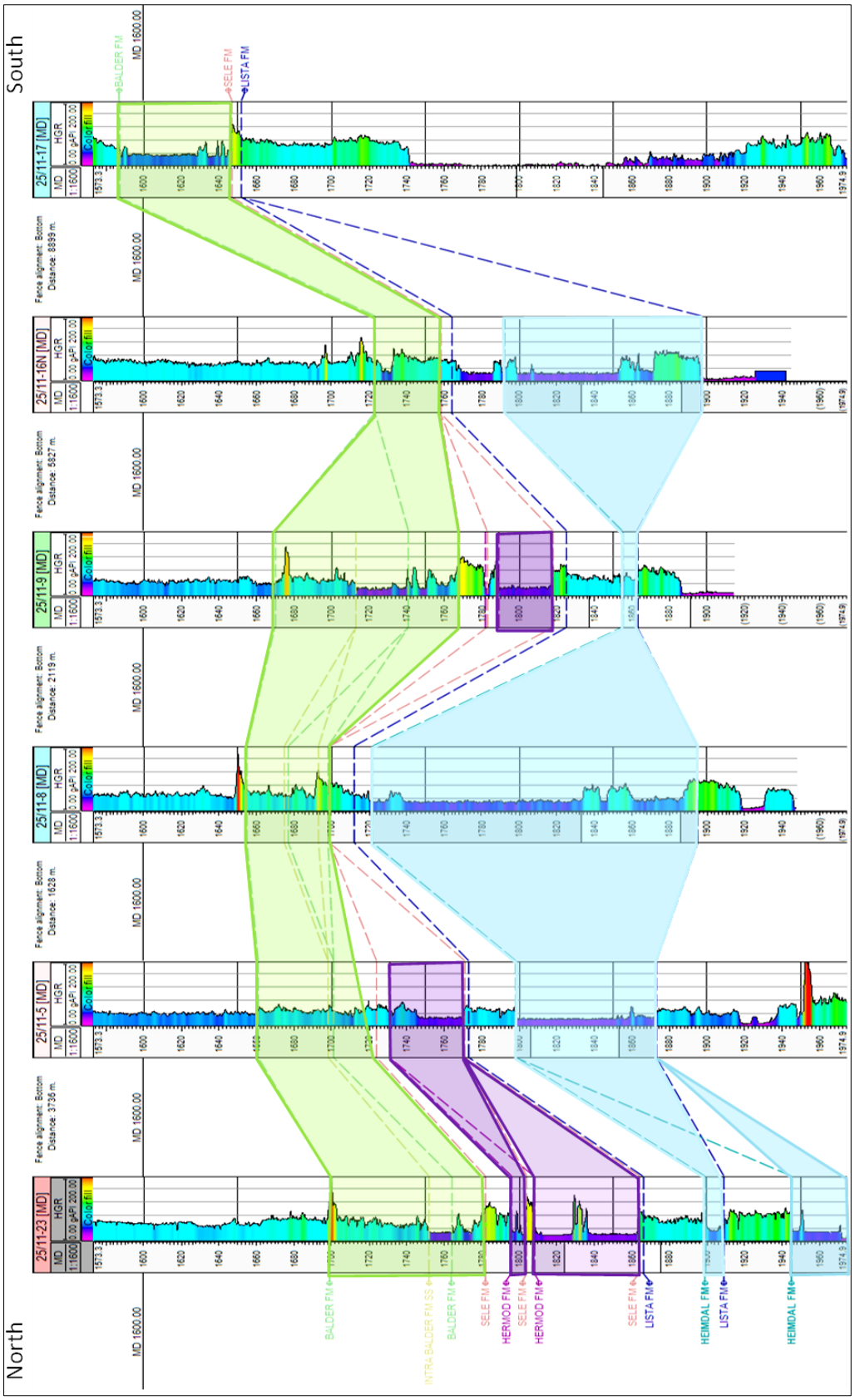

Figure 2.18 Stratigraphic cross-sectional view across the Balder field for reservoir formations. The light green, purple and light blue polygon presents the thickness variation of the Balder, Hermod and Heimdal formations respectively.

2.4.4 Traps and Migration

The Balder field traps categorized as structural-stratigraphic traps. It has independent structural closure from 1660-1720 m subsea (Sarg and Skjold, 1982). The Balder field is a highly quartzose sand-prone suprafan complex belonging to the age of Middle to Late Paleocene, which have prograded and channelized suprafan lobes (Sarg and Skjold, 1982; Jenssen et al., 1993). A mounded upper surface on the reservoir sequence was caused by the depositional topography and submarine erosion (Sarg and Skjold, 1982). The shale occur as hemipelagic drape over the entire suprafan complex which also serves as the seal (Briedis et al., 2007; Sarg and Skjold, 1982). Sand injections and faults geometry plays important role to control oil-water contact and common pressure system across the Balder field (Jenssen et al., 1993).

The field comprises of seven structurally and stratigraphically trapped oil accumulations in three separate stratigraphic intervals (Fig. 2.19) (Briedis et al., 2007). Heimdal sand intervals contain mounds 1, 2, and 3, Paleocene Hermod sand intervals contain mounds 5 and 6, whereas Eocene Balder sand intervals contain mound 4 and 2 (Fig. 2.19) (Briedis et al., 2007).

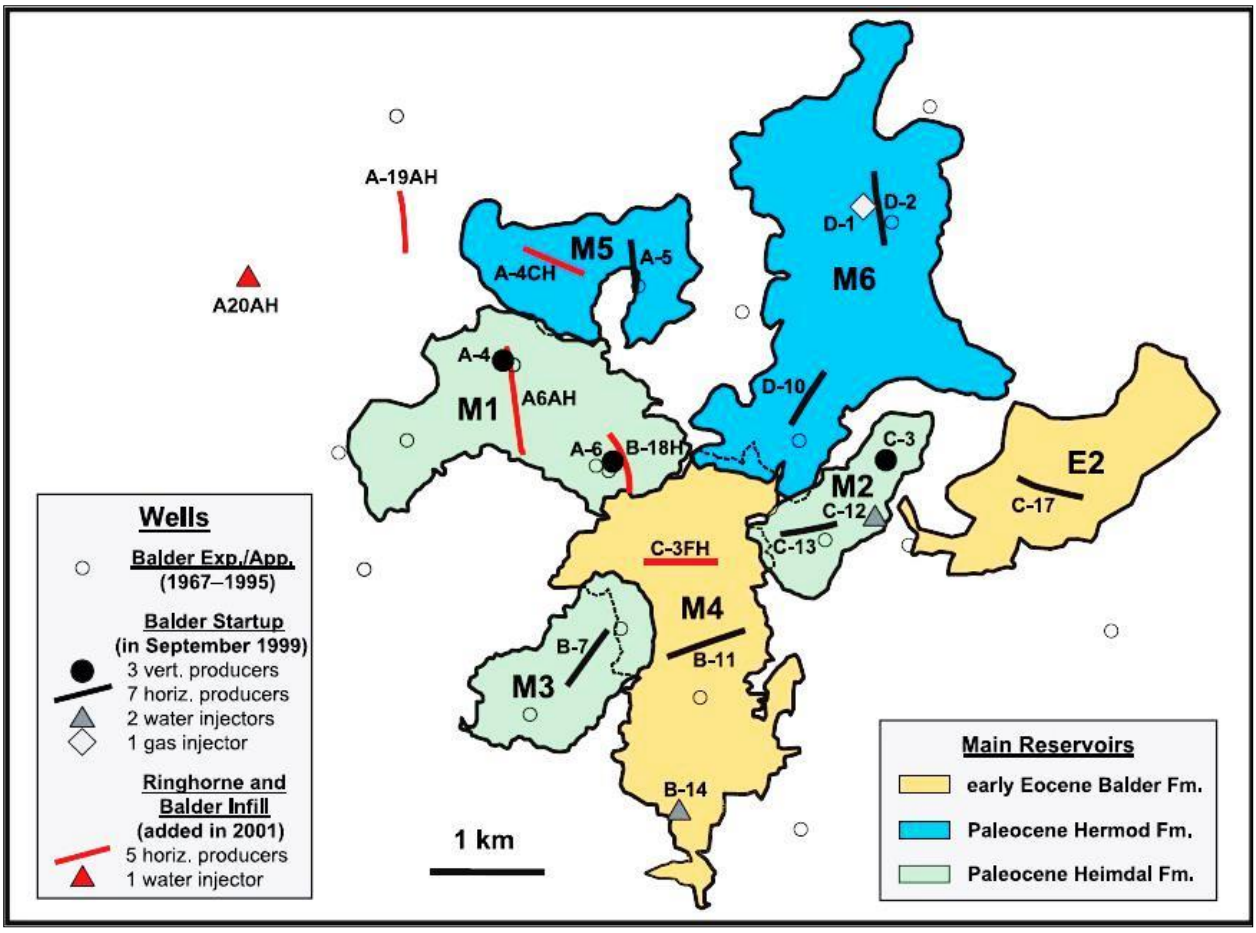

Figure 2.19 The Balder field production map, main structural-stratigraphic trapped accumulations and key wells (Source: Briedis et al., 2007).

The Draupne and Heather Formation are main source rock in the area, the hydrocarbon expulsion and migration started in Latest Cretaceous (Justwan and Dahl, 2005; Lonergan et al., 1998).

Many authors like Barnard and Cooper, (1981); Cornford, (1990) and Newman et al., (1993) has described and established the relationship in their study that Tertiary reservoir filled by the Kimmeridge Clay Formation equivalent (Lonergan et al., 1998). Newman et al., (1993) explained in their study that some reservoirs, which directly lie above the source rocks are filled by the vertical migration through the faults. The Tertiary reservoirs filled by the fracture system that extended in both vertically and horizontally (Fig. 2.20) (Lonergan et al., 1998).

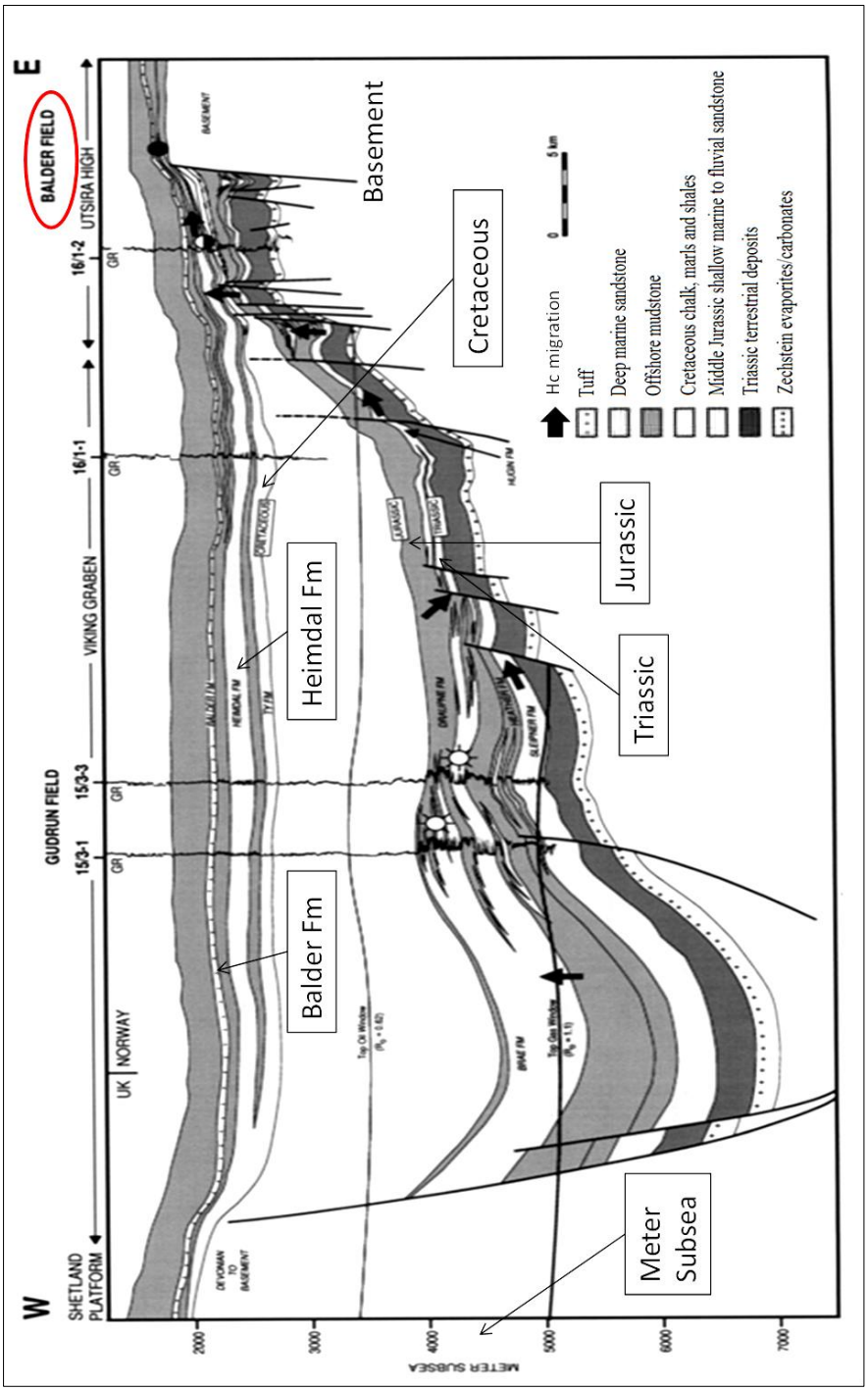

Figure 2.20 Migration of hydrocarbons from the source to reservoir rocks, the Balder field area highlighted by the red circle (modified from Isaksen and Ledje, 2001).

Chapter 3: Methodology and theoretical background

This chapter focuses on the methods and theoretical background, which are utilized to conduct this study. It has divided into four parts under the headings: Data handling, petrophysical analysis, compaction analysis and rock physics diagnostics. This chapter also illustrates common uncertainties of the well log measurements and estimation of rock properties form the well log data.

3.1 Data handling

This study utilizes a suite of twenty five well log data of the Balder field, Norwegian North Sea. One of the early challenge is to get familiar with the well log data sets, their limitations and uncertainties related to extraction of rock properties that not measured directly. Other than that, learning the different geological and geophysical softwares (eg. Interactive Petrophysics, Petrel) used in this study to handle different data formats are also challenging. It is very important to know what exactly the softwares are calculating/estimating behind the scene.

3.1.1 Softwares

This study utilizes different software packages, the license provided by the respective companies to the Department of Geosciences, University of Oslo.

Microsoft Office 2007 (Excel, Word and PowerPoint) is used to handle the data, writing thesis and making presentations for the group discussion and the final thesis defense. Interactive Petrophysics software provided by Senergy is used for most of the petrophysical analysis. The software is also used to generate the crossplots to interpret the data for compaction study and rock physics diagnostics of reservoir rocks of the Balder field. Petrel provided by Schlumberger is used for the correlation study of the source, reservoir and cap rocks units. It is also used to generate the contours maps to understand geothermal gradient and subsurface temperature distribution within the Balder field..

3.1.2 Log editing and quality check

The well log data (composite logs) provided by the NPD (Norwegian Petroleum Directorate) are LAS and ASCII formats. Before analyses, the data quality check is performed on each set of well log. In few wells, the neutron log and in most wells, the shear sonic are missing (Table 3.1). In some wells, the density log is incomplete and similarly in few wells, sonic and deep resistivity logs are not recorded either through stratigraphic intervals penetrated by the wells (Table 3.1).

No major well log editing is required, as all the well logs are up to the standard to conduct the research. For compaction study and rock physics analyses, the caliper log is also utilized to observe the bad borehole conditions. Where caliper log shows disturbed readings and density correction more than 0.5 g/cc that data points are excluded from the analyses. Other than that analysis of carbonates is not included either in this study and so excluded from the data during editing phase.

Table 3.1 The data check availability and quality of 25 studied wells (Source: NPD 2013).

Well No.	Depth (m) RKB	BHT ^{O}C	DT	DTS	Density	NPHI	R_D	Gr
25/10-1	2092	76	✓	x	❖	x	✓	✓
25/10-2	3181	82	✓	x	❖	x	✓	✓
25/10-3	1921	63	❖	x	❖	x	❖	✓
25/10-4	2550	75	✓	x	❖	❖	✓	✓
25/10-5	2011	55	✓	x	❖	x	✓	✓
25/10-8	2653	x	x	x	❖	❖	❖	✓
25/11-1	2459	71	✓	x	❖	x	✓	✓
25/11-2	1824	61	❖	x	❖	x	❖	✓
25/11-3	1858	63	❖	x	x	x	❖	✓
25/11-4	1896	71	❖	x	❖	x	❖	✓
25/11-5	2164	60	✓	x	❖	❖	✓	✓
25/11-6	1948	65	✓	x	❖	❖	✓	✓
25/11-7	1944	x	✓	x	❖	❖	✓	✓
25/11-8	1950	77	✓	x	❖	❖	✓	✓
25/11-9	1910	57	✓	x	❖	❖	✓	✓
25/11-10	1988	55	✓	x	❖	❖	✓	✓
25/11-11	1960	55	✓	x	❖	❖	✓	✓
25/11-12	1918	60	✓	x	❖	❖	✓	✓
25/11-13	1932	55	✓	x	❖	❖	✓	✓
25/11-15	2035	85	✓	x	❖	❖	✓	✓
25/11-16	1945	71	❖	❖	❖	❖	✓	✓
25/11-17	2255	105	❖	x	❖	❖	❖	✓
25/11-18	1875	83	x	x	❖	❖	✓	✓
25/11-20	1828	76	❖	x	❖	❖	✓	✓
25/11-23	2014	x	❖	x	❖	❖	✓	✓

Legend
✓ Available
❖ Partially available
X Not available

3.1.3 Work flow

This study follows the following work flow to characterize the reservoir horizons of Balder field. Using only the well log data to perform reservoir characterization is obviously a big

challenge where several uncertanities may mislead the interpretation of data. To achieve better understanding the reservoir rocks using the well log data the following work flow is adopted (Fig. 3.1).

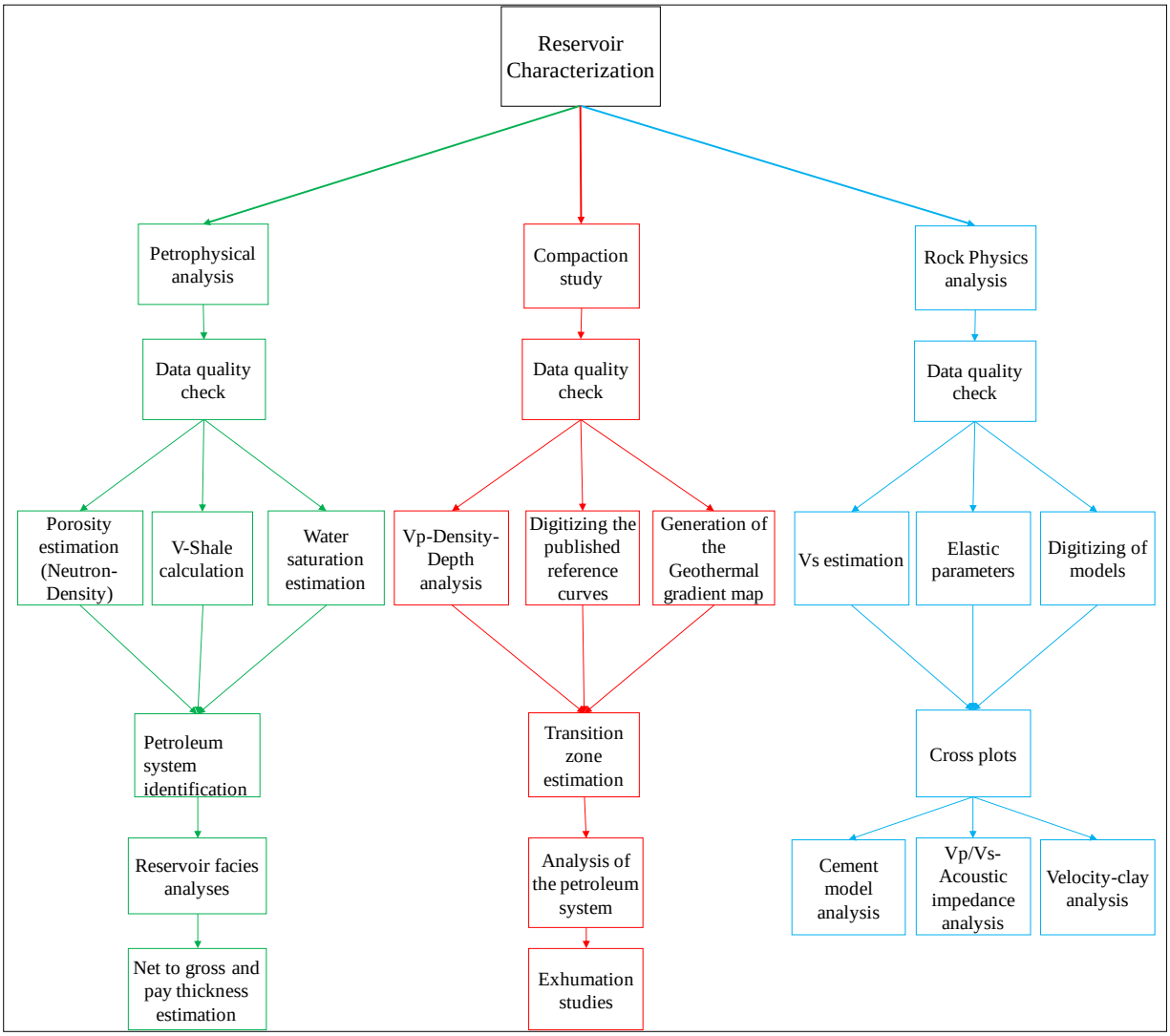

Figure 3.1 A detail work flow used in this study.

3.2 Petrophysical Analysis

In petrophysical analysis reservoir parameters like porosity (φ), shale volume (Vsh) and water saturation (Sw) are calculated. Petrophysical analysis also focuses on defining the net pay and reservoir intervals from the gross formation thickness. This part of the study not only gives the basic platform to conduct the compaction and rock physics analyses but also gives the idea about the sensitivity of different parameters utilize in calculations. Moreover, an effort is made to investigate and to understand the lateral variations and vertical thickness of different reservoir units. For this purpose, the correlation of formation tops, lithology units, and reservoir contour maps are created and presented in the chapter 4 using the well log data.

3.2.1 Uncertainty to estimate in porosity, shale volume and water saturation

Petrophysical analysis includes many parameters, which can be directly or indirectly disturbed by the background noises. Porosity values calculation from well log are uncertain to some extent because borehole readings can be influenced by the drilling mud salinity and mud invasion. Specifically, porosity values calculated from density logs are uncertain for any bad borehole condition, formation gases and barite in drilling mud give the false readings, where density correction are more than 0.5 g/cc (Rider and Kennedy, 2011). The caliper log should be kept along with density log during the evaluation. These kinds of condition somehow affect the actual logging readings. The other uncertainty in density porosity calculation is using the matrix density values. In nature, sedimentary rocks constitute different minerals and variations of their size, shape and sorting. Like this study area, the reservoir rocks are composed by sandstones that interbedded with siltstones, mudstones and shales. To calculate more accurate porosity these units must be separated on the basis of shale volume, as the matrix density of these sands and clays varies significantly. Similarly, the neutron log values are uncertain when it is measured in the shale or a zone saturated with hydrocarbon. In most cases, neutron log over esitmate the porosity in shales, as neutron tool is more sensitive to the hydrogen index associated with clay bound water, while density log underestimates the porosity. To avoid these uncertanities the average porossity can be better instead of porosity from a single log measurement (Fig. 3.2) (Cluff and Cluff, 2004; Rider and Kennedy, 2011; Soubotcheva and Stewart, 2004).

Calculating the shale volume is one of the basic yet another controversial parameter in the petrophysical analysis. The Vsh estimation not only helps to differentiate the reservoir intervals from the gross formation but also helps to calculate more accurate porosity to some extent (Hamada, 1996). The formation clay content can be indicated by the several logs like gamma ray, spontaneous potential, caliper or neutron-density log but results are unreliable to some extent (Poupon et al., 1970; Soto et al., 2010). In most cases gamma ray and self-potential (SP) log are used. On land, the Vsh calculation can be done more accurately using the SP log but on off-shore rigs like the Balder field, this cannot be done with 100% accuracy, as there is no land available to measure the potential difference between two layers (Rider and Kennedy, 2011). In most cases off-shore floating rigs, a riser is used, but readings can be disturbed by the different rig's electrical noises (Rider and Kennedy, 2011).

The gamma ray log records the formation radioactivity. The measurements can be influenced by the logging speed, if logging speed is too high or slow it will mix the bed boundaries. The other main influence on gamma ray log is increase of drilling mud between the measuring tool and the actual formation due to the caving. This effect will show lower gamma ray values. The gamma ray log also gives lower values in bad borehole conditions (Rider and Kennedy, 2011). All these factors should be considered while analyzing the gamma ray log. Other than that, the two main parameters used in volume of shale calculation are GR_{Max} and GR_{Min}, choosing the values of these two parameters will surely give uncertainty in results itself.

Water saturation calculation from well logs is also uncertain to some extent. As the methods/equations which are used to calculate the water saturation can not account all the factors accurately. This will influence the relationship between the formation resistivity and water saturation. For this study Archie equation (1942) is used. This equation has six different parameters [saturation exponent (n), tortuosity constant (a), formation water resistivity (R_w), porosity (φ), cementation exponent (m) and true resistivity (R_t)] which itself create the uncertainty in the results (Crowell et al., 1995; Rider and Kennedy, 2011; McCoy

and Grieves, 1997). Without petrographic study of the cores, it is not possible to calculate those parameters used in calculation of water saturation accurately.

3.2.2 Porosity estimation

Porosity is the pore volume of the rock. It can be filled with hydrocarbons, moveable water, capillary water or clay bound water (Cluff and Cluff, 2004; Hook, 2003; Rider and Kennedy, 2011; Shepherd, 2009). Its unit can be fraction or percentage. Porosity is one of the main parameter to estimate compaction trends (Dvorkin and Nur, 2000), cementation prediction or differenciating the hydrocarbon zones (Dvorkin et al., 2002). In this study, the porosity estimation is based on two well logs (Neutron, and Density log).

Neutron porosity

Neutron log is used to measure the porosity in the formation. In most cases like in limestone lithology, it can be read directly from the neutron log. For the other lithology, it should be used by taking the average of porosity calculates from density and neutron logs to get rid of the lithologic effects (Glover, 2005; Rider and Kennedy, 2011). Neutron tool give same values for water and oil saturated formation, as the hydrogen index for both fluid is almost same (Glover, 2005). Glover, (2005) explain further that in gas saturation lithology neutron log gives lower values for porosity, which can be corrected by using the following equation (3.1).

$$\Phi_{N} = \Phi\ [1 \text{ x } S_{xo} + HI_{Gas} \text{ x } (1 - S_{xo})] \quad \ldots\ldots (3.1)$$

$\Phi_{N \text{ is the}}$ Neutron porosity, Φ is apparent values from the neutron log, HI is the gas index (Hydrogen index) and S_{xo} is the saturation of mud filtrate (Glover, 2005). Further, the Figure 3.2 illustrates that the porosity from the neutron log overestimate the values compared to the average porosity in shales, while in sandstones, it almost gives the same values.

Density Porosity

Density log is useful to discriminate lithology as well as to calculate the porosity and hydrocarbon density. The general scale of measurement is from 1.95 to 2.95, with units of g/cm^3 (Rider and Kennedy, 2011). The general equation (3.2) to measure the porosity expresed by (Rider and Kennedy, 2011)

$$\Phi = (\rho_{ma} - \rho_{b}) / (\rho_{ma} - \rho_{f}) \quad \ldots\ldots (3.2)$$

ρ_{ma} = Density of the matrix material

ρ_{f} = Pore fluid density

ρ_{b} = General density log reading

Densities of common lithologies are shown in the Table 3.2 (Modified from Rider and Kennedy, 2011).

Table 3.2 Matrix density parameters

Lithology	Range (g/cm^3)
Clays – Shales	1.85 – 2.75
Sandstones	1.9 – 2.65
Limestones	2.2 – 2.71
Dolomites	2.3 – 2.87

Further the Figure 3.2 illustrates the density porosity underestimate the value of porosity as compare to the average porosity in shales while in sandstones it gives almost the accurate porosity values. The value of matrix density, which are used during porosity calculation varied with respect to the volumetric percentage of shales presence in the formation.

Average porosity from Neutron and Density logs

Further the Figure 3.2 illustrates the density porosity underestimate the value of porosity as compare to the average porosity in shales while in sandstones it gives almost the accurate porosity values. The value of matrix density, which are used during porosity calculation varied with respect to the volumetric percentage of shales presence in the formation.

$$\emptyset_{Avg} = \sqrt{\frac{\emptyset_{density}^2 + \emptyset_{neutron}^2}{2}} \ldots \ldots \ldots \ldots (3.3)$$

The porosity estimated from the equation is used in this study to avoid uncertanities to interpret the data (Rider and Kennedy, 2011). Furthermore the Figure 3.2 illustrates the average porosity calculated in different lithologies.

Effective porosity

For better understanding of the reservoir permeability without core data, it is better to estimate the effective porosity (Eq. 3.4). It also considered that the effective porosity show, how well connected the pores are and by which fluid can easily move. The shaly sandstone is not that much productive compared to the clean sandstone intervals (Rider and Kennedy, 2011). The effective porosity will not only help to calculate the water saturation with less uncertainity but it also helps to mark the reservoir interval from the main formation. The reservoir interval may also mark more precisely to separate effective pay zones. Effective porosity mostly used in marking the reservoir intervals from the gross interval. It is considered that this type of porosity available to produce the hydrocarbons (Cluff and Cluff, 2004). In shale dominated sandstone most of the porosity is occupied by the clay bound water or small clay particles, which may not producible and have no economic interim of the petroleum industry. To avoid these kind of uncertainties, effective porosity is used instead of total porosity, while calculating and marking the pay zones intervals from reservoir intervals (Cluff and Cluff, 2004; Rider and Kennedy, 2011). To calculate the effective porosity the following Eq. 3.4 is used as defined by Cluff and Cluff, 2004. Furthermore, the Figure 3.2 illustrates that the effective porosity underestimate the value of porosity in shale zone, while in sandstone, it gives same values compared to the average porosity.

Effective porosity = Porosity x (1-Vsh) . . . . (3.4)

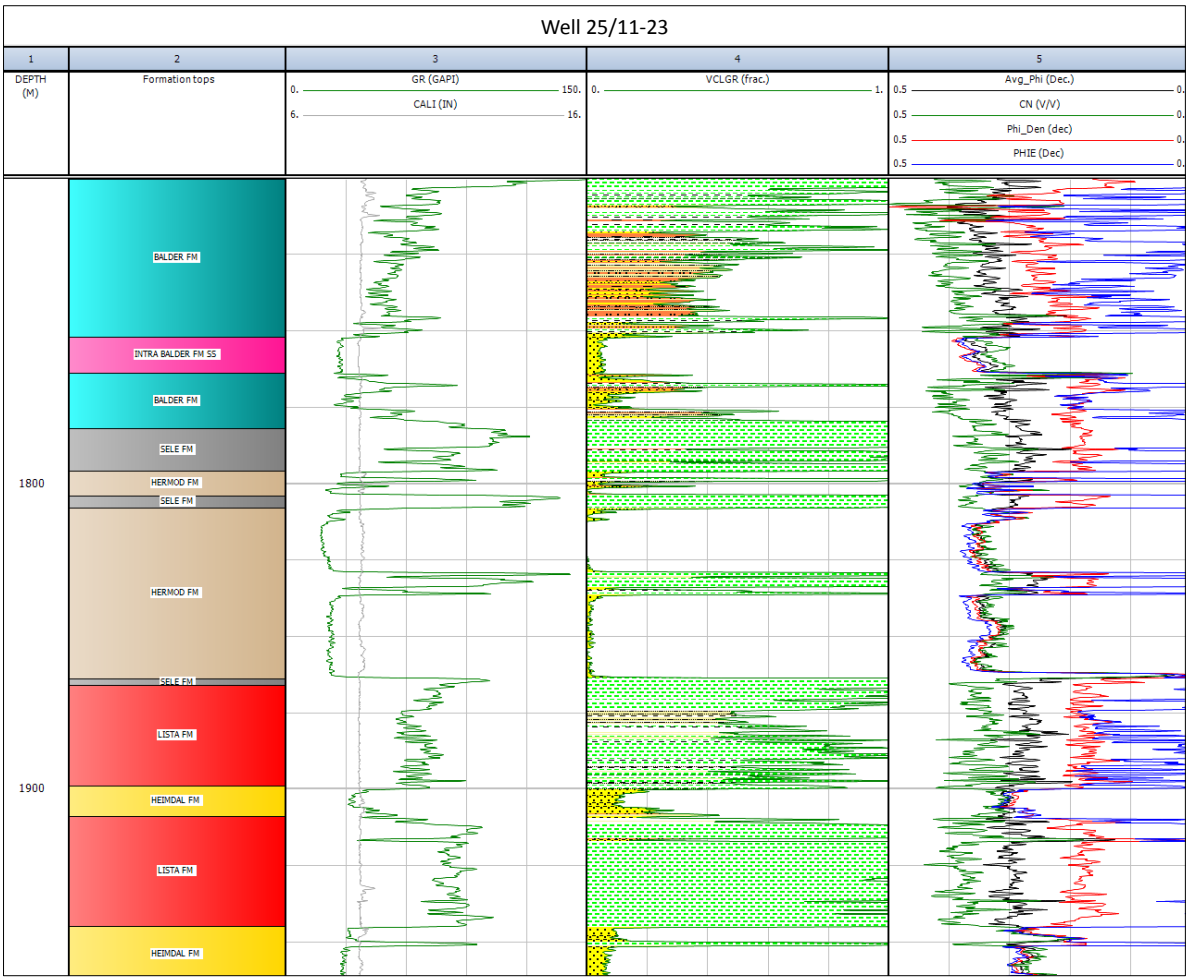

Figure 3.2 Comparison of estimated porosity for different lithologies from the well 25/11-23.

In the Figure 3.2 Average porosity (Avg_Phi) showed by the black line, neutron porosity (CN) showed by the green line, density porosity (Phi_Den) showed by the red line, and effective porosity (PHIE) showed by the blue line.

3.2.3 Lithology discrimination

The gamma ray and density logs are very useful to descriminate lithology. On the basis of gamma ray log sandstones, shales and carbonates sequences can be marked (Soto et al., 2010). For this study gamma ray readings are used to define different lithologies as shown in the Table 3.3. Furthermore, to distinguish sandstone and carbonate the density log is used parallely with the gamma ray log.

Table 3.3 Gamma ray reading for the different lithologies which are used in this study.

Lithology	**Range (API)**
Carbonates	<15
Sandstones	>15 and <40
Shaly Sandstones	>40 and <65
Sandy Shale	>65 and <80
Shale	>80

3.2.4 Shale volume calculation

The main step before calculating the shale volume is to calculate the gamma ray index, which can be calculated by the following Eq.3.5 (Cluff and Cluff, 2004; Rider and Kennedy, 2011).

$I_{gr} = (GR_{log} - GR_{Min}) / (GR_{Max} - GR_{Min})$ . . . . . .(3.5)

Where

I_{gr} = Index of Gamma ray (Fraction)

GR_{log} = Gamma Ray Log in the zone of interest (API Unit)

GR_{max} = Gamma Ray Maximum (API Unit)

GR_{min} = Gamma Ray Minimum (API Unit)

For taking the GR_{max} and GR_{min} values, a histogram is run on the well data in order to mark the maximum average and minimum average values (Fig. 3.3).

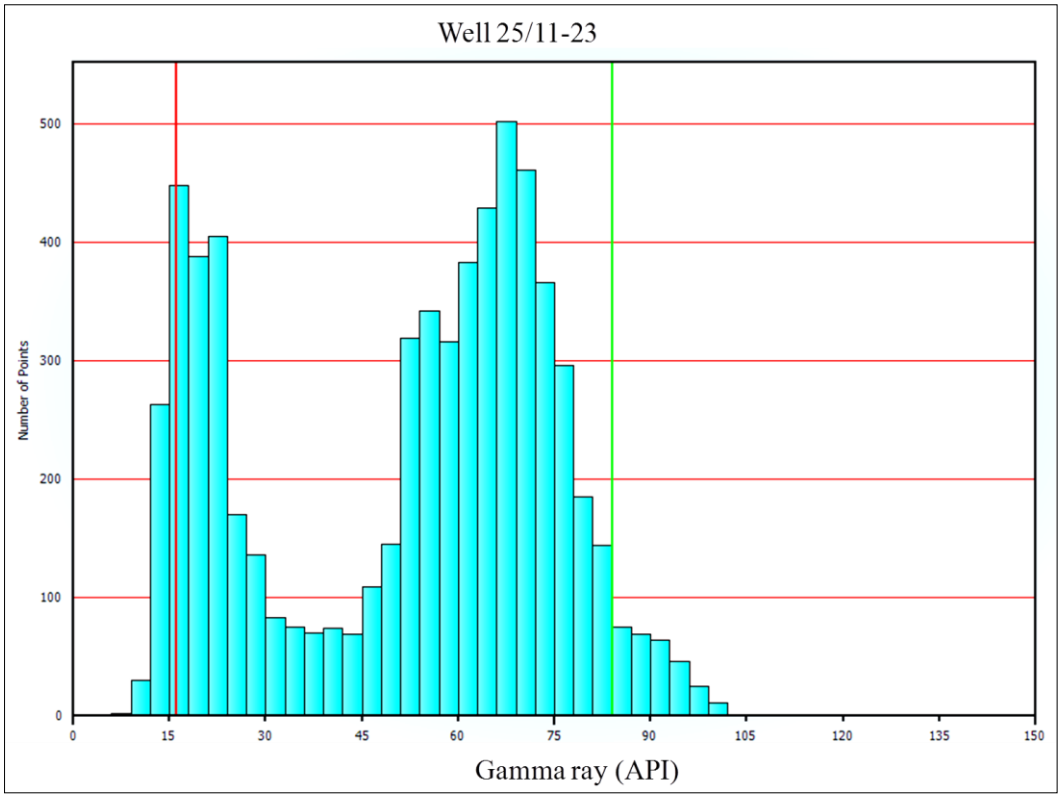

Figure 3.3 Gamma ray histogram from the well 25/11-23

In the Figure 3.3, the red line is for the gamma ray minimum (16 API) and the green line is for the gamma ray maximum (84 API).

After calculating Gamma ray index, volume of shale is calculated. In this study Larionov (1969) equations are used for shale volume calculation (Rider and Kennedy, 2011).

Larionov (1969) gives following equations for different rocks on the basis of their age.

Older Rocks $V_{sh} = 0.33\ (2^{2xIRA} - 1.0)$ . . . .(3.6)

Tertiary Rocks $V_{sh} = 0.083\ (2^{2.37x\ IRA} - 1.0)$ . . . . . .(3.7)

In this study following Vsh values are used to differentiate different lithologies as shown in the Table 3.4.

Table 3. 4 Vsh ranges for different lithologies, used in this study.

Lithology	**Range (Frac.)**
Sandstones	< 0.25
Shaly Sandstones	>0.25 and <0.5
Sandy Shale	>0.5 and 0.75
Shale	>0.75

3.2.5 Water Saturation

Water saturation is calculated by using the Archie (1942) equation in Interactive Petrophysic software. Porosity is used from the Eq. 3.3, which calculate average porosity. Cement value (m) is taken as 1.5; tortuosity factor (n) is taken as 2. Deep resistivity values are used from R_D. On the basis of water saturation, pay zone is separated from reservoir intervals. The R_w values are estimated by using the histogram. Following, Archie, (1942) equation is used, as define in Worthington et al., (2011).

$S_w = [a/ \Phi_m * R_w/R_t]$ . . . . . (3.8)

There is large uncertainty associated with water saturation calculation as no petrographic or core data analyses are available to get better more reliable values of porosity, cementation exponent or water saturation factors. But still results are good enough to do the analyses and further interpretation and discussion of outcomes. These results are quite comparable to the data published like Bergslien, 2002; Briedis et al., 2007; Jenssen et al., 1993; NPD, 2013.

Hydrocarbon saturation

For hydrocarbon saturation (S_{hc}) calculation, the following equation is used as define by Shepherd, (2009).

$S_{HC} = (1- S_w)$ . . . . . (3.9)

*S_w in fraction.

3.2.6 Net-to-Gross and pay zone

Gross interval is a total thickness of the reservoir formation. It includes all zones (productive zone, non-productive zone, tight zone, shaly or silty zone), no cutoff has applied. Net reservoir interval contains the rock of good reservoir quality sorted by V_{sh} and porosity cutoff. Net reservoir interval also contained the fully water saturated and hydrocarbon saturated zones. Pay zone interval contained the commercially producible hydrocarbon. Pay zone interval obtained by putting the cut off values of water saturation as well. Pay zone also

eliminate depth below the Oil-Water-Contact (OWC), which is fully water saturated (Cluff and Cluff, 2004; Dean, 2007; Egbele et al., 2005; Gaffney, 2010; Li et al., 1997; Shepherd, 2009).

On the basis of the effective porosity, Vsh and water saturation, reservoir intervals and net pay zones are marked from the gross formation intervals. In this study for defining the reservoir interval, the effective porosity is greater than 20% and volume of shale less than 30% are used. For net pay or producible zones marking, water saturation less than 30% are taken along with the other parameters deifined early.

3.3 Compaction analysis

Compaction depends upon the mineral composition, grain size, shape, sorting and packing of the grains (Bjørlykke et al., 2009; Bjørlykke and Jahren, 2010; Storvoll et al., 2005; Marcussen et al. 2009; Weaver, 1959). The sediments drive to lower porosity and higher density as over burden increases with respect to depth (Bjørlykke and Jahren, 2010; Sheldon et al., 2003; Storvoll et al., 2005). Two main processes which are active during the compaction of sediments as define by Bjørlykke and Jahren, (2010) are

- Mechanical Compaction
- Chemical Compaction

Mechanical compaction

The mechanical compaction starts as soon as sediments deposit (Storvoll et al., 2005). The mechanical compaction causes the packing and crushing of grains, hence reduces the porosity without changing any chemical properties of the sediments (Bjørlykke, 2010). In sedimentary basin mechanical compaction caused by the vertical effective stress, which is difference between total stress and pore pressure (Bjørlykke et al., 2010; Mondol et al., 2008). Bjørlykke et al., 2010 define the following equation for effective stress estimation.

$$\sigma'_v = \sigma_v - u \qquad (3.10)$$

σ'_v = Vertical stress

σ_v = Total stress

u = Pore-pressure

From the Eq. 3.10, it can be observed that more the pore pressure, lesser will be the magnitude of the vertical stress, hence it can be interpreted that in high pore pressure regime the porosity will be preserved (Bjørlykke et al., 2010). Further, the effective stress is carried through mineral grain framework (Fig. 3.4) (Bjørlykke et al., 2010; Storvoll et al., 2005).

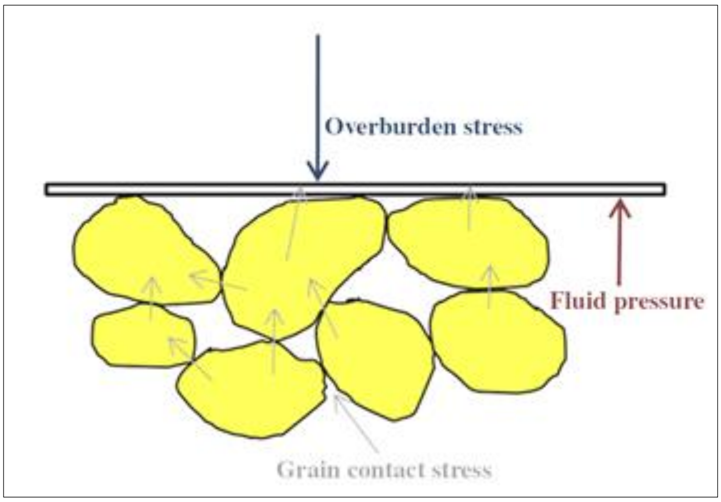

Figure 3.4 Mechanical compaction, effective stress from overburden carried by the mineral grain framework (Source: Bjørlykke et al., 2010).

Chemical compaction

The chemical compaction is controlled by the temperature (Dræge, 2011). It can alters the properties of the sediments chemically and transforms them to more thermodynamically stable form (Bjørlykke, 2010; Dræge et al., 2004). The chemical compaction drives the sediments to much lower porosity by dissolution of minerals and precipitating the mineral cements (Bjørlykke, 2010; Storvoll et al., 2005). Mineral types, pore fluid compositions and time-temperature are the main controlling factors for the chemical compaction process (Bjørlykke, 1998; Marcussen et al., 2010; Peltonen et al., 2008). Mineral cement like quartz precipitates, when temperature exceeds 60-80 ^{o}C (Bjørlykke and Aagaard, 1992). The sonic velocity sharply increase even with the small amount of cement precipitated on grains contact (Avseth et al., 2005; Dvorkin and Nur, 1996; Storvoll et al., 2005). There are number of sources for quartz cementation in sedimentary rocks like stylolites or transformation of less stable clays to more thermodynamic stable form (Bjørlykke and Jahren, 2010). In the Balder Formation, the main source of cementation is from alternation of volcanic clast (amorphous-silica) and smectite to illite transformation (equation 3.11), where temperature is exceeding 60 ^{o}C (Bjørlykke and Aagaard, 1992). Further, Bjørlykke and Aagaard, 1992; Bjørlykke, 2010 defined the following reaction (Eq. 3.11) for transforming of smectite from one form to another.

Smectite + K^+ = illite + quartz + H_2O. . . . .(3.11)

3.3.1 Uncertainty in estimation of geothermal gradient, interpretations of cross-plots and exhumation study

This study only relies on the well log data, so accurate estimation of the paleo-geothermal gradient are nearly impossible. The present day geothermal gradient map is generated using the bottom hole temperature (BHT) data available at the NPD website. These data are somehow uncertain, as the quality check for the published data unknown. Other than that taking average surface temperature, somehow, is not absolute either. All these factors increase the uncertainty in the results, as transition zone heavily emphasizes on the temperature gradient in subsidizing regime (most cases). Therefore, the interpretations on the cross-plots by utilizing the well logs only, create the uncertainty in the analyses, to some extent. The interpretation than discussions are depends upon the information, which is

gathered by observing and tweaking the well logs and then comparing the observation to published literature. The interpretation and discussion portion surely have uncertainty, which cannot eliminate simply by this study where well log data is only considered.

Other than that, the experimental compaction curves, which used in this study are generated in very control environments. The conditions at some extent may not be the same that may represent in the natural setup. Furthermore, it is quite clear and established concept that the study area is a subsidizing basin. No major upliftment is observed or marked after the deposition of the reservoir rocks. But conducting the exhumation studies on the data, from this kind of basin, will help to understand the evolution history of the basin.

3.3.2 Geothermal gradient estimation

In compaction analysis, it is important to estimate the geothermal gradient in the study area. For this purpose the following Eq. 3.12 is used (Source: Theweatherprediction, 2013).

Thermal gradient = (BHT – Mean annual surface temperature) / Total depth. . . . . .(3.12)

Borehole temperatures (BHT) and total depth are taken from the Table 3.1 (Source: NPD, 2013). Mean annual surface temperature is considered 4 ^{o}C (Source: Met, 2013).

3.3.3 Reference curves

For compaction analysis, three experimental curves (Marcussen et al. 2010 for sand, Mondol et al., 2007 for Kaolinite-Smetitie (80:20) and Mondol et al., 2009 for; Kaolinite-Silt (50:50) are used in this study (Fig. 3.5). These theoretical curves are generated by performing the controlled laboratory experiments. These curves are valid only for mechanical compaction. This kind of experiments are relative easy to perform in the laboratory compared to the experiment of chemical compaction, where time and temperatures are major issues. This gives even the benefit in a way that one can easily separate the mechanically compacted regime to chemical compacted regime. For better results in this study, water depth is excluded and all the data points are plotted with respect to the BSF (Bellow Sea Floor) depth.

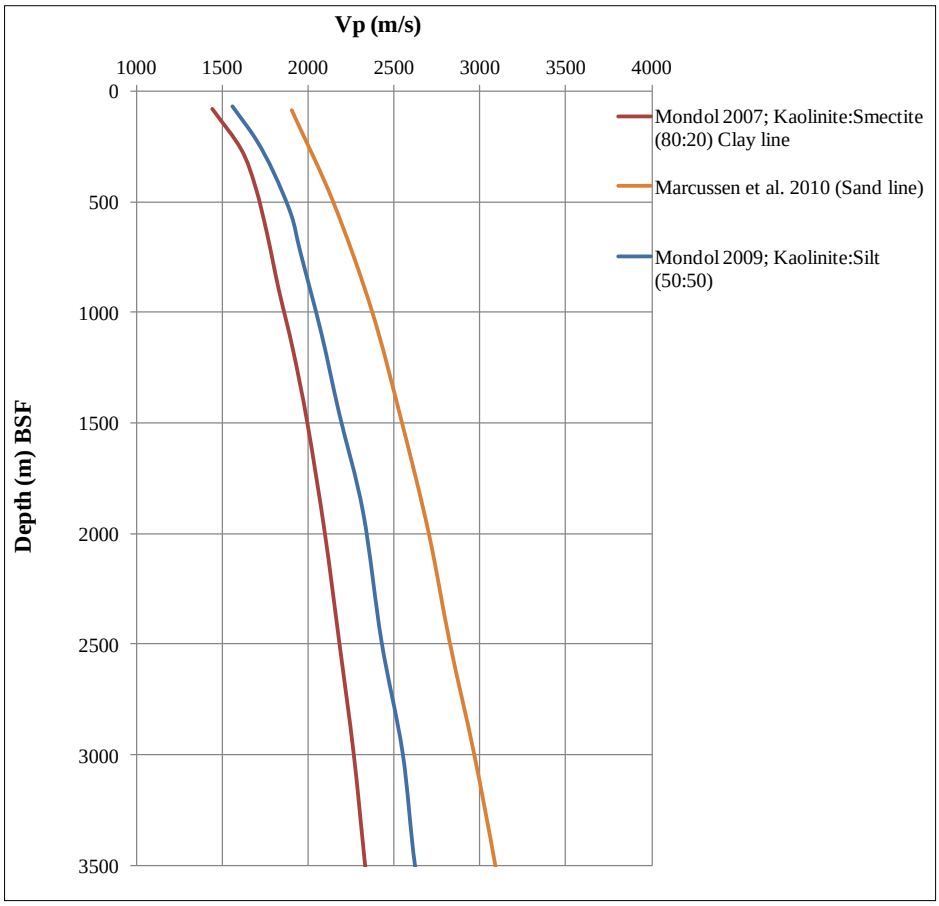

Figure 3.5 Trends of mechanically compacted sand, clay and clay-silt mixtures used in this study.

Marcussen et al., (2010) trend line is valid for the sandstone lithology. Marcussen et al., (2010) used sandy sediments in laboratory from the Etive Formation from depth level of 1600 m. Then, these sandy sediments are put under different stress conditioned to compact, the ultrasonic device take continuous reading as well. These different stress conditions are then translated to the overburden load. This overburden load is further represents the depth interval. Then the sonic velocity reading and the translated depth reading presented as shown in Figure 3.5.

Similarly Mondol et al., (2007, 2009) curves are generated by performing experiments in the laboratory. The samples used in this case were Mondol et al., (2007), koalinite-smectite (80: 20) and Mondol et al., (2009), kaolinite-ilt (50:50). Mondol et al., 2009 is further used for estimation of upliftment, as this curve take the account of silt and clay mixures comparable to natural mudstones.

3.3.4 Over pressure effect

Compaction of sediments may increase the pore pressure (Bjørlykke et al., 2010; Charlez, 1997; David and Dupin, 2007). Over pressure develops in those sedimentary sequences, where rate of sedimentation is high and ineffective dewatering of sediments help to retain the porosity, hence retard the compaction process (Bjørlykke et al., 2010; Goulty et al., 2012; Katahara, 2006; O'Connor et al., 2011). These overpressure zones can be marked by wire line

sonic logs (Rider and Kennedy, 2010) and compare it to the experimental curve like (Mondol et al., 2009). The analysis for over pressure regime is done in the chapter 5.

3.3.5 Exhumation study

The study area went under lots of structural evolutions throughout the geological history (see the chapter 2 for better overview). To understand the reservoir quality, it is important to estimate any upliftment in the study area. It is very important to know that if these reservoir rocks went to high temperature regime, where intensive quartz cementation can be initiated. This quartz cementation may derives the reservoir to much lower porosity, hence compromised the reservoir quality (Bjørlykke and Jahren, 2010). For this purpose, well data is compared with published Mondol, (2009); Kaolinite: Smectite (50:50) curve. Any mismatch with the laboratory reference curves may indicate the upliftment in the study area. Only data from shaly horizons are considered for the exhumation study. For this, the data are sorted on the basis of the shale volume. To eliminate the carbonate lithology effects, the data from carbonate lithology are excluded from the analysis.

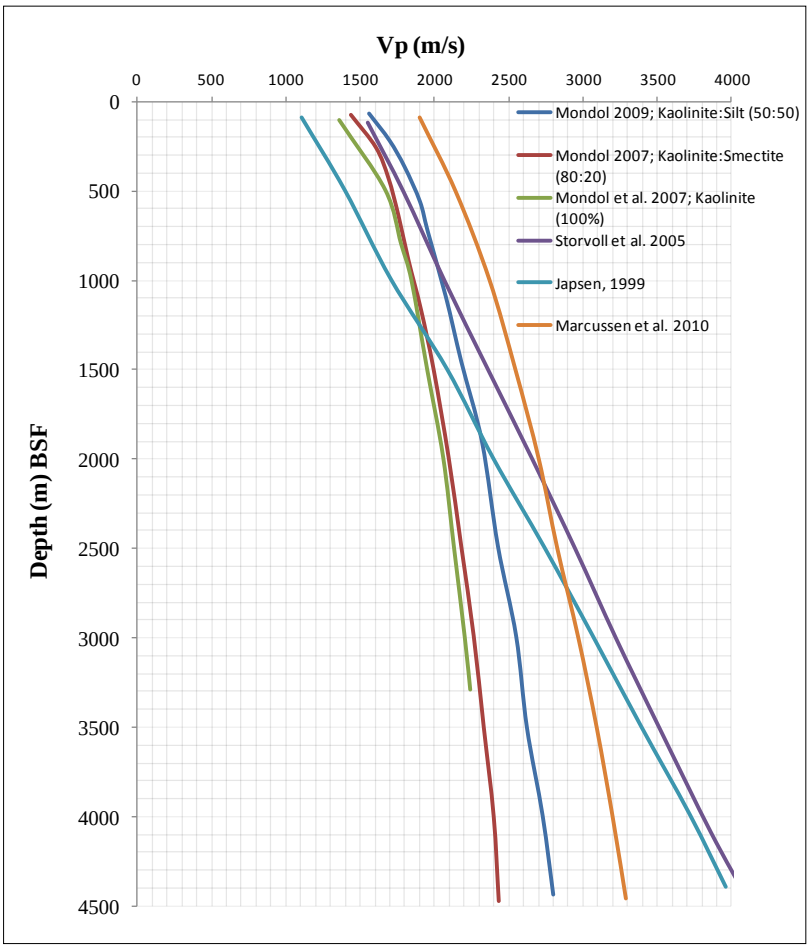

Figure 3.6 Several experimental compaction curves as a function of depth are used to estimate exhumation in the study area.

3.4 Rock physics diagnostics

This part of the study aims to characterize the reservoir properties of the Balder field by using different rock physics templates. Rock physics established the relation between the reservoir

properties (lithology, porosity, volume of shale and water saturation) to elastic properties (velocity, impedance and Vp/Vs ratio) (Avseth, 2010; Avseth et al., 2009; Chi and Han, 2009; Dewar, 2001; Dvorkin and Nur, 1996; Dvorkin et al., 2002; Dvorkin et al., 2004; Miller, 1992; Mukerji and Mavko, 2006; Ødegaard and Avseth, 2004). Rock physics analyses rely on the empirical relations and cross-plots defined and practiced by number of workers (Carr et al., 2002; Omudu and Ebeniro, 2005; Sayers and Boer, 2011). Different cross-plots used to predict the lithology variation across the Balder field, which can affect the reservoir quality (Pelletier et al., 2004). It may helpful for selecting different seismic attributes, predict and calibrate different seismic response during interpretation (Avseth et al., 2005; Dvorkin et al., 2003; Pelletier et al., 2004). Additional, different established rock physics trends help to characterize the reservoir further (Avseth, 2005; Avseth et al., 2005; Ødegaard and Avseth, 2004). It also helps us to differentiate the reservoir rocks from the non-reservoir rocks (Avseth et al., 2001; Walls et al., 2004).

3.4.1 Uncertainty of the results

In rock physics analysis, Vp (P-sonic velocity), Vs (Shear velocity) and density are the most fundamental parameters (Avseth et al., 2010). Vp and density are commonly logged but Vs unfortunately not widely logged, especially the wells which drilled in 1960s, 70s and 80s. Most of the wells consider for this study were drilled in the 1960-1980s and so Vs is only available in well 25/11-16. The well with Vs, have very poor coverage especially in reservoir sections (Fig. 3.7) (Rider and Kennedy, 2010).

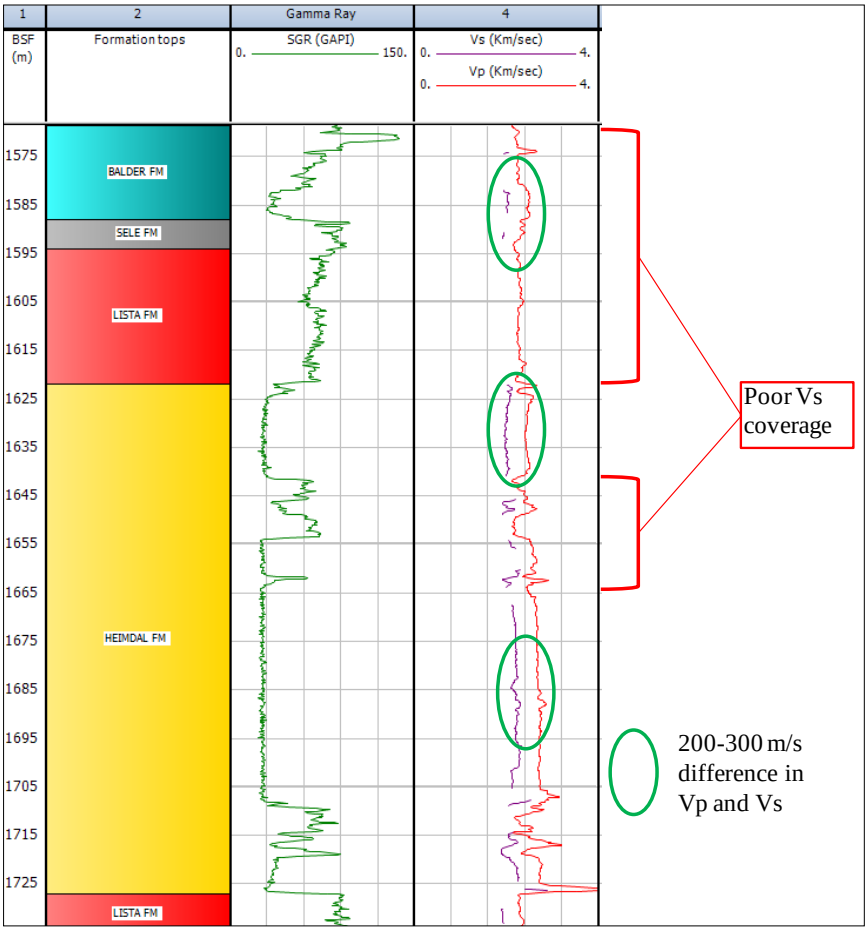

Figure 3.7 Vs quality check for the well 25/11-16.

Other than that, the difference between Vp and Vs value is just between 200-300 m/s (Fig. 3.7). This difference of values is not normal, as in ordinary situations (common lithology i.e. sand and shale) the Vp values mostly 1.5-2 times more than the values of Vs (Emery and Stewart, 2006; Miller, 1992; Xu and Bancroft, 1998). After these uncertain values, still by Vp-Vs cross-plot, a 2nd derivative equation is derived later (Fig. 3.9). The results with the linear equations, which has been defined or given by their respective authors are compared in the Figure 3.8. This shows difference of 900 m/s for a single lithology.

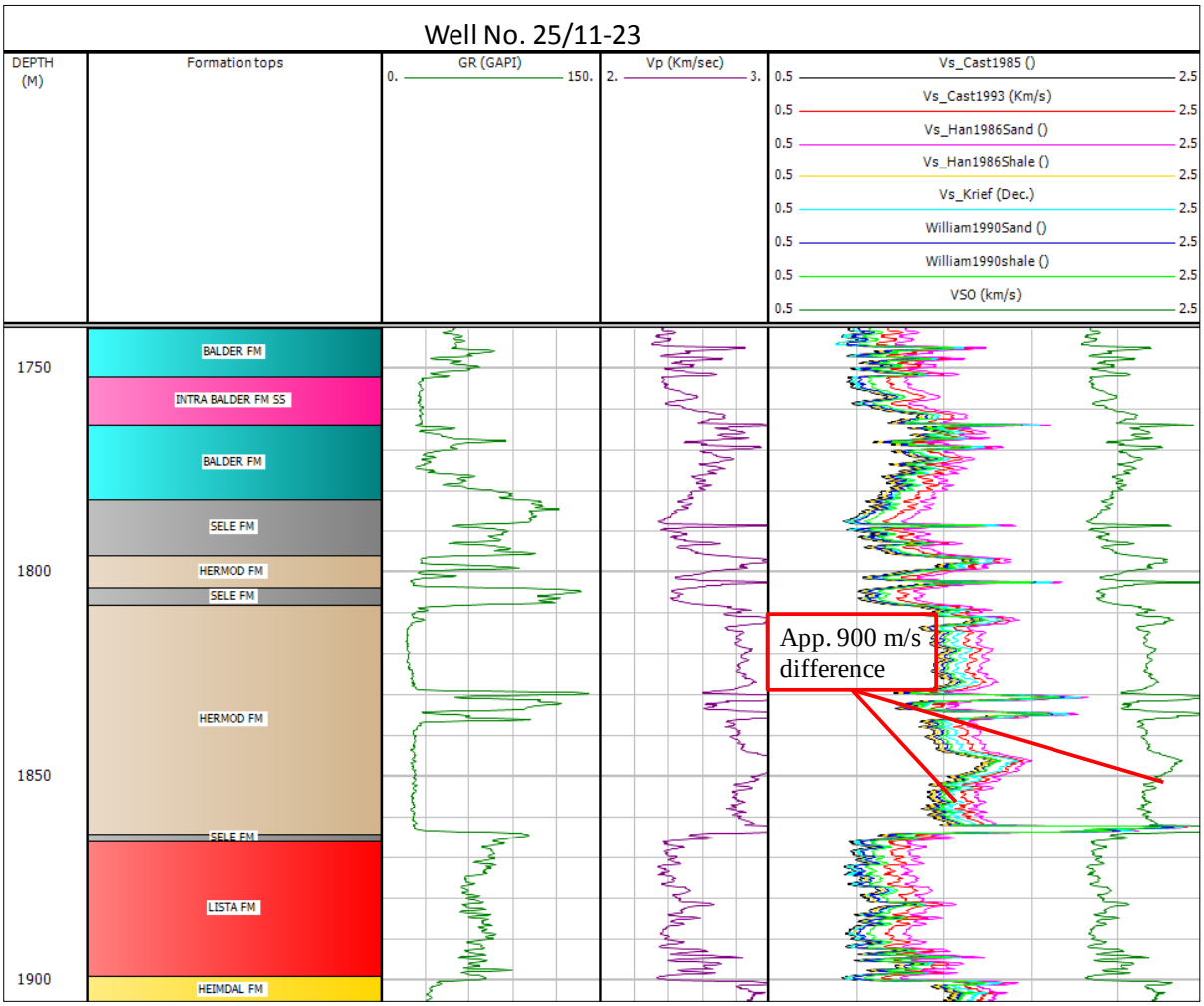

Figure 3.8 Different Vs (km/s) comparing in different formation with varying lithology.

The empirical relations published by the authors are defined in the next section. The results from these empirical relations also have uncertainty, as it is very hard and tough job to know, what kind of sediments are being utilized during these experiments? What were the conditioned and precautions taken during the experiments? The sonic frequency which are used for these experiments not known at some extent. These kinds of questions put the big question mark on the reliability of the results. Due the uncertainty in Vs estimation, the other elastic parameters like bulk modulus, shear modulus, Vp/Vs ratio, Poisson's ratio, shear impedance and lame parameters are uncertain to some extent. But still, the results which have been shown and discussed further in the chapter 6 are interesting, and comparable with the published literatures.

3.4.2 Calculations of rock physics parameters

Vs estimation

Vs known as shear velocity is fundamental parameter in rock physics. The wells which are under consideration (Table 3.1), don't have direct measurement of Vs, except one well (25/11-16). The Vs from this well (25/11-16) is used to derive the Vp-Vs relation (Fig. 3.9) equation. The results from this relation are highly uncertain and totally contradict with the published literature, which have been pointed out in the previous section.

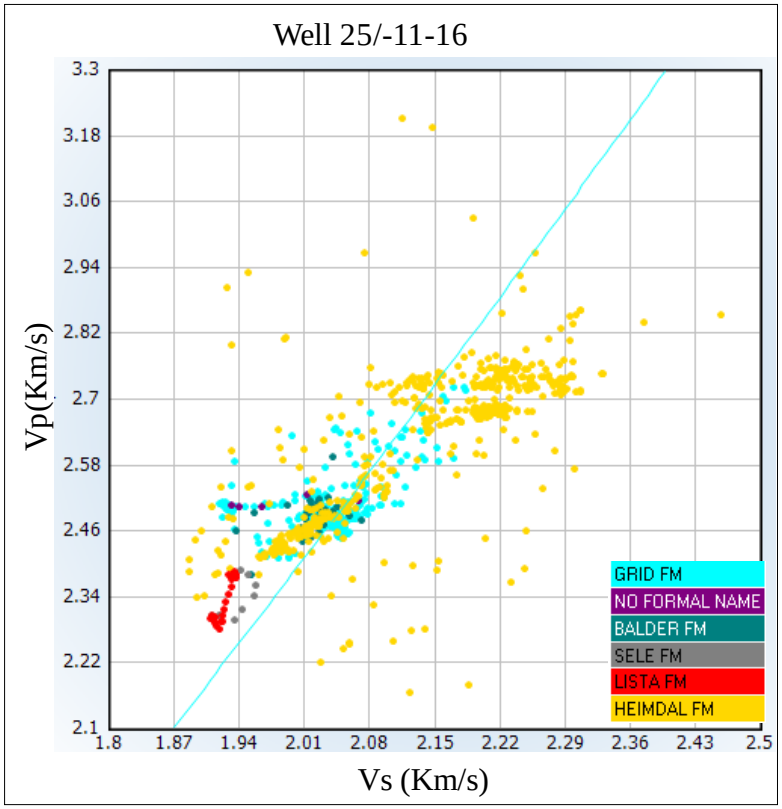

Figure 3.9 Vp-Vs cross-plot form the Well 25/11-16 to derive the local Vs.

The following Vp-Vs relationship is derived from the cross-plot (Fig. 3.9) of data from the well 25/11-16.

Vs = 0.185376184 + 0.916843042 x Vp - 0.0679041133 x Vp ^2 (R_2= 0.930496075) . .(3.13)

Castagna et al., (1993) give the following empirical relationships to estimate Vs from Vp.

Vs=0.804 x Vp-0.856 . . . . . (3.14)

Castagna et al., (1985) for mud rock, give the following empirical relationship for Vp and Vs

Vs=0.862 x Vp-1.172 . . . . . (3.15)

Han et al., (1986) give the two following empirical relationships for the Vs for sandstone and shale lithologies after conducting large data sets of porosity and clay variation content as define by Dvorkin, (2007).

For Sand (Clay content less than 25 %) Vs = 0.794 x Vp – 0.787. . . . . (3.16)

For shale (Clay content greater than 25 %) Vs = 0.842 x Vp – 1.099 . . . . . .(3.17)

William, (1990) used well log data and give the following two equations for water bearing sand and shales, as define by the Dvorkin, (2007).

For Sand Vs = 0.846 x Vp −1.088. . . . . .(3.18)

For Shale Vs = 0.784 x Vp − 0.893. . . . . .(3.19)

Impedance (Ip and Is) calculation

After measuring Vp and Vs, P and S impedance (Ip and Is) can be derived from simple impedance equation as define by the Goodway (2001).

Acoustic Impedance (Ip) = Vp x Rock density . . . . . .(3.20)

Shear Impedance (Is) = Vs x Rock density . . . . . .(3.21)

Lame's parameters (Lambda and Mu) calculation

Lambda-Rho (λp) and Mu-Rho (μp) parameter, as defined by Goodway et al., (1997), can be calculated by the following equations.

$\lambda p = Ip^2 - 2Is^2$ . . . . . .(3.22)

$\mu p = Is^2$ . . . .(3.23)

Lambda (λ) and Mu (μ) parameter, as defined by Goodway, (2001), can be calculated by the following equations.

$\lambda = \text{Density} \times (Vp^2 - 2 \times Vs^2)$ . . . . . (3.24)

$\mu = \text{Density} \times Vs^2$ . . . . . .(3.25)

3.4.3 Rock physics templates (RPTs)

Rock physics templates (RPTs) are used to predict lithology (reservoir quality) and fluid discrimination (hydrocarbons or water) (Avesth et al., 2005). The most widely used RPT is the acoustic impedance (AI) versus Vp/Vs ratio (Ødegaard and Avest, 2004).

Vp, Vs, porosity and clay volume cross-plots

Vp versus Vs

Vp-Vs ratio/cross-plots are used to determine the lithology and pore-fluids properties (Arns et al., 2002; Castagna 1993; Emery and Stewart, 2006; Gassmann 1951; Goodway et al. 1997; Guliyev and Davis, 2006; Miller, 1992; Pickett, 1963; Tatham, 1982). This simple cross-plot separate the water saturated and gas saturated lithology on two narrow parallel trend lines (Avseth et al., 2005). But in this study, shear velocity has poor quality and derived shear velocity from the equation give the linear trends (Fig. 3.10). In these circumstances, this

cross-plot is not much usable. But from this plot, a linear trend can be selected, on the basis of its average behavior with respect to the other trends.

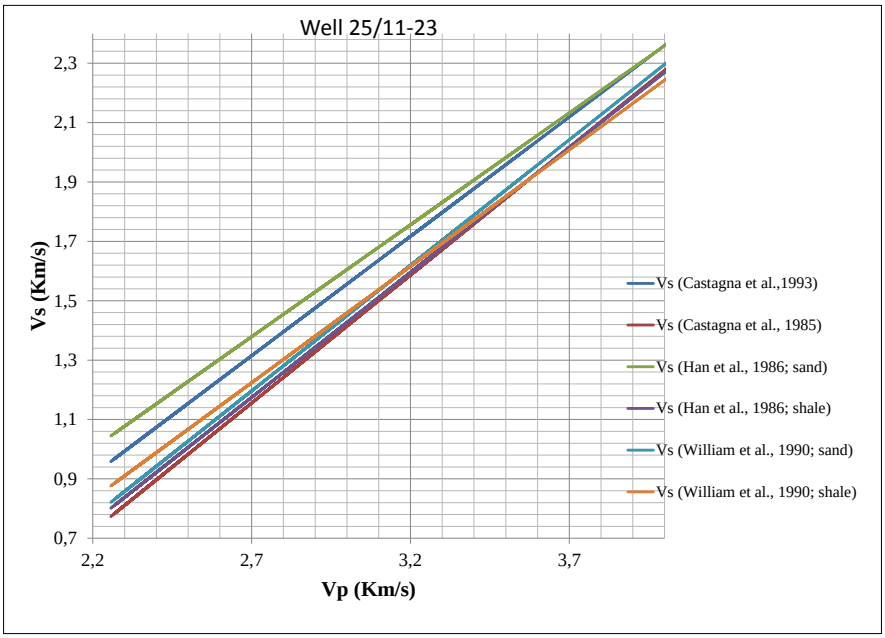

Figure 3.10 Vp versus Vs (Data points from the Heimdal Formation)

Vp vs Porosity (Clay model)

This model was introduce by the Han, 1986. In this model effect of the varying clay contents on the porosity and sonic velocity can be observed (Fig. 3.11). Han, 1986 model is the clean sandstone data points with varying clay content are considered. The reservoir formations in the study area are of clean sandstone lithology. The clay volume till 35% are taken to study its effect on the sandstones. Furthermore, this experiment also takes the account of the porosity variation due to the introducing of the clay content in sandstone. This analysis will help us to understand the reservoir formations in better way, in term of porosity and clay volume (Avseth et al., 2005).

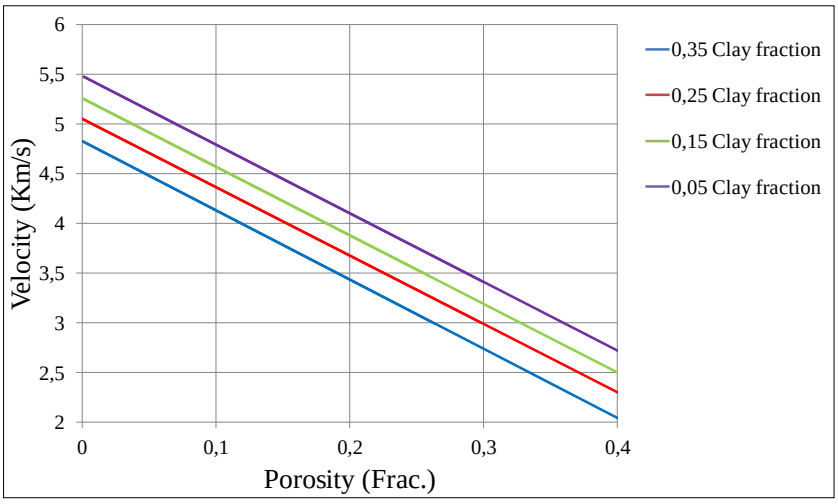

Figure 3.11Porosity-Vp cross-plot, varying clay volume trend lines (Digitized and modified after Han et al., (1986) cited in Avseth et al., 2005)

Vp/Vs versus IP

This cross-plot is useful for the fluid and lithology discrimination (Fig. 3.12) (Avseth et al., 2005; Guliyev and Davis, 2006). The low impedance (AI) and Vp/Vs ratio can be categorized as gas or highly porous sands (Chi and Han, 2009). The overall effect of the gas/hydrocarbon saturation will decrease the elastic properties of the rocks. Vp/Vs versus IP cross-plot will also help to differentiate the clean reservoir intervals from gross formation (Feng et al., 2007; Mukerji and Mavko, 2006; Russell and Smith, 2007). Furthermore, the contact cement line will surely help to identify the poorly cemented intervals as well (Avseth et al., 2009).

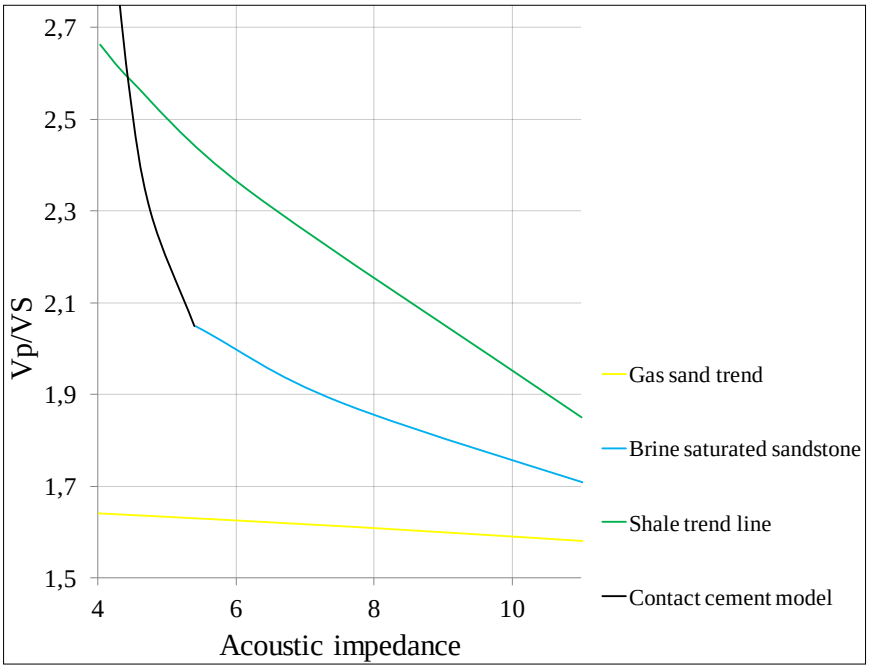

Figure 3.12 Ip-Vp/Vs cross-plot (Digitized after Avseth et al., 2009).

Lame's parameters (Lambda-Rho and Mu-Rho) cross-plot

This cross-plot is useful for separating the gas sand zone from the rest of data (Fig. 3.13) (Xu and Bancroft, 1997). Lambda-Rho (λp) is sensitive to (incompressibility) lithology, porosity and fluid content, while Mu-Rho (μp) is sensitive to matrix (rigidity) i.e. lithology (Contreras and Verdin, 2004; Feng et al., 2007; Goodway et al., 1997). This cross-plot also help to differentiate the reservoir intervals from the gross formation.

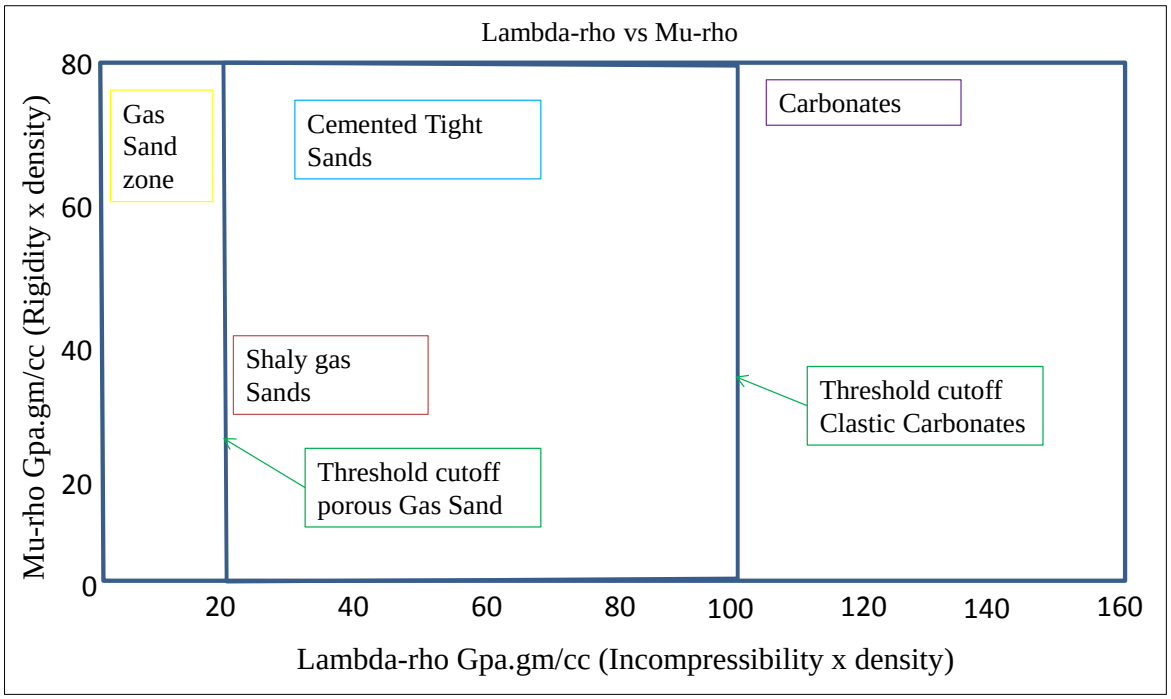

Figure 3.13 Generalize cross-plot, of Lambda-Rho (λp) versus Mu-Rho (μp) (Modified from Goodway et al., 1997).

Rock physics cement models

These models are mostly used to estimate the packing of sediments, more specifically concentration of the cement volume in rocks (Fig. 3.14). It utilizes the data from the sonic velocity and porosity. These models also help to understand the depth related diagenetic or depositional effect on the formation (Avseth et al., 2005; Avseth et al., 2010).

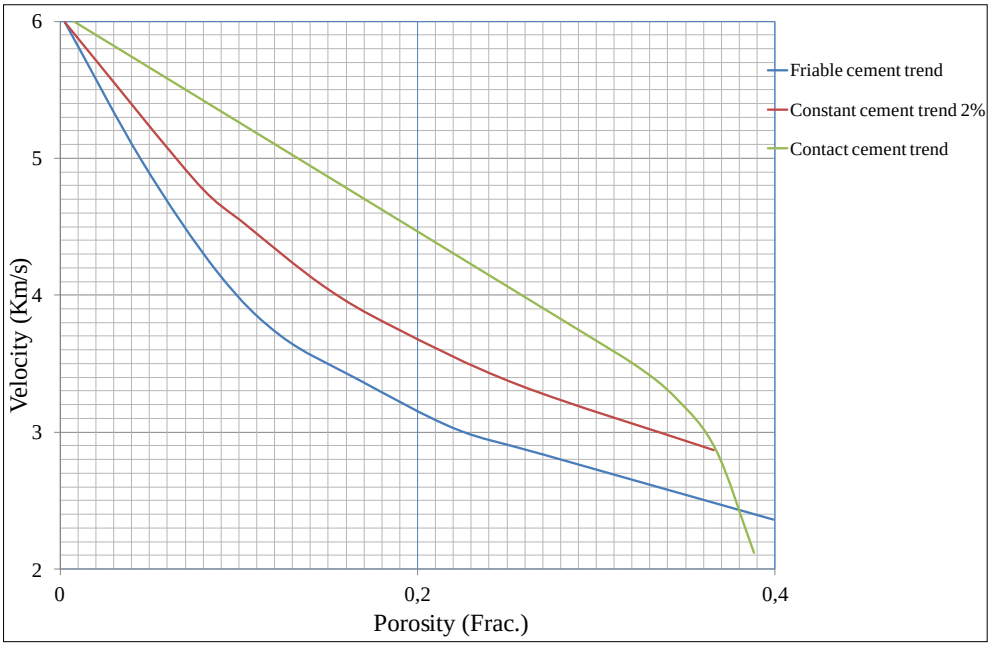

Figure 3.14 Schematic descriptions of the three rock physics cement models (Modified and Digitized from Avseth et al., 2005).

The friable-sand model

The friable-sand model is well known for the high porosity sands, which reflects the velocity-porosity relation with respect to the degree of sorting (Fig. 3.15) (Avesth et al., 2005). This model introduced by Dvorkin and Nur, (1996). The critical porosity of well sorted sand grain is around 40% (Mukerji and Mavko, 2006), but with addition of smaller grains like clay in pores will reduce the porosity and sorting, hence elastic impedance increases (Avesth et al., 2005; Avesth et al., 2010; Marion, 1990). The friable sand model precedes the poorly sorted grains as the well sorted grains.

The Contact cement model

Sandstones get cemented as the burial depth, overburden and temperature increases (Avseth et al., 2005). This cementation increases the stiffness of the sandstone, as the initial cementation at grain contacts strengthen the rock. It will decrease the porosity (negligible) but increase the elastic impedance of rock (Fig. 3.15) (Avseth et al., 2000; Avseth et al., 2005; Avesth et al., 2010). The contact cement model shows the relationship between velocity-porosity with respect to cement volume (Mukerji and Mavko, 2006).

The Constant cement model

The constant cement model takes account of both friable sand model and contact cement model, it considers not only the cementation at grain contacts but also cementation within the void spaces (between the grains) (Fig. 3.15). This model was introduced by Avseth et al., 2000. It shows the velocity-porosity relations with respect to specific cement volume (Avseth et al., 2000; Avesth et al., 2010; Mukerji and Mavko, 2006).

Chapter 4: Petrophysical Analysis of the Balder field

This chapter focuses on the petrophysical studies of the Balder field using the well log data to evaluate the reservoir properties. The essential parameters require to characterize the reservoir rocks have been calculated and their derivation briefly illustarted in this section. It is challenging to display all the analysis and results especially calculation stages of basic parameters in limited expansion. Initially MS Excel is used to calculate required parameters and to prepare a spreadsheet for every well and later Interactive Petrophysics software is used for petrophysical analysis. The results demonstrate here in many cases consider only single well analysis to highlight some particular issues. Similar analyses and outcomes can be seen in the Appendix I.

4.1 Results

4.1.1 Petroleum system analysis

4.1.1.1 Source rocks

The source rock can be identified by the five common well logs i.e. gamma ray, sonic, bulk density, neutron and deep resistivity. All five log curves plotted for the well 25/11-17 (Fig. 4.1). The high gamma ray values of approximately 300 API are observable for the source rock, the Draupne Formation (Fig. 4.1) (Cooper et al., 1995; Cornford, 1998; Justwan and Dahl, 2005).

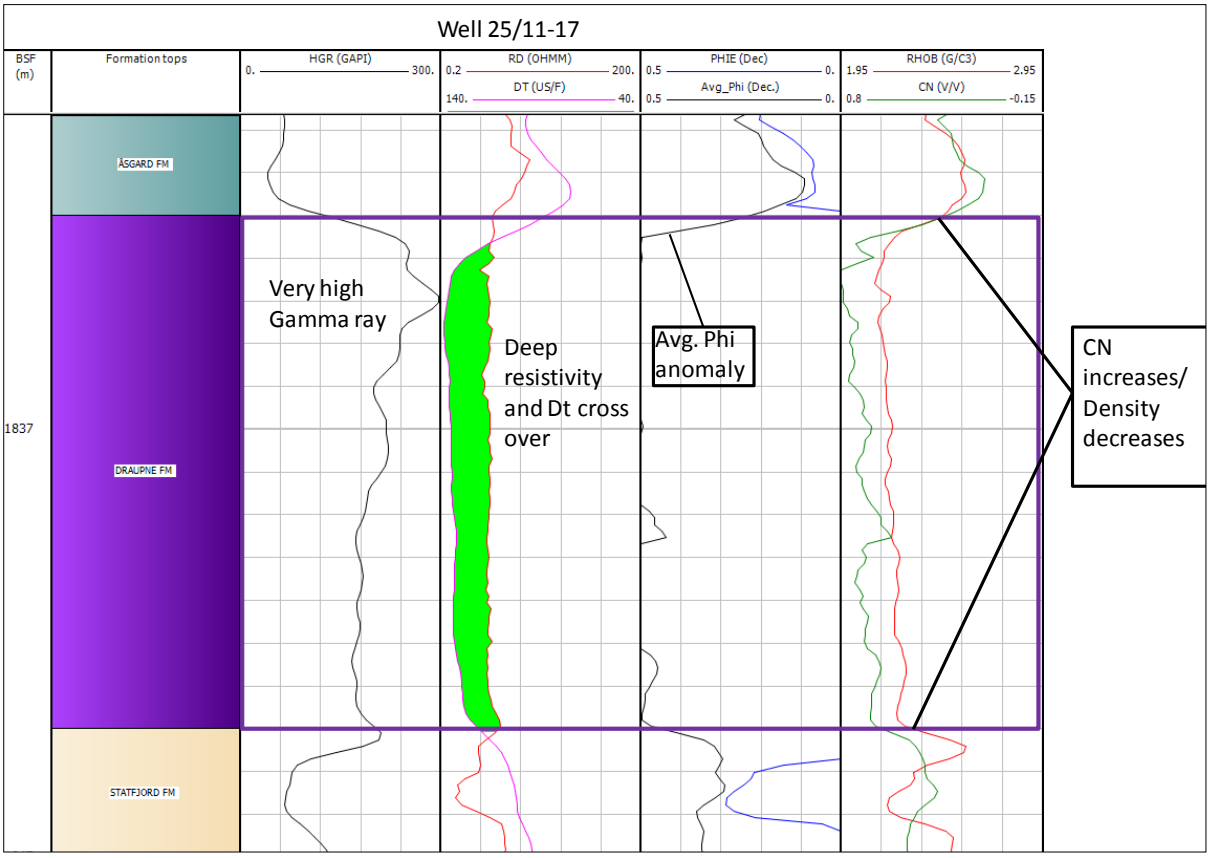

Figure 4.1 Source rock characterization of the study area, example from the well 25/11-17.

In this high gamma ray interval (Fig. 4.1), the neutron log shows very high values whereas, the bulk density decreases sharply. These phenomena lead an increase of the average porosity, as the neutron log overestimate the value and bulk density underestimate it. Furthermore, due to the high gamma ray index, the effective porosity decreases to almost zero, as it shows 100% shaly interval. Other than that, the sonic log (transit time) increases and makes crossover with the deep ressistivity log (filled with the green color). All of these anomalies on the well logs may indicate the presence of the source rocks (Autric and Dumesnil, 1985; Dellenbach et al., 1983; Passey et al., 1990).

Similarly in the well 25/11-15 the gamma ray log has been plotted along with the spectral gamma ray log for potassium, thorium and uranium (Fig. 4.2). In this well log plot anomalies are observable for the source rocks as well. The gamma ray log value increases sharply to approximately 380 API along slight increase of the spectral gamma ray log values. The sonic log, fairly increases in the source rock intervals and makes crossover with the deep resistivity log (filled with the green color). The high resistivity values indicate the presence of hydrocarbons (non-conductors). This however is not a good indicator for high TOC. The bulk density and deep resistivity logs also crossover in this high gamma ray log interval (filled with the pink color). The neutron log shows high values whereas the bulk density log decreases rapidly. The Vp log also shows the velocity reversal in this zone. All of these anomalies may indicate the presence of organic-rich source rocks (Passey et al., 1990).

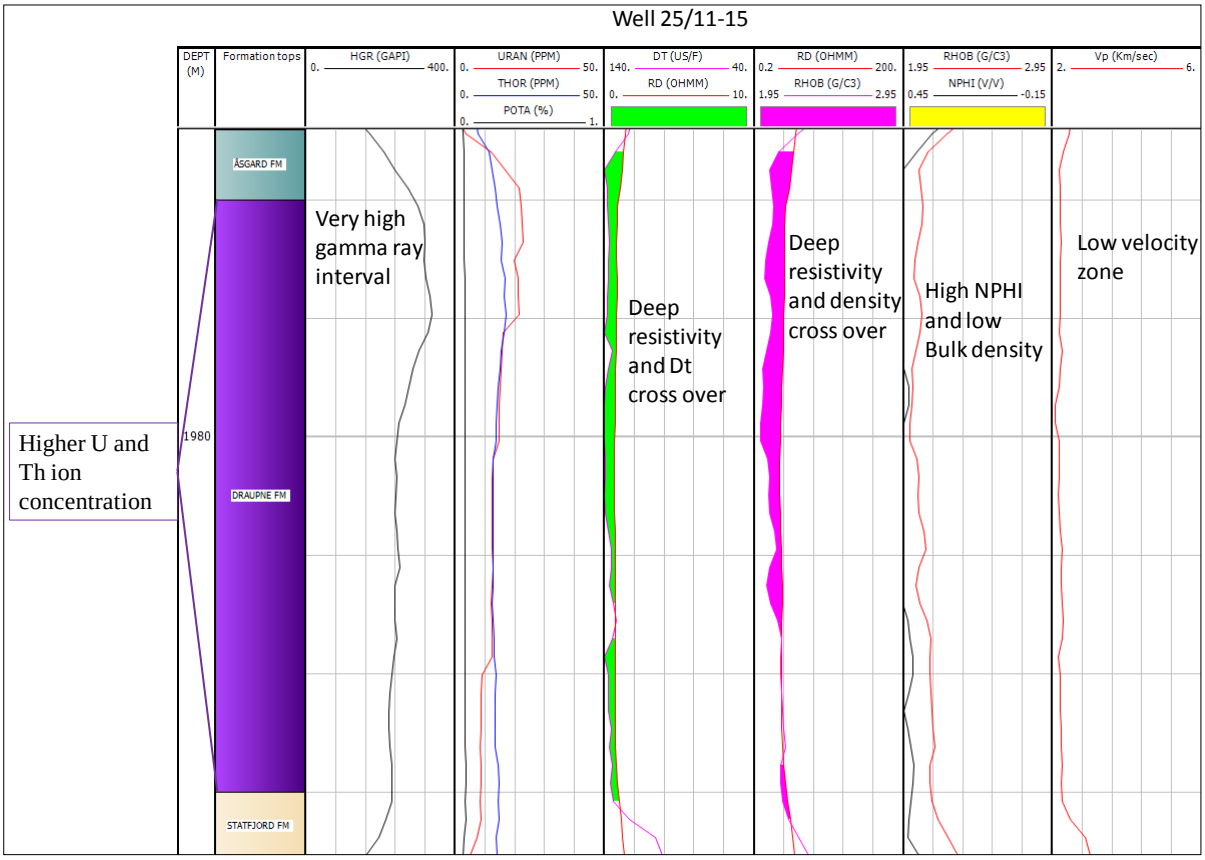

Figure 4.2 Source rock characterization of the study area, example from the well 25/11-15.

Shale content in the source rock

The shale content in the source rock have been calculated by the method defined in the chapter 3. It is previously established that the source rock contains high gamma ray values,

which may indicate high shale content as well. The clay volume histogram contains data points from four different wells (Fig. 4.3). It may be observable that the average mean value in histogram is approximately 0.80 (fraction) or 80%, while the mode is at 1 (fraction) or 100 %. This simple (Fig. 4.3), yet informative histogram indicates that the source rock is highly rich in the shale content (Passey et al., 1990).

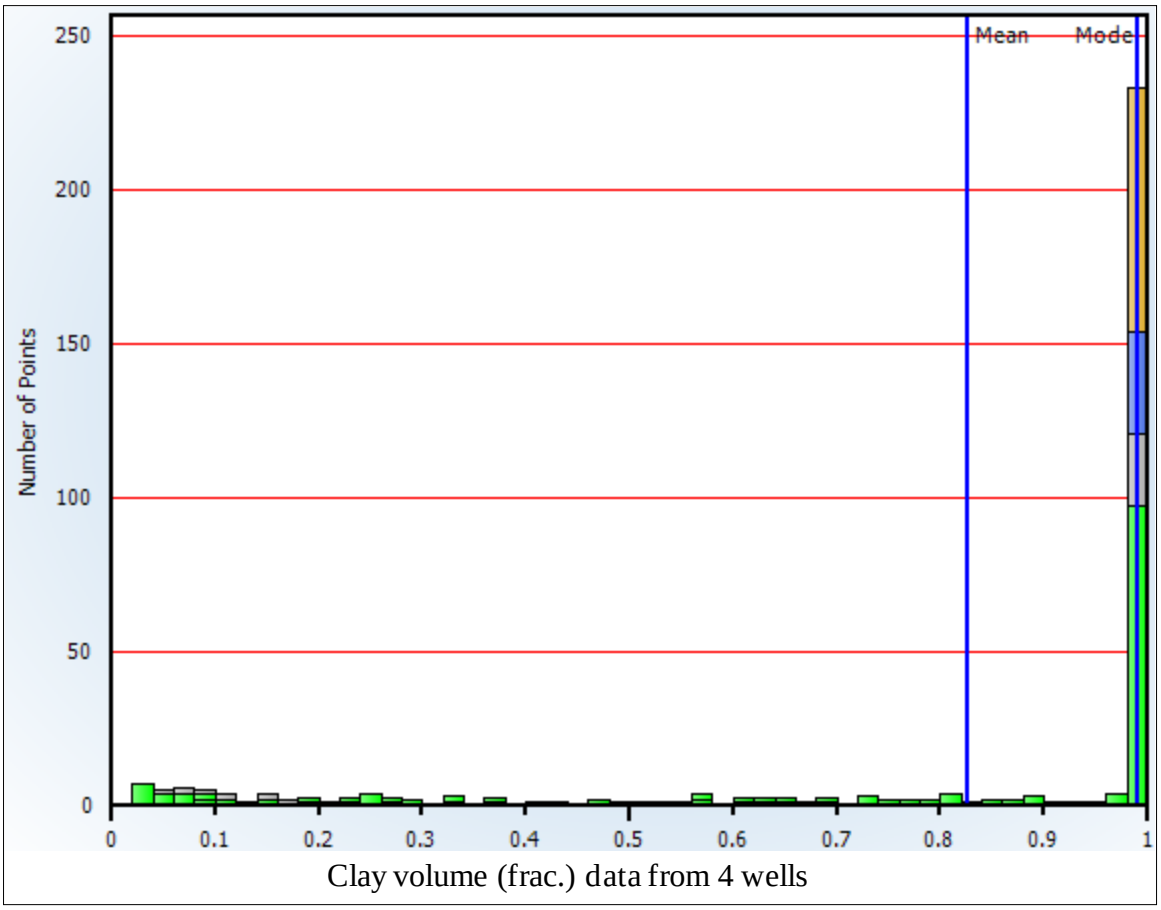

Figure 4.3 Histogram of the source rock in the study area display the calculated shale volume.

Porosity in the source rock

The average porosity in source rocks have been calculated by the method defined in the chapter 3. It is previously explained that the source rocks response have high neutron log values and low bulk density, which may indicate the presence of kerogen (Rider and Kennedy, 2011). All data points from four wells have been plotted in the porosity histogram (Fig. 4.4). It may be observed that the mean value in histogram is approximately 0.25, while the mode is at 0.22. From above observation it can be concluded that the calculated porosity values for source rocks may have significant error (if the well log data is the only source of porosity estimation in source rock intervals).

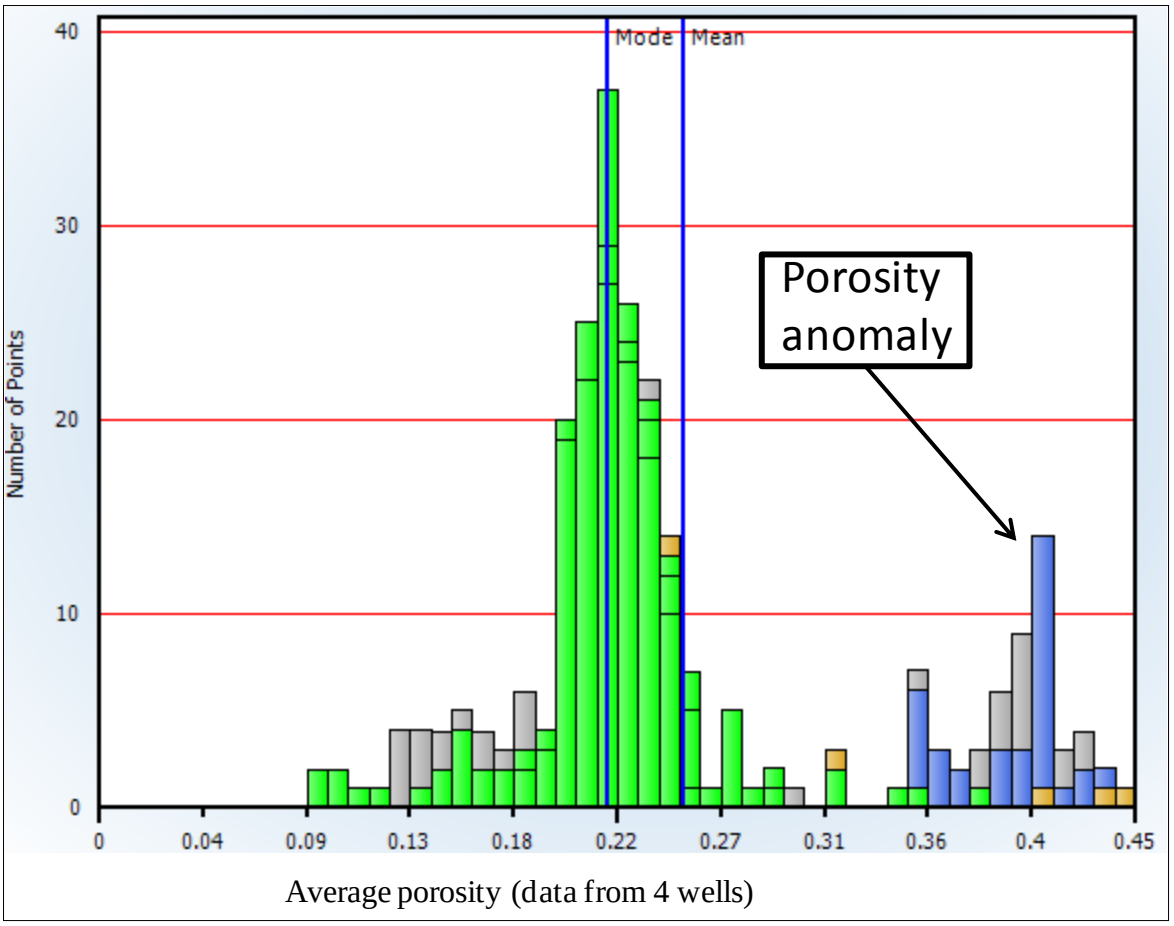

Figure 4.4 Histogram of the source rock (Draupne Formation) for porosity, data from four wells.

The porosity histogram (Fig. 4.4) shows some anomalies as well, because the neutron and bulk density have error readings (some points shows the values above 0.4, data points are from 1800-2000 m interval below the sea level). The neutron log overestimate the value, which may indicate the presence of hydrocarbon (higher hydrogen index). The bulk density shows the low values, indicating that these intervals are less dense and may have the organic matters (Passey et al., 1990).

4.1.1.2 Reservoir rocks

Correlation of reservoir rocks

It is important to visualize the lateral expansion of the formation/surface before conducting any kind of analysis. Due to lack of seismic data for this study, it is very uncertain what may have between the two wells, as well logs have only good vertical resolution. A well correlation was performed to visualize how these reservoir formation's thickness varies across the Balder field? To perform the well correlation (Fig. 4.5), gamma ray log and the information relative to the formation tops used from the NPD's website. In Figure 4.5, it can be observed that the reservoir rocks thickness decreases from north to south and from west to east across the Balder field. The north-western part of the field has more deeper reservoir zones as compared to the south-eastern part (Fig. 4.5). The reservoir sandstones: Balder, Heimdal and Hermod formations are pinching out in south-eastern wells (Fig. 4.5). These variation of lithology may indicate the deposition pattern and direction of sediments source,

which in this case may be from west. Further, it also illustrates that during the Paleocene-Eocene time the reservoir sediemnts had transported from East Shetland Platform, due the tectonic upliftment of the Atlantic rift margin (Timbrell, 1993). Most of these sediments transpoted as submarine flows, which may prograded (low system tract) and pinch out in east, against the Utsira High (Faleide et al., 2010; Fitzsimmons et al., 2005; Timbrell, 1993; Wild and Briedis, 2010).

The well log data have used to generate the surface contour maps for each reservoir horizon (Fig. 4.6). They show very intresting features of the Balder field, known as mounds and lows, discussed by many authors like Bergslien, 2002; Jenssen et al., 1993; Wild and Briedis, 2010. Only with well logs, it has limitation to elaborate how these mounds have been formed. The only information which may be extracted here with less uncertainty from correlation (Figs. 4.5, 4.6 a, b and c) and interpretation of gamma ray log (Fig. 4.13) that these mounds are thick deposits of sands. Further from the blocky nature (Boxcar trend) and low gamma ray response, it marks as submarine fan/turbidite deposits (Milton and Emery, 2008). The clean sandstone intervals may be associated with the channel deposits of submrine fans (lobes), while the mudstone/shale belong to the flood plains or leeves deposits (Fig. 4.23) (Milton and Emery, 2008; Timbrell, 1993).

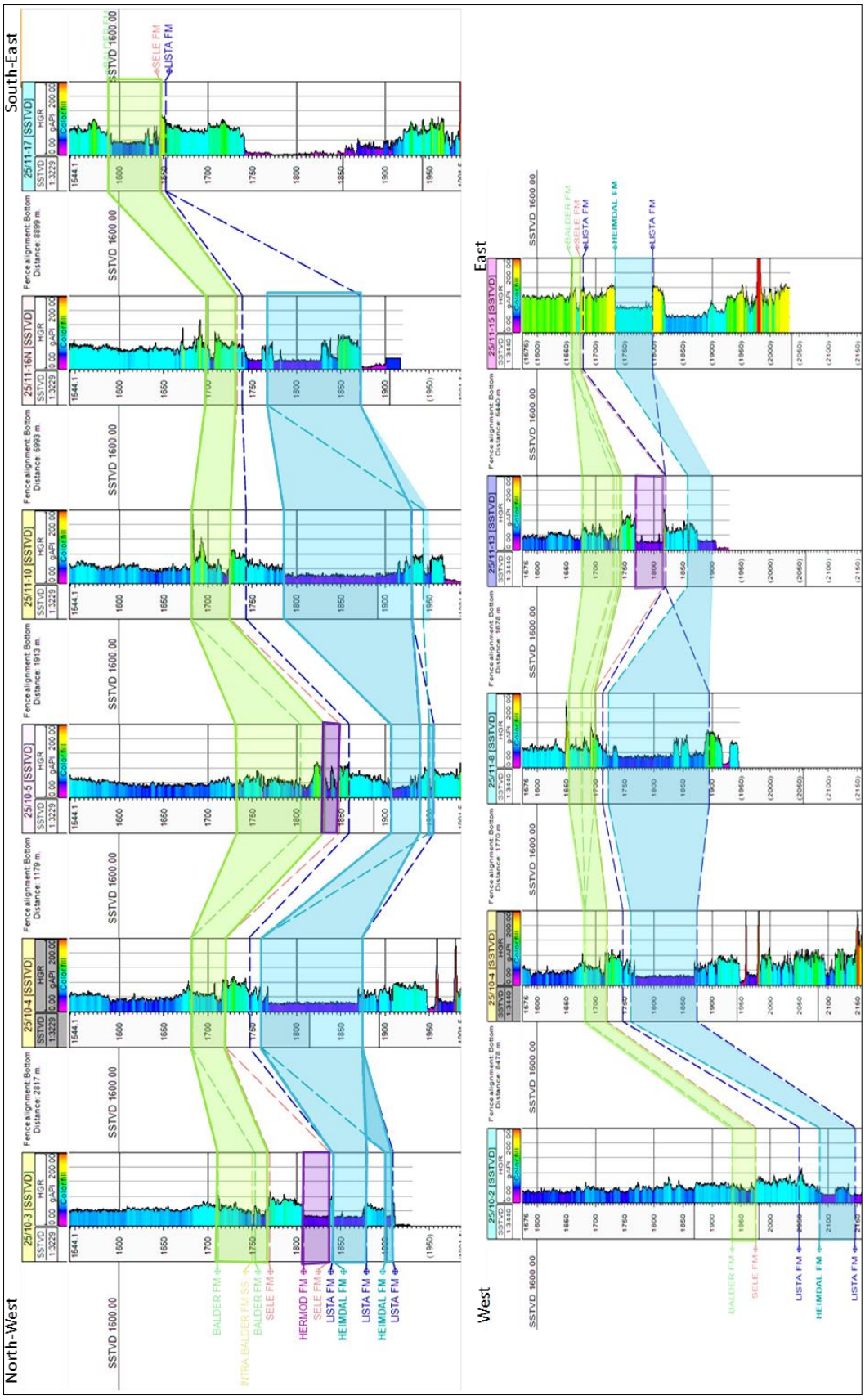

Figure 4.5 Correlation of reservoir rocks of Balder (Light green polygon), Hermod Formation (Purple polygon) and Heimdal Formations (light blue polygon).

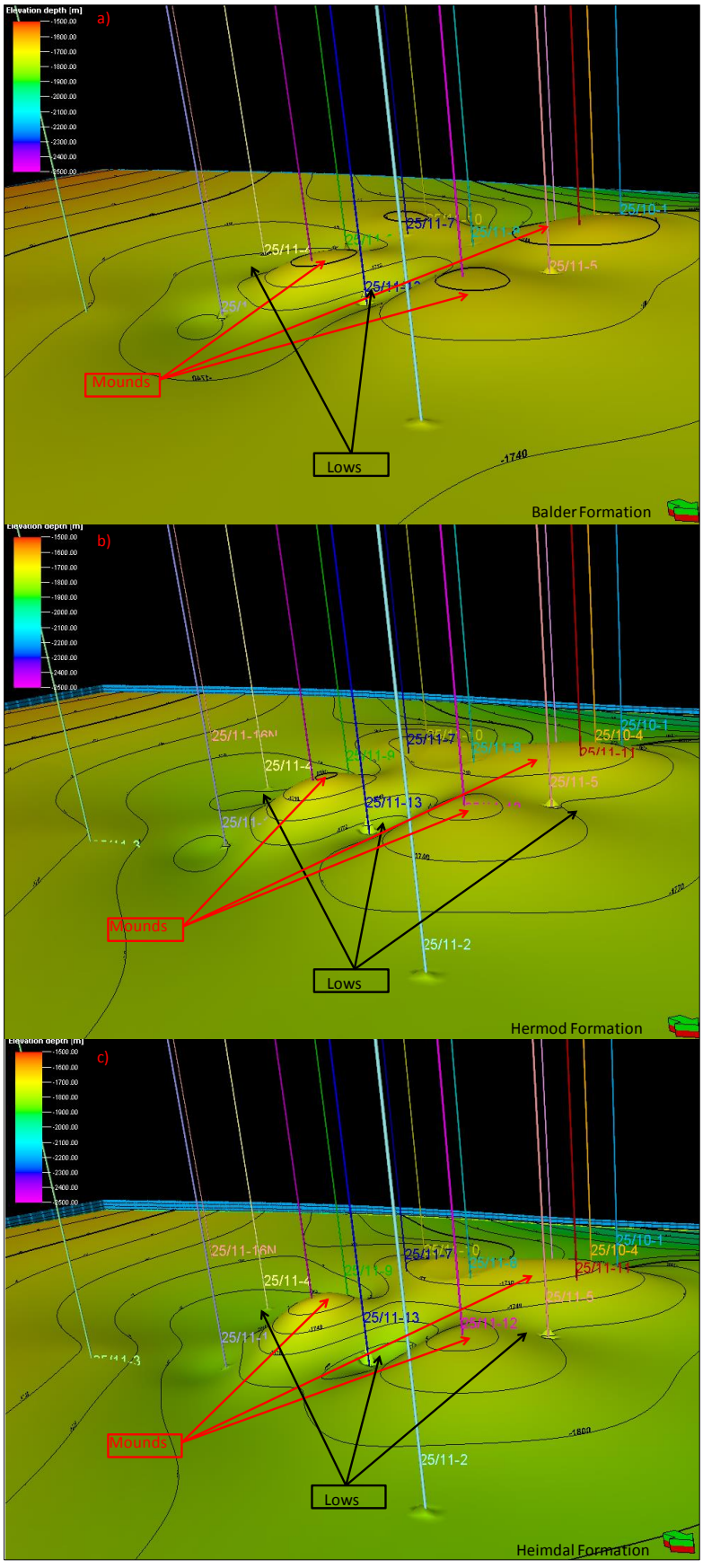

Figure 4.6 Illustrate mounds and lows in the area, (a) Balder, (b) Hermod and (c) Heimdal formations surfaces generated from well log data.

Identification of reservoir rocks

In the neutron-density cross-plots (Fig. 4.7), data points from the seventeen wells from the Balder, Hermod and Heimdal formations have been plotted. Overlay lines data are taken from IP. Only the points with less than 25% shale (Vsh<0.25) have been plotted. By using this cutoff, the shale intervals are removed from data as this plot (overlay lines) only valid for pure sandstone, limestone and dolomite. Figure 4.7 demonstrate that only few points do not fall outside the pure sandstone line, which may belong to calcite or data from the intervals of bad boreholes.

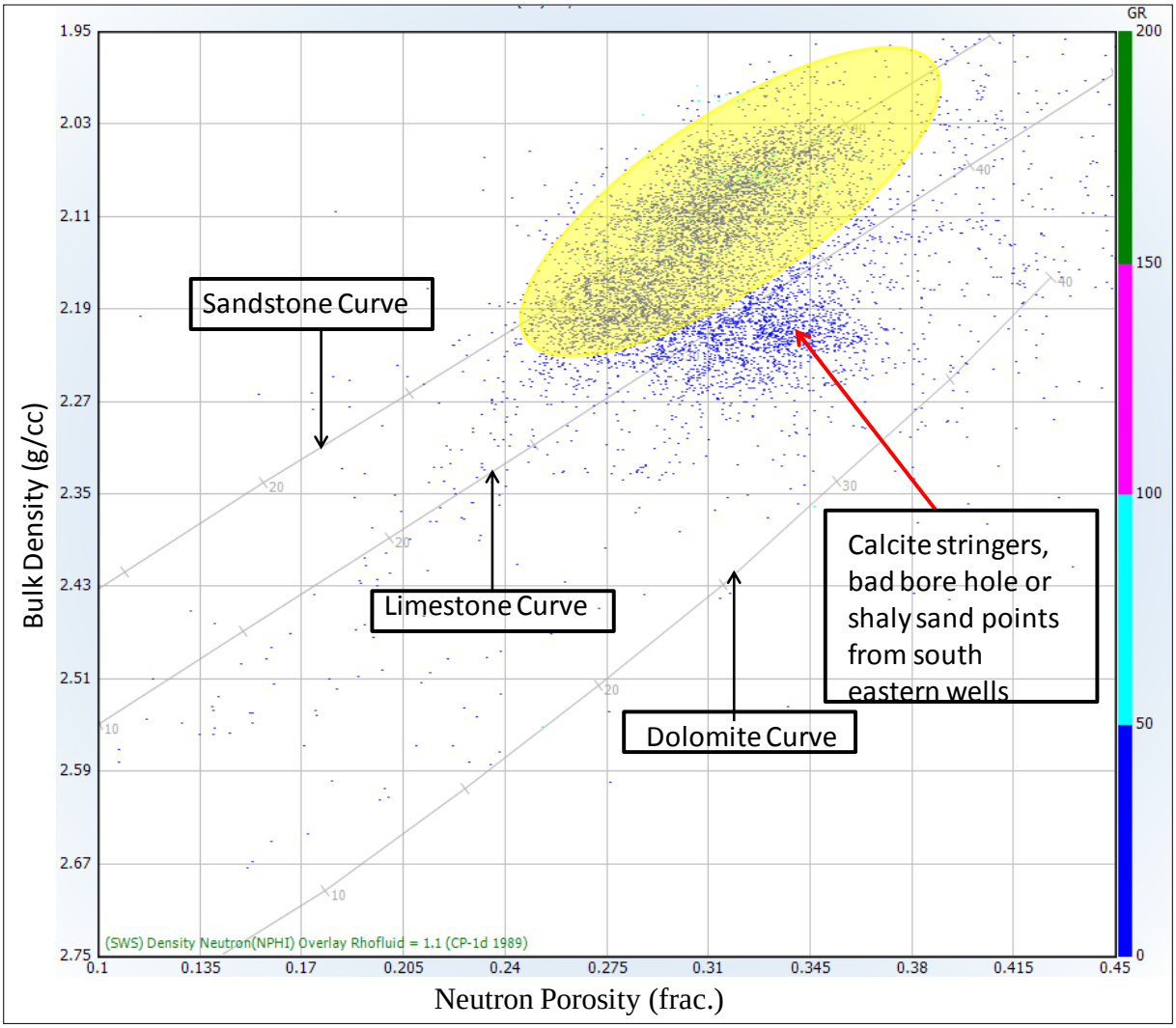

Figure 4.7 A crossplot of Neutron versus bulk density logs. The data from reservoir formations i.e. Balder, Hermod and Heimdal from seventeen wells fall mostly on the sandstone line.

In Neutron-Sonic crossplot (Fig. 4.8) overlays line data incorporated from Wyllie overlay lines. Data points from the Balder, Hermod and Heimdal formations have been plotted that sorted by IP. Similarly, the reasons that mentioned above, only those points have been plotted which contains Vsh less than 0.25 . In the Figure 4.8, few points plunge off from the sandstone line. These anomalies are further discussed in the section 4.2.

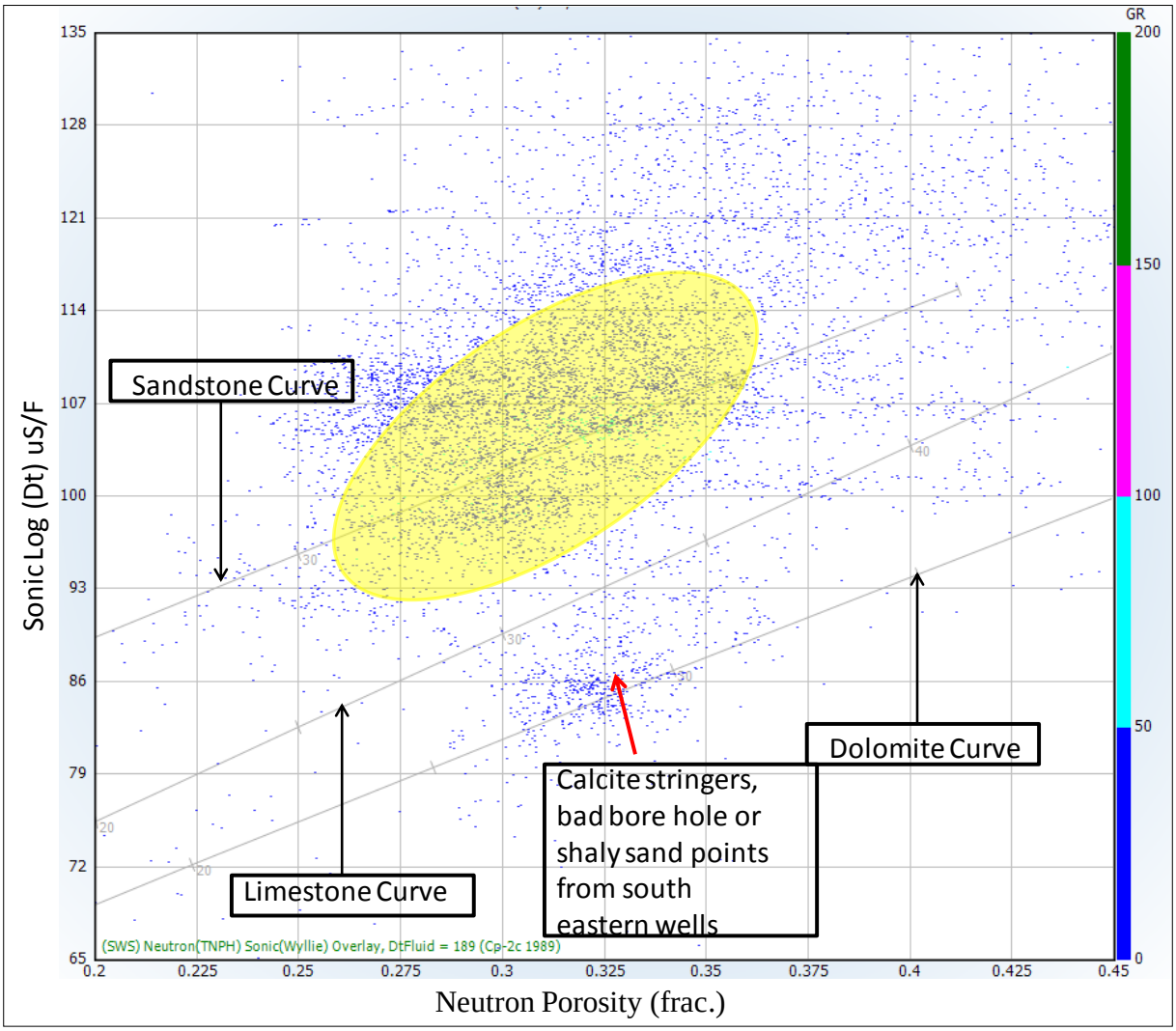

Figure 4.8 Crossplot of Neutron and Sonic logs. The data plotted here only from the reservoir formations of Balder, Hermod and Heimdal.

Shale content in reservoir rock

From the petrophysical analysis and literature (Norlex, 2013; NPD, Bulletin-5) it is clear that the three reservoir sandstones of Balder, Hermod and Heimdal Formations in the Balder field area contains interbedded sandstones and shales. The estimated volume of shale may helps to differentiate the sand and shale beds, which helps to mark the commercial reservoir intervals (Fig. 4.9). Further, all data points of shale volume from twenty five wells relative to the three reservoir fromations have been plotted in histogram. It is observed that the mean value is approximately 0.18 while the mode is 0.05. This simple yet informative histogram shows that the reservoir intervals have clean sandstone with only minor shale content (Rider and Kennedy, 2011). For further discussion, please see the section 4.2.

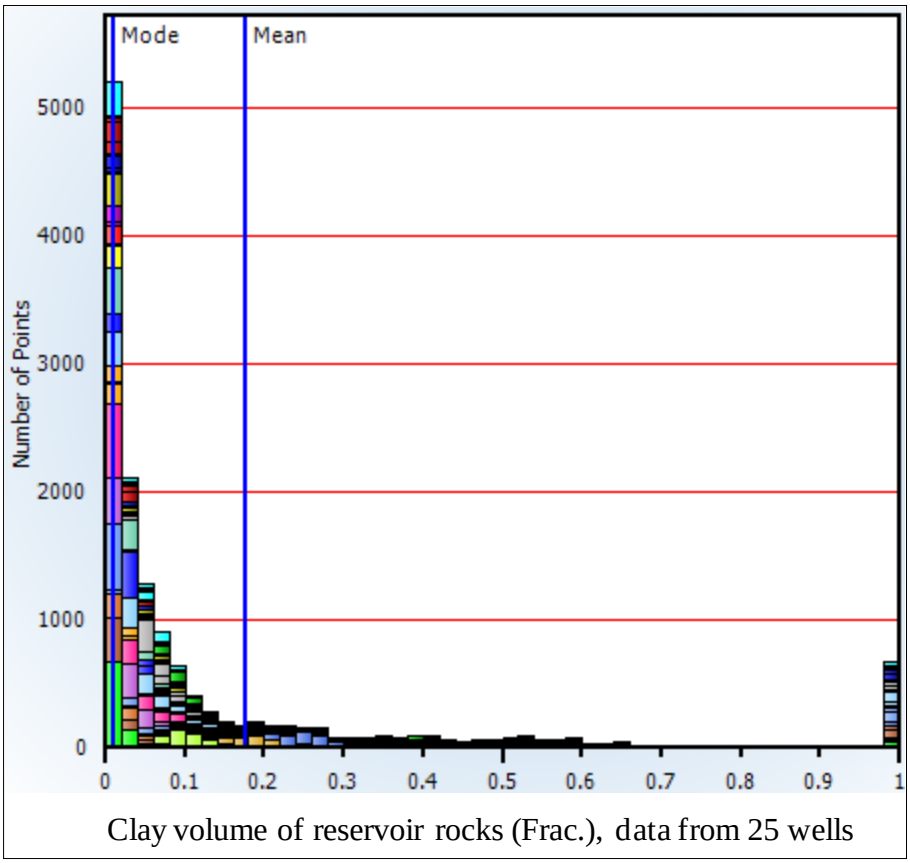

Figure 4.9 The Shale data points from 25 wells of three reservoir formations; Balder, Hermod and Heimdal.

Porosity in reservoir rock

Porosity is one of the fundamental parameters to define the reservoir quality. The porosity logs (Neutron, Density and Sonic) may give different values under varied lithologies. The porosity of reservoir rocks have been estimated and described further by standard methods (porosity prediction from neutron and density logs), as well as combination of two or three porosity logs to estimate average porosity and effective porosity. The single log porosity estimation, like porosity from neutron log overestimate the value in shales (Fig. 4.10, zone b), as they are more sensitive to the hydrogen index, which may present in shale/clay lithology as bounding water (Rider and Kennedy, 2011). The density value underestimate the value in shaley zone, even different value of matrix density have been used in calculation of density porosity as mentioned earlier in the chapter 3 (Fig. 4.10, zone b). The average values however provide better results (Fig. 4.10). The effective porosity indicates the connectivity of the pores. It may takes the account of the clay/shale effect from the values (Fig. 4.10, zone b), in clean sand intervals. Further, the effective porosity is almost zero in zone b (Fig. 4.10), as comapared to the zone a (Fig. 4.10), because shale dominates in the zone b (Rider and Kennedy, 2011).

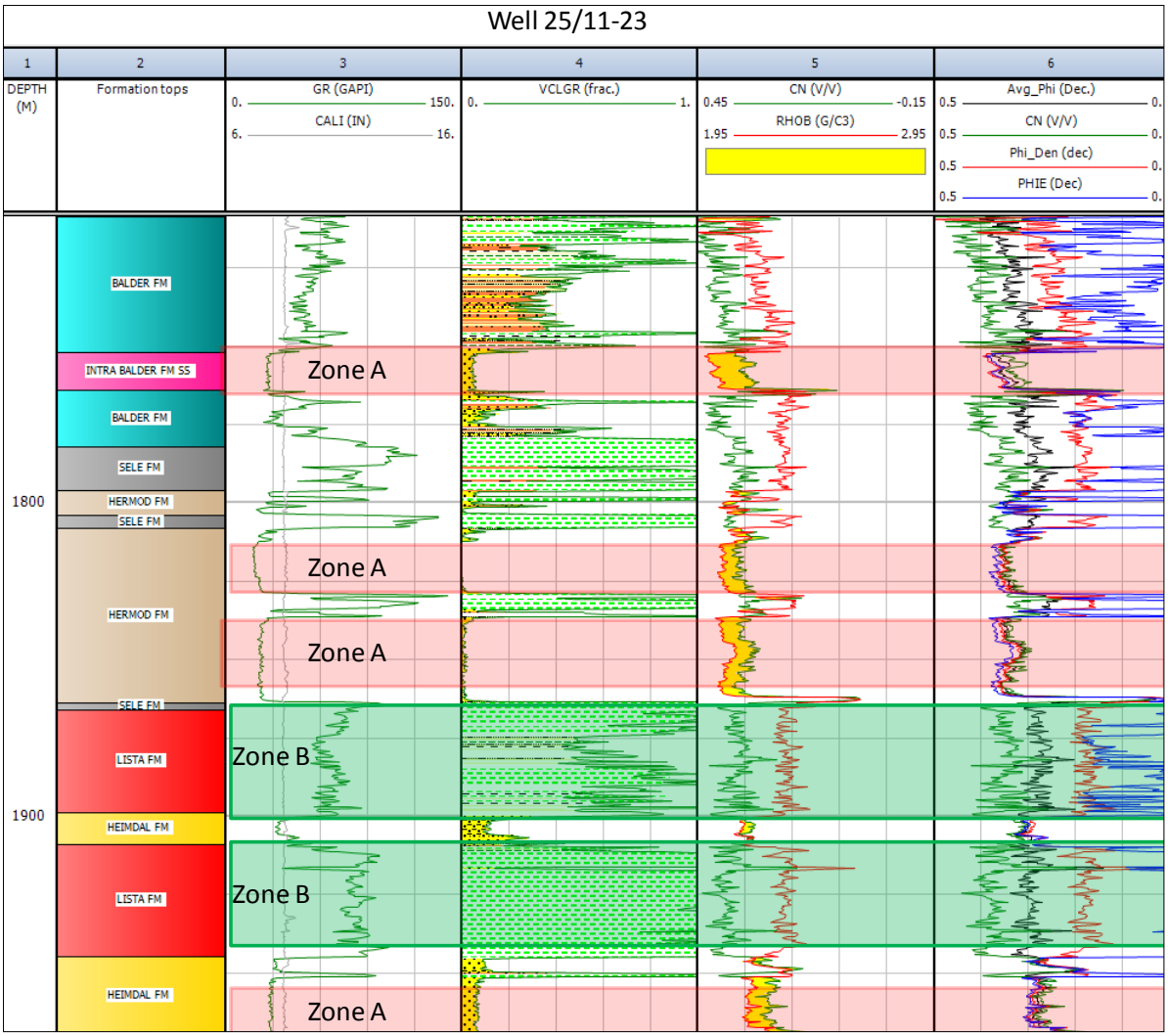

Figure 4.10 A composite log plot of the three reservoir formations showing variation of porosity in different zone.

For better understanding of the porosity values, all data points of average porosity from the seventeen wells of the three reservoir formations have been plotted in a histogram (Fig. 4.11). The mean value is 0.31 with the mode of 0.30 which show that the reservoir has decent porosity. For further discussions, please see the section 4.2.

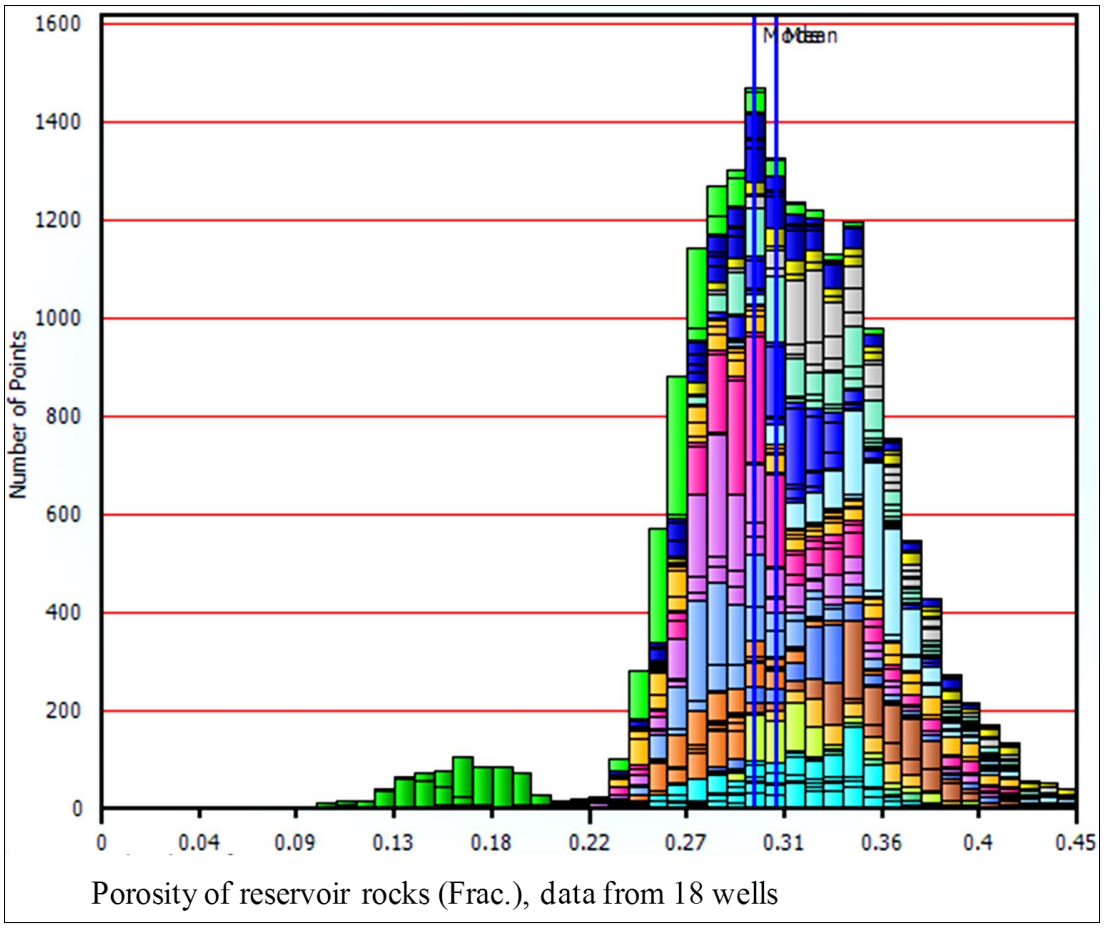

Figure 4.11 Histogram of porosity distributions in three reservoir intervals in the Balder field.

Hydrocarbon saturation in the reservoir rocks

In the petrophysical analysis to calculate hydrocarbon saturation the resistivity logs are the most important one. It may quite easy to separate the hydrocarbon saturated zone from the water saturated zone with the help of deep resistivity log (Fig. 4.12). The water saturation has been calculated after estimating the porosity and the volume of shale. On the basis of the water saturation, the hydrocarbon saturation have been estimated. In the reservoir interval highlighted by the red color, water saturation is in average between 0.1-0.2, which indicates that hydrocarbon saturation in this zone almost 0.8-0.9. The fully water saturated zone is highlighted by the light blue color in the Figure 4.12, while the hydrocarbon saturated interval highlighted by the red color. It may be observed in the Figure 4.12 that the shale barrier act as the cap rock for the reservoir rocks, which may stop the migration of relatively heavy hydrocarbons in the Balder field (Rider and Kennedy, 2011). For further discussion, please see the section 4.2.

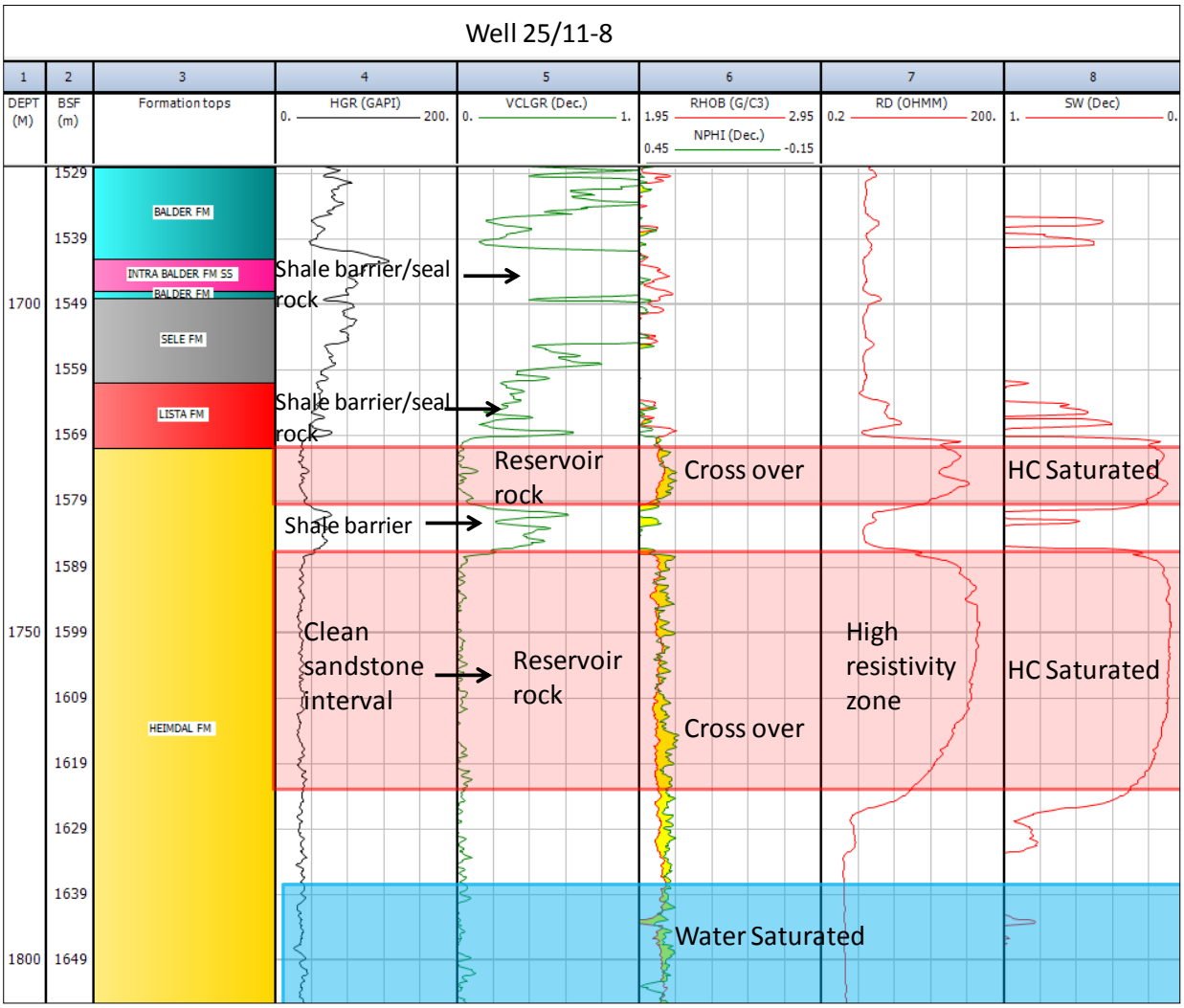

Figure 4.12 Well 25/11-8 log plot, hydrocarbon interval marked on the basis of deep resistivity log and water saturation values.

Calculations of N/G and pay thickness

After calculating basic parameter like porosity, volume of shale and water saturation the reservoir zones have been marked. Further a pay zone interval is estimated within the reservoir zones. At this step following cutoff limits are used, effective porosity 0.2, Vsh 0.3 and water saturation 0.3. For further discussion, please see the section 4.2.

The gross thickness of the Balder, Hermod and Heimdal formations, with net reservoir and pay zone intervals are shown in the Tables 4.1a, b and c respectively. The average porosity of the reservoir and pay zone with their water saturation percentage also calculated and presented in the tables.

Table 4. 1 a Shows, Balder Formation gross interval, reservoir thickness with net pay.

Well No.	Gross Interval (m)	Net Reservoir (m)	Net Pay (m)	Average Porosity % (Res. Zone)	Average Porosity % (Pay Zone)	Water Saturation % (Res. Zone)	Water Saturation % (Pay Zone)	Formation
25/10-1	36.1	25	0	25	N/A	96	N/A	Balder
25/10-2	40	13.75	0	22	N/A	95	N/A	Balder
25/10-3	58.37	25	1	25	28	85	30	Balder
25/10-4	38.5	21.4	0	25	N/A	99	N/A	Balder
25/10-5	87	58	0	27	N/A	80	N/A	Balder
25/10-8	47	34	0	25	N/A	87	N/A	Balder
25/11-1	80	70	3	28	33	85	25	Balder
25/11-2	66.14	43.13	1	26	32	89	25	Balder
25/11-3	35	9	0	33	N/A	100	N/A	Balder
25/11-4	78.75	43.25	0	30	N/A	86	N/A	Balder
25/11-5	62.79	9.14	0	22	N/A	90	N/A	Balder
25/11-6	41	8.23	1	25	34	86	38	Balder
25/11-7	44.2	15.7	6.4	30	32	37	25	Balder
25/11-8	44.04	8.84	0	29	N/A	66	N/A	Balder
25/11-9	98	25.25	25	36	36	40	12	Balder
25/11-10	42	13.56	0	21	N/A	100	N/A	Balder
25/11-11	58.38	14.13	0	28	N/A	66	N/A	Balder
25/11-12	54.88	18.25	0	24	N/A	100	N/A	Balder
25/11-13	66	23.63	1	24	30	80	27	Balder
25/11-15	14.17	2.74	0	25	N/A	65	N/A	Balder
25/11-16	33	5	0	25	N/A	96	N/A	Balder
25/11-17	59	0	0	N/A	N/A	100	N/A	Balder
25/11-18	16	5.8	0	21	N/A	99	N/A	Balder
25/11-20	12	0	0	N/A	N/A	N/A	N/A	Balder
25/11-23	83.06	20.42	15.24	31	33	17	9	Balder

Table 4.1 b Shows, Hermod Formation gross interval and reservoir thickness with net pay.

Well No.	Gross Interval (m)	Net Reservoir (m)	Net Pay (m)	Average Porosity % (Res. Zone)	Average Porosity % (Pay Zone)	Water Saturation % (Res. Zone)	Water Saturation % (Pay zone)	Formation
25/10-1	22	10	1	31	34	54	28	Hermod
25/10-3	27.5	27	0	35	N/A	96	N/A	Hermod
25/10-5	18	12	0	27	N/A	98	N/A	Hermod
25/11-1	22.25	22	0	33	N/A	96	N/A	Hermod
25/11-2	37.03	31.55	0	33	N/A	99	N/A	Hermod
25/11-4	24.63	23.25	0	35	N/A	96	N/A	Hermod
25/11-5	39.17	26.37	16	32	33	36	30	Hermod
25/11-9	30.5	0.5	0.4	35	35	34	39	Hermod
25/11-13	48.38	45.50	9	28	31	76	17	Hermod
25/11-23	67.67	54.79	1	34	21	93	7	Hermod

Table 4.1 c Shows, Heimdal Formation gross interval and reservoir thickness with net pay.

Well No.	Gross Interval (m)	Net Reservoir (m)	Net Pay (m)	Average Porosity % (Res. Zone)	Average Porosity % (Pay Zone)	Water Saturation % (Res. Zone)	Water Saturation % (Pay zone)	Formation
25/10-1	156	119	0	33	N/A	96	N/A	Heimdal
25/10-2	60.5	54.1	0	25	N/A	97	N/A	Heimdal
25/10-3	67.8	46.1	0	32	N/A	98	N/A	Heimdal
25/10-4	112	106	16	27	27	87	19	Heimdal
25/10-5	33.25	27.5	0	26	N/A	99	N/A	Heimdal
25/10-8	44	40	0	31	N/A	98	N/A	Heimdal
25/11-5	76.2	72.62	0	33	N/A	97	N/A	Heimdal
25/11-6	130.3	113.92	49	30	32	51	7	Heimdal
25/11-7	125.43	107.82	34.9	32	32	67	10	Heimdal
25/11-8	173.58	136.63	45	33	34	66	13	Heimdal
25/11-9	6.5	0	0	N/A	N/A	N/A	N/A	Heimdal
25/11-10	157	141	0	26	N/A	100	N/A	Heimdal
25/11-11	141.25	132.81	25	27	28	77	12	Heimdal
25/11-12	104.75	86.56	0	28	N/A	100	N/A	Heimdal
25/11-13	4.13	1.63	0	23	N/A	100	N/A	Heimdal
25/11-15	63.86	45.8	38.25	25	26	24	15	Heimdal
25/11-16	104	87	17.68	33	35	71	10	Heimdal
25/11-18	56	55	39.85	29	32	31	11	Heimdal
25/11-23	25	22.71	0	28	N/A	98	N/A	Heimdal

Facies interpretation of reservoir formations

The three potential reservoir formations present in the study area are Balder, Hermod and Heimdal formations. These reservoir formations are deposited in the different geological age, hence their depositional environment also varies, which result in a difference of the vertical thickness and horizontal distributions of the rocks. In the Figure 4.13, finning and coarsening upward trends are marked on the basis of the gamma ray log. The mound features also marked by utilizing the gamma ray log with the geological model of the Balder field, proposed by Breidis et al., 2007. It can be observable in the Figure 4.13 that most of the sand units pinch out in eastern wells. The geological model also illustrate that the deposition of the relatively young Paleocene reservoir rocks are controlled by the depositional pattern of the older formations (Breidis et al., 2007; Martinsen et al., 2005).

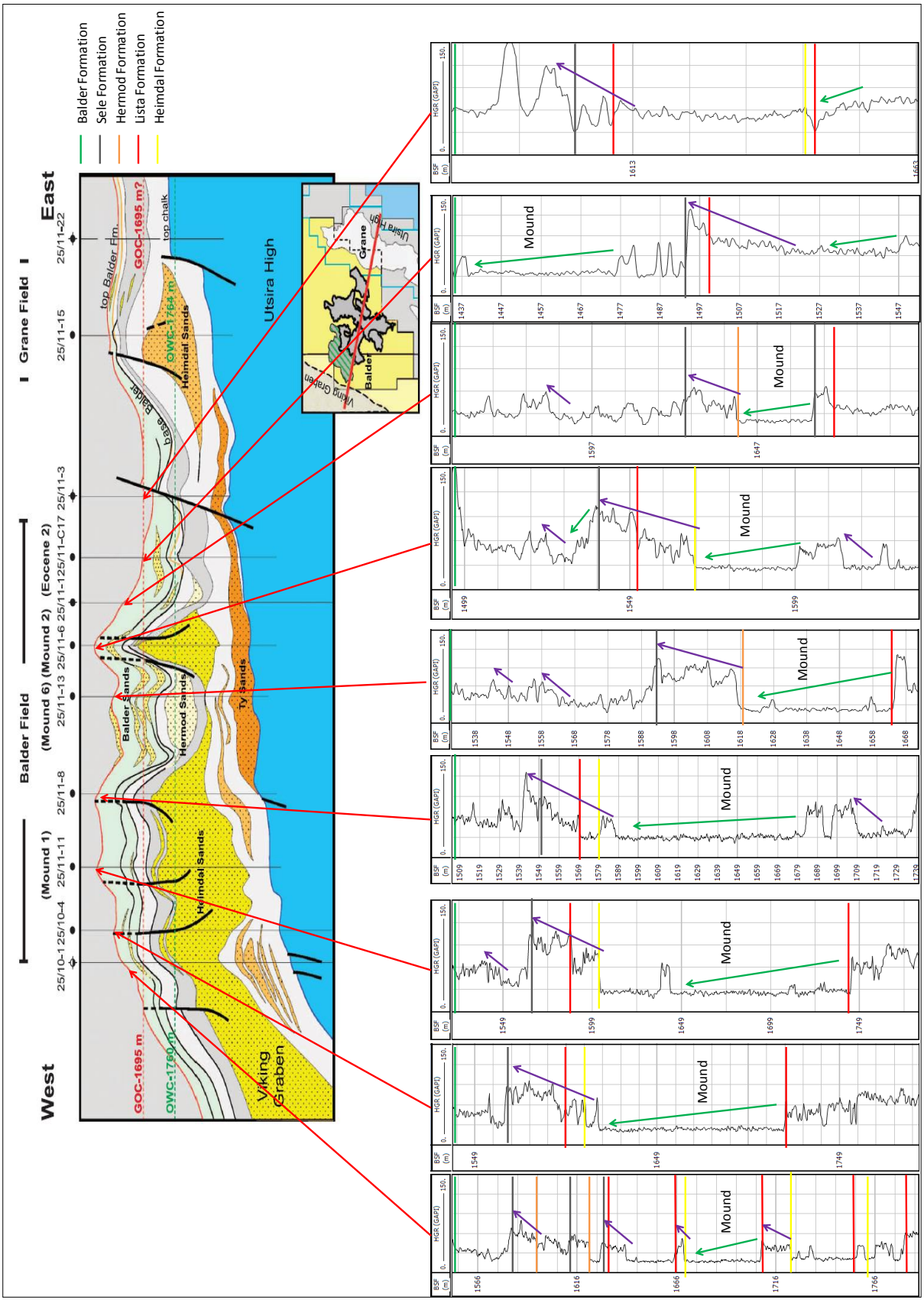

Figure 4.13 Gamma ray response of studied well at different stratigraphic position (modified after Briedis et al., 2007).

The facies distribution also varies due to the varying geological event during their deposition. The facies are interpreted by using the wells log, but due to the limitation of other resources (e.g seismic data), the results may contain some errors. In this part of the analysis three wells are selected from the geological model (Fig. 4.13) for better understanding of the depositional environment. In Figures 4.14, 4.15 and 4.16 different facies have been marked on the basis of the gamma ray and sonic log response. The lower boundary and upper boundary also marked on the basis of the gamma ray and sonic logs.

In the Figure 4.14, the Heimdal Formation plotted from the well 25/11-8 only for the gamma ray and the sonic log data. The upper boundary can be easily picked on the basis of sharp change of the low gamma ray log and high sonic velocity of the Heimdal Formation into the high gamma ray log and low sonic velocity of the Lista Formation. Similarly the lower boundary may be easily picked on the basis of the sharp change of high gamma ray log and low sonic velocity of the Lista Formation into the low gamma ray log and high sonic velocity of the Heimdal Formation (Norlex, 2013; Sarg and Skjold, 1982). It may be interpreted from gamma ray and sonic log response that the Facies 1 has more clay and the Facies 2 has more cleaner thick sands (clean gamma ray trend). It is more likely the mound, as its thickness almost reaches 80 m. The Facies 3 has interbedded claystone and shale deposits (Milton and Emery, 2008). For further discussion, please see the section 4.2.

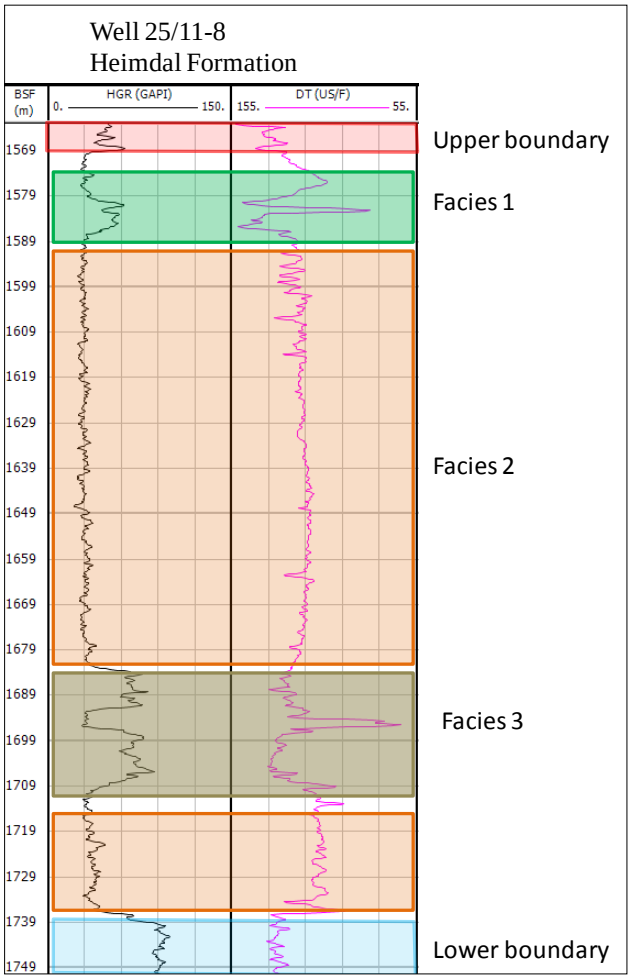

Figure 4.14 The Heimdal Formation, upper and lower boundary with three distinct facies identified based on the gamma ray and sonic log responses.

In the Figure 4.15, the gamma ray and sonic logs responses of the Hermod Formation plots from the well 25/11-13. The upper boundary may be easily picked on the basis of the sharp change of low gamma ray log and the high sonic velocity of the Hermod Formation into high gamma ray log and low sonic velocity of the Sele Formation. Similarly, the lower boundary can be easily marked on the basis of the sharp change of high gamma ray log and low sonic velocity of the Sele Formation into the low gamma ray log and the high sonic velocity of the Hermod Formation (Norlex, 2013; Sarg and Skjold, 1982). The two distinguish facies have been marked on the basis of the gamma ray and sonic log response. The Facies 1 has clean thick sandstone bed (low gamma ray trend), which more likely a mound, as it is almost 37 m thick. The Facies 2 has clay content, increases in the lower part of the formation (Milton and Emery, 2008). For further discussion, please see the section 4.2.

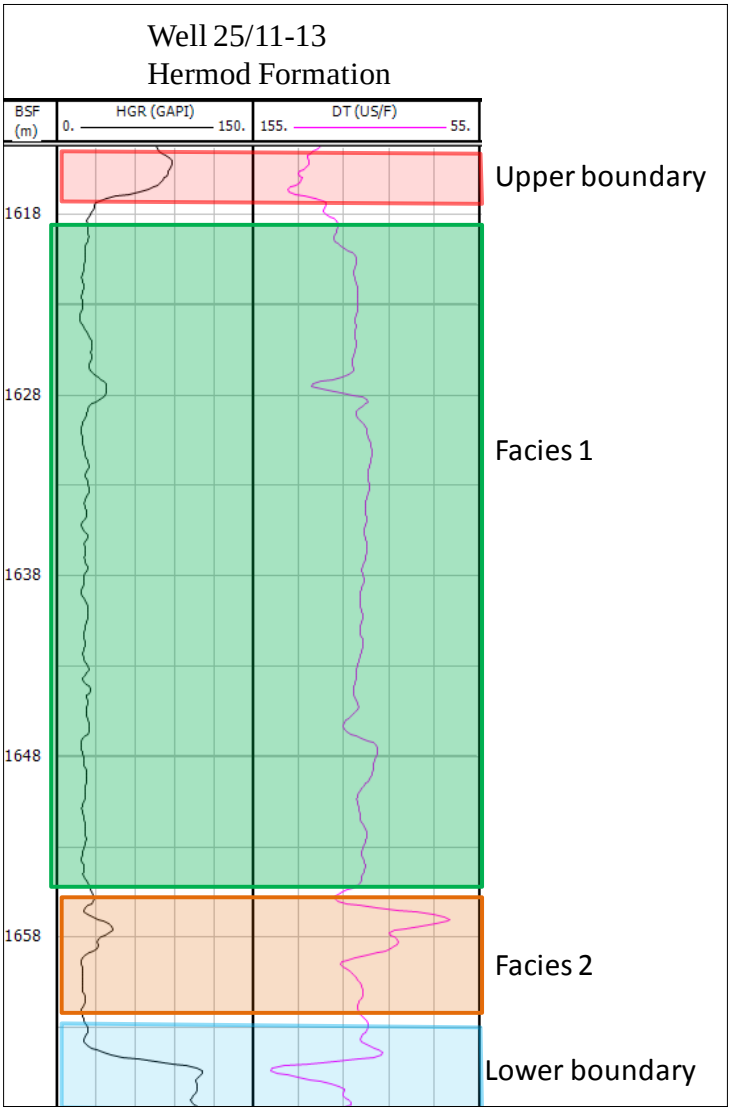

Figure 4.15 Hermod Formation, upper and lower boundary marked on the basis of gamma ray and sonic logs. Two distinguish facies also marked in the Hermod Formation.

In the Figure 4.16, the gamma ray and sonic log responses of Balder Formation is plotted from the well 25/11-6. The upper boundary may be easily picked on the basis of the high gamma ray log and low sonic velocity. The lower boundary may also be marked on the basis of sharp change of high gamma ray value and low sonic velocity of the Sele Formation into the low/intermediate gamma ray value and high sonic velocity of the Balder Formation

(Norlex, 2013; Sarg and Skjold, 1982). Three distinguish facies have been marked on the basis of the gamma ray and sonic log responses.

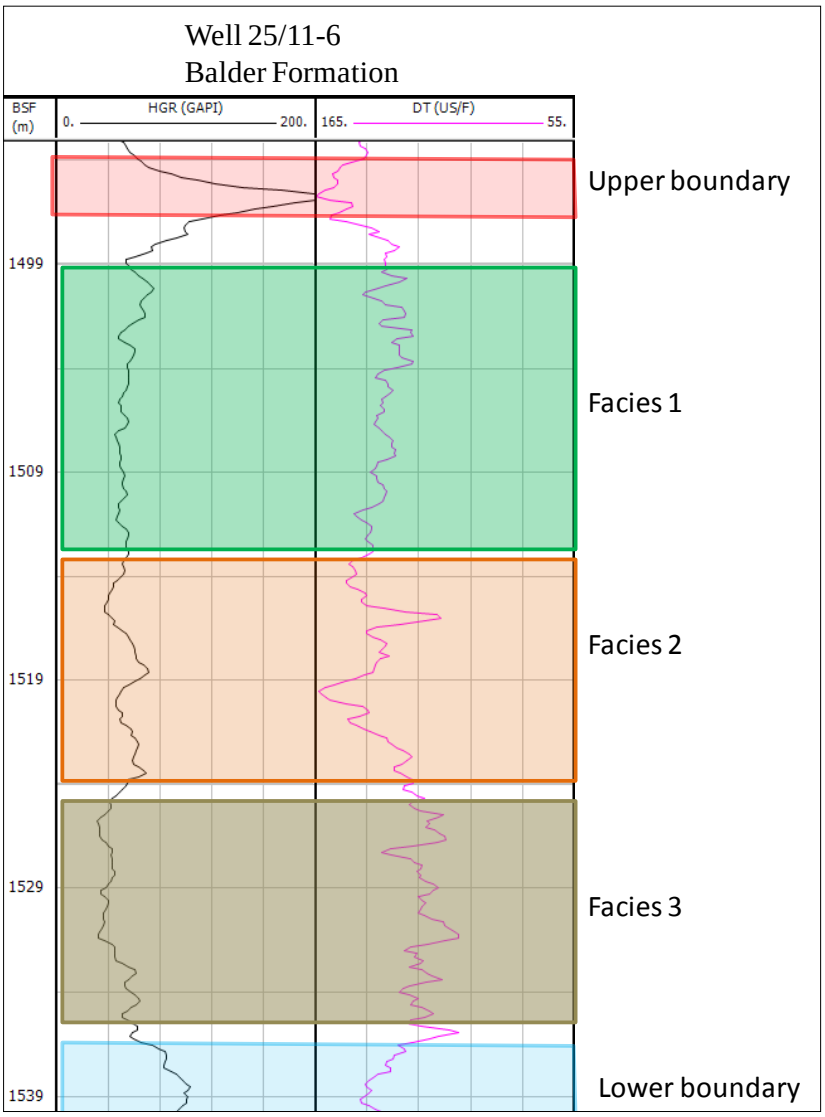

Figure 4.16 The Balder Formation lower and upper boundary marked on the basis of gamma ray and sonic log. Three different facies are identified in the Balder Formation.

The Facies 1 has clean thick sandstone bed (clean gamma ray trend), which more likely a mound. The Facies 2 contains the varying content of clays, which may show the variation in depositional environment. The facies 3 has more clay content with low sonic transit time, which may indicate more compaction (Milton and Emery, 2008). For further discussion, please see the section 4.2.

4.1.1.3 Cap rocks

Correlation of cap rocks

In the study area three formations i.e. Balder, Sele and Lista are acting as the seal/cap rocks. The thickness of these formations varies in the study area. The Balder Formation is also acting as the reservoir, but it has thick intervals of shale units as well. These intervals are impermeable enough to hold the hydrocarbons. The Sele and Lista formations acting as the

seals for the Hermod and Heimdal formations respectively. These cap rocks thin out in the eastern wells (Fig. 4.17).

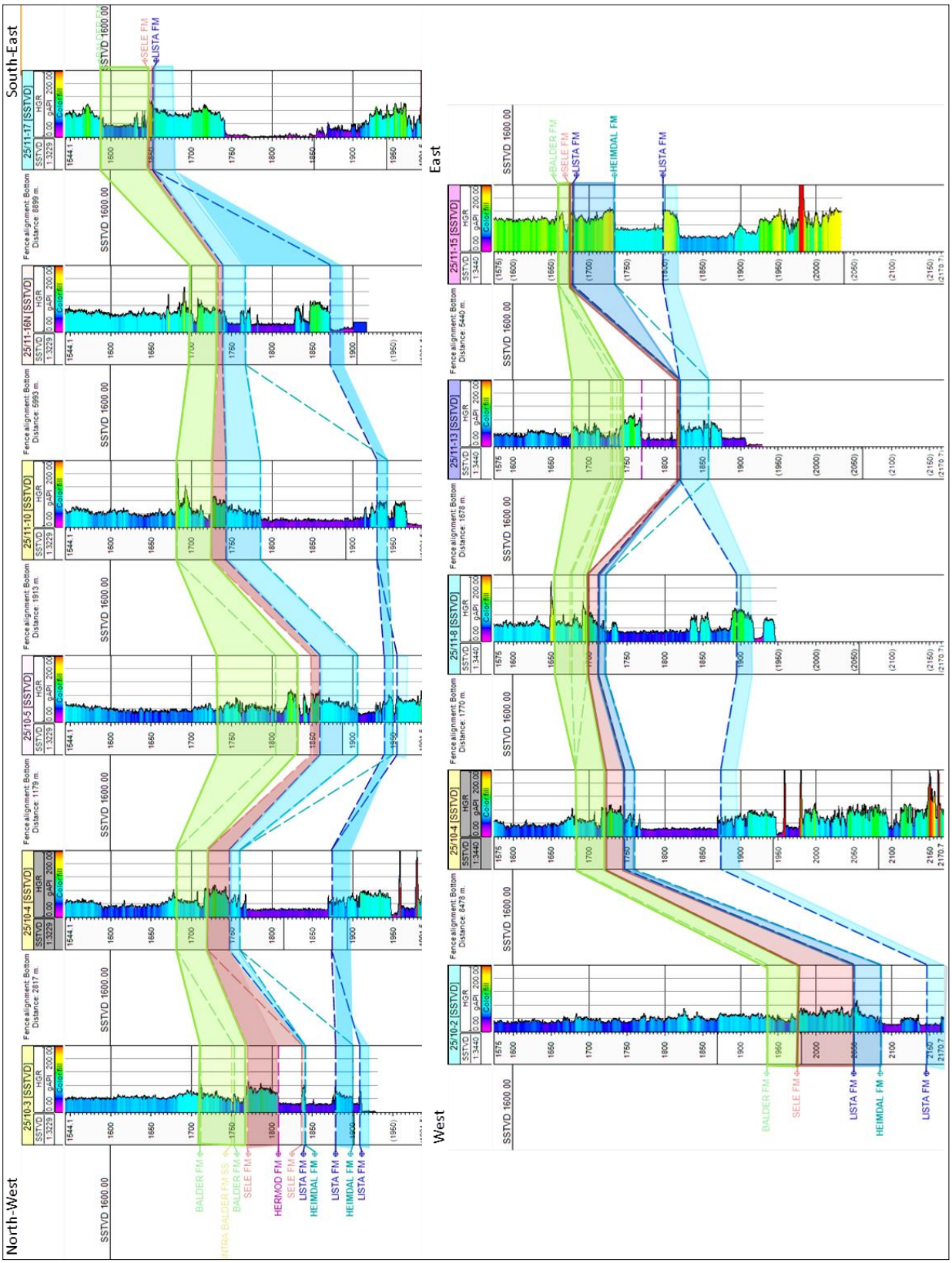

Figure 4.17 The correlation of cap rocks, the Balder (Light green polygon), Sele (Light brown polygon) and Lista Formations (Light blue polygon).

Identification of cap rocks

Cap rocks can be marked on the well log data. For better understanding and evaluation of the cap rocks through well logs, the gamma ray, sonic, resistivity and bulk density logs have been plotted together (Fig. 4.18). The gamma ray values increase within the cap rocks, which may lead to high clay volume within the formation. The high shaly zone is highlighted by the green box (Fig. 4.18). In this zone no distinctive crossover of the density and neutron log can be observed. The deep resistivity value is very much less in cap rocks as compared to the reservoir and source rocks. The reservoir section saturated with hydrocarbon is marked by the yellow color. In reservoir zones distinctive crossovers of density and neutron logs can be seen. The resistivity values are much higher, which indicate that this section may saturated with hydrocarbons. Water saturated zone marked by the blue color on the basis of low resistivity value (Rider and Kennedy, 2011). For further discussion, please see the section 4.2.

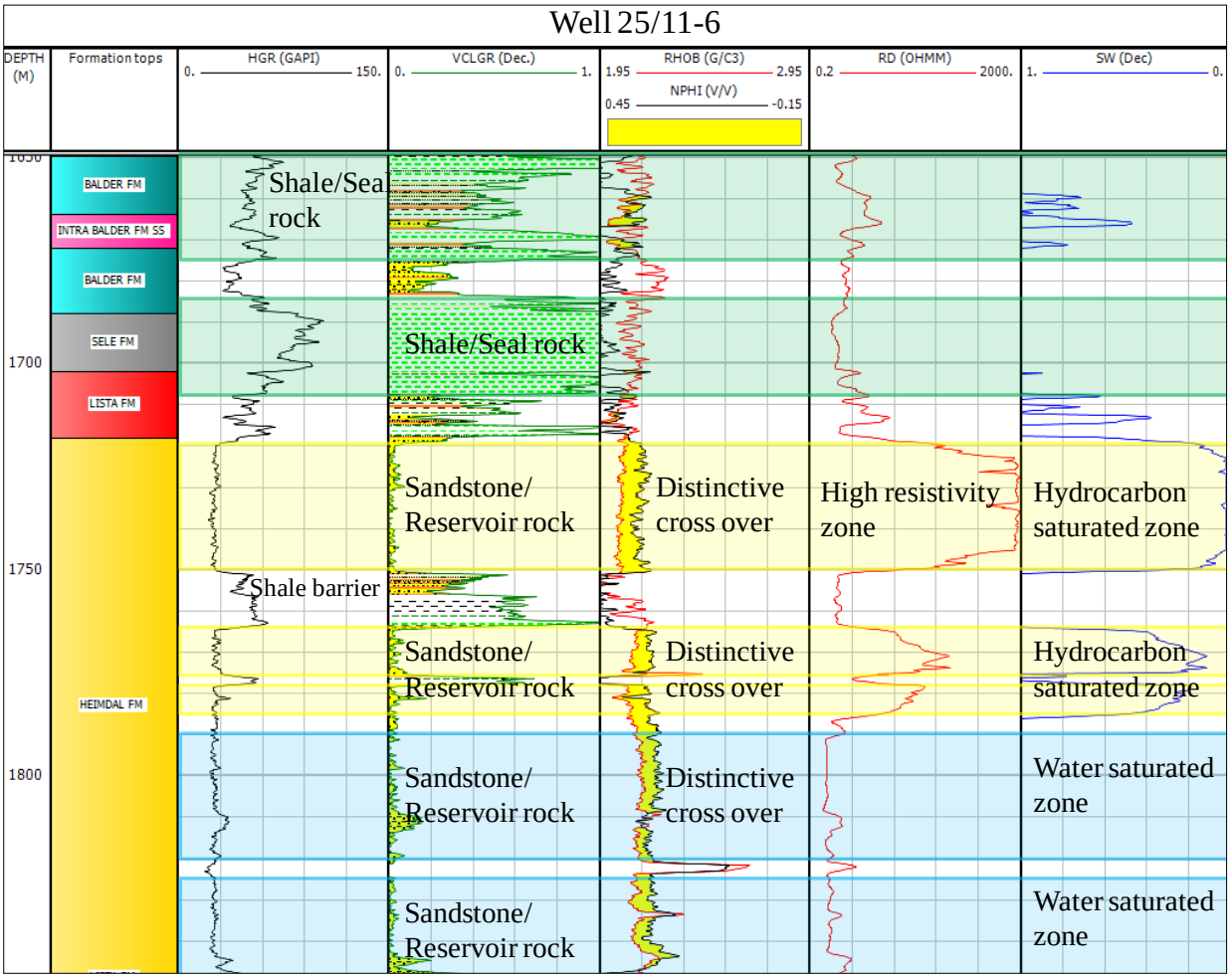

Figure 4.18 The log plot of 25/11-6 showing different reservoir sections (yellow color) and effective cap rocks (green color).

Clay content in the cap rocks

The Balder field cap/seal rocks belong to the Balder, Sele and Lista formations (Norlex, 2013; NPD, Bulletin-5). The estimated shale volume help to mark these intervals. For better understanding these data points have been plotted in the histogram (Fig. 4.19). It may be seen that the mean value is approximate 0.6, with mode of 0.9. This simple yet informative histogram shows that the seal/cap intervals have high amount of shales with very less sand contents. For further discussion, please see the section 4.2.

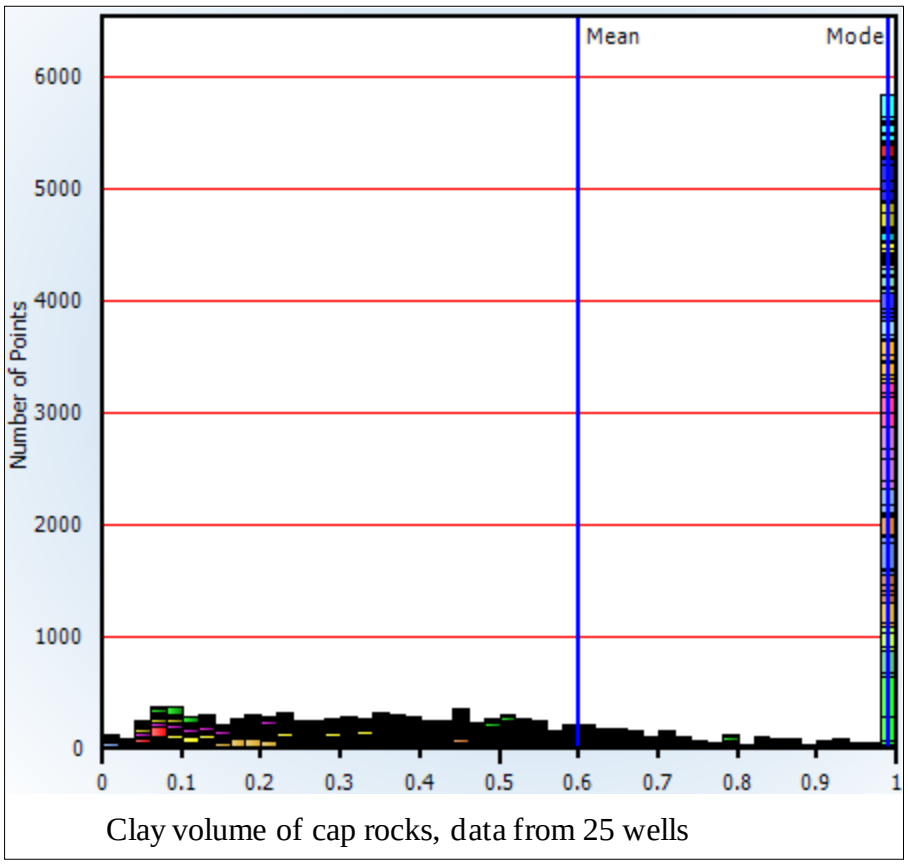

Figure 4.19 Histogram display clay volume in the cap rocks, data points plotted from the cap rocks from all 25 studied wells.

Porosity in the caps rocks

In the cap rocks, it is better to calculate and observe the effective porosity. As the effective porosity indicate that how the pores are connected and whether there have enough network of pores to transmit the fluids or not (Rider and Kennedy, 2011). For this purpose, effective porosity have been plotted in histogram from the three caps rock formations. It can be seen in the Figure 4.20 that the mean value of porosity is almost 0.13, with the mode is 0.01. It may indicate that the cap rocks are impermeable for hydrocarbon migration. For further discussion, please see the section 4.2.

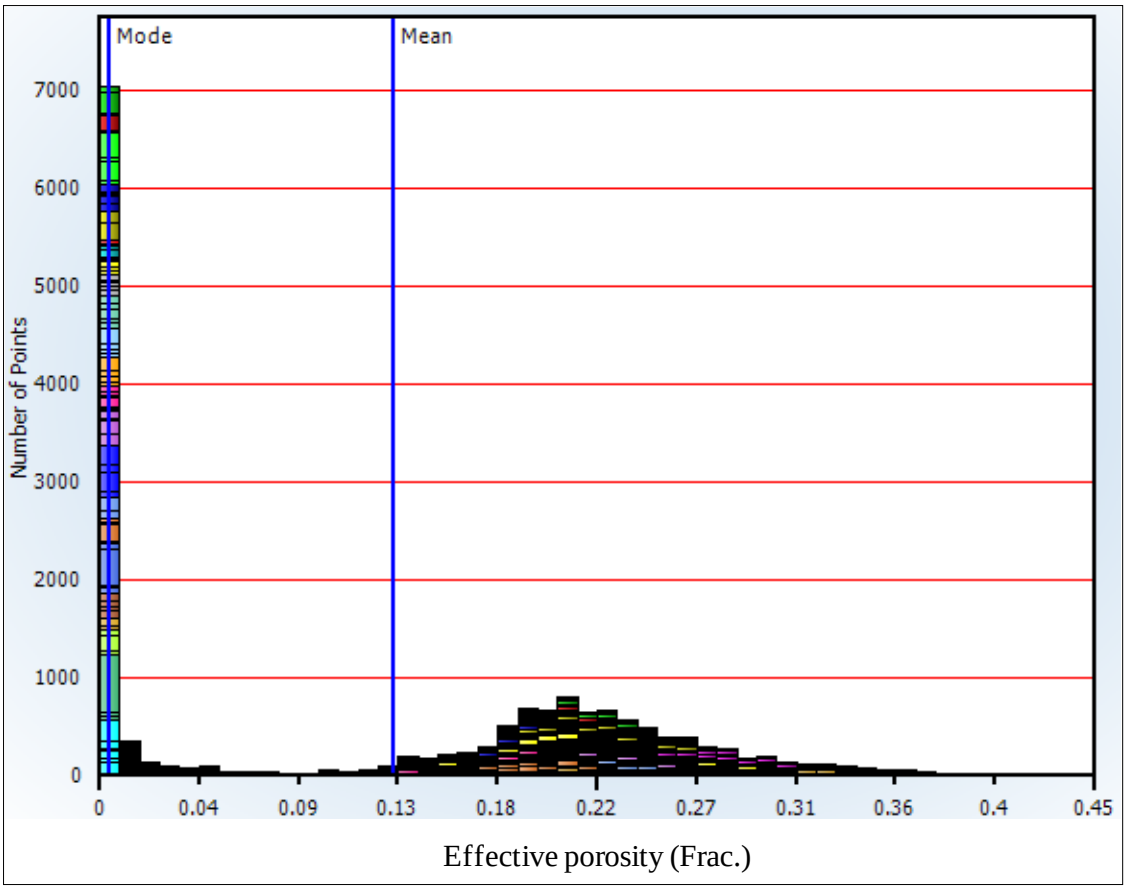

Figure 4.20 Histogram display effective porosity data points from the three cap/seal formations i.e. Balder, Sele and Lista formations (Data points from nineteen wells).

4.2 Discussions (identification of the petroleum system in the Balder area)

4.2.1 Source rocks

In general, source rocks are composed of three main components i.e. rock matrix, solid organic matter and fluids filled in the pore spaces. The source rock is easily identifiable by high gamma ray response (Fig. 4.1) and higher content of shale as shown in the histogram in the Figure 4.3 (Beers, 1945; Fertl and Chilingar, 1988; Hinds and Berg, 1990; Keym et al., 2006; Passey et al., 1990; Schmoker, 1981). The presence of organic matter within the rock can be detect by the spectral gamma ray log, which contains the information of the uranium, potassium and thorium as the organic-rich intervals (dark organic rich shale) have high spectral gamma ray values (Fig. 4.2) (Fertl and Rieke, 1980; Fertl and Chilingar, 1988; Soto et al, 2010; Supernaw et al., 1978; Swanson, 1960; Passey et al., 1990). This high organic content also illustrates that the environment of deposition was calm and anaerobic, as gamma ray response showed fining upward trend in these intervals (Brooks et al., 1987; Fertl and Chilingar, 1988; Milton and Emery, 2008). It may have deposited in restricted bottom circulation in marine environment (Keym et al., 2006; Norlex, 2013). The higher uranium values also illustrate that the environment of deposition is reducing, which could be deep marine. The reducing conditions are ideal for the deposition and accumulation of uranium with organic material, as solubility of uranium is much more in sea water as compared to fresh water. (Bjørlykke and Jahren, 2010; Fertl and Chilingar, 1988; Yang et al., 2010). In the Figures 4.1 and 4.2, the clear separation between the resistivity and sonic log indicate the maturation level of the source rock, as the source rocks contain the significant amount of the

organic matter. The source rocks contained kerogen, which is soft as compared to surrounding matrix (sonic log transit time increases in soft lithology) (Brooks et al., 1987; Dellenbach et al., 1983; Fertl and Chilingar, 1988; Hinds and Berg, 1990; Passey et al., 1990; Peters and Cassa, 1994; Storvoll et al., 2005). The bulk density log detects the less dense intervals, which may constitute of organic material as the common density of organic material is 1.05 g/cm^3, as compared to the surrounding rocks, which may have 2.5 g/cm^3 density. The neutron logs give very high values, which indicate the high hydrogen index may be present in the kerogen as hydrocarbons (Fertl and Chilingar, 1988; Hinds and Berg, 1990; Meissner, 1978; Murray, 1968; Nixon, 1973; Passey et al., 1990; Schmoker, 1979).

Moreover, all these indicators discussed above illustrate that the source rock may deposited in the marine environment, which can produced more oil than the gas as the marine source rock have high hydrogen/carbon ratio (Brooks et al., 1987). The interpretation on the well logs indicate that this interval of source rock (High gamma ray log) may deposited in sediment starved basin (accumulation of organic matter and clay deposition) (Milton and Emery, 2008). These starved basin condition indicates that the accommodation space may increased rapidly due to the rifting and transgression phase (Cornford and Brooks, 1989; Faleide et al., 2010). This may lead depletion of the clastic sediments supply. Further, the restricted bottom water circulation leads the anoxic conditioned prevailed. These conditioned may lead the deposition and accumulation of the organic rich shale with laminated clays. Further, thick condensed section indicate the basin deepning (rise of sea level), which may be due to the rifting or climate changed (Cornford and Brooks, 1989; Dawers et al., 1999; Nøttvedt et al., 2000). In well 25/10-4, a thick sandstone interval of 19 m is also encounter in the western part of the field. This thick deposit of the sandstone may indicates the submarine fan channel deposits. The deposition and presence of the sandstone body in such a high gamma ray intervals indicate the forced regression period. It can be interpreted that as in rift basin setting, the source of these sandstone can be from the flank of the basin during the low stand period. (Myers and Milton, 2008; Isaksen and Ledje, 2001; Nøttvedt et al., 2000). Further, the focus of this study is not on the Jurassic sandstone, so further discussion and comments are not possible, without more detailed study. Other than that the Intra Draupne sandstone only encountered in one well, which are under consideration, so commenting and discussion on such a limited data, will also put lot of uncertainty. It is also not suitable to construct the effect of the deposition of this sand deposit in the organic rich shale only from the well log data analysis.

4.2.2 Reservoir rocks

Formation evaluation

In petrophysical analysis, there are number of ways by which reservoir lithology may be determined. The gamma ray log may be helpful to determine the shale and sand intervals. The low gamma ray indicates sandstone intervals, while the high gamma ray indicates the shale intervals. But, it is difficult to estimate how much carbonates intervals are present in the reservoir rocks, as these intervals can not be clearly detectable on the gamma ray log. In these kinds of situation density-neutron-sonic cross-plots (Fig. 4.7 and 4.8), somehow is much better approch to predict the type of matrix lithology (Rider and Kennedy, 2011). The overlay lines by the Schlumberger (IP) and Wyllie (1956) are very useful to estimate the carbonates amounts in sandstone lithology, but still in these kinds of plots there are large uncertainities, as only clean sandstone data is rare. Other then that bad borehole conditions may disturbed the log measurements of the neutron-density-sonic logs. Furthermore, most of these reservoir

intervals are saturated with the hydrocarbon, which can influenced the neutron log as well as density and sonic log responses. On these cross-plots some of the data, which are not influenced by the bad borehole, hydrocarbon or shale effect, can be from the stingers of calcites, which are ocassionally present in these reservoir formations especially in the Balder Formation (Norlex, 2013; Rider and Kennedy, 2011; Sarg and Sjold, 1982). But majority of these data point fall on the sandstone line, which indicate that the main part of the reservoir rocks belong to the sandstone lithology with good reservoir quality (porosity and permeability). The other uncertainty of density-neutron-sonic logs are already pointed out in the chapter 3.

Further, evaluation of these reservoir formations, a histogram is utilized to determine the shale quantity (Fig. 4.9). The histogram (Fig. 4.9) clearly indicates that most part of these formations belong to the clean sandstone intervals. There are few shaly intervals which may act as the barrier between different reservoir sections. Moreover, water saturation is one of the important parameter to mark the hydrocarbon intervals in the reservoir rocks. The reservoir intervals, where water saturation is less indicate that these zones may be filled by the hydrocarbons (Fig. 4.12). The interpretation can be confirmed by the high resistivity values present against these intervals as the hydrocarbon zone have high resistvity values. In the Figure 4.12, it can also be observed that shales make the barriers within the reservoir formations, which may control the hydrocarbon saturation. It can be interpreted here that these shale barriers are less permeable (Rider and Kennedy, 2011).

Porosity, Vsh and water saturation are the fundamental parameters for the reservoir characterization. On the basis of these parameters reservoir zone and net pay thickness can be estimated. In this study different cutoff limits are used. For the effective porosity 0.2 cutoff is used as it is assumed here that below that value the permeability will be much lower and hydrocarbons cannot be extracted efficiently. For the Vsh 0.3 cutoff value is used and it assumed that only the sandstone intervals are good for hydrocarbon production and above the limit permeability of reservoirs may not be that good for economic point of view. Further, for water saturation 0.3 cutoff value is used to separate the oil/gas bearing zones from the water saturated zones. It is assumed that above this limit the production of water will be much higher as compared to hydrocarbon and it would not be economically feasible. Furthermore, N/G are marked on the basis of these cutoff parameters (Tables 4.1 a, b and c) (Haynes et al., 2000; Li et al., 1997; Rider and Kennedy, 2011; Shepherd, 2009). Average porosity and water saturation is also marked. Other than that, if the information from the Figure 4.5 collaborate with the Table 4.1, it gives the better idea where the good quality sand intervals can be found. The Paleocene-Eocene reservoir intervals at the Balder field contains 80% net reservoir of good quality permeable sandstones. These reservoir intervals are well sorted, fine to medium grains thick sand deposits (Ostvedt et al., 1990; Sarg and Skjold, 1982).

Furthermore, the Balder field has regional oil water contact at 1760m (Bergslien, 2002). The reservoir sands which are below this depth filled with the water and those reservoir sands unit which lies above this depth may partially to fully saturated with the oil/gas. This is the main reason that good intervals of reservoir sands which have been mentioned in Tables 4.1 a, b and c are not filled with the hydrocarbons and have zero net pay intervals.

Well log interpretation

The well log analysis illustrates that the reservoir and cap rocks may depsoited during the regression and transgression cycles respectively. These cycles illustrate that during the regression phase, the siliciclastic input (sand deposition) dominates (Myers and Milton,

2008). These cyclic deposits can be associated with the regional upliftment caused by the Icelandic plume (Nadin et al., 1997). The erosion of uplifted basin margins cause the siliciclastic deposition in the basin. Further, may be climatic control or basin subsidence increase the sea level, which may initiate trangression cycle. During transgression period, clay dominated formations deposited as well, which act as the cap/seals rocks in the area (Faleide et al., 2010; Kjennerud et al., 2001; Martinsen et al., 2005). The main process of the transportation of reservoir sediments from flanks to the basin may due to the gravity flow deposits associated with the submarine fan system/turbidites, as the thick sand intervals can be observed on the well logs (Bergslien, 2002; Fitzsimmons et al., 2005; Shell, 1982; Kjennerud et al., 2001; Wild and Briedis, 2010).

The Heimdal Formation overlies the Lista Formation. It is overlain by the younger rocks of the Sele Formation. Heimdal Formation is deposited as thick sandstone unit mainly as sandy debries (Bergslien, 2002). Heimdal Formation's gamma ray response (Fig. 4.10) of coarsening upward indicates that formation is dominated by the sandstone lithology. The thick deposit of the sands like mounds indicate that it may be deposited as submarine fan lobe of deep marine environment (Figs. 4.5 and 4.10). It may also indicates that these are the submarine fan channel deposits (Myers and Milton, 2008; Norlex, 2013; NPD bulletin-5; Sarg and Skjold, 1982). The deposition of the Heimdal Formation is mainly influenced by the complex depositional pattern of the Ty Formation (Guargena et al., 2007). The massive sand deposits marked as mound in the Figures 4.5 and 4.10 may prograded as sub-marine fan in southeastward direction. These sand-rich deposits pinchout in eastern and southern wells (Fig. 4.10). The three facies can be observed from gamma ray log. The Facies 1 contains shale beds, but from the sonic log it may also indicate that this unit contained the small laminated bed of sandstone as well. It may be deposited as the turbiditic shale (Bergslien, 2002; Fitzsimmons et al., 2005). The Facies 2 show boxcar trend, which indicates that it may have contained coarser sediements like sandstone (80 m of thick sandstone interval in well 25/11-8) with sharp upper and lower boundaries. The clean gamma ray trend indicates that this unit contains well sorted sediments with minor amount of clay and can be graded as clean sandstone intervals (Myers and Milton, 2008). It also indicates that sediments were moderately sorted before transportion and deposition in the study area (the distance between the proposed source area East Shetland was ~100 km during the deposition of reservoir sandstones (Ostvedt et al., 1990; Sarg and Skjold, 1982). This facies may be deposited as the sandy debrites (Bergslien, 2002; Fitzsimmons et al., 2005). The Facies 3 contains thinner sandstone bed (approximate 2 m thick) interbedded with shale units. The decreasing tendency of the sonic transit time indicates that this sandstone bed is well laminated. This facies can be graded as sandy turbidite (Bergslien, 2002; Bergslien et al., 2005; Fitzsimmons et al., 2005; Okiotor and Imasuen, 2011; Ostvedt et al., 1990; Shell, 1982; Torsvik et al., 2002; Wach et al., 2000).

Hermod Formation's gamma ray response (Fig. 4.10) of coarsening upward (cleaning upward) indicates that the formation is dominated by the sand lithology. The thick deposits of the sand like mounds indicates that it may be the lobe depsoit, which is the part of the submarine fan system (Myers and Milton, 2008). Hermod Formation deposited in lows and along the flanks of prextisting topography (Figs. 4.5 and 4.10) (Bergslien, 2002; Fitzsimmons et al., 2005). Gamma ray and sonic log boxcar trend indicate that the Facies 1 may contain thick deposits of coarser sediments i.e. sandstone. It can also be observed that this unit contained less amount of clay, which indicate the well sorted sediments. It may be deposited as the sandy debrites (Bergslien, 2002; Fitzsimmons et al., 2005; Myers and Milton, 2008). In the Facies 2, gamma ray indicates the increase of the clay content as well as sharply decrease

of the sonic transit time. This indicate the laminated bed, which may be part of the turbiditic shale sequence (Bergslien, 2002; Fitzsimmons et al., 2005; Okiotor and Imasuen, 2011; Shell, 1982; Wach et al., 2000).

Further, different sequences of the coarsening and fining upwards are marked on the basis of gamma ray log in the Balder Formation (Fig. 4.10). The finning upward sequences in the Balder Formation may indicate the deccrease of sand input. It may also indicate the calm and deeper marine environment. These fining upward trends indicate the shale lithology domination. Further these coarsening upward sequence and the blocky (boxcar) nature of the gamma ray indicates that sandstone intervals (marked as mound in the Balder Formation; Figs. 4.5 and 4.10) deposited as turbidite deposits with the hemipelagic sediments input (ash deposits) (Bergslien, 2002; Bergslien et al., 2005; Molyneux et al., 2002; Myers and Milton, 2008; Norlex, 2013; Timbrell, 1993). The lateral variation of these mounds also indicates that the older formation may be controling the depositional pattern of the Balder Formation (Martinsen et al., 2005; Timbrell, 1993). During the deposition of Balder Formation, it avoided the structurally high area (mounds) and deposited in the lows (Fig. 4.6a) (Guargena et al., 2007). The Balder Formation overlies the Sele Formation. The three facies have been marked on the basis of gamma ray response. The Facies 1 has high gamma ray and low sonic velocity response which may indicate the shale deposition. This facies may be deposited as the hemipelagic sediments (Bergslien, 2002). It also indicate that, this facies may be deposited during the transgressive phase with less clastic input in the basin. It is also indicated that these sequences may have deposited during high system tract (Myers and Milton, 2008). The Facies 2 may be belonged to the turbiditic shale deposits (Bergslien, 2002). As in the Facies 2, gamma ray indicates both coarsening and finning upward sequences. These parasequences indicate the cyclic change in water depth by climate. These sequences may deposited as the lowstand fan, which can be associated with the lowstand system tract (Myers and Milton, 2008). In the Facies 3, the gamma ray indicates the clean sandstone sequence in the upper part but in the lower part of the Facies 3 it indicates the much more shaly. The decrease in sonic transit time indicates that this part of the formation is well laminated. Further, this increase in the sonic velocity indicates more compaction of the lower part of the formation. It may be due to the cementation precipitated from the volcanic ash, which is significantly present in the Balder Formation (Bjørlykke and Aagaard, 1992; Bjørlykke, 2010). This ash is associated with the volcanic activity associated with the opening of the Atlantic Ocean, which separated the Greenland and Norway (Kjennerud et al., 2001; Norlex, 2013; Torsvik et al., 2002). The Facies 3 is also act as regional seismic marker for the Balder Formation (Norlex, 2013). The sand injections are the other main features in the Balder field more specifically in the Balder Formation. These sand injections are quite hard to be marked and study on the well logs without analyzing the core and seismic data, which is unfortunately not considered in this study (Bergslien, 2002; Newman et al., 1993; Norlex, 2013; Okiotor and Imasuen, 2011; Shell, 1982; Torsvik et al., 2002; Wach et al., 2000).

4.2.3 Cap rocks

The cap rocks are the rocks which have very small pore throats and the permeability. The good cap rocks may have high entry capillary pressure, which can hold large volume of the hydrocarbons. Cap rocks can be belonged to any lithology like evaporites, fined grained clastics, organic rich shales or any other lithology which has greater high capillary pressure then the hydrocarbons zone (Downey, 1994; Ingram et al., 1997). In the study area the cap rocks belong to shale as it can easily be identifiable from the unusually high gamma ray

response (green zone) which contained high volume of shale (Fig. 4.18). The reservoir section can be easily separated from the cap rocks by the low gamma ray response (clean sandstone) with the high resistivity values (hydrocarbon saturated zone). This hydrocarbon zone is sealed by the cap rocks of Lista and Sele formations. Furthermore, it can be observed that in the Figure 4.18 the yellow zone, the neutron deflects on the right side and density deflects on the left side give nice sepration, more like ballon effect (markeded by the yellow color). It indicates the good sandstone intervals, which may be filled by the light hydrocarbons (Ulasi et al., 2012). In the Figure 4.18 the green zone, the neutron log run on left and density log run on right side, it may indicate the shaly zone with less or no hydrocarbons. These type lithologies can be act as the cap or seal rocks. In few wells the shale wedge intrusion in these thick sand bodies acts as barrier for hydrocarbon migration. These shale wedge may be deposited as the hemipelagic anoxics shales. These thin shale beds also indicate that during these intervals the clastic input may be halted, which may indicate the transgressive phase and subsidence of basin (Asquith and Krygowski, 2004; Dypvik, 1983; Emery and Keith, 2008; Faleide et al., 2010; Guargena et al., 2007; Ingram et al., 1997; Kjennerud et al., 2001; Quintero and Bassiouni, 1997; Torsvik et al., 2002).

The Lista Formation finning upward gamma ray response (Fig. 4.10) indicates that the formation is dominated by the shale lithology and deposited in calm marine environment. The upward cleaning and dirtying trends also indicate that the formation deposited in varying sea level. The influx of the siliciclastic input also varied during its deposition (Kjennerud et al., 2001; Milton and Emery, 2008; Norlex, 2013). It is deposited as the hemipelagic sediments draped over the Heimdal Formation (Bergslien, 2002). It is thin out in the south-eastern wells (Fig. 4.5). The Sele Formation finning upward gamma ray response (Fig. 4.10) indicates that the formation is dominated by the shale lithology which may deposited in the calm and restricted environment (Emery and Keith, 2008; Norlex, 2013). It can be categorized as turbiditic shale draped over the Hermod Formation (Bergslien, 2002). As it can be easily observe in the Figure 4.5 that pinching and thinning of the formation from the west to the east. This also shed light on the source of sediments, which is from north-east direction (Hempton et al., 2005).

4.2.4 Overview of the Balder field (integration of learning from the chapters 2 and 4)

The Balder field reservoir and cap rocks belonged to the post rift sediments (Bergslien, 2002). The well log (fining upward) trends of these formations may indicate that these formation deposited in deep marine settings. The rise in sea level may be associated with the subsidence. This subsidence can be associated with the reduction in heat flow. (Johnson and Fisher, 1998, 1998; Kjennerud et al., 2001; Martinsen et al., 2005; Ziegler and Hoorn, 1989). The correlation of the reservoir and cap rocks indicate that the depositional pattern was influenced by the underlying fault blocks. The underlying chalk formation (Cretaceous age) indicates that before the deposition of these thick sandstone formation (Tertiary age), the basin was starved from the clastic input. But, after the opening of the Atlantic Ocean which lead the upliftment of the East Shetland Platform, coarser sediments (Sandstones) deposited by the deep marine turbidite system (Johnson and Fisher, 1998; Jenssen et al., 1993; Kjennerud et al., 2001; Milton and Emery, 2008; Thyberg et al., 2000; Torsvik et al., 2002). These deposits contained well sorted thick sandstone intervals (Heimdal and Hermod formation, clean gamma ray), which act as the good reservoir bodies. These intervals gradually thinned in Late Paleocene-Early Eocene and in some cases deposited as the deep marine mudstones (Balder Formation mudstone; Flood plain deposits) (Figs. 4.21 and 4.23) (Johnson and Fisher, 1998; Milton and Emery, 2008; Timbrell, 1993). The wells (25/11-20;

25/11-18; 25/11-17; 25/11-16; 25/11-15) which are more in the south-eastern side of the field (Fig. 4.22, map generated by IP) have vey low net-to-gross (Table 4.1a), specifically in the younger reservoir intervals (Balder Formation). These intervals may be deposited as the distal sub-marine fan deposits (Fig. 4.23). These distal deposits rich in mud and contained very less amount of sandstone (Johnson and Fisher, 1998; Milton and Emery, 2008;).

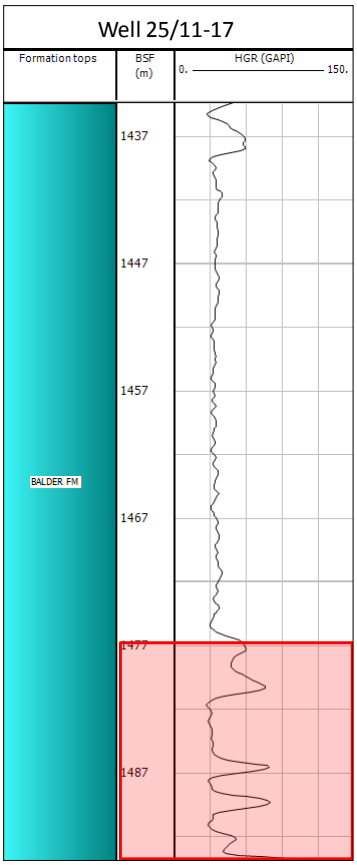

Figure 4.21 The Balder Formation, mudstone interval highlighted by the red box whereas the much cleaner sandstone is in the upper part.

In the Balder field, specifically in the Balder Formation sand remobilization and the liquefaction (sand injections) have very imporatant role between the communication of different reservoir units (Bergslien, 2002; Jenssen et al., 1993). The lacking of petrographical thin section study and other alternative data sets put the limitation on broad discussion on their origin. Further, the traping mechanism of the Balder field can be associated with the stratigraphic as well as structural (Jenssen et al., 1993). As this study is more focuses the analyses of well logs, so it would quite uncertain to discuss about the structural traping. But, from the well logs, it can be observed that the trap mechanism of hydrocarbons is also influenced by the stratigraphy. The sub environment of these deep marine system indicated that most of the reservoirs can be associated with the channel deposits of turbidite system (Well 25/11-23 North western), while the cap/seal rocks may deposited as the levees of turbidite system (25/11-17, south eastern well) (Fig. 4.23) (Milton and Emery, 2008; Sarg and Skjold, 1982; Timbrell, 1993). The stacking of the channel sandstone bodies and than lateral movement of these deep marine depositional system may help to create pinchout of sands bodies more specifically to create the seal/cap rocks (Figs. 4.18 and 4.23) (Jenssen et al., 1993; Sarg and Skjold, 1982). Further, the distal deep marine mud fan deposits may also help to create these kinds of seals. The Balder field may has more likely traps the

hydrocarbon in this way (Johnson and Fisher, 1998; Martinsen et al., 2005). The deposition of the hemipelagic sediments (volcanic ash) creates good vertical seals. These all geological influences help to create a good reservoir rocks with high quality seals (Bain, 1993; Johnson and Fisher, 1998; Jenssen et al., 1993; Norlex, 2013; Timbrell, 1993). From the well correlation (Chapter 2, Figure 2.18), it indicates that the source rock is well distributed under the Balder field. The generation of hydrocarbons from the Upper Jurassic is still continuing to the present day, this can fill any good trap present (Cornford, 1998). The migration path of hydrocarbon is more likely from the Mesozoic fault and fracture systems. The defective seal of chalk help it to migrate into Paleocene-Eocene sandstone bodies (Cornford, 1998; Isaksen and Ledje, 2001).

"All of above mentioned geological features, their deposition and origin in this section have been covered and referenced in chapter 2 with more indepth reveiwed."

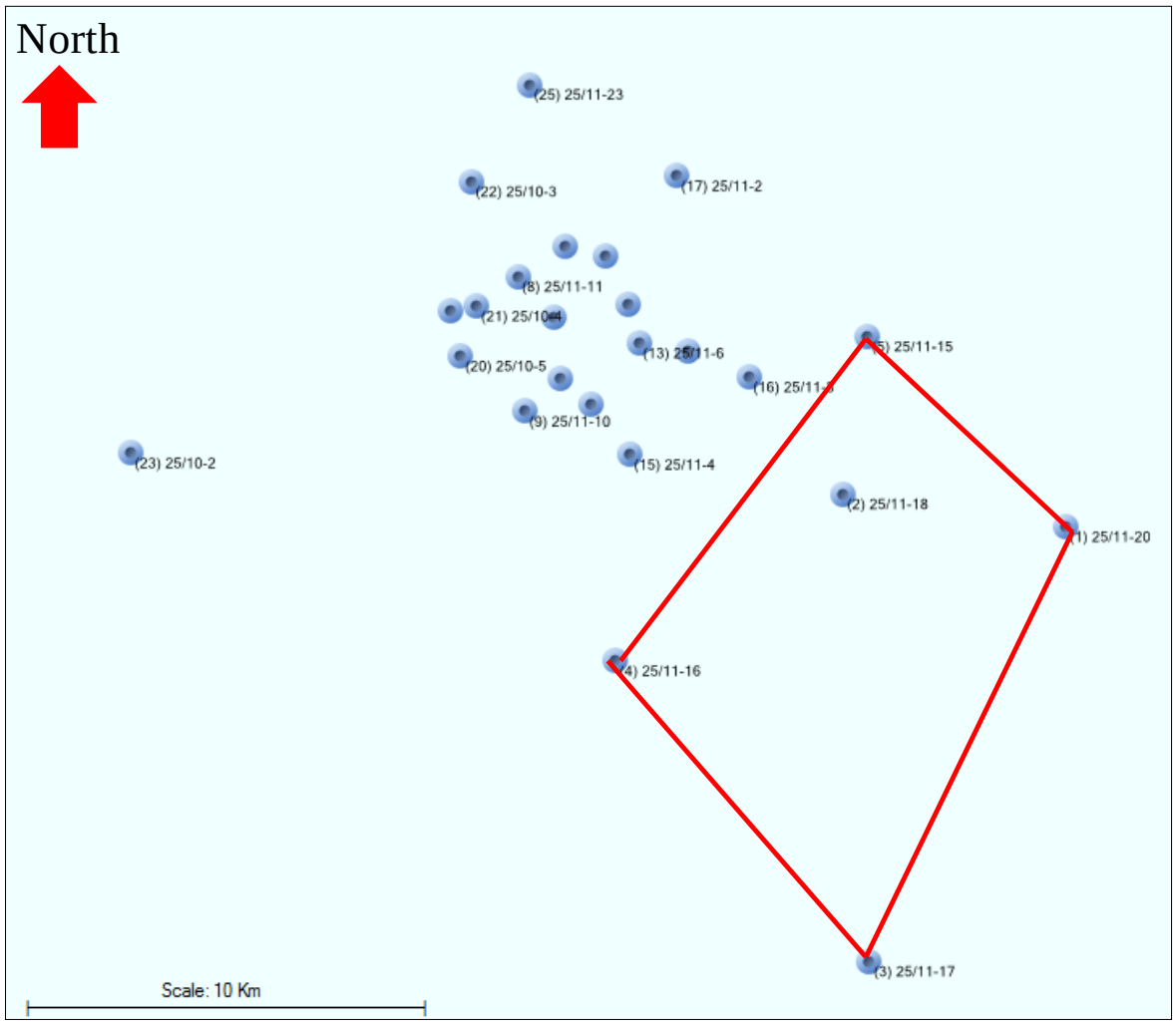

Figure 4.22 The Balder field well location. The red polygon shows well location of southeastern wells with less amount of sandstone intervals in Balder Formation.

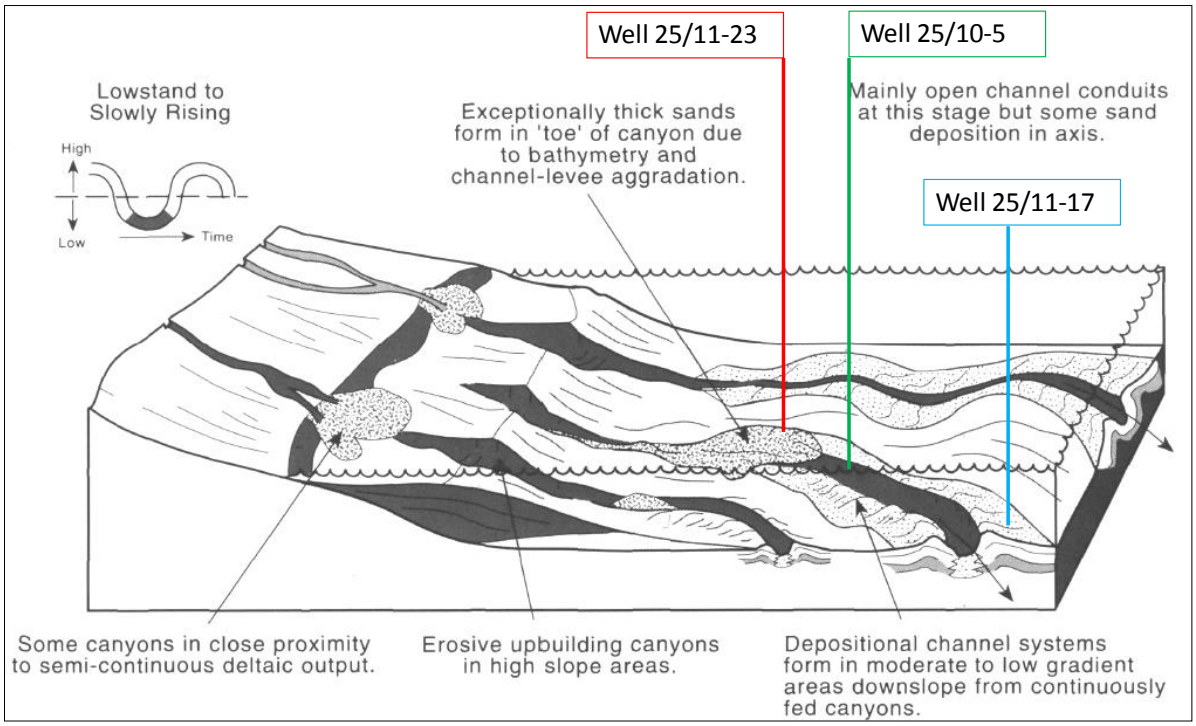

Figure 4.23 Conceptual model of deposition of the reservoir formations (modified after: Timbrell, 1993).

Chapter 5: Compaction study of the Balder field

In this chapter compaction study and rock property evolution of the Balder field is carried out using well log data. The chapter focuses exclusively the results and discussion of the compaction study of different stratigraphic horizons penetrated by the 25 wells. In the first section different cross-plots are used to demonstrate the compaction trends within the Balder field and later the major findings are discussed. The results demonstrated below also carried on several wells can be seen in the Appendix II. The detail discussion of the compaction study are concentrated in the reservoir horizons but the compaction results of other zones (overburden and underburden of the reservoirs) are also discussed but not very extensively.

5.1 Results

5.1.1 Geothermal gradient

One of the very first steps related to compaction study for any hydrocarbon field is to determine whether the reservoirs are mechanically or chemically compacted. So to start the compaction analysis, it is very important to know about the geothermal gradient of the field, as temperature is the one of essential elements in the compaction analysis (Bjørlykke et al., 1986; Ehrenberg, 1990; Storvoll et al., 2005; Walderhaug, 1994b). As with limited resources for this study, borehole temperature data of twenty two wells were utilized to generate the approximate geothermal gradient map of the Balder field (Fig. 5.1). The following geothermal gradient map (Fig. 5.1) is to analyzed further to interprete the compaction behaviour and to mark the transition zone of mechanical and chemical compactions within the study area. For further discussion see the section 5.2.

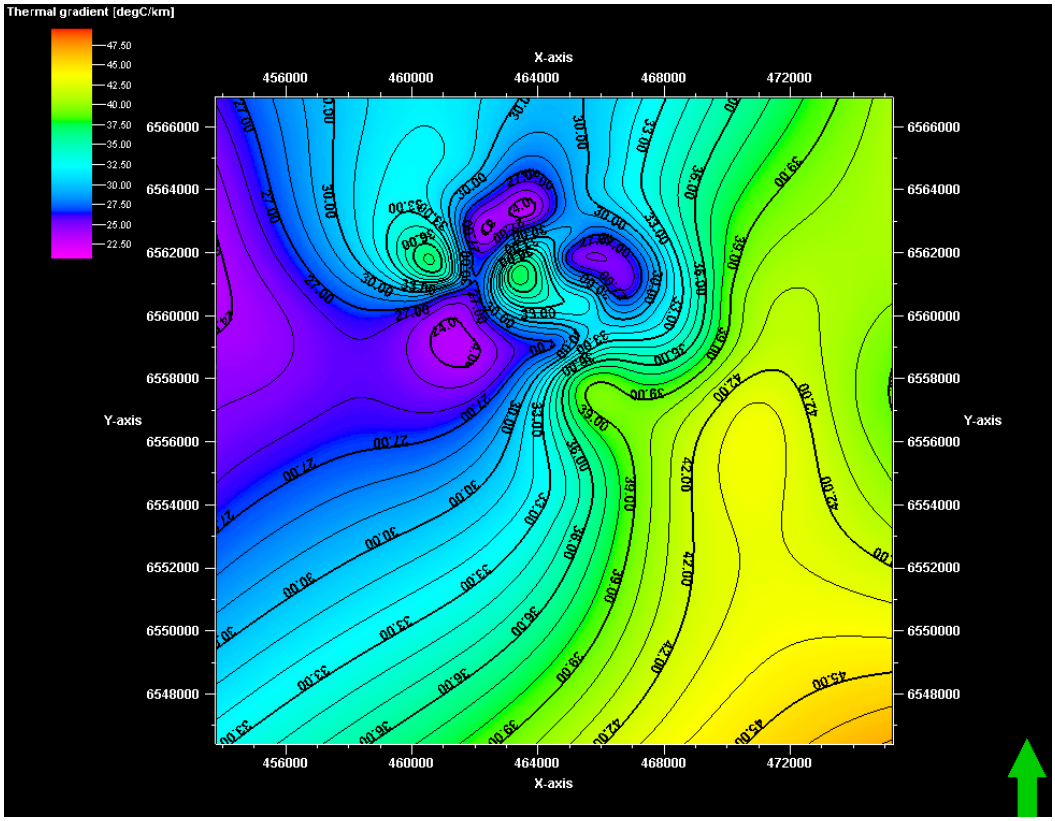

Figure 5.1 The present day geothermal gradient in and around the Balder field. The map is constructed by utilizing the BHT data available in the NDP website.

5.1.2 Compaction trends

The velocity and density trends with respect to depth of the Balder field show different compaction behaviors within the area. The velocity-depth plot shows different zonal velocity trends from the twenty three wells data points (Fig. 5.2).

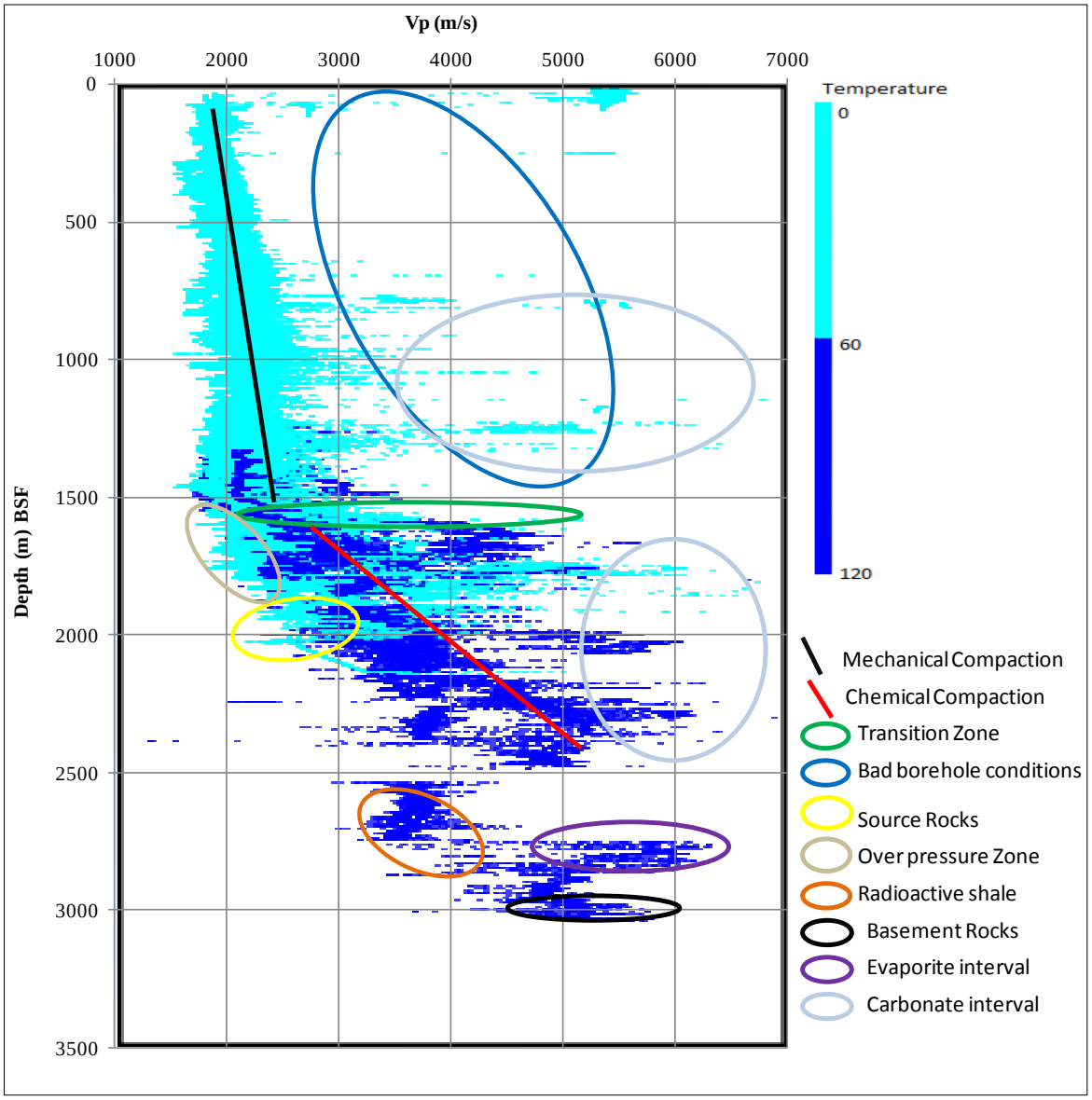

Figure 5.2 Compaction trends of 23 studied wells. All the P-wave velocity data points color coded by the temperature against the depth.

By analyzing the velocity data, two different zones have been marked (Fig. 5.2). This trend showed the two different compaction regimes in the study area. The velocity-depth trends show in general an increasing trend with the burial depth. But in a narrow zone, which have been marked as the transition zone, the behavior changes as the velocity data shows an abrupt increase, indicating more stiffness of the grain frameworks (Fig. 5.2). After this zone the sharp increase in velocity trend is easily identifiable, which may indicate chemical compaction marked by the red line (Fig. 5.2) (Marcussen et al., 2010; Storvoll et al., 2005). The other anomalies of Vp data which marked in the Figure 5.2, are discussed in the section 5.2.

Further, the bulk density data from twenty four wells plotted against the depth (Fig. 5.3). The bulk density data shows different zones within the study area. At initial stage, where the mechanical compaction dominates, the bulk density data show gradual increase compared to the transition zone. The bulk density increases significantly in the transition zone which reflects better packing and stiffness of the sediments (Fig. 5.3) (Mondol et al., 2009; Storvoll et al., 2005). Different zones marked due to variation and anomalies of the bulk density data. These zones, further discussed in the section 5.2.

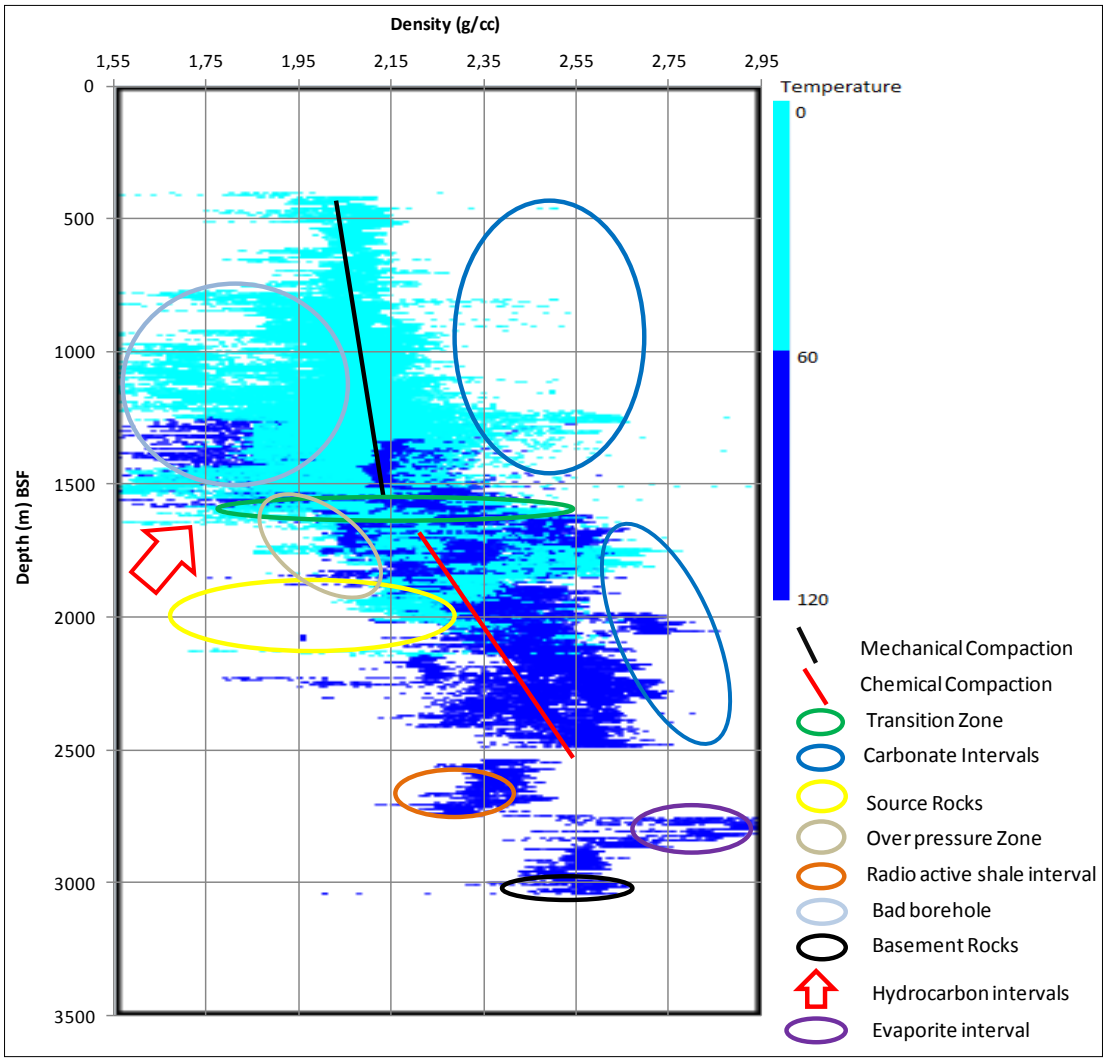

Figure 5.3 Bulk density data of twenty-four wells color-coded by the temperature.

To investigate it further, a crossplots of the Vp and bulk density color-coded by the borehole temperature is utilized (Fig. 5.4).

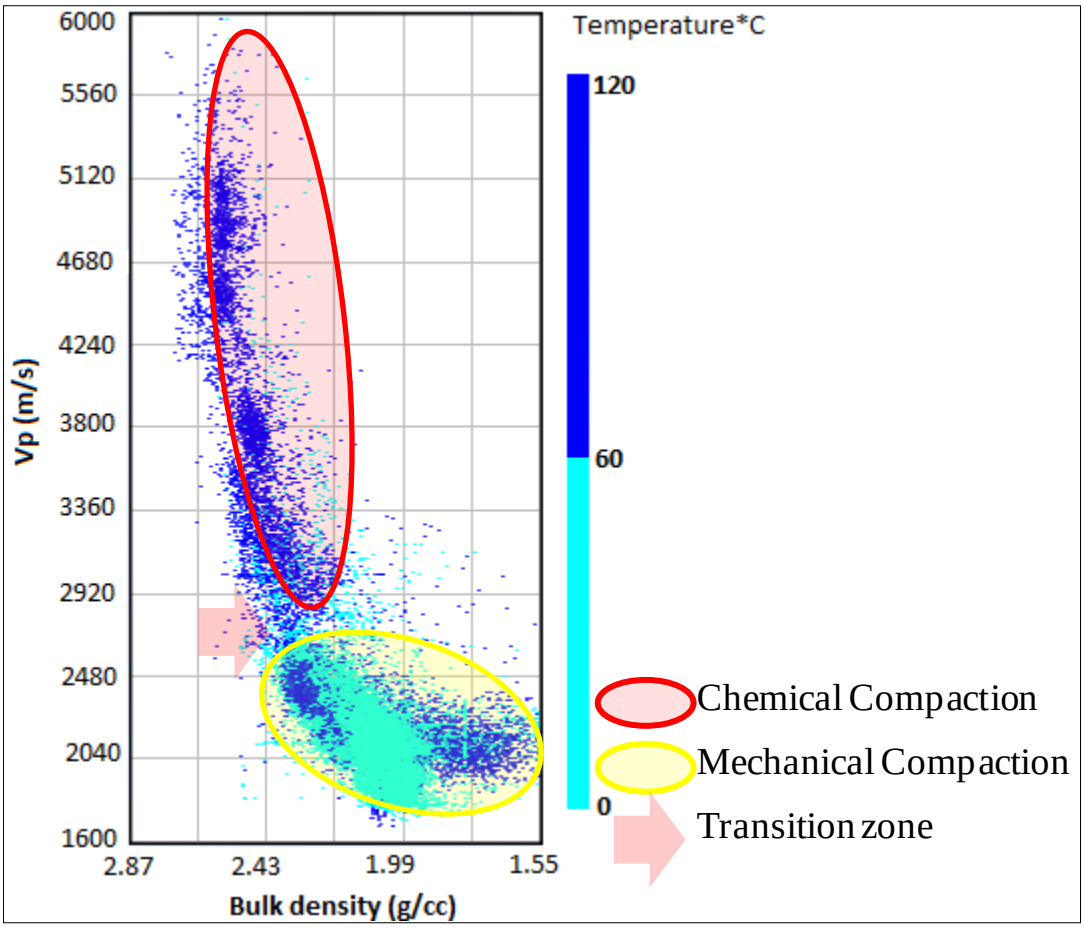

Figure 5.4 Only the shale data points from the twenty-three wells plotted the bulk density and Vp color-coded by the temperature.

In the Figure 5.4, it is easily obervable that the Vp and bulk density increase significantly within the studied wells. Two different data clusters are identifiable within the plot. The knee bend between two clusters of data represent the transition zone where the Vp, density and temperature increases significantly compared to the mechanical compaction zone. This may indicates the sudden increase of stiffness of the sediments (Avseth et al., 2005). For further interesting observations and discussion are shown in the section 5.2.

The porosity-velocity cross-plot color codded by temperature of only shale data points (Vsh>0.75) from the seventeen wells has been utilized for further interpretation. The average porosity values have been plotted against the Vp for better understanding of the transition zone (Fig. 5.5).

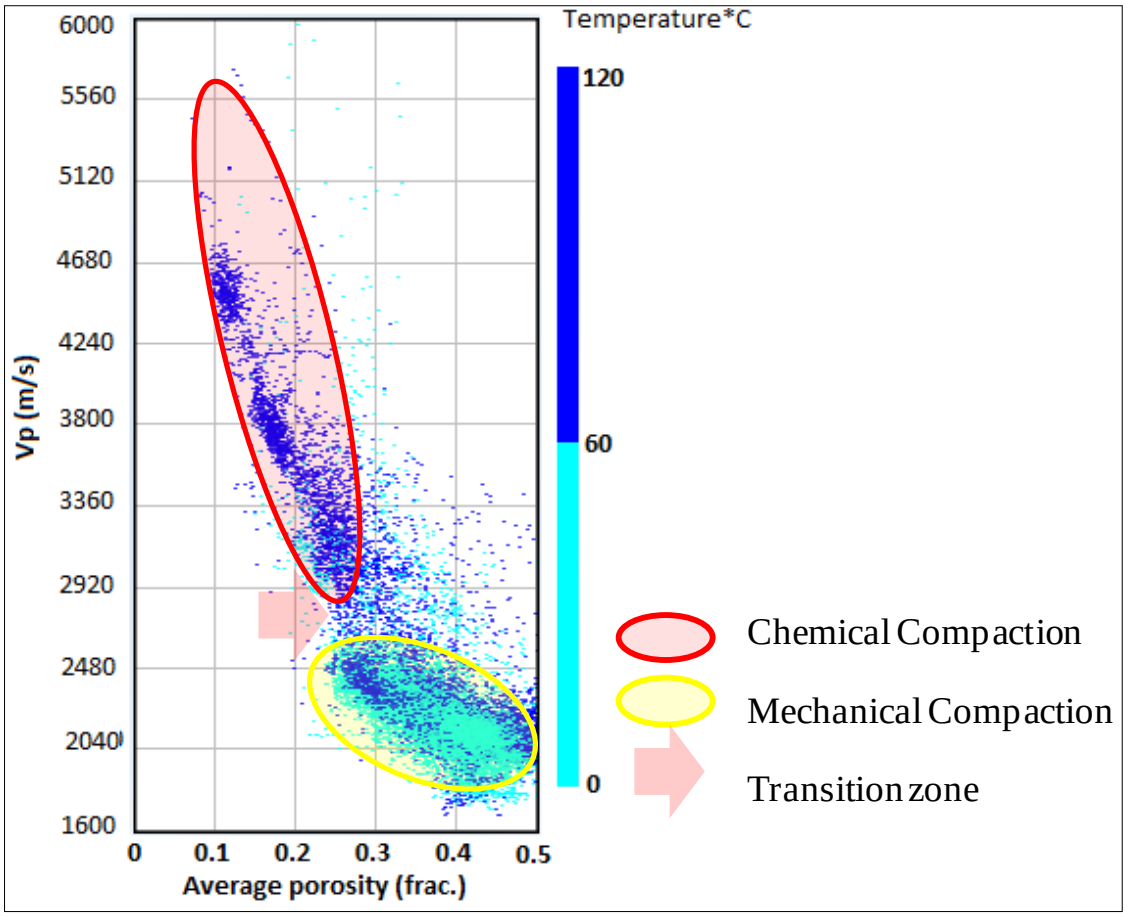

Figure 5.5 Shale data points from seventeen wells of bulk density against the Vp data color-coded by temperature.

Similar like earlier plots (Figs. 5.2 and 5.4) two different data clusters marked on the cross-plot. The sharp increase of velocity and decrease in porosity may indicate the better packing of the sediments (Avseth, 2010). For further discussion, see the section 5.2.

5.1.3 Sand and shale compaction

In nature, rocks composed of sediments vary in mineralogial and textural compositions. The two common and most abundant lithologies in the clastic sedimentary basins are sandstones and shales. Hence, to study the compaction trend of these two lithologies, Vp data have been sorted on the basis of shale volume and plotted against the depth. For better understanding of the compaction of these lithologies, the three published curves are used as references (Fig. 5.6).

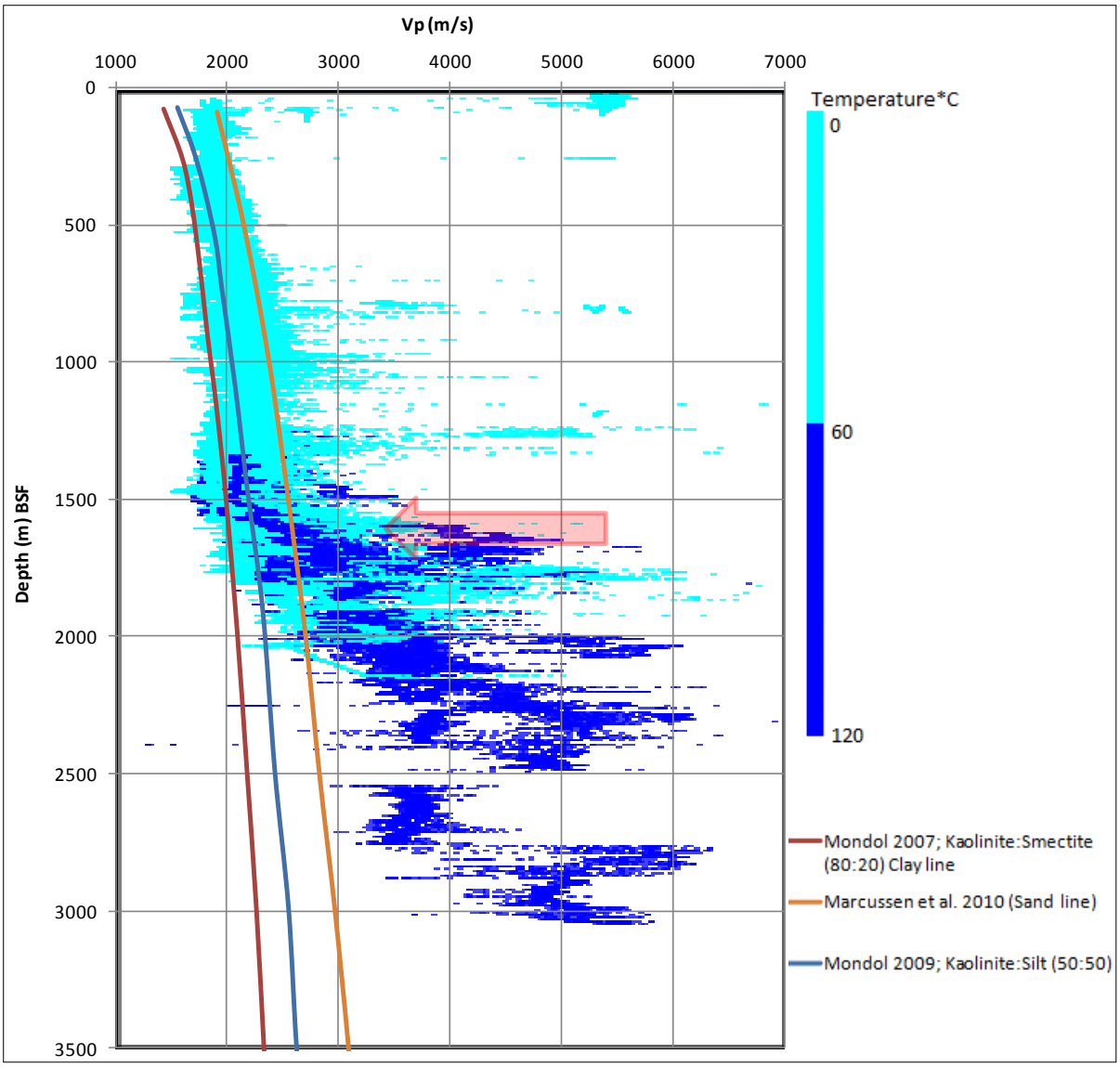

Figure 5.6 Three reference curves with all Vp data points of twenty-three wells, data color-coded with temperature.

In the Figure 5.6 the red arrow shows the transtion zone, in which the velocity-depth trend deviates from the reference curve. Initially, all the Vp data points from twenty-three wells have been color-coded with the temperature, plotted with the three reference curves. In mechanical compaction regime, the data points are following at least one of the dipping trends of the reference curves. In and after the transition zone (marked by the red arrow), the Vp data start deviating from the published curves. Specifically, in the high temperature regime (the Blue color) only few data points matched with the reference curves.

Furthermore, the data sorted out by shale volume in order to get better look at individual lithologies. For analyze the sandy lithology, the Vp data point of twenty-three wells, which contained less than 25% of the shale volume plotted against the depth with Marcussen et al., (2010) sand line (Fig. 5.7). The data points color-coded with the temperature plotted for better understanding of the compaction behavior of sand and sandstones.

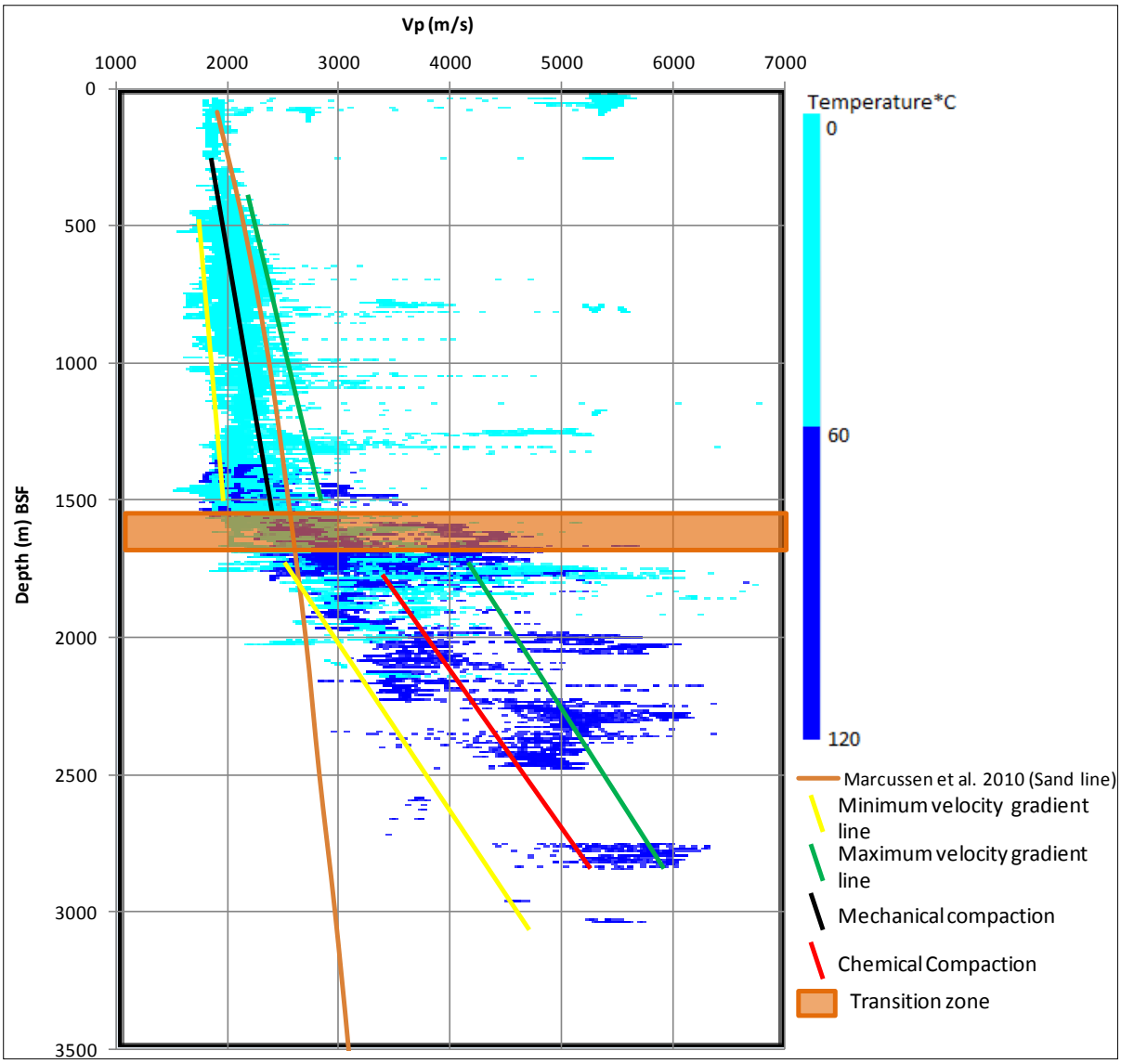

Figure 5.7 Vp versus depth data of sand points only, color-coded by the temperature from the twenty-three wells.

It is not that eassy to isolated carbonate only by petrophysical analysis. So, the plotted data may also contained carbonates as well (Fig. 5.7). The data ponits from the carbonate intervals for individual well also sorted and clearly marked (see the Appendix B). Similarly, as demonstrated in the previous section, the sand data almost follow the dipping trend of the reference sand line, but as soon as it reached the transition zone, the Vp increases significantly and start deviating from the normal compaction trends. This increase in Vp indicates the more stiffness of the sediments. The average lowest Vp value in the mechanical compaction zone for sandstones is 1700-1900 m/s and the average highest Vp value in the mechanical compaction zone for sandstone is 2200-2600 m/s. The average lowest Vp value in the chemically compacted zone for sandstone is 2900-3400 m/s whereas the average highest Vp value in the chemically compacted zone for sandstone is 3800-4200 m/s.

For analyzing the shaly lithology, the Vp data point of twenty-three wells which have more than 75% Vsh plotted against the depth and compared it to Mondol, (2007) and (2009) experimentally compacted mudstone curves (Fig. 5.8). The data points also color-coded by temperature for better understanding of the compaction behavior of shales.

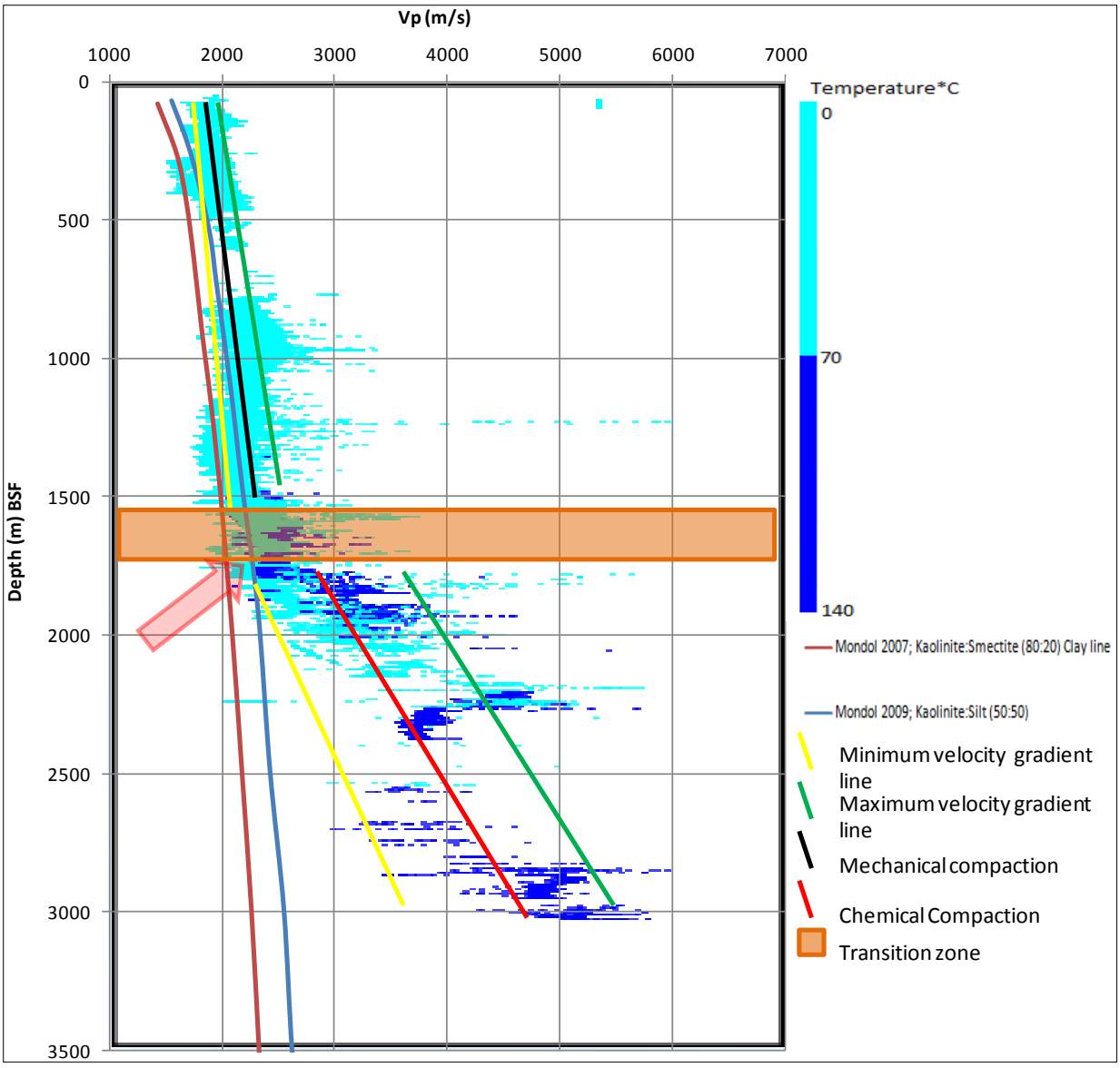

Figure 5.8 Only the shale points, Vp versus depth data color coded by temperature from the twenty-three wells. Expected velocity reversal zone marked by the red arrow.

The average lowest Vp value in the mechanically compacted zone is about 1700 m/s and the average highest Vp value in the mechanical compacted zone for shale vary between 1900-2300 m/s. The average lowest Vp value in the chemical compacted zone varies from 2700 to 3400 m/s and the average highest Vp value in the chemical compacted zone varies from 3600 to 3800 m/s. The velocity reversal zone (possible zone of MC and CC) is also marked by the red arrow.

Further the density data points of the shaly lithologies are shown in comparison with Mondol (2009); Kaolinite: silt (50:50) published compaction trends to better explanation of the compaction behavior of shale units (Fig. 5.9). In this plot, only those data points used, which have more than 75% shale volume. The density data also color-coded with the temperature. In the Figure 5.9, it is easily observable that after the marked transition zone the density start increasing significantly. Before the transition zone the average maximum density varies about 2.10-2.15 g/cc but, as soon as the transition zone encounter the average values of density increases. Below the transition zone, the density values increase significantly and deviates

from the published mechanical compaction trend line. Further in the Figure 5.9 different anomalies zones also marked which are discussed in the 5.2 section.

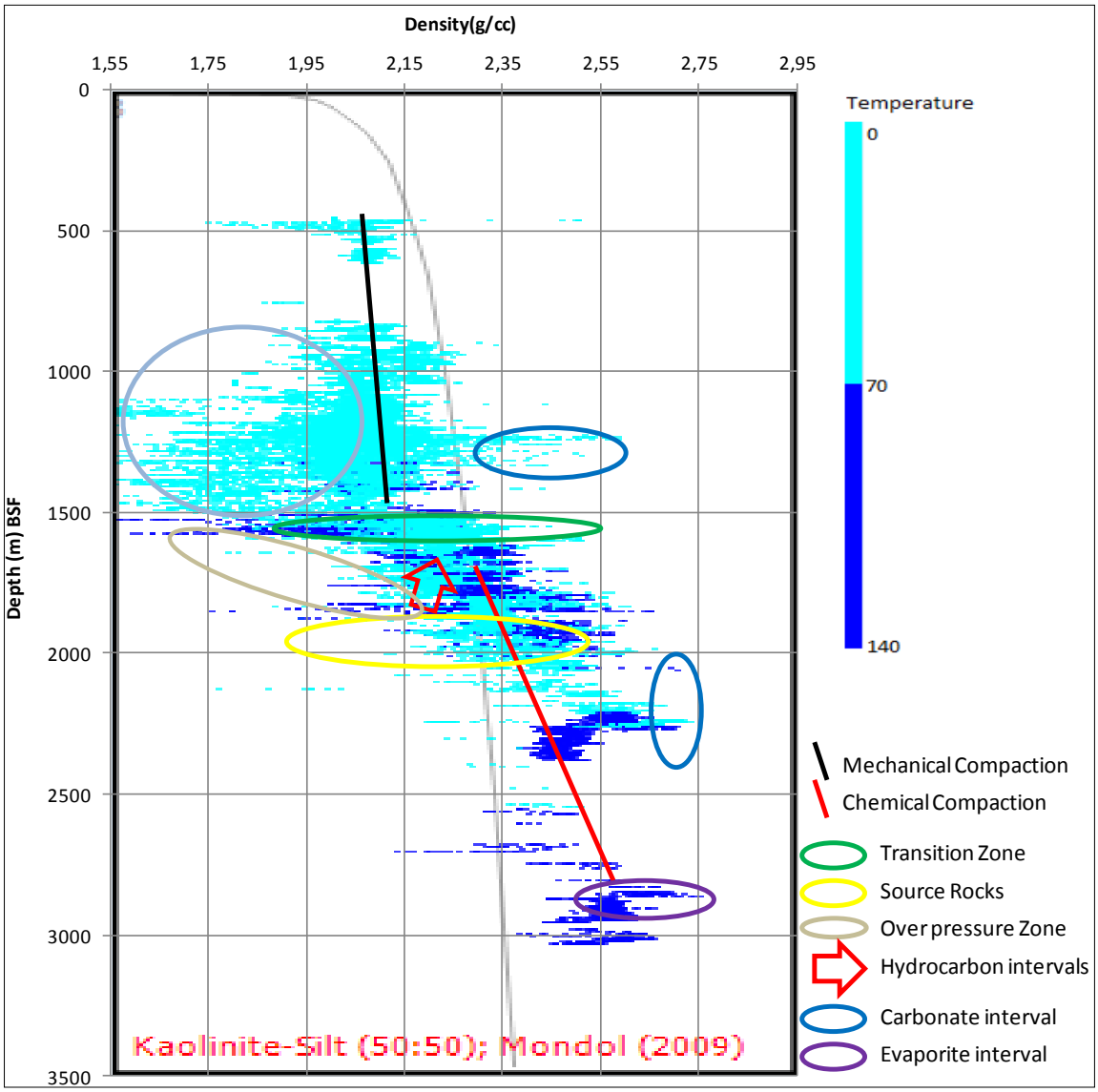

Figure 5.9 Depth-density cross-plots, the shale data from the twenty-three wells, color-coded with the temperature and compared with the Kaolinite-Silt (50:50) reference curve (Mondol, 2009).

5.1.4 Analysis of the source rocks

In study area two major source rocks are present, the Draupne and Heather Formation. The Draupne Formation penetrated by four wells in the study area while the Heather Formation penetrated by the one well. The thickness of the Draupne Formation varies from 3 to 24 m, whereas the thickness of the Heather Formation is 18 m in the well 25/10-4. For the compaction analysis of the source rocks, the shale data points of the source rocks plotted in the Vp-depth relation with two mechanically compacted reference curves (Fig. 5.10). The data also color-coded by temperature which have ranged between 60 and 80 ^{0}C.

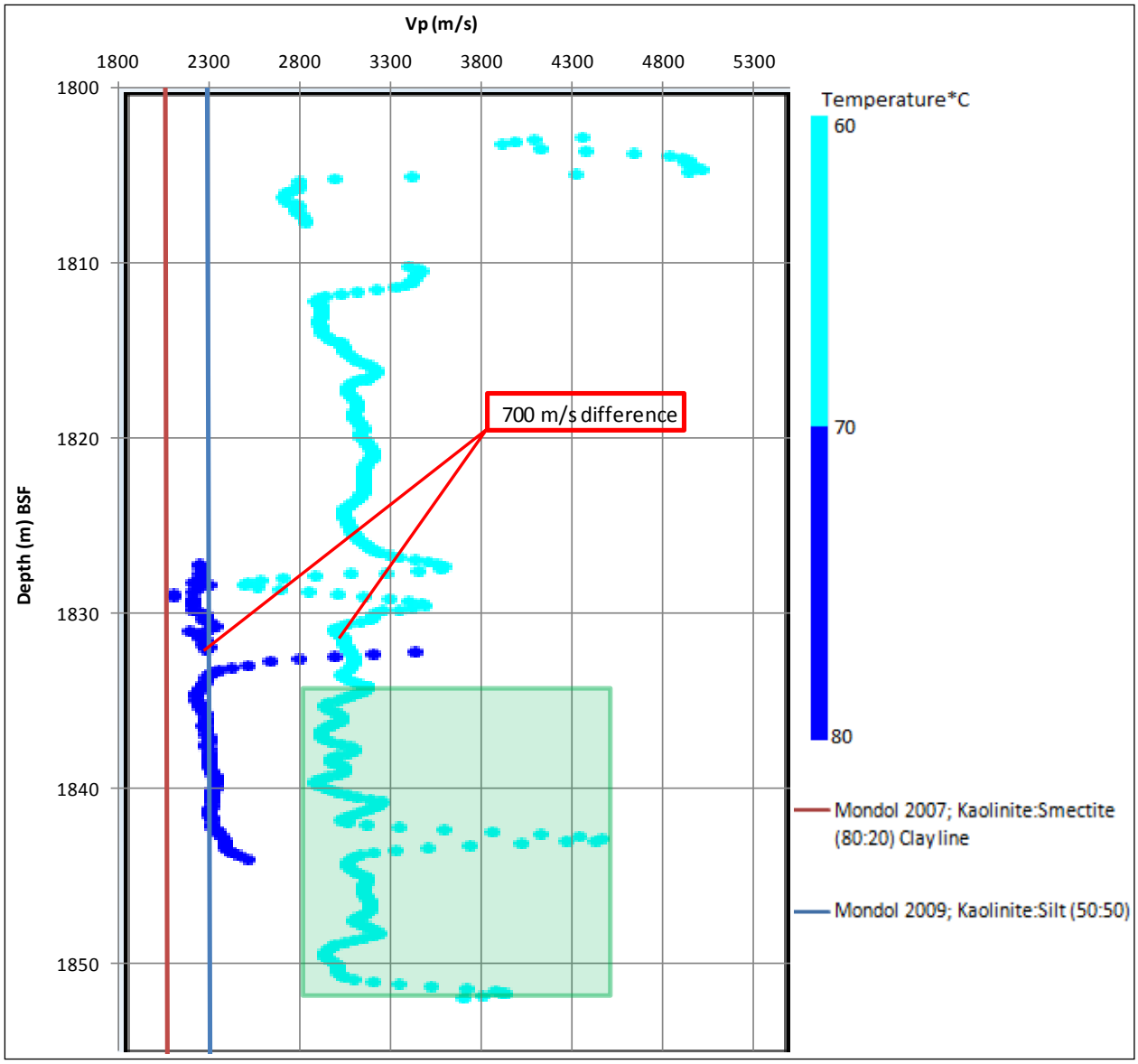

Figure 5.10 Shale data points from the source rocks (Draupne and Heather formations) from four wells with two reference curves.

In the Figure 5.10, the green highlighted box area belongs to the Heather Formation data points, while rest points are from the Draupne Formation. It is clearly observed that the data points of the source rocks, which have temperature higher then 70 ^{0}C, show low velocities and follow the Mondol et al., (2009) reference curve. While the data points having temperature less than 70 ^{0}C, show higher velocities and do not match with any of the curves. It also demonstrate that the same rocks but at different temperature regime with the same stratigraphic depth have velocity difference about 700 m/s. For further discussion, see the section 5.2.

5.1.5 Analysis of the reservoir rocks

In the Balder field, three formations; Balder, Hermod and Heimdal holds the commercial quantities of hydrocarbons. The thickness and stratigraphic positions of these formations have been already discussed and mention in the second and fourth chapters. For the compaction study of these reservoir rocks only sand data points considered, since most of the producible

interval belonged to the sandstone lithologies (Fig. 5.11). Marcussen et al., (2010) curve also used for the better understanding of the compaction behavior of the reservoir sandstones. The data points also color-coded by the temperature.

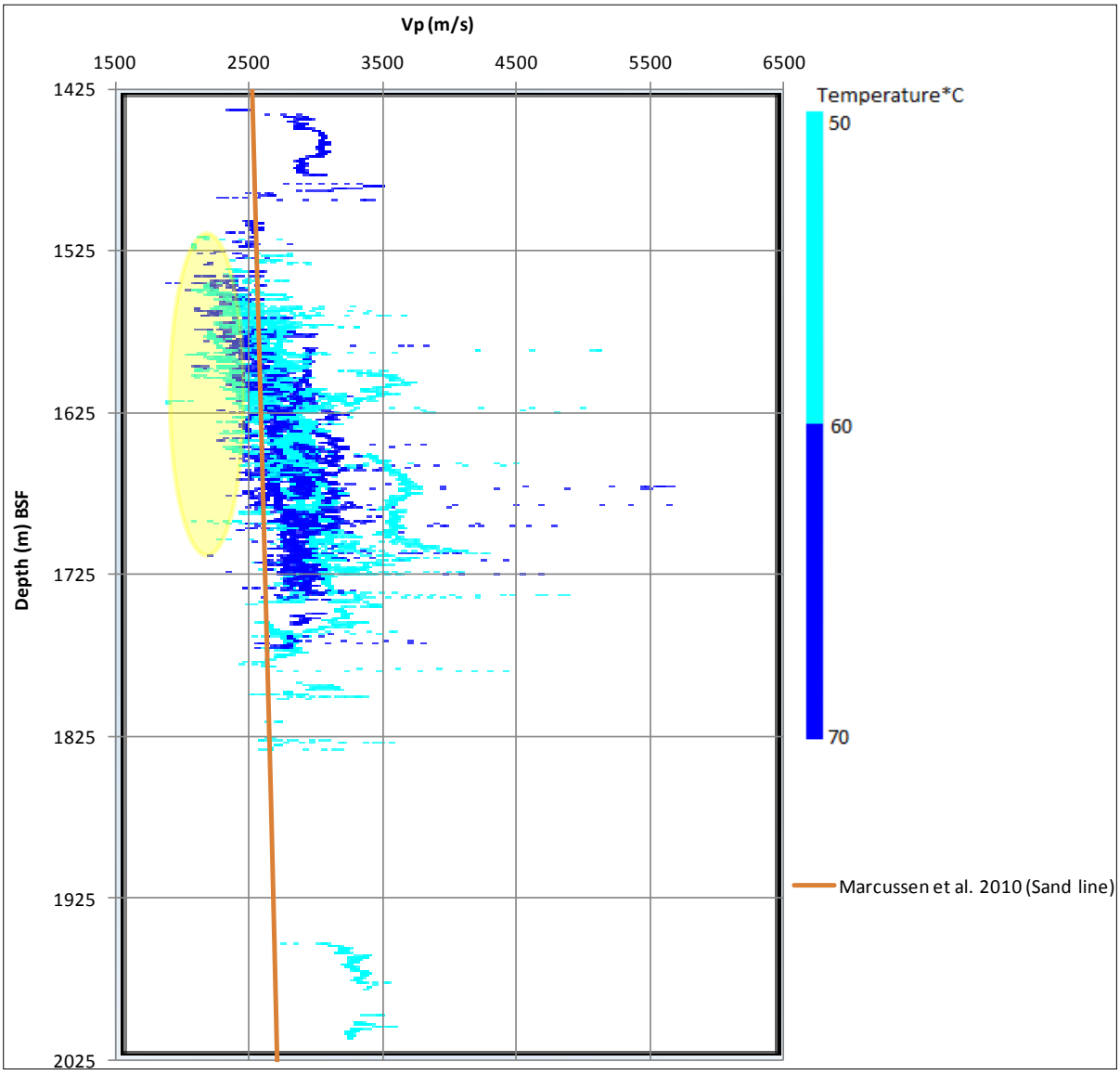

Figure 5.11 Sand data points of the reservoir rocks (three formations) from the twenty-three wells with sand reference lines (Marcussen et al., 2010).

In the Figure 5.11, the yellow highlighted ploygon shows the hydrocarbon filled reservoir zone. It is easily observable that most of the data points scattered across the Marcussen et al., (2010) published curves. There are quite small intervals where data points show very high velocity as well. This interval may indicates the stiffness of sediments. Hydrocarbons have tendency to decrease the sonic velocity which have been marked by the yellow ellipse, as few intervals show very low velocity zones (Rider and Kennedy, 2011).

5.1.6 Analysis of the cap rocks

In the Balder field, the three reservoir intervals interbedded by the seal rocks that belonging to the Balder, Sele and Lista formations (Results from the chapter 4). For the compaction analysis of these rocks only shale data points have used for the better understanding of the

compaction trends with respect to the published reference curves (Fig. 5.12). The data are color-coded by the temperature ranges from the 60-80 ^{0}C. The thickness and stratigraphic positions of these rocks have been already discussed and mentioned in the second and fourth chapters.

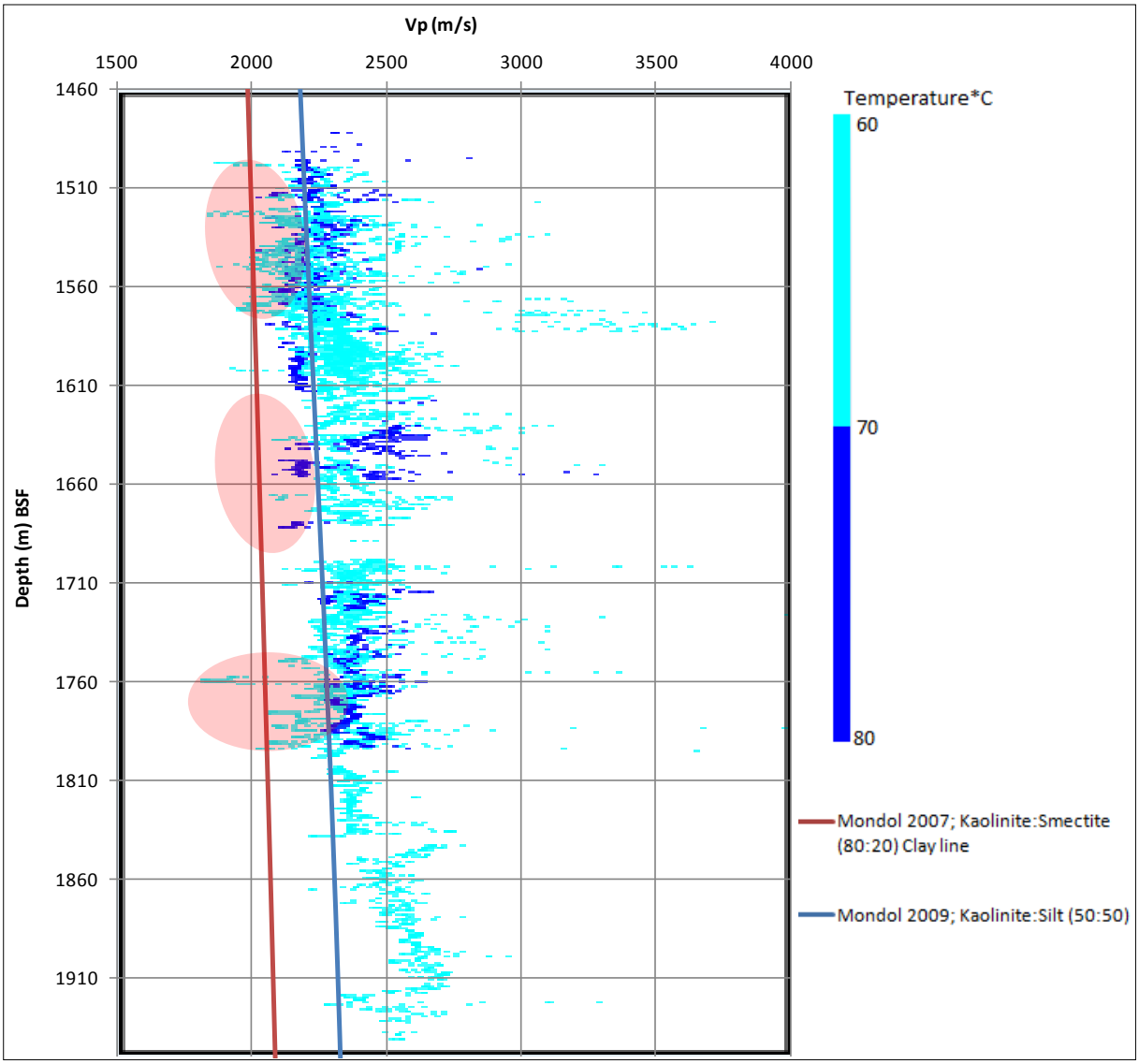

Figure 5.12 Shale data points of cap rocks (three formations) from twenty-three wells compared with two-reference clay compacted lines.

In the Figure 5.12, the red highlighted polygon shows the velocity reversal or the over pressure zone. It is also observable that most of the data points scattered across the Mondol (2007) and (2009) curves. The borehole temperature is quite within the range to initiate the quartz cementation, but only few data point show the high peaks above 3000 m/s. Other than that few intervals also show very low velocities than the general compaction trends of the reference curves. This can be interpreted as the velocity reversal due to over pressure zones (Bjørlykke et al., 2010; Storvoll et al., 2005).

5.1.7 Effect of time-temperature on compaction

In early sections, it has been demonstrated that the temperature is an important factor for controlling the compaction of sediments in the deeper part (Bjørlykke, 2010). For better understanding and demonstration Vp, depth and density cross-plots are utilized. The data is also color-coded by the temperature (Fig. 5.13).

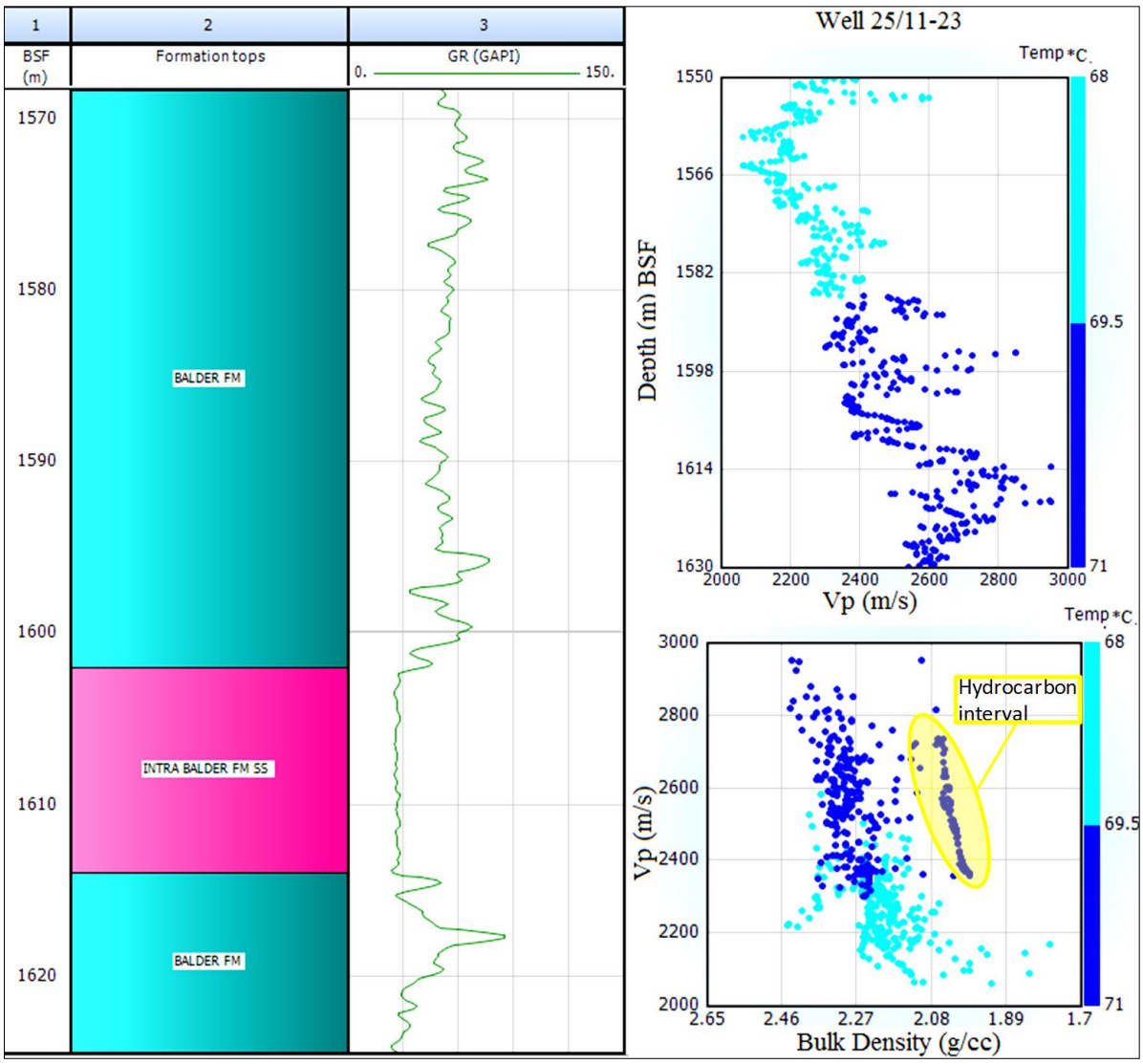

Figure 5.13 Vp, density and depth cross-plots color-coded by temperature of data from the well 25/11-23.

In the Figure 5.13, it can be easily seen that as soon as the temperature cross approximately 70^{O}C, the significant increase of velocity occurs without any significant change in the lithology. Similarly, the Figure 5.13 also illustrates it further with Vp-density cross-plot, color-coded by the temperature. When the temperature reach approximately 70^{O}C, the velocity and density increases significantly. The increase of velocity from 2000 m/s to 3200 m/s just within the 80 m interval (Fig. 5.13) demonstrate that it may not be the influence of mechanical compaction. The temperature can initiate the quartz cement precipitation at the grain contacts. This kind network of grains get stiffer to give such a higher peak values of the Vp within the small depth intervals (Marcussen et al., 2010; Storvoll et al., 2005).

5.1.8 Transition zone

In the previous sections, the transition zone is marked within the study area using the well log data. The transition zone has been marked clearly within the following wells (Table 5.1) by using the series of same cross-plots on each individual wells (Appendix B). These results are presented in the Table 5.1.

Table 5.1 Approximate transition depth in the study area with respect to wells and formations

Well No.	Transition zone Depth (m) BSF	Formation
25/11-23	1586	Balder
25/11-17	1505	Balder
25/11-15	1630	Heimdal
25/11-13	1655	Hermod
25/11-12	1580	Balder
25/11-11	1705	Heimdal
25/11-10	1720	Heimdal
25/11-9	1635	Hermod
25/11-8	1592	Heimdal
25/11-7	1553	Balder
22/11-6	1520	Balder
25/11-5	1576	Balder
25/10-4	1680	Heimdal
25/10-2	1821	Balder

5.1.9 Exhumation studies

It is important to conduct the exhumation studies, when doing the compaction analysis. Any major uplift in the area, may nullify the compaction trends especially, when using only the well logs and the temperature gradient to estimate the transition zone. Before moving further on the exhumation, it is important to mention that from chapter two of this study, it is easily understandable that the study area characterized as the subsidizing regime. So estimating the upliftment will not only make this interesting but one can see, how sometime these analyses can help us for better understanding of the tectonic evolution.

For this purpose, the Vp data from well 25/10-4 is plotted against the different theoretical compaction trends (Fig. 5.14). These theoretical compaction trends are better known as the experimental reference curves. In this part of the analysis, reference curve is plotted with the Vp data against the BSF depth. At this stage only the shale data points are plotted in order to eliminate the carbonate intervals from this analysis. Theoretically, for the normal subsidizing basin and the compaction of sediments, the Vp data points should follow the dipping trend of these experimental curves. Any mismatch from the reference curves may be result of upliftment in the study area.

It is clearly observable in the Figure 5.14a, that the Vp data don't match with any of the reference curves. At this point, present day BSF will be adjusted in that way, it can match with the any of the theoretical compaction trend. Any variation between the present day BSF and corrected depth may show the upliftment in the area.

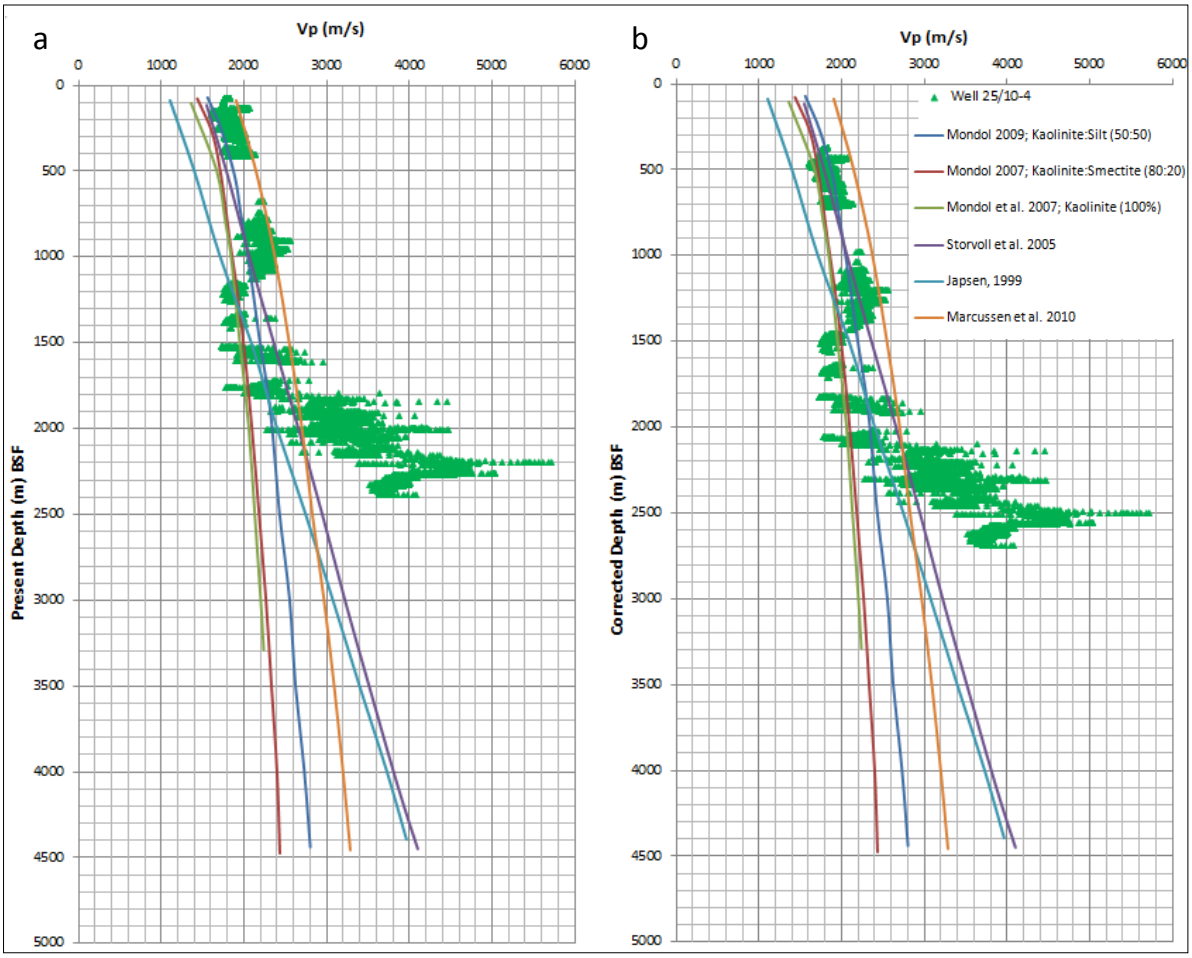

Figure 5.14 Vp data from the well 25/10-4 compared with a series of published reference trends.

To analyze it further, 300 m is added to the present day depth. In the Figure 5.14b, the cross-plot illustrates that after the correction applied, well data follow the trend of Mondol et al., (2009); Kaolinite: Silt (50:50) trend.

For further evaluation, the Vp data without any corrected depth have been plotted against the BSF depth with the three different reference curves as shown in the Figure 5.15a. The Figure 5.15b, the blue curve is of Mondol, (2009) Kaolinite-Silt (50:50), shows approximately 300 m of uplift. In the Figure 5.15c, the red curve of Mondol, (2007) Kaolinite-Smectite (80:20), shows approximately 700 m of uplift. In the Figure 5.15d, the light green curve of Mondol, (2007) Kaolinite (100%), shows approximately 900 m of uplift in the area.

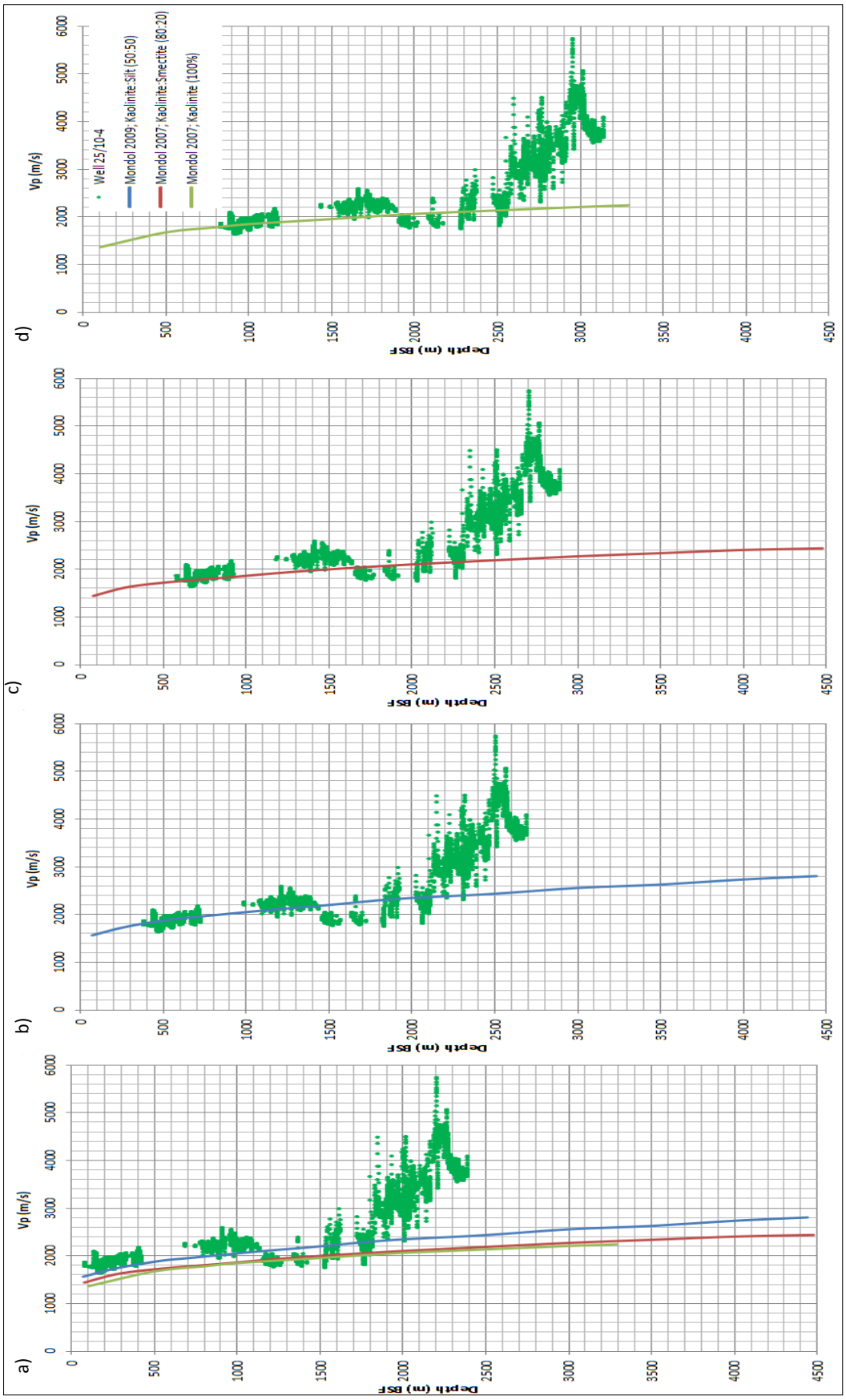

Figure 5.15 Uplift estimation, well 25/10-4, the Vp data with the three different compaction curves.

The compaction of sediments depend upon the mineralogical composition, shape, size and size of the grains (Bjørlykke and Jahren, 2010). Mondol, (2009); Kaolinite:Silt (50:50) curve provides average mixture of two different lithologies, which represents a better field conditions. This curve is further used to evaluate the other wells (see Appendix B), for these cross-plots. Table 5.2 demonstrates different exhumation observed in different wells. From the initial observation, exhumation decreased from north to south and west to east across the Balder field.

Table 5.2 The estimated exhumation by using the well log data.

Well No.	Total Exhumation (m)
25/11-23	300
25/11-17	150
25/11-15	250
25/11-13	250
25/11-12	250
25/11-11	250
25/11-10	300
25/11-9	250
25/11-8	200
25/11-7	250
22/11-6	300
25/11-5	100
25/10-4	300
25/10-2	250

5.2 Discussion

This part mostly relies on the observations, which are direct interpretations of the compaction study. Most of these discussed points demonstrated or assumed here have some uncertainties as the only data type used in this study is the well logs. Still there are many interesting findings and observations that supported by the published literatures.

5.2.1 Geothermal gradient of the Balder field

Geothermal gradient is one of the important elements in the compaction study. The temperature is the main controlling factor to initiate or halt the chemical compaction (Bjørlykke et al., 1986; Ehrenberg, 1990; Marcussen et al., 2010; Murphy et al., 1989; Storvoll et al., 2005; Walderhaug, 1994a, 1994b and 1996). For better understanding of this factor and before starting the compaction analysis, it is better to know, how the geothermal gradient varies across the study area. The approximate geothermal gradient map of the Balder

field has been established (Fig. 5.1). In the Figure 5.1, it can be seen that the geothermal gradient varies across the field significantly, from 25^0 C/km (north-west) to 45^0 C/km (south-east) of the Balder field. The variation in geothermal gradient may be the main reason for the shallow transition zone in the south east compared to north-west of the Balder field (Bjørlykke, 2010b).

5.2.2 Well log analysis

Before moving to the discussion on the compaction trends, it is better to point out the anomalies, which are marked in the early part. These anomalies can give uncertainty in the results. During this whole analysis the borehole condition kept under observation for better constrain of the analyses and results. The bad borehole conditions add uncertanities in logging where the we may see under or overestimate the values especially for density and sonic log, even if the corrections are applied (Rider and Kennedy, 2011). These could give uncertainty in results, which should be kept in mind. A series of cross-plots is utilized to analyze theindividual well to mark any bad borehole conditions (see the Appendix B).

The carbonate intervals are also pointed in the early part (Figs. 5.2 and 5.3). The position of these intervals within the study area is doubled checked by NPD wells reports. These carbonate intervals have tendency to show high Vp values at lower and higher depths, compared to the other lithologies like sandstones and shales (Rider and and Kennedy, 2011). These intervals are marked in individual well and shown in the Appendix B. The thickness of these carbonate intervals at shallower depths are negligible (just over a meter in few cases). These carbonate intervals are not dominated in the study area to halt the mechanical compaction at shallower depths. It can be seen in the cross-plots (Figs. 5.2 and 5.3). The carbonate lithology is not a part of this study, as these analyses are more focused on reservoir sections, which is dominated by the sand/shale lithologies. Other than that, with limited amount of data and time, it is not possible to utilize other methods to study the impact of these interval on overall compaction trends within the study area.

The low velocity regimes also marked within the study area by utilizing the well logs (Figs. 5.2 and 5.3). These zones maintain the porosity, hence sonic velocity decreases. These low velocity zone can be marked as overpressure zones (Avseth et al., 2005; Fert et al., 1994; Kan and Sicking, 1994; Li et al., 2012). In the study area these low velocity zones are encountered within the Balder, Sele and Lista formations. These formations mainly composed of clays and minor volacnic ash except the Balder Formation where it contains high amount of volcanic ash, deposited in anoxic basin condition. The deposition of such sediments makes these formation even less permeable (Mondol et al., 2008; Norlex, 2013; NPD, 2013; Sarg and Skjold, 1982). The low velocity/over pressure zones also marked on individual well (see the Appendix B).

The study area has significant potential of hydrocarbons reserve within the three reservoir intervals of Balder, Hermod and Heimdal Formations (NPD, 2013). Due to the presence of hydrocarbons in these formations, the logging tools especially sonic and density may underestimates the values compared to real responses (Li et al., 2012; Lin and Salisch 1993; Rider and Kennedy, 2011). This point has been kept under consideration, during the whole analysis. A red arrow is marked on the cross-plots, where potential reservoir intervals can be found (Figs. 5.2 and 5.3). Other than that analysis is carried out on each individual well to mark the high resistivity zones, see the Appendix B for the individual well analysis. For further discussion on these hydrocarbon zones, see the section 5.2.4 includes analysis of the petroleum system.

The compaction trend of sediments in the study area is almost similar in all wells (Figs. 5.2 and 5.3). The Vp data from wells (Figure 5.2) shows different increasing trends in mechanical and chemical compaction zones. In mechanically compacted zone, the general gradient of Vp is marked by black line, which shows normal increase in Vp due to overburden. This increase in Vp may indicates systematic compaction and packing of sediments with burial depth without changing their chemical composition (Bjørlykke, 1998; Bjørlykke and Jahren, 2010; Giles et al., 1998; Mondol et al., 2008; Peltonen et al., 2009). The transition zone marked by the green circle, as few intervals show the increase of Vp values, which indicates more stiffening of the grain frameworks (Avseth et al., 2005). After the transition zone, the Vp increasing significantly means more compacted due to chemical compaction that marked by the red line. The reason which can be interpreted here for getting kicks in Vp values in transition zone then sharply increase of the average Vp trend is due to the precipitation of the quartz cements on the grains contact. The theoretical temperature to initiate for quartz cementation is 60-70^{o}C. The transition zone, which is marked has this temperature regime (Avseth et al., 2005; Bjørlykke et al., 1986 and 2010; Ehrenberg, 1990; Maast et al., 2011; Storvoll et al., 2005; Vemik and Nur, 1992; Walderhaug, 1994b).

Similarly, the density-depth cross-plot verifies the same situation (Fig. 5.3). The trend of the density in the mechanically compacted regime show normal increasing trend as burial depth increases but within transition zone the density starts increasing significantly and deviates from the normal trend. This behavior of density shows more compaction of sediments in and after the transition zone. The reason which can be interpreted here for getting increase in density value can be attributed to the precipitation of the quartz cement. As the quartz cement reduce the porosity results increase the overall bulk density and so the rock strength (Avseth et al., 2005; Bjørlykke et al., 2009; Bjørlykke and Jahren, 2010).

The Vp versus density shows the two different clusters of data points (Fig. 5.4). The significant increase of Vp and density at certain temperature, may indicate onset of quartz cementation. Similarly, the Vp versus porosity also show the similar clusters of the data points (Fig. 5.5). The porosity reduced significantly as the velocity data gets higher values. This indicates that the precipitation of the quartz cementation, may reduce the porosity. The reduction in porosity increase more compaction and the more intense packing of the grains, which results in increase of the sonic velocity (Avseth et al., 2005; Avseth, 2010; Chuhan et al., 2002; Giles et al., 1998; Lang, 1994; Storvoll et al., 2005).

5.2.3 Sand and shale compaction

Sandstone and shale are the most abundant sediments in many sedimentary basins. These two lithologies have different mineralogical composition, size and shape of the grains. These variations lead them to behave differently under the same diagenesis conditions, as their porosity and velocity varies (Avseth et al., 2005; Fawad et al., 2011). Right after the start of burial, the shales have approximately 80% porosity while the sandstones have 45-50% (Chuhan et al., 2002; Marcussen et al., 2009). The main cause of difference in intial porosity at such extent is the difference of grain sizes. The compaction processes start as soon as sediments deposited (Bjørlykke and Jahren, 2010). Initially, mechanical compaction dominates in the first few hundreds meter of burial depth than unstable minerals start to precipitate to attain more thermodynamically stable form which results in more compaction known as chemical compaction. This cementing minerals further control the compaction trends of the sediments (Bjørlykke and Jahren, 2010; Oelkers et al., 1992 and 1996; Ramm and Bjørlykke, 1994; Storvoll et al., 2005). The source of quartz cementation in the sandstones is from dissolution of the grains, approximately starts at 60^{o}C. On the other hand,

in shale it is from the transformation of the clay minerals to more stable forms, starts at approximate 70-80^{o}C (Bjørlykke, 2010; Maast et al., 2011). The amount of quartz cement availability in sandstone mainly dependent upon the grain to grain contact and dissolution (Bjørlykke and Jahren, 2010). In shale it mostly dependent upon the release of quartz from the transformation of clay mineral to much thermodynamically stable form (Bjørlykke, 2010; Bjørlykke and Aagaard, 1992).

To study the individual compaction trend for these two lithologies, Vp data is sorted on the basis of shale (Fig 5.7, 5.8 and 5.9). But it is not possible to study pure clean sandstone or shale data individually, by just using the well logs. This limitation increases the uncertainty in the whole study. But still an effort is made to give an idea of how these individual lithology affects compaction trends within the study area. At the beginning of the mechanical compaction regime the shale velocity is much less compared to sandstone. As soon as burial depth increases the velocity of shale is higher compared to sandstones (Avseth et al., 2005). But in and after transition zone the sandstone shows sharp increase of velocity trend where as the shale shows almost decreasing trends (Velocity reversal trend). In shale dominated intervals, over pressure develops, which halts further compaction, hence velocity reversal can be observed (Fig. 5.2) (Storvoll et al., 2005; Thyberg et al., 2000). In the chemical compaction regime (with further burial and increase temperature), dramatic increase of velocity can be observed which is marked by the red line. The gradient of the red line is much higher in sandstones when compared to shales. This may be explained by the crushing of grains and precipitation of the cement. The sandstone has much larger grain size which may crush and generate stylolites to precipitate the cement (Bjørlykke and Jahren, 2010) while in shale lithology it could be from the transformation of clay (Bjørlykke, 2010). An experimental Depth-Density relation for shale data points was compared with the Mondol et al., (2009) compaction trend. It shows the similar relation, the density increases significantly after the transtion zone which may indicates the chemical compaction (Avseth et al., 2005; Bjørlykke et al., 2009 and 2010; Chuhan et al., 2002; Lang, 1994; Revil et al., 2002; Storvoll et al., 2005; Weller, 1959). The sand density relation is not utilized because it's hard to separate the influence of carbonate and other lithologies by considering the shale volume estimated from the well logs.

5.2.4 Analysis of the petroleum system

The Balder field has significant amount of hydrocarbons. To analyze the compaction trends through the use of only well logs not only make a challenging task, but also put uncertainty in the results. The logging tools sometime under or overestimates the values due to the presence of hydrocarbons (Lin and Salisch, 1993). Other than that most of the wells have been from the 1960s and 1970s, which also add limitation on the quality of the data.

Source rocks

The source rock analysis is carried out by using the Vp data from the four wells (25/10-4, 25/11-5, 25/11-15 and 25/11-17). Out of twenty five wells, only these four wells have good quality of Vp and porosity data. These wells are deep enough to penetrate the source rocks. Moreover, the distribution of these four wells in the Balder field is enough to carry out the analysis. It can be seen in the Figure 5.10 that the data points which have higher temperature fall on the reference curve, while with lower temperature data points have higher values of Vp. This observation can be interpreted, as that lower velocity and density of the source rocks with higher temperature indicates that it may still holds the hydrocarbons. It indicate as well that the kerogen is quite soft compared to the surrounding matrix. It may be overpressured

due to the generation of hydrocarbon, this may lead in porosity reversal phenomena (Palciauskas, 1991; Pepper and Corvi, 1995; Storvoll et al., 2005). The higher velocity and density indicates that these intervals of source rocks have less amount of kerogene material and/or residual hydrocarbon. It also indicate that these intervals of the source rock may have slight quartz cementation within it, as the depth with respect to temperature to initiate the cementation is quite feasible (Avseth et al., 2005; Lin and Salisch, 1993; Rider and Kennedy, 2011; Storvoll et al., 2005).

Furthermore, the generation/expulsion of hydrocarbons may lead the higher porosity values, which cause further collapse of the pores due to the overburden stress. This lead to the micro fractures in the rocks. These fractures can give doubtful values on well logs (Neutron or density). These conditions may results in the low sonic velocity in source rocks as well (Bjørlykke, 2010; Passey et al., 1990; Storvoll et al., 2005). Further organic matter fills the pores between the grains, these conditions will overall decrease the density of the rock matrix, which results in decrease of the velocity (Løseth et al., 2010).

The other mechanism, which lead the velocity reversals in the source rock intervals is related to the ineffective drainage of fluids. The permeability is affected by the many factors like grain size, specific surface area, arrangment of minerals and fluid types (Broichhausen et al., 2005). The permeability significantly decreases as the compaction increases. Similarly, the organic matter in clay matrix will reduce the permeability, which causes ineffective explusion of the fluid. This lead in development of overpressure (Bjørlykke et al., 2010; Storvoll et al., 2005). This overpressure zone may carry the overburden load, which results in less compaction of the organic matter. This overpressure may help to retain the porosity and retard the compaction process. This can be detected by the decrease in sonic velocity (Avseth et al., 2010; Broichhausen et al., 2005; Løseth et al., 2010; Storvoll et al., 2005).

In addition, it can also be observed within the study area that the organic and clay dominated shale have different velocity at almost similar depths but in different formations (Fig. 5.16). In well 25/11-15, the source rock (Draupne Formation) is present, while in well 25/11-11 clay dominated Lista Formation is present (Chapter 4 results). Figure 5.16, illustrate that at even shallower depth interval (~1789 m) shale in well 25/11-11 shows higher velocity than the deeper depth (~1825 m) level shale interval in well 25/11-15. In general considering the compaction trend for sediments, the deeper interval should have higher velocity than the shallower sediments because of more crusing and packing of grains (Avseth et al., 2005; Bjørlykke and Jahren, 2005). This may shows that the compaction is also controlled by the presence of the kerogen in the rocks. The presence of mature kerogen increase pore pressure, which may retard compaction process. This may lead in velocity reversal (Bjørlykke, 2010; Storvoll et al., 2005). But these kinds of interpretations need cross verifications, which is beyond the scope of this study, due to the limitation of data. The depositional environment of the source rock is already discussed in the chapter 4.

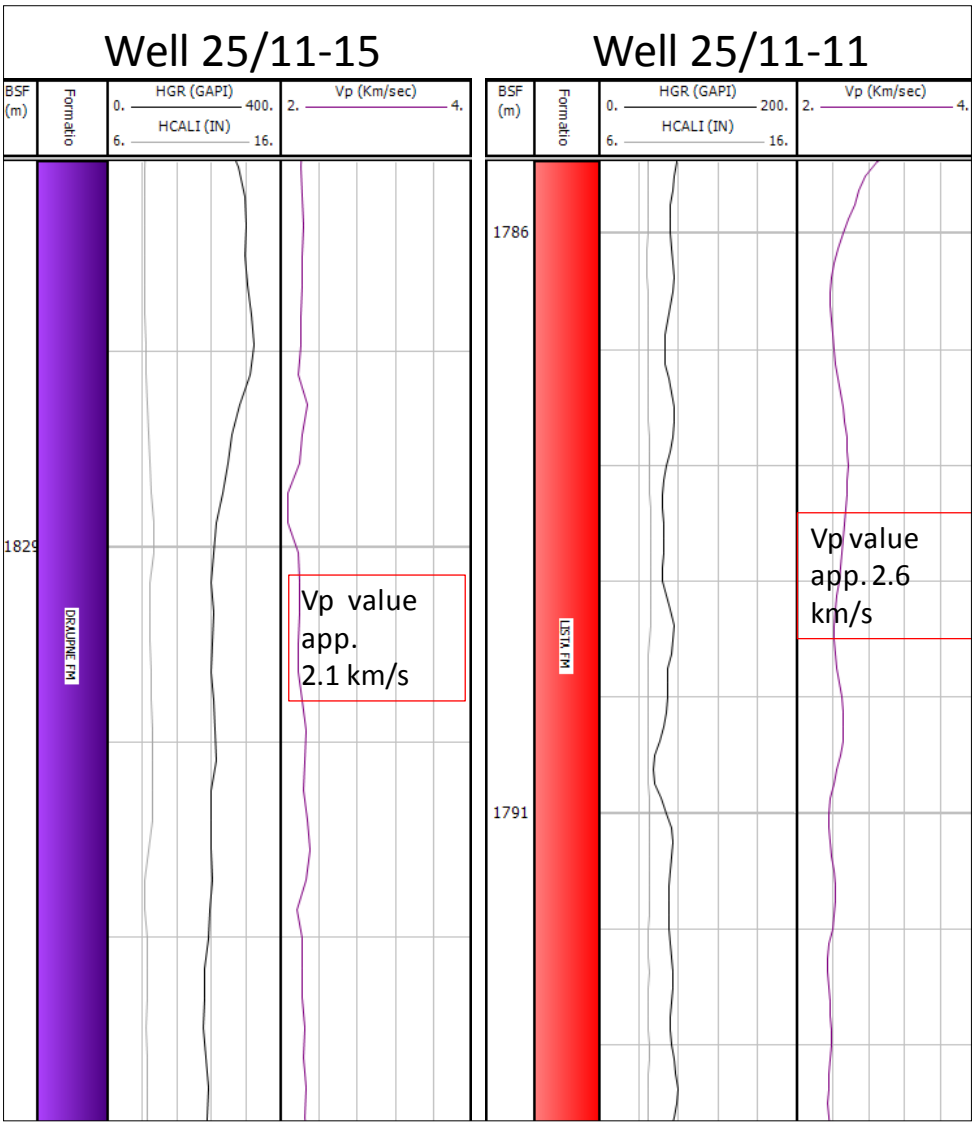

Figure 5.16 Velocity comparison of potential source rock (Well 25/11-15) with the shale dominated formation from well 25/11-11.

Reservoir rocks

The reservoir intervals show different behaviors on the Vp-density-porosity-depth cross-plot (Fig. 5.11). The intervals which are stratigraphically deep enough to the temperature ranges between 60 and 70 ^{o}C shows a sharp increase in the Vp values. This sharp increase in Vp indicates stiffness of the grain frameworks, which can be associated with the quartz cementation (Avseth, 2010; Bjørlykke, 2010). Moreover, the depth-porosity relation also indicates that these reservoir intervals have high porosity values (30%-35%). This illustrats that these intervals are poorly cemented and somehow, it retains the high porosity at such depth (1500 m-1800 m). This high porosity (low velocity zones) indicate that these intervals may develop overpressure (under compacted) specifically in the Balder Formation, which may contain significant amount of smectite (Bjørlykke and Aagaard, 1992; Thyberg et al., 2000).

Moreover, the base of the Balder Formation contains laminated mudstones. These mudstone intervals show high velocity peaks may represent the cement, as these beds are adjacent to the

tuff rich intervals. The volcanic ash layers (tuff) are few centimeters thick within the Balder Formation (Bjørlykke and Aagaard, 1992). These ash deposits are associated with the NE Atlantic opening, due to the volcaninc activities (Norlex, 2013; Peltonen et al., 2008). The ash layers (tuff) can be sourced for direct precipitation of quartz or can convert to smectite and then smectite to illite transformation to precipitate quartz cement (Bjørlykke, 2010; Bjørlykke and Aagaard, 1992). As described by the Karlsson et al., (1979)

$$\text{Glass (volcanic ash)} + H_2O \longrightarrow \text{smectite + silica +zeolite + metallic ions}$$

and the Boles and Franks, (1979)

$$\text{Smectite} + K + Al \longrightarrow \text{illite + silica + metallic ions} + H_2O + O^{-2} + OH^-$$

The higher porosity and low sonic velocity values indicate that the overpressure may be developed specifically in smectite-rich intervals (Balder Formation and cap rocks; shale dominant intervals) (Thyberg et al., 2000). Because the smectite-rich intervals are difficult to compact, as it can retain the bound water and have high specific area. These properties of smectite make it less permeable and much more resistive to the effective stress (Bjorlykke et al., 2009; Bjørlykke and Aagaard, 1992; Mondol et al., 2008; Peltonen et al., 2009; Thyberg et al., 2000).

Moreover, quartz cement can be precipitated within the volcanic ash layers or adjacent beds, by moving of silica-rich water (Bjørlykke and Jahren, 2010). The above transformations are mainly dependent upon the temperature. Volcanic glass alteration to smectite can be initiated at lower temperature (Karlsson et al., 1979), whereas smectite-illite alteration is at higher temperature (Bjørlykke, 2010). The deeper part of the basin may have less amount of the volcanic glass and smectite (Thyberg et al., 2000). But these assumptions have to be confirmed by other methods, which are beyond the scope of this study. The Balder Formation also contains the siliceous microfossils (diatoms) in the lower part, which may precipitate the cement as well, at much lower temperature (Bjørlykke and Aagaard, 1992; Bjørlykke, 2010; Norlex, 2013). Furthermore, the formation of opal-CT or micro quartz can also gives the peaks in Vp data at high porosity zones. Opal-CT can be formed at lower temperature by alteration of the volcanic ash or biogenic silica (opal-A). The amount of silica released from volcanic ash or by biogenic material is difficult to be quantified from the well logs (Aase et al., 1996; Avseth et al., 2005; Boles and Franks, 1979; Bjørlykke, 2010; Bjørlykke and Aagaard, 1992; Compton, 1991; Huggett et al., 2005; Jahren, 1993; Jahren and Ramm, 2000; Martinsen and Dreyer, 2001; Norlex, 2013; Ostvedt et al., 1990; Peltonen et al., 2008; Peltonen et al., 2009; Srodon, 1999; Storvoll and Bjørlykke, 2004; Storvoll et al., 2005; Towe, 1962; Weaver, 1959)

The pore water composition also plays a vital role in the precipitating of silica. However, environment of the deposition has fundamental control on the pore water composition (Bjørlykke and Jahren, 2010). The marine sandstone intervals (Hermod and Heimdal formations) are less likely to precipitate the early cement associated with the kaolinites. These deep marine (turbidites deposits) sandstone bodies may not be connected to the fluvial water influx or the influence of meteoric water flushing (Bjørlykke and Jahren, 2010). The shales of Sele and Lista formations have low permeability and effective porosity, which may restricts the flow of water. All of these circumstances lead to less cementation within these formations as kaolinitization needs meteoric water flushing. (Bjørlykke, 1996; Bjørlykke and Aagaard, 1992; Bjørlykke and Jahren, 2010; Keer et al., 1997).

Moreover, Huggett (1992), proposed that the source of silica can be from the reworking of the pyroclastics land deposits into the basin, during complex sequences of regression and transgression phases. This may increase the concentration of silica saturation in water, which leads to precipitation of quartz within the formation (Bjørlykke, 2010). These cementation processes give kicks not only in the Vp values of well logs but also on the seismic data as high positive amplitudes (Avseth et al., 2005). On the other hand, these reservoir formation still shows high porosities. This anomalies of high porosities decrease the sonic velocity in few intervals as well. It can be interpreted here that these formations are mostly in transition zone and poorly cemented. The reservoirs have good quality sandstones (Marcussen et al., 2010; Storvoll et al., 2005). These reservoir sands show less cementation related to the depth. For these kinds of assumptions and analyses, one have to do the thin section study to calibrate the results and discussion.

Cap rocks

The cap/seal rocks of the study area belongs to the Balder, Sele and Lista formations. These formations marked as the overpressure zone, which have been already explained earlier (Fig. 5.12). These formations may have high entry point of capillary pressure and act as the impermeable barriers, which may restrict the vertical movement of the hydrocarbons (Chatellier et al., 2011; Ingram et al., 1997; O'Connor et al., 2011). The permeability of these rocks are very low, it could be due to the several reasons, as these formations deposited during the volcanic events taken place in the North Sea (Faleide et al., 2010). The volcanic materials may convert to the smectite-rich clays, which deposited within these formations. Smectite-rich clays have itself low permeability and can retain porosity by entrapment of the bounding water (Bjørlykke and Aagaard, 1992; Peltonen et al., 2008; Thyberg et al., 2000). These conditions may lead to the overpressure development, when the compaction is applied (stress by overburden) (Marcussen et al., 2009; Storvoll et al., 2005). These over pressure regimes can directly decrease the sonic velocity, which are marked on the logs (Rider and Kennedy, 2011). In addition, the high gamma ray responses and low velocity intervals indicate the condensed section (Fig. 5.17). This may be deposited during the restricted and anoxic deep marine conditions (Myers and Milton, 2008; Milton and Emery, 2008; Myers and Milton, 2008; Timbrell, 1993).

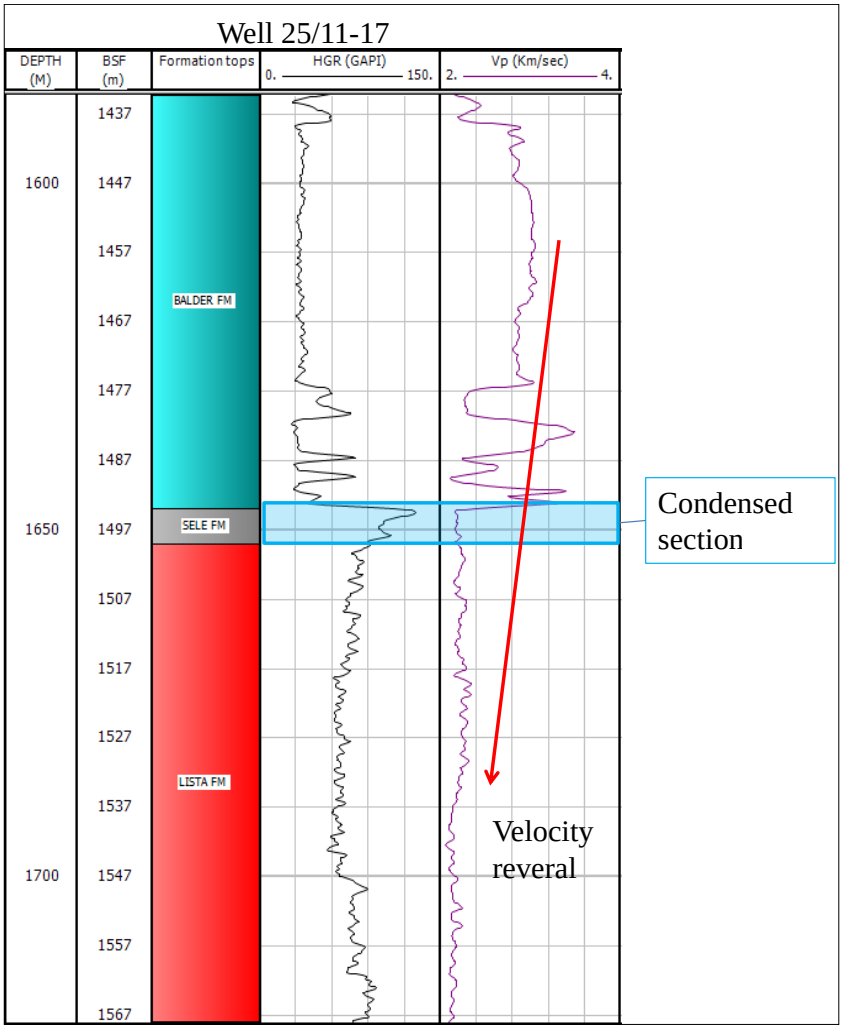

Figure 5.17 The high gamma ray peak and velocity reversal.

5.2.5 Transition zone and temperature effect

The transition zone is the interval, which may separates the chemical compacted regime from the mechanical compacted regime. This zone is not a just a line or a plane, it can be ranged of few tens of meters in depth. After this zone, the chemical compaction dominates as the rigidity of grains increase, hence restricts the further dominance of the mechanical compaction (Bjørlykke and Jahren, 2010). This zone can be marked by the sudden increase in the Vp values with respect to the depth, as only small amounts of cement may required for increasing the stiffness of the grains (Avseth et al., 2010; Bernabe´ et al., 1992; Dvorkin and Nur, 1996; Storvoll et al., 2005; Vernik and Nur, 1992).

Temperature is one of the key component for compaction analysis. Figure 5.13 demonstrate that the Vp and density increases due to the temperature variations. The Vp-density-depth cross-plot color-coded with the temperature is adopted. It can be seen in the Balder Formation that the Vp increases from 2000 m/s to 3200 m/s in less than 80 m section and with only slight change in the temperature. This significant increase of the Vp is not possible only due to the mechanical compaction. The temperature is quite high (~ 60-70 ^{O}C), where quartz cementation can be started (Bjørlykke, 2010). It can be interpreted here that the quartz cementation may started within the Balder Formation at the grain contacts, which stiffen the network frame of the sediments. This stiffness increases the velocity and density, which may

observed on the log response (Bjørlykke and Jahren, 2010; Murphy et al., 1989; Walderhaug, 1994a, and 1996). But overall effects of the chemical compaction is not that much to drive the sediments to much lower porosities (Average porosity of reservoir are 30-34%). The transition zone depth estimationtion is identified by series of cross-plots for each well (see the Appendix B). In detailed analysis and investigation through the well log data, the transition zone depth between the mechanical and the chemical regime, varies within the area (Table 5.1). In few wells , the transition zone is in the Balder Formation. The TZ is also observed in the Hermod and Heimdal formations in few wells. The main reason, which can be interpreted here for variation of depth in the transition zone is due to the difference of the geothermal gradient of the Balder field. The distance between the northern most well i(25/11-23) and the southern most well (25/11-17) is just over 21 km, but the geothermal gradient varies from 25^0 C/km (north-west) to 45^0 C/km (south east). This raise of the geothermal gradient causes more heat in the sedimentary layers which may lead to initiate the quartz cementation. The influence is much less in the Tertiary reservoir formations, but not negligible (Bjørlykke, 2010 and 2010b; Johnson and Fisher, 1998).

5.2.6 Uplift estimation

Uplift estimation is one of the important phases during the exploration and development of the field. It can affect the maturity of source rocks, quality of reservoir rocks or formation of seal rocks. The Balder field is located in the North Sea, which is well known as subsidizing basin (Faleide et al., 2010; Kjennerud et al., 2001). In compaction analysis, there is quite a practice to conduct the exhumation analysis by establishing the link between the Vp data from well logs to published compaction trends, with some uncertainty (Marcussen et al., 2010). Similarly, in this study the same methods are adopted. As in the Figure 5.14a, it can be observed that Vp-depth plot did not match with any of the published curves, which may represents the uplift. But to investigate it in more detail, the data is plotted with Mondol, (2009); Kaolinite:Silt (50:50) (Fig. 5.15b). This curve gives promising and spectacular result in the Barent Sea basins, which are well known for the upliftment. It can be seen that this curves only give the estimation between 200-300 m in the Balder field. This can be associated with the rotated fault block or the particularly lifted area on the Utsira High (Faleide et al., 2010; Kjennerud et al., 2001). In addition, 200-300 m upliftment can be associated with the regional upliftment associated with the Icelandic plume or related phenomena (Faleide et al., 2010; Nadin et al., 1997). It can also be associated with the post glacial rebound (18,000 years ago) or isostatic rebound (Bungum et al., 2010; Lambeck, 1995). The uncertanities of paleogeothermal gradient compared to the present day geothermal gradient may mislead the results. On the otherhand, uncertanity to measure the BHT (the main source of the present day geothermal gradient) may also misguide the results.

Chapter 6: Rock physics diagnostics of the Balder field

This chapter is mainly focused on the rock physics diagnostics of the Balder field using the well log data. The analysis relies on the results, which are generated in the early part of the study (Chapters 4 and 5). An effort is made to analyse the rock properties of the reservoir rocks utalizing different rock physics templates (RPTs). These templates are digitized from the literatures data published by several authors (Avseth et al., 2005 and 2009;), which have already been explained in the chapter 3.

6.1 Results

6.1.1 Analysis of reservoir rocks

In chapter two and four, it has been recognized that the study area has three reservoirs in the Paleocene and Eocene sandstones. The Balder, Hermod, and Heimdal formations contained thick sandstone intervals, which saturated with hydrocarbons depending upon their stratigraphic location and depth. It predicted in the chapter 5 that these reservoir formations possess poorly cemented intervals. In this section, published rock physics templates and the field log data linked together to understand further the reservoir horizons. This investigation is not only help us to understand the reservoir formations, but also help to understand the relationship between fluids, lithology, and sonic/seismic parameters. These parameters in one or another way around may affect each other; hence compromise the reliability of results. Moreover, for the better understanding, each of the reservoir formations, a series of cross-plots utilized for interpretation of reservoir quality.

Balder Formation

In this part of diagnostics, data points from 17 wells are plotted in each model.

Velocity-Porosity-Clay relationships

In this step, variation and the effect of velocity and porosity, due to the presence of the clay content, in the reservoir formations are studied. Han (1986) model used to demonstrate and compare the results, with the laboratory data to the field data. The data sorted and divided into four categories, depending upon the clay contents, as described in the third chapter. For better understanding of the reservoir formations, the data sets also color-coded by water saturation, shale volume, and depth.

In the Figure 6.1, data points from the Balder Formation of the water-saturated points plotted with Han (1986) model. In the Figure 6.1a, the selected data color-coded by the water saturation showed that none of the sorted data is following any trend line suggested by Han (1986). In Figure 6.1b, the data color-coded by the shale volume showed that a cluster of data shows different behavior than rest of the data. By further investigation it comes out that these points are from one particular well (25/10-2), which has bad borehole conditions. However, in this well, the stratigraphic depth of the Balder Formation is deeper compared to the other wells (Fig. 6.1 c).

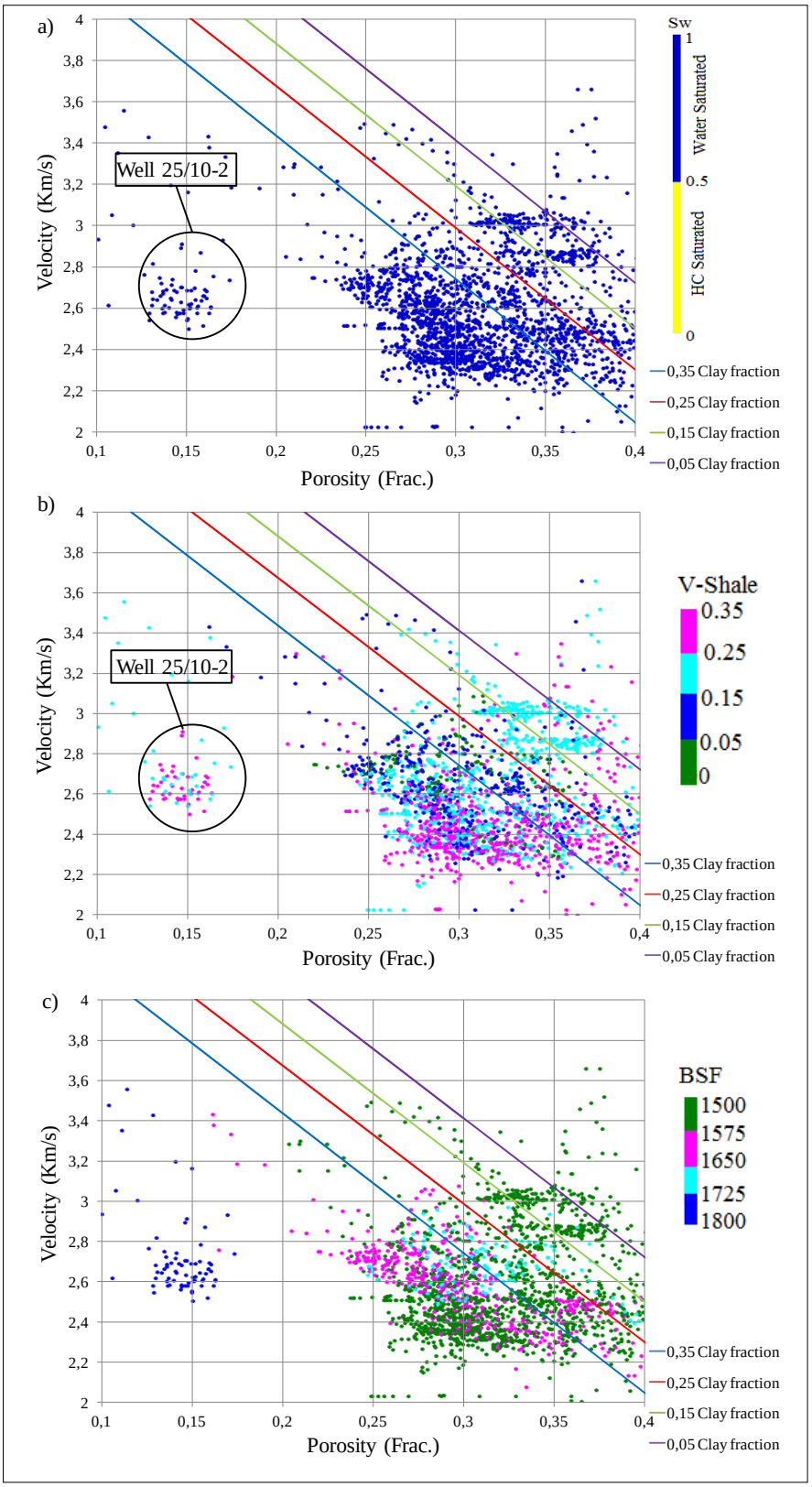

Figure 6.1 The Balder Formation data superimposed on Han (1986) model for porosity-velocity cross-plots color-coded by a) Water saturation b) Vsh and c) Depth (BSF).

The sediments from the deeper part of the basin (well-25/10-2), show lower porosities as compare to the shallower part. This may represent that the effective stress reduced the

porosity (Fig. 6.1c) (Bjørlykke et al., 2010). Furthermore, in the Figure 6.1b, it is observed that the data that contained 0.05 fraction of clay or less, does not follow the 0.05 fraction clay Han's line instead most of the data points scattered below the 0.35 clay trend line. The data, which contained clay content of 0.05-0.15 fraction mostly, scattered between 0.25-0.35 and below the 0.35 fraction of the clay trend lines. The data, which contained clay content of 0.15-0.25 fraction mostly, fall between the 0.15-0.25 clay trend lines. In addition, the data, which contained clay content of 0.25-0.35 fraction mostly, fall between 0.25-0.35 fraction and below 0.35 clay trend lines. When the same data color-coded with depth, it is easily observable that overburden stress has great influenced on the porosity and velocity relation. The sediments, which represent the deeper parts of the basin specifically from the well 25/10-2, shows decreased trend in porosity, as compared to the shallow buried sediments. However, there are quite few types of sediments, which have showed lower velocity with high porosity and do not follow their respective clay content trend lines. In the Figure 6.2, hydrocarbon saturated data is used. It is easily observed that clean sandstone intervals (clay volume less than 5%) do not follow the 5% clay trend line. Similarly, sediments ranging between 0.15-0.25 shale volumes do not follow their respective experimental trend line either. It is easily observable here that the presence of hydrocarbon decreases the P-wave velocity (Avseth et al., 2005).

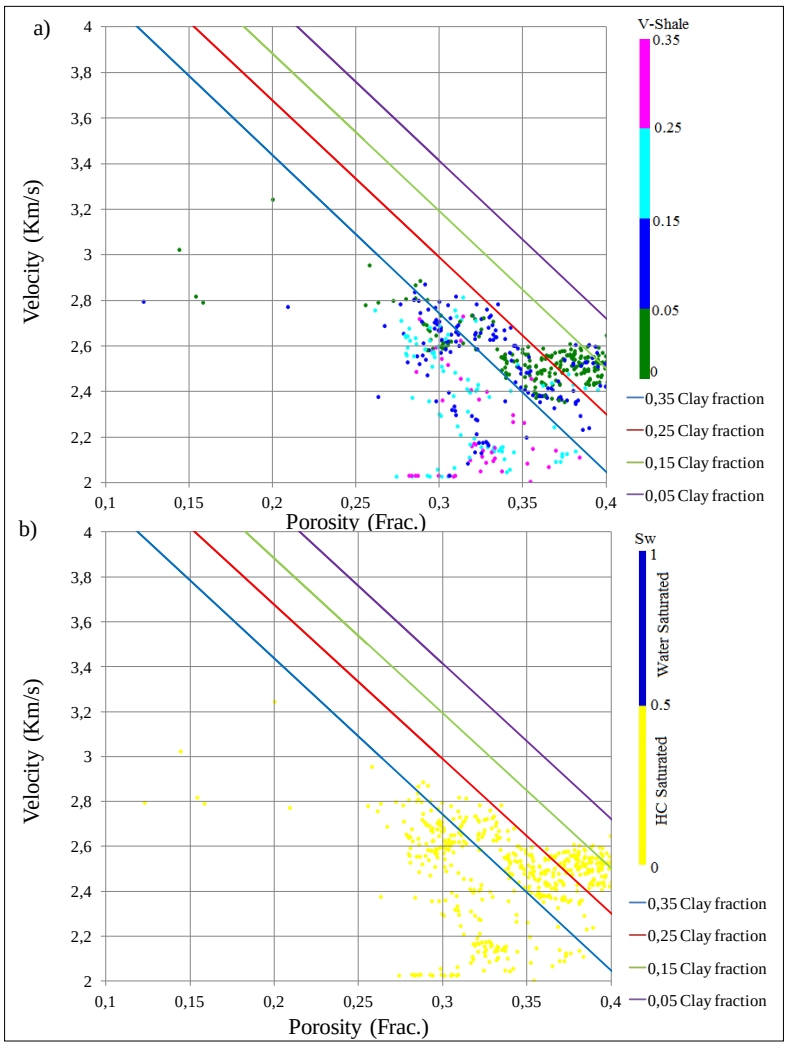

Figure 6.2 The Balder Formation and Han (1986) model superimposed in velocity-porosity crossplots color-coded by a) Vsh and b) Water saturation.

Rock physics cement models

It was previously investigated that the reservoir formations may have a small amount of quartz cement, but the porosity is relatively high (results from the chapters 4 and 5). To investigate it further, rock physics cement models (Dvorkin and Nur, 1996) are utilized. These models account the data of the porosity and velocity color coded by the Vsh, Sw and depth. A different approach is used in this analysis to understand better the reservoir rocks.

In the Figure 6.3, data points from the Balder Formation plotted with the three rock physics cement models. In this plot (Fig. 6.3a), only the water saturated data points are used. It can be observed from the Figure 6.3b that the data cluster display entirely different behavior in contrast to the other data points. These data points are particularly from well 25/10-2, which pointed out early to have poor quality porosity data, because of bad borehole condition, but represent the deeper part of the basin. Furthermore, one data cluster, plunge on the constant cement line. This cluster belongs to the well 25/11-17. It shows higher velocity, which may indicate the quartz cementation (Avseth et al., 2005). This well is from the southern part of the Balder field, where geothermal gradient is higher due to the shallow basement rocks (analysis in the chapter 5).

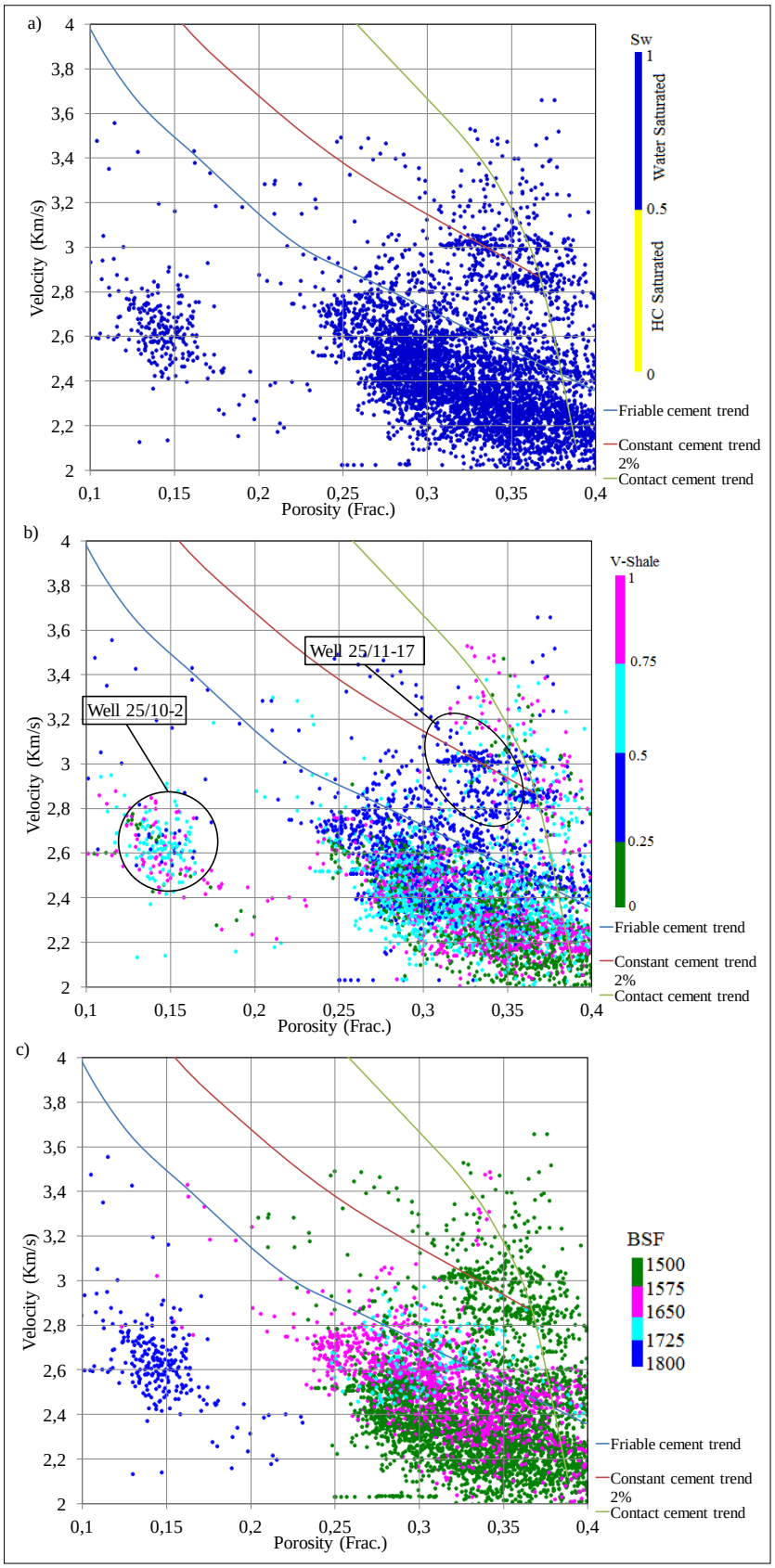

Figure 6.3 The Balder Formation data superimposed with rock physics cement models color-coded by a) Water saturation b) Vsh c) BSF depth. Overlay lines digitized from Avseth et al., 2005.

In the Figure 6.4, only the hydrocarbon-saturated data points from the Balder Formation are plotted with the three rock physics cement models. For better understanding and visualization, the hydrocarbon saturated data points are plotted (Fig. 6.4b). It can be observed (Fig. 6.4 a) that most of the data points scattered on or below the friable sand model. This could be due to the saturation of the hydrocarbon. The hydrocarbons have strong influenced to decrease the sonic velocity.

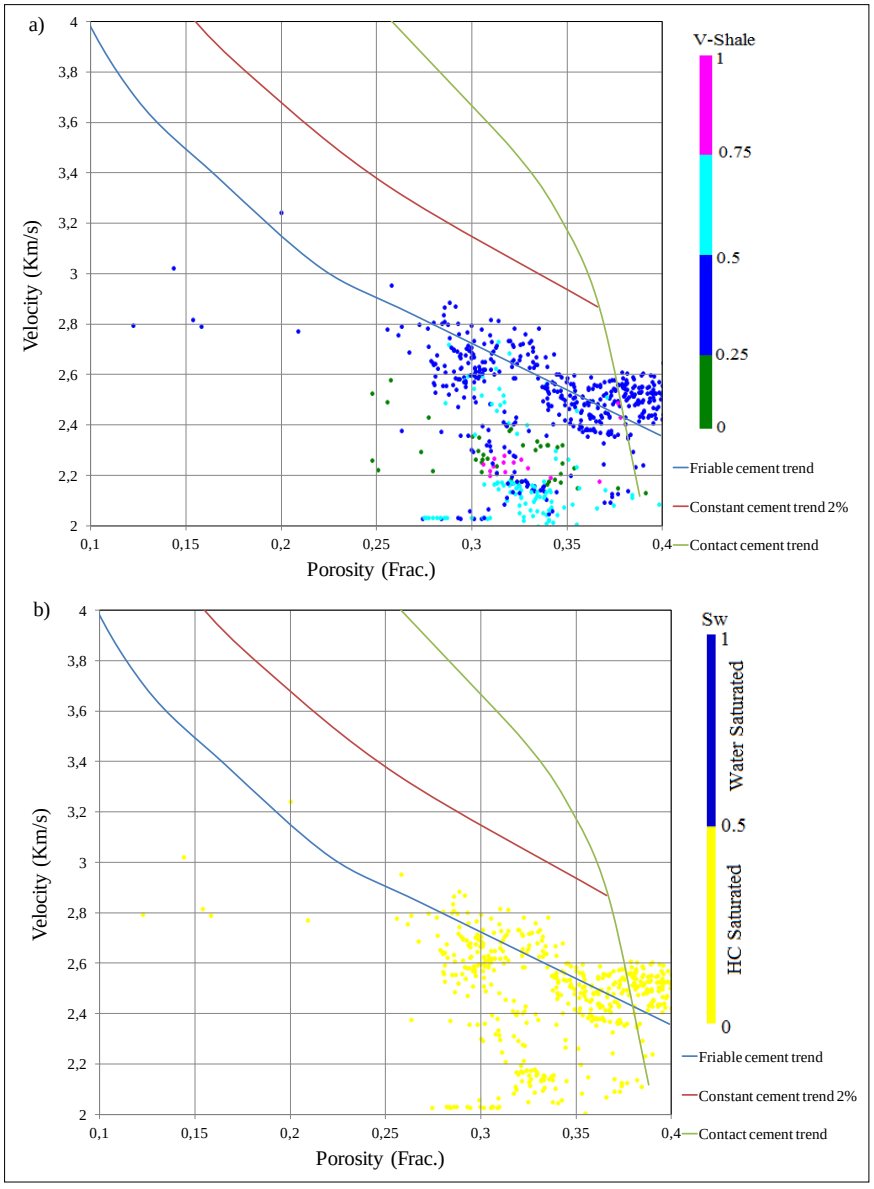

Figure 6.4 The Balder Formation hydrocarbon saturated data superimposed with the rock physics cement models, color-coded by a) Vsh b) Water saturation. Overlay lines digitized from Avseth et al., 2005.

Acoustic impedance versus Vp/Vs

The standard rock physics templet (acoustic impedance versus Vp/Vs ratio cross-plot) is used. The reference curves, which are used in these plots are digitized from Avseth et al., 2009. The Vp/vs versus IP crossplots helps to distinguish the reservoir sands from the shaley

lithology and then hydrocarbon saturated reservoir sands to brine saturated reservoir sands. This plot is also helpful for separating poorly cemented sands as well.

In the Figure 6.5, the data points from the Balder Formation plotted. The Figure 6.5a, data is color-coded by the shale volume. It is easily observable that the shale and the sandstone lithology separated on this plot. The separation is not that much distinct as compared to the shale line but it is adequate to mark the reservoir interval by color coding the data with Vsh. Furthermore, the same data color-coded by the water saturation (Fig. 6.5b). In the Figure 6.5b, it is clear that the hydrocarbon isaturated data separate from the brine saturated data points, which follow the poorly cemented and water saturated sandstone curves. None of the points have followed the gas saturated line.

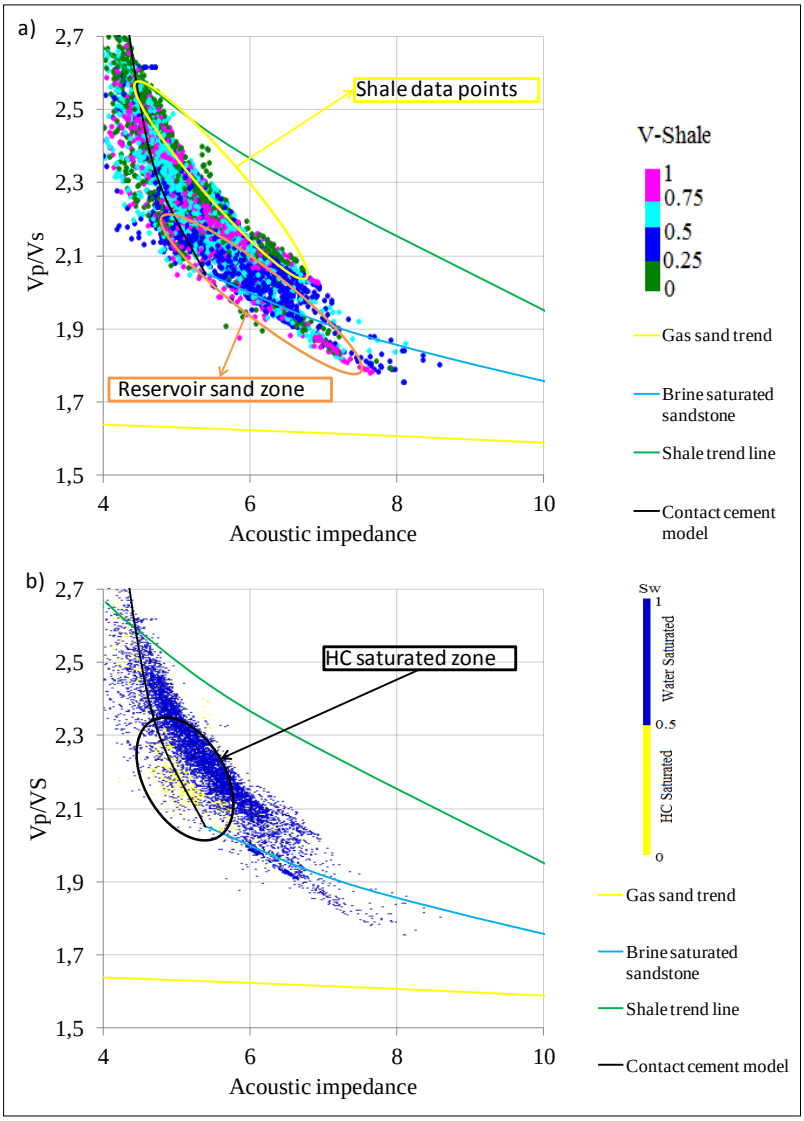

Figure 6.5 Vp/Vs-AI cross-plots, The Balder Formation, data points color-coded with a) Volume of shale b) Water saturation. Overlay lines digitized from Avseth et al., 2009.

Lambda-Mu-Rho cross-plots

The Lambda-Mu-Rho cross-plot are used to demonstrate the reservoir response. In these cross-plots, the data color-coded with the shale volume and water saturation. In the Figure

6.6a, the data points from the Balder Formation plotted and color-coded with the shale volume. It is easily observable (Fig. 6.6a) that the potential sand intervals separated from the shale units. This plot indicates that the Balder Formation have high amounts of shale, which may act as the cap/seal rock for the reservoir intervals. The same data points color-coded with water saturation (Fig. 6.6 b), indicate that sandstone intervals saturated with hydrocarbon plunge to the lower left side as compared to the those points saturated with brine.

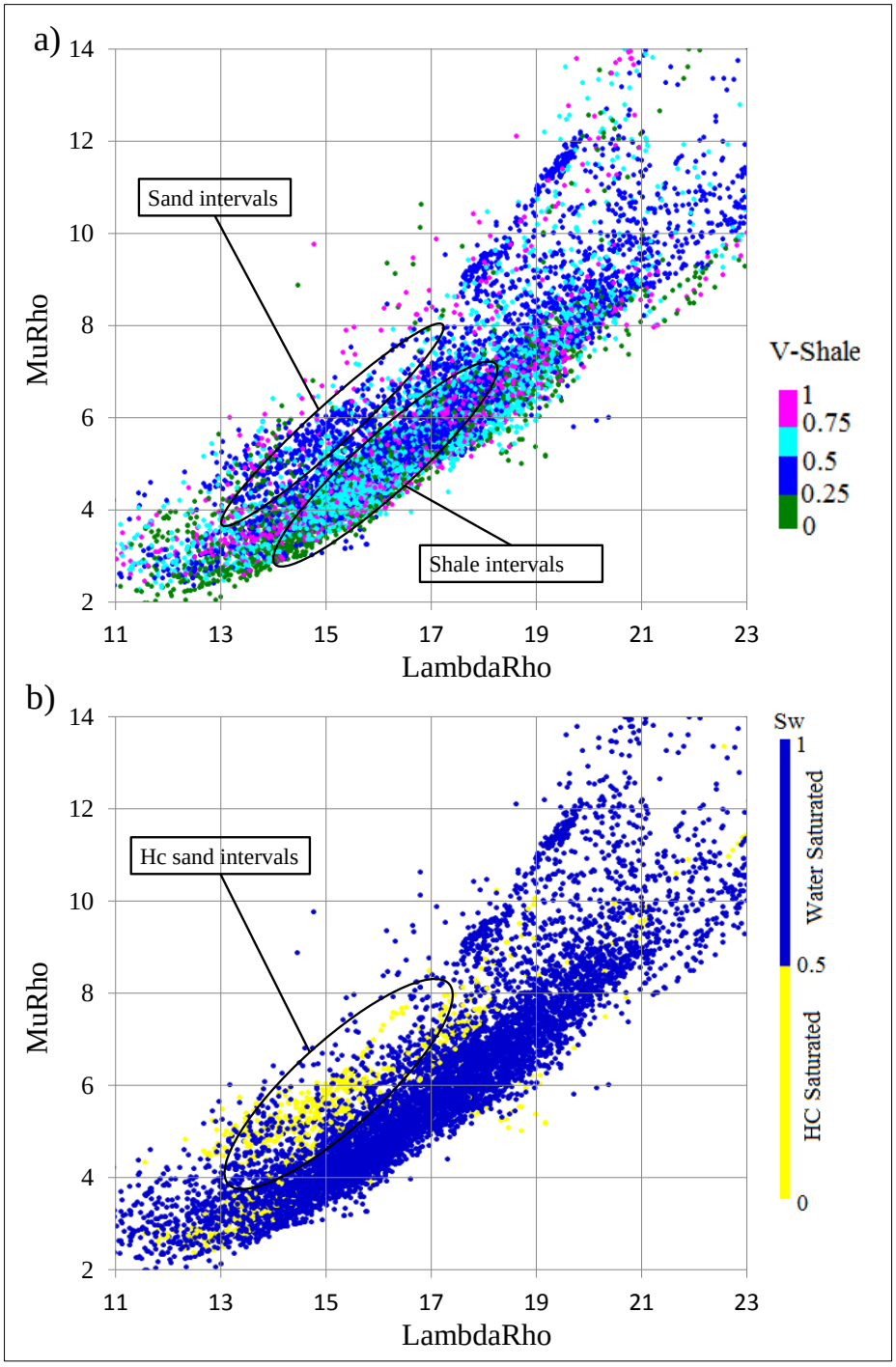

Figure 6.6 LMR cross-plots, the Balder Formation data points, color-coded with a) Vsh and b) Water saturation.

Hermod Formation

In this part of diagnostics, data points from 5 wells are plotted in each model.

Velocity-Porosity-Clay relationships

The velocity-porosity data plotted with Han (1986) experimental curves for the better understanding of clay content in the reservoir sands. In the Figure 6.7, only water saturated points used. The water saturation color-coded points also plotted in the cross plot (Fig. 6.7a). In the Figure 6.7b, the data color-coded by shale volume, for better understanding on distribution of clays in the Hermod sands. Two data cluster marked on the clean sandstone interval, both have same velocity but different porosity. To investigate it further, the same data points color-coded by the depth and plotted in the Figure 6.7c. It is easily observable that low porosity points belong to the shallower part, while higher porosity fits to the deeper part. This expresses that the compaction of sediments in this formation interval is mostly due to the depositional environment than to the depth related diagenetic influence (Bjørlykke et al., 2010). Most of the data points are from the clean sandstone intervals (Less than 0.05 fraction), but these points do not follow the clean trend line (less than 5% clay line).

In the Figure 6.8, hydrocarbon-saturated points plotted for the Hermod Formation. It is easily noticeable that one of the data sets shows different behavior compared to the rest of the data cluster. With further examination, these data points are from the well 25/11-5. These points show the 0.05-0.15 volume of shale range. These points show higher velocity in contrast to the model proposed by Han (1986). This could be due to the quartz cementation initiation. Other clusters of the clean sandstones (0-0.05 clay volume) show lower velocities than predicted values by Han (1986). It could be due to the presence of the hydrocarbon.

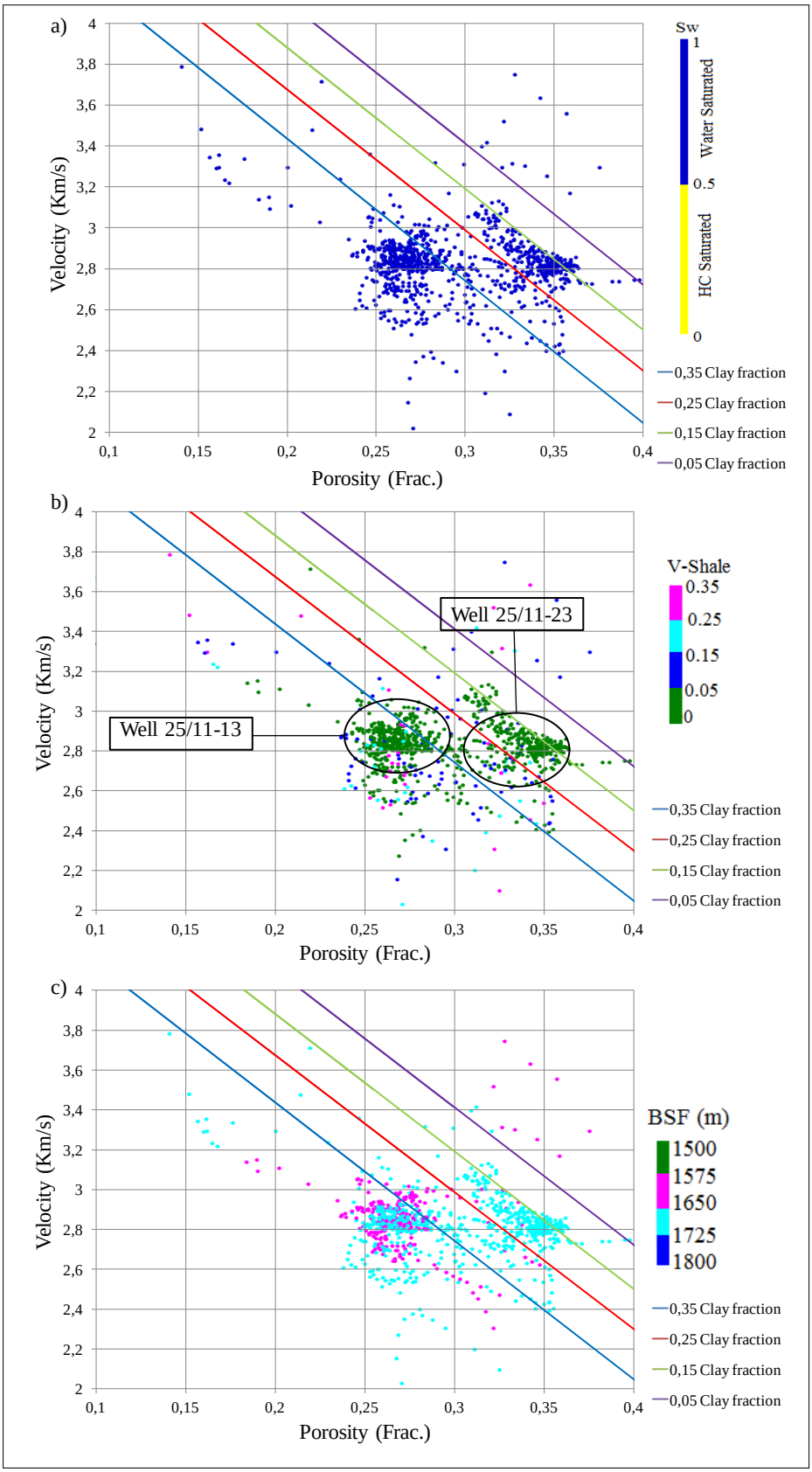

Figure 6.7 The Hermod Formation data and Han (1986) model, color-coded with a) Water saturation b) Vsh c) BSF depth.

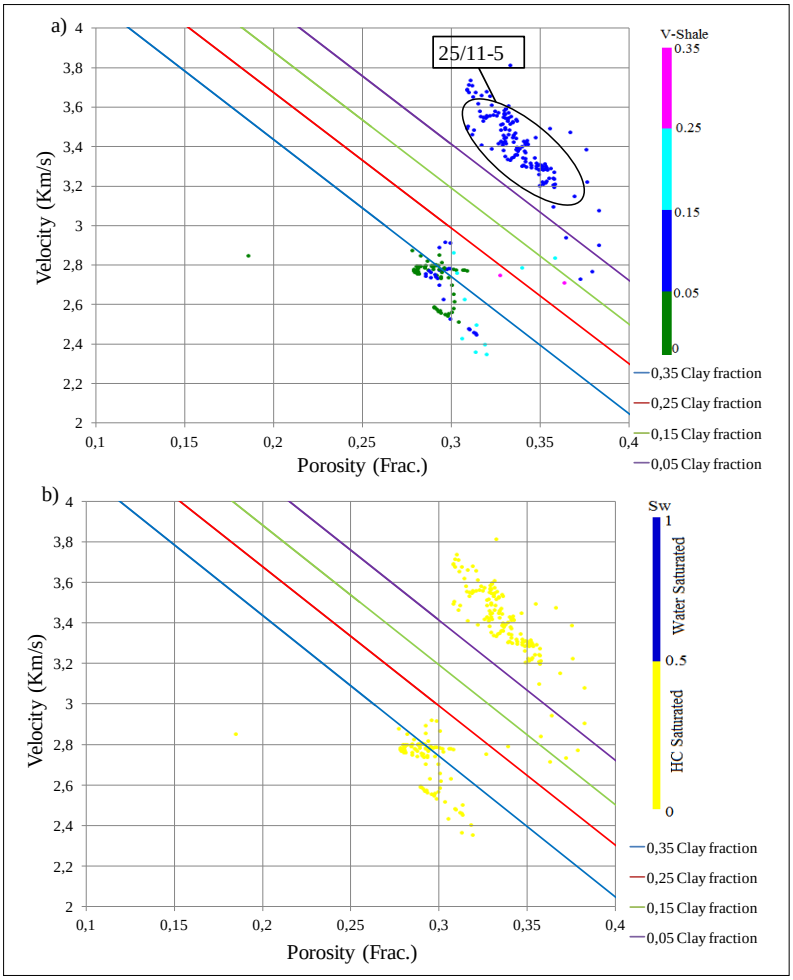

Figure 6.8 The Hermod Formation and Han (1986) model superimposed in velocity-porosity crossplots color-coded by a) Vsh and b) Water saturation.

Rock physics cement models

The comparison of Han (1986) model and the data from the Hermod Formation gives different anomalies. In this investigation, data color-coded by the water saturation, Vsh and depth.

In the Figure 6.9, the data points from the Hermod Formation plotted with the rock physics cement models. It is observed that the most of the data points plunge on the friable sand model line and some points plunge between the friable and constant cement lines. This may indicates that the Hermod Formation possess poorly cemented intervals in the studied wells. However, few points also plunge on the contact cement line. These points are from the same well 25/11-5. This particular well may have initial cementation. In the Figure 6.9b, the clean sandstone intervals (shale volume less than 0.25), shows different porosity values. The higher porosity values plunge across the constant sand line, while lower porosity values plunge across the friable cement line. Furthermore, when same data points, color-coded with the depth (Fig. 6.9 b) it reveals that the higher porosity data points are from the shallower zone.

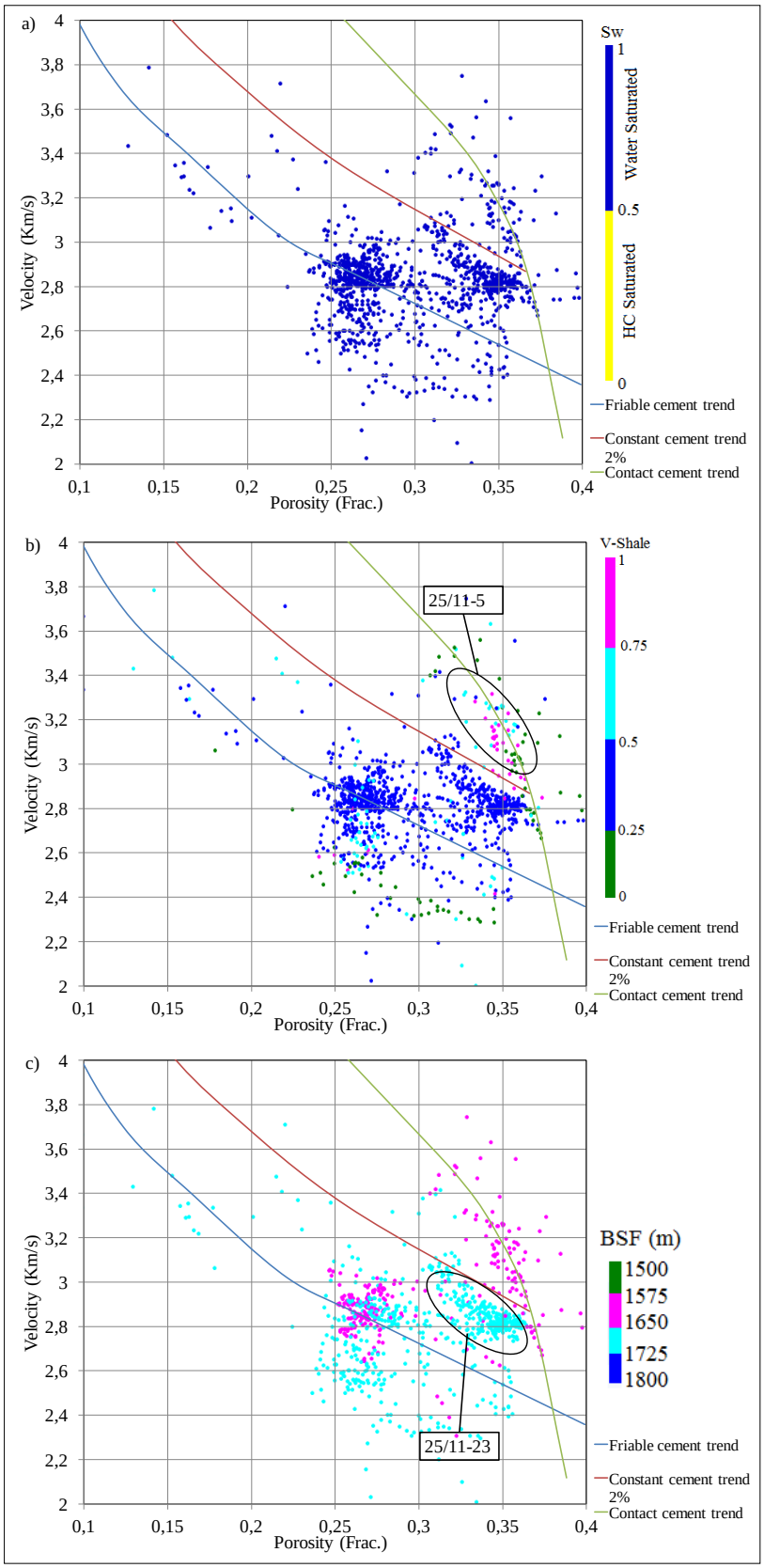

Figure 6.9 The Hermod Formation, hydrocarbon-saturated data superimposed with the rock physics cement models, color-coded by a) Vsh b) Water saturation. Overlay lines digitized from Avseth et al., 2005.

In the Figure 6.10, the data points from the Hermod Formation plotted with the three rock physics cement models. Only hydrocarbon saturated sediment data points plotted. For better understanding and visualization, the hydrocarbon saturated color-coded data points also plotted (Fig. 6.10b). It is clear (Fig. 6.10a) that one data cluster shows entirely different behavior than the other. These data points are particularly from the well 25/11-5. As explained before, these points plunge directly on the contact cement line, which may indicates that this intervals experienced the cementation. But the porosity is still high, which may indicate the the initial cementation stage (Avseth et al., 2005).

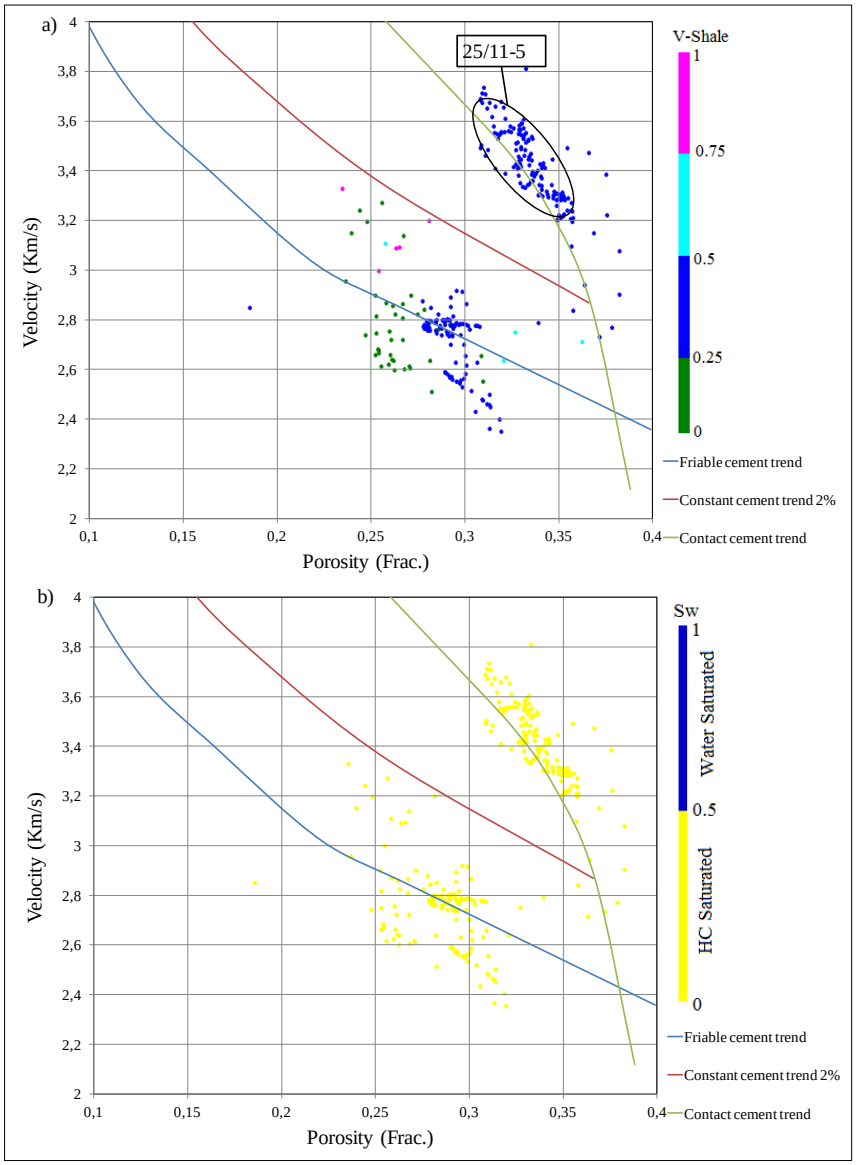

Figure 6.10 The Hermod Formation, hydrocarbon-saturated data superimposed with the rock physics cement models, color-coded by a) Vsh b) Water saturation. Overlay lines digitized from Avseth et al., 2005.

Acoustic impedance vs Vp/Vs

The data points from the Hermod Formation plotted on the standard rock physics acoustic impedance versus Vp/Vs cross-plots (Fig. 6.11). These points color-coded with the shale

volume in the Figure 6.11a. The shale and sand lithologies separation is easily observable in this plot. For the same reason which mentioned earlier, shale and sandstone separation is not that much as the model curves. Furthermore, the same data points from the Hermod Formation color-coded by water saturation. In the Figure 6.11b, it is noticed that hydrocarbon intervals separated, which may follow the contact cement curve and crosses the water saturated sandstone trend. But hydrocarbon saturated intervals do not scatter on or near the gas saturated line.

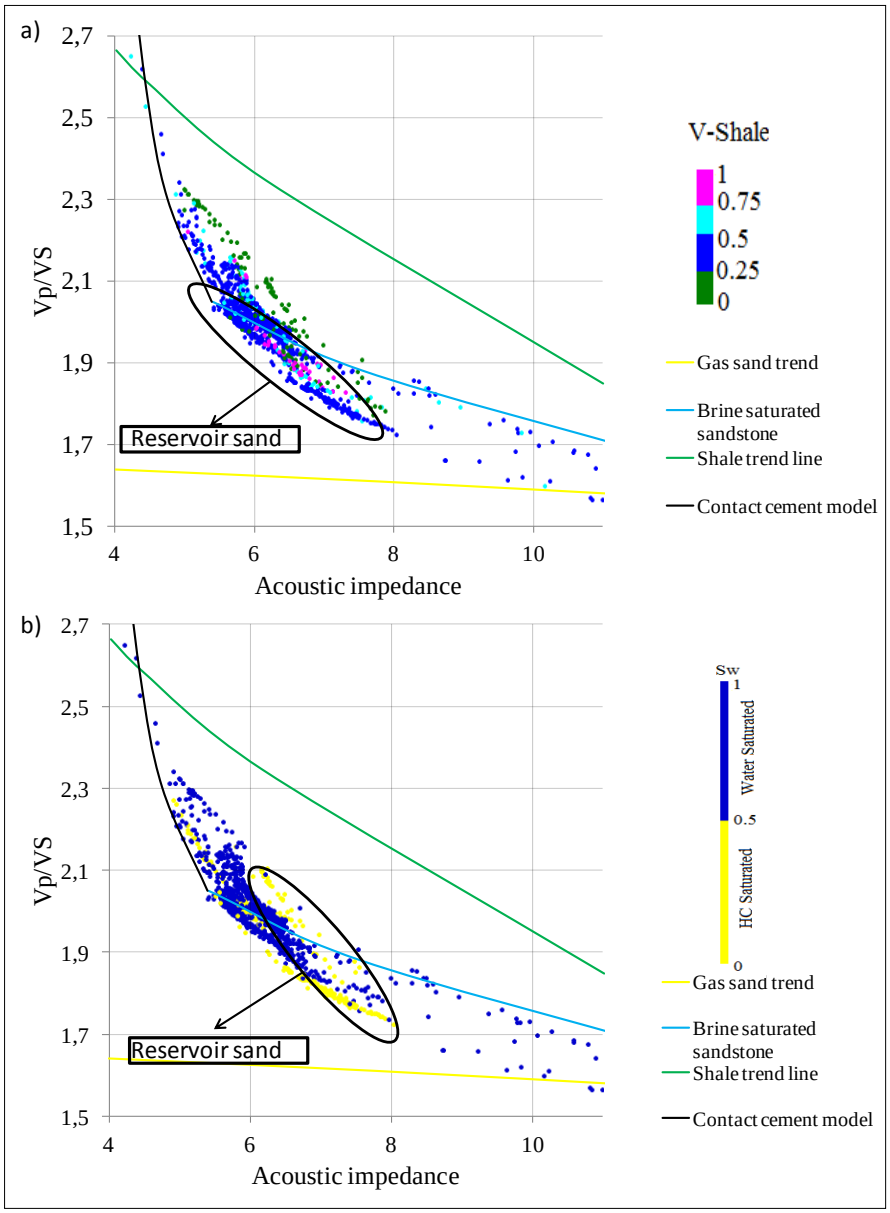

Figure 6.11 Vp/Vs-AI cross-plots, the Hermod Formation data points color-coded with a) Vsh b) Water saturation. Overlay lines digitized from Avseth et al., 2009.

Lambda-Mu-Rho cross-plots

As same as the Balder Formation, the same series of LMR cross-plots used to diagnose the Hermod Formation. In the Figure 6.12a, the data points from the Hermod Formation plotted and color-coded by the shale volume. It is observed (Fig. 6.12a) that the potential reservoir sand intervals separated from the shale units. It also shows that the Hermod Formation not

only have good reservoir quality sands but also has high net-to-gross ratio. Furthermore, in the Figure 6.12b, the same data points color-coded by the water saturation. Other than main cluster of sandstone points, a small patch of the sandstone also marked, which belongs to the well 25/11-5. This well has been diagnosed before as with early cementation stage. Mu-Rho is sensitive to lithology, which may also indicate that this cluster of the sediments have initial sign of cementation (Goodway et al., 1997).

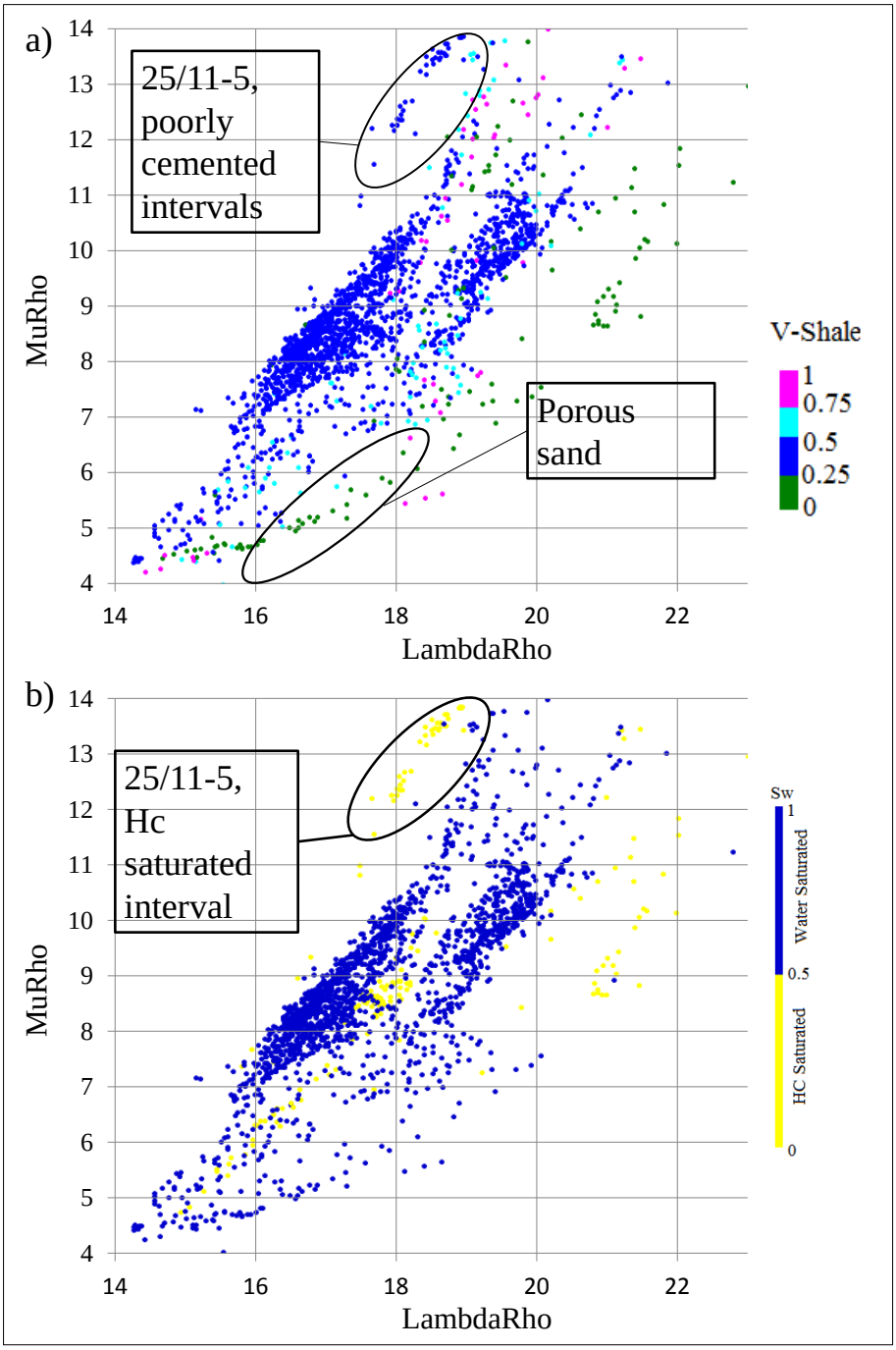

Figure 6.12 LMR cross-plots, the Hermod Formation data points, color-coded with a) Vsh and b) Water saturation.

Heimdal Formation

In this part of diagnostics, data points from 15 wells are plotted in each model.

Velocity-Porosity-Clay relationships

The velocity-porosity data plotted with Han (1986) experimental curves (Fig. 6.13). In Figure 6.13, only the water saturated data points are plotted. The data is color-coded with the water saturation (Fig. 6.13 a). It is easily observed in Figure 6.13 b that most of the field data do not follow the experimental curves established by the Han (1986). Only data points which contained 15-25% of shale volume plunge across the 15% clay line. Other than that, the three clusters of data are marked. One cluster of data showed low porosity behavior than the rest. These points are from the well 25/10-2. The porosity data disturbed due to the bad borehole conditions. Furthermore, this cluster also represents the deeper points of the basin. This may indicates that the effective stress reduce the porosity (Bjørlykke and Jahren, 2010). The other cluster of data has higher velocity. These data points are from the well 25/11-5, which mentioned before, during the Hermod Formation diagnostic. These data points may have poor cementation, by which the velocity data gives peaks without affecting the porosity (Avseth et al., 2009). Furthermore, it is easily observable (Fig. 6.13 a) that the Heimdal Formation contains clean sandstone intervals with less than 5% clay content. These intervals do not match with the any of the reference curves, particularly the clean sandstone experimental curve (Han's 5% clay line). In Figure 6.13 b, it is easily observed that none of the sorted points follows the Han's clay trend line. It may be due to the errors in porosity or Vsh calculations or the uncertainties in the p-wave velocity. In Figure 6.14, hydrocarbon saturated data points from the Heimdal Formation plotted with the Han (1986) model. The data is mostly from the clean sandstone intervals. This clean sandstone points (shale volume less than 5 %), do not match the Han's clay line of 5%, but it plunge underneath it.

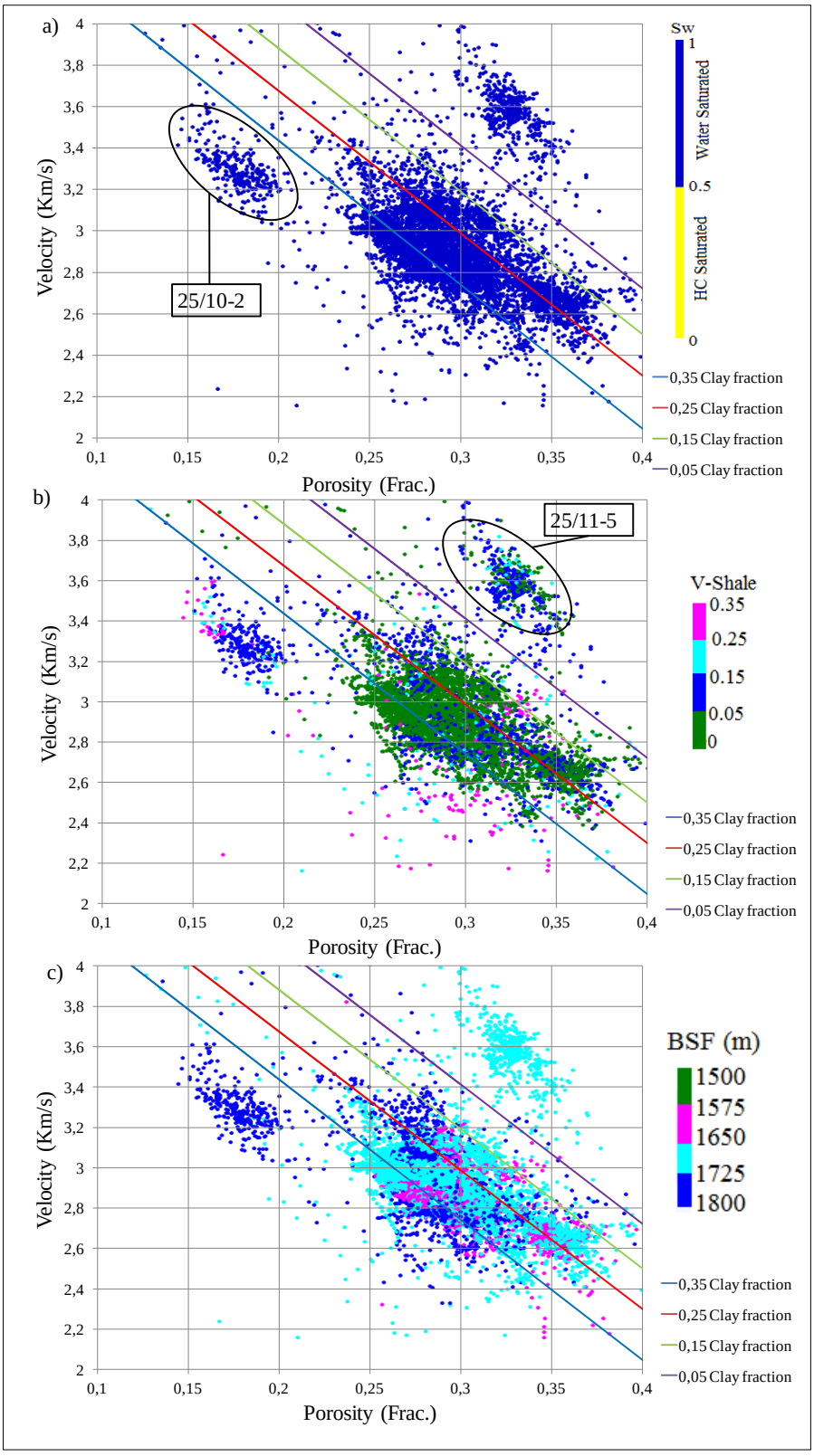

Figure 6.13 The Heimdal Formation data superimposed on Han (1986) model for porosity-velocity cross-plots color-coded by a) Water saturation b) Vsh and c) Depth (BSF).

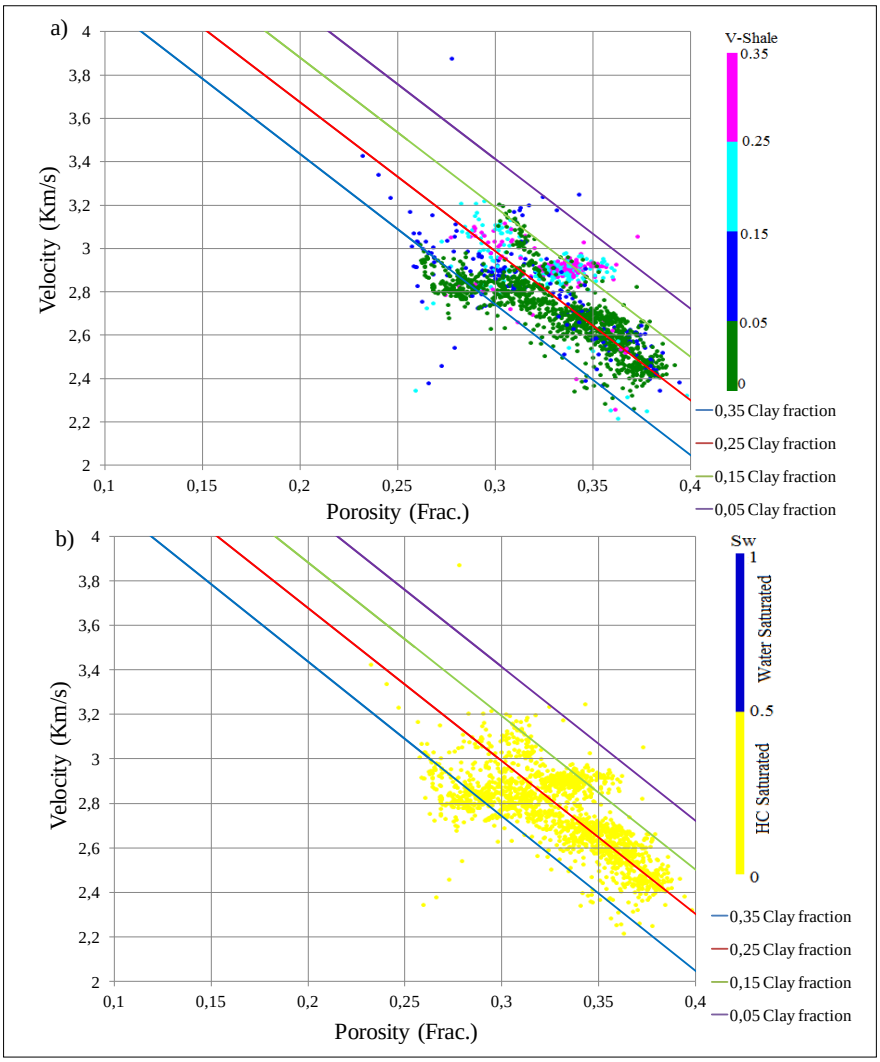

Figure 6.14 The Heimdal Formation and Han (1986) model superimposed in velocity-porosity cross-plots color-coded by a) Vsh and b) Water saturation.

Rock physics cement models

In the Figure 6.15, data points from the Heimdal Formation plotted with the three rock physics cement models. Data points are of the water saturated intervals (Fig. 6.15 a). It is easily observable that the two data cluster shows different behavior from main cluster of data (Fig. 6.15 b). The data cluster from the well 25/11-5, which have been discussed before, plunge on the contact cement line, but the porosity values are still high. This may indicate the initial cementation at grain contacts, which gives peaks in the sonic velocity (Avseth et al., 2005). The other data cluster is from well 25/10-2, which discussed early. These data points are from the deeper part of the study area, which spectacles low porosity. But these data points plunge on the friable cement line which may specify that these intervals are not cemented. The Figure 6.15 b also illustrate that most of the data points plunge between the friable and constant cement models. This may show the poor cementation within the Heimdal Formation. Furthermore, hydrocarbon saturated data points plotted on the rock physics cement models. In the Figure 6.16, it is easily observable that most of the points plunge between the friable sand line and constant cement line model. It may show these intervals are mostly poorly cemented. Other than that these intervals also saturated with the hydrocarbons, which may have tendency to decrease the sonic velocity (Avseth et al., 2005).

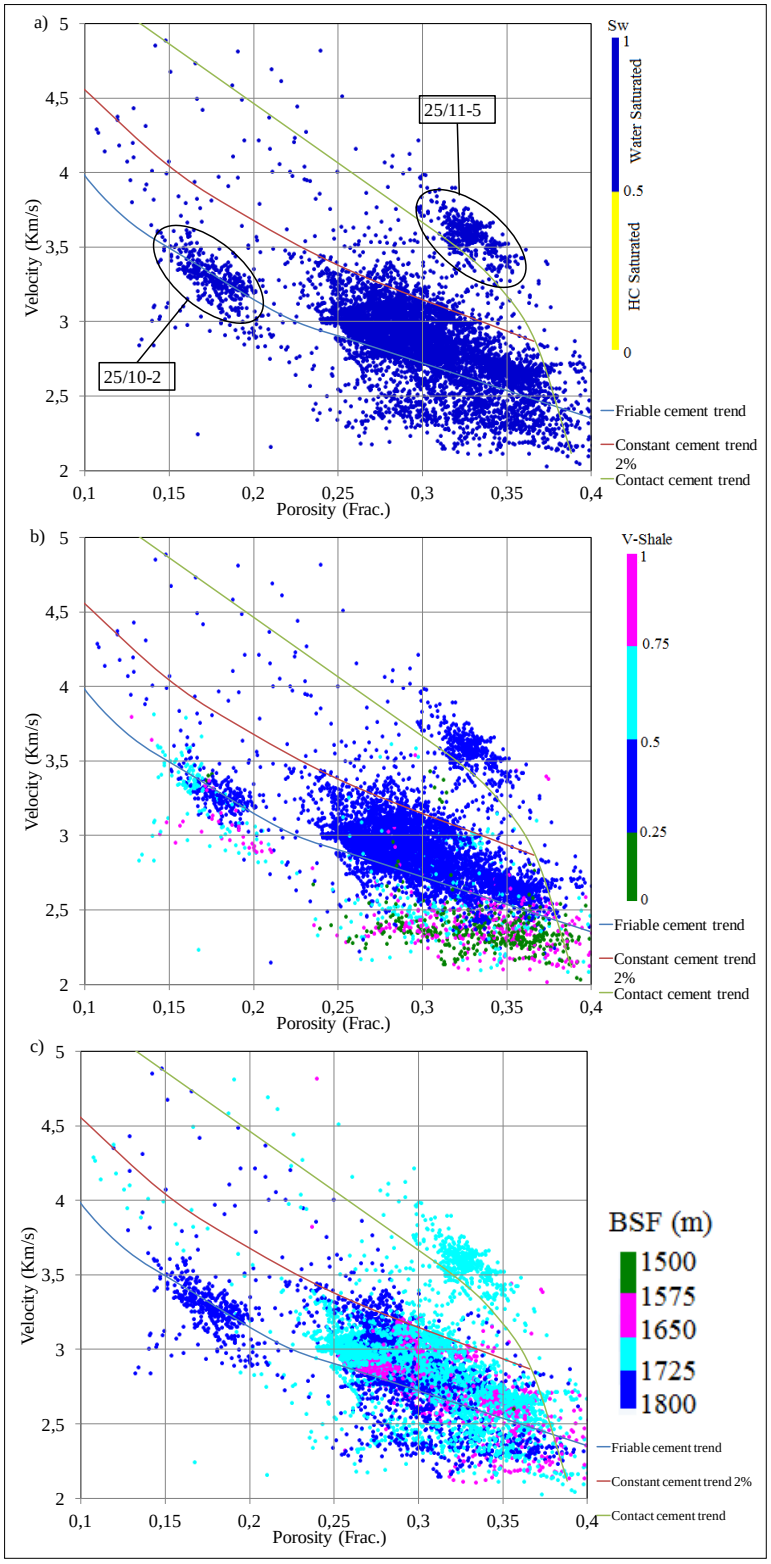

Figure 6.15 The Heimdal Formation data superimposed with rock physics cement models color-coded by a) Water saturation b) Vsh c) BSF depth. Overlay lines digitized after Avseth et al., 2005.

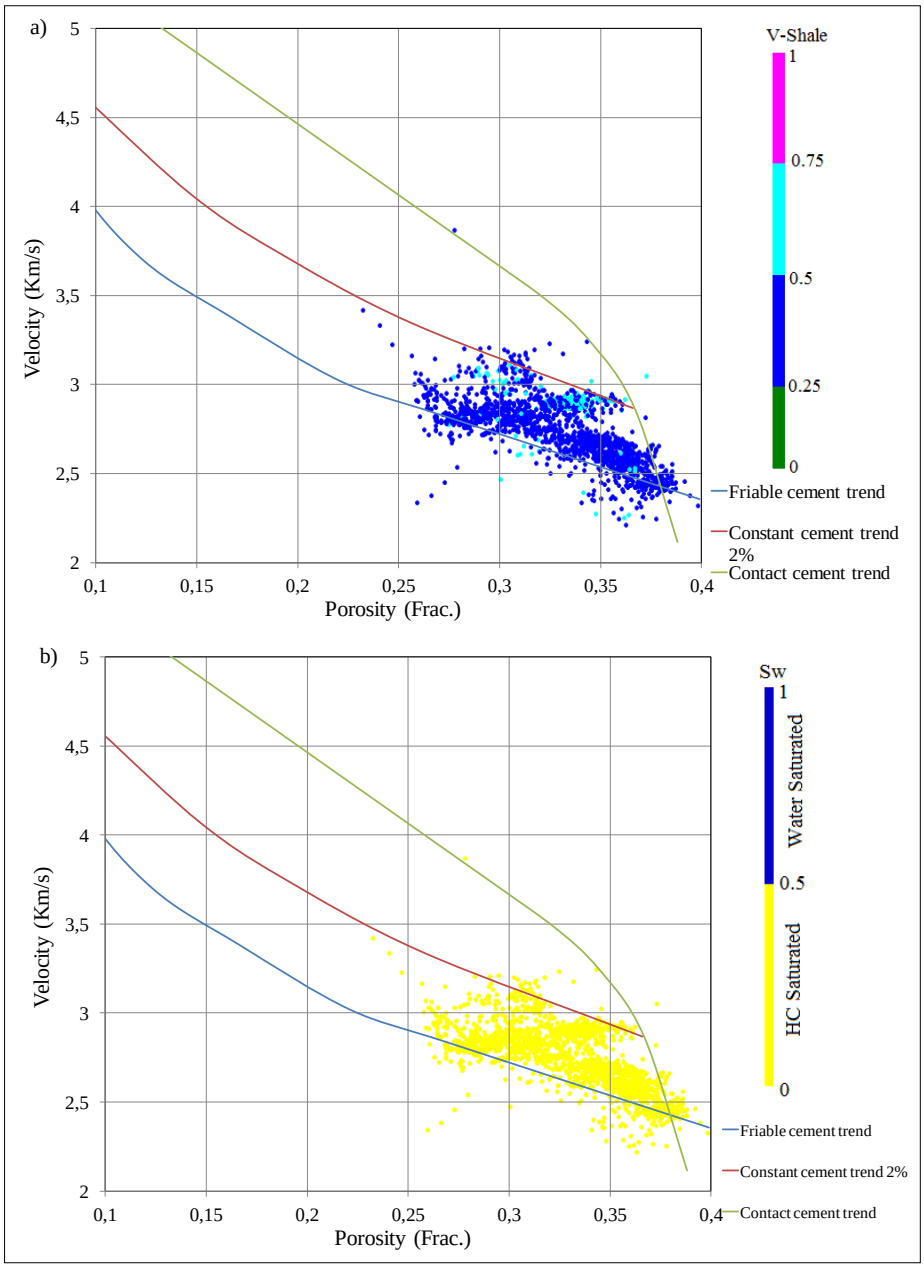

Figure 6.16 The Heimdal Formation hydrocarbon saturated data superimposed with the rock physics cement models, color-coded by a) Vsh b) Water saturation. Overlay lines digitized after Avseth et al., 2005.

Acoustic impedance versus Vp/Vs

The acoustic impedance and Vp/Vs ratio cross-plots used to diagnose the Heimdal Formation. In this plot (Fig. 6.17 a), data points color-coded with the shale volume plotted. It is easily observable that most of the data points plunge across the water saturated sandstone and contact cement line. This may specify that the Heimdal Formation is poorly cemented, as most of the intervals show no cementation. Furthermore, when the same data points color-coded with the water stauration (Fig. 6.17 b), it indicates that the some points which show poor cementation, also contains the hydrocarbon.

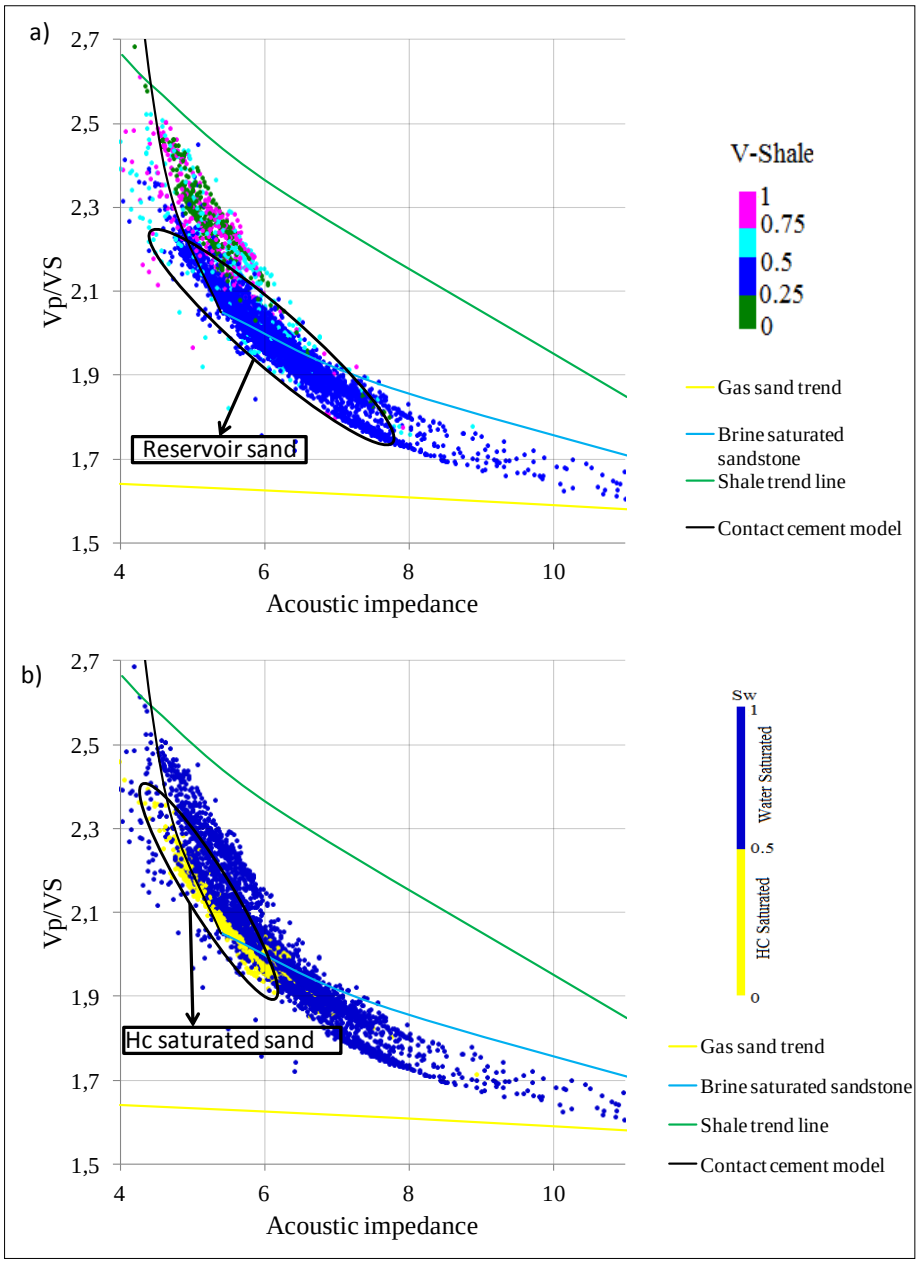

Figure 6.17 Vp/Vs-AI cross-plots, the Heimdal Formation data points color-coded with a) Vsh b) Water saturation. Overlay lines digitized from Avseth et al., 2009.

Lambda-Mu-Rho cross-plots

The same series of LMR cross-plots used to diagnose the Heimdal Formation as well. In the Figure 6.18a, data points from the Heimdal Formation plotted and color-coded with shale volume. It is easily observable (Fig. 6.18a) that the potential sand intervals separated from the shale units. This plots help to diagnose that the Heimdal Formation contained good quality of reservoir sandstone with very high net-to-gross ratio. Furthermore, in the Figure 6.18b, the same data points color-coded with the water saturation. These sandstone intervals which marked initially, may saturated with hydrocarbons. Other than main data cluster, hydrocarbon saturated points are marked. These points plunge lower left corner of plot, which may marked as the porous sand intervals.

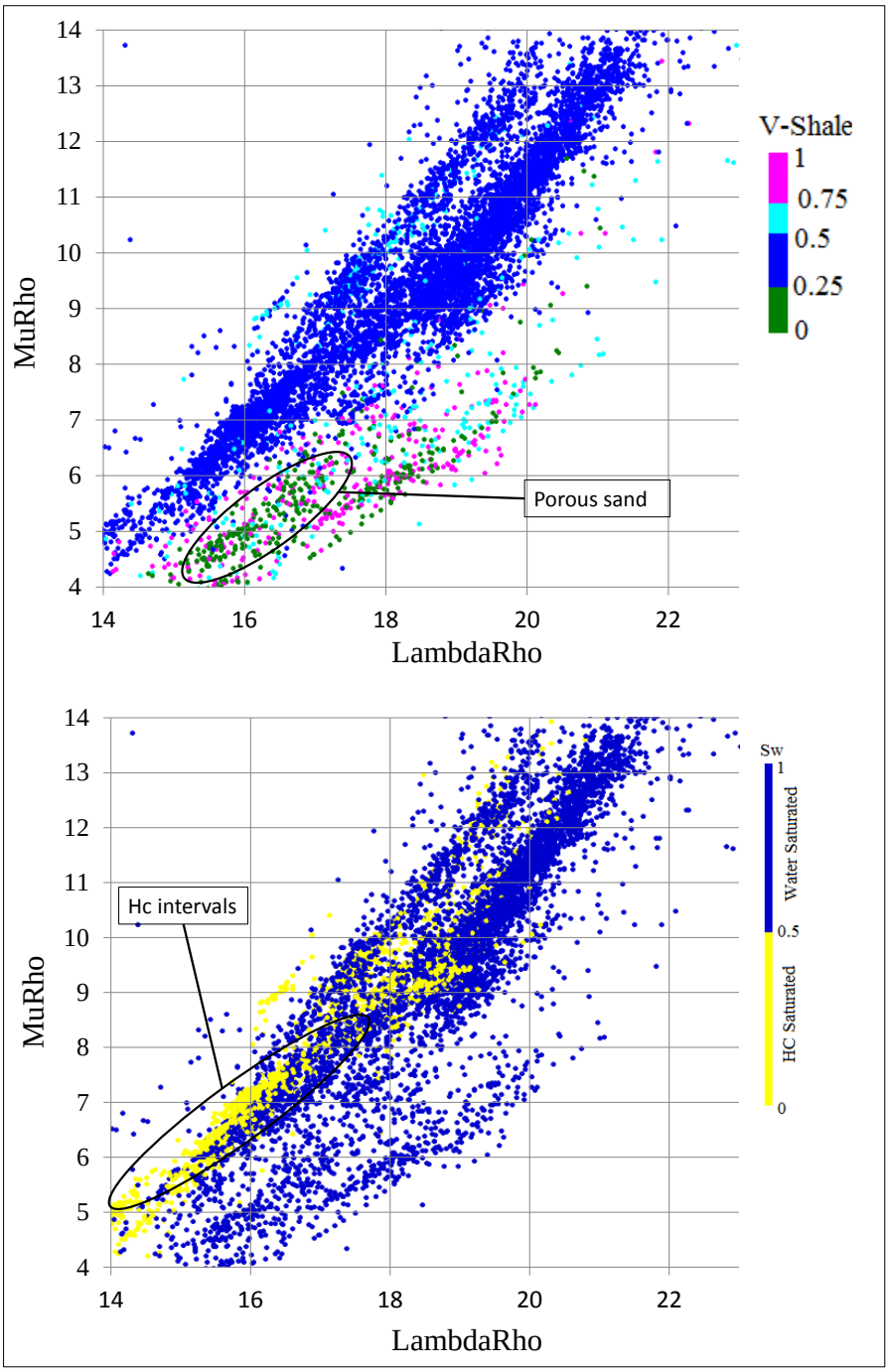

Figure 6.18 LMR cross-plots, the Heimdal Formation data points, color-coded with a) Vsh and b) Water saturation.

6.2 Discussion

As discussed earlier, the Balder, Hermod and Heimdal formations are the reservoir intervals of the Balder field. These sand intervals are separated by the thick shale formations, acting as the seal rocks (Bergslien, 2002). These reservoir formations are poorly cemented, which makes them a good quality reservoir. These formations deposited in the different ages, hence in different climates, depositional environments and tectonic settings. The influence of depositional environment on rock physics properties is significant. The change in depositional environment can deposit different types of the facies within the same formation

(Myers and Milton, 2008). The facies change within the same formation leads to the different clusters of the data points in rock physics cross-plots. These anomalies in most cases contribute to understand the reservoir properties in a more sophisticated way, sometime it introduces the uncertainty, especially if the study just relies on the well log data (Avseth et al., 2005; Avseth, 2010; Marcussen et al., 2010).

Different facies have been marked within the reservoir formations, during the petrophysical analysis (Chapter 4). The facies influence and lithologic variations are also demonstrated in the rock physics cross-plots. This variation of the facies and lithology (both horizontally and vertically) make the study area complex. These complexity most of the time leads to the uncertainty not only in the rock physics analysis, but also put the question mark on reliability of the well log data. An effort is made during the analysis to point out the anomalies, which are associated with the bad borehole, as well as with the rock physics templates itself.

6.2.1 Rock physics and facies relationship

The rock physics results indicate that the reservoir formations (Balder, Hermod and Heimdal) are unconsolidated to the poorly cemented. The depositional environments and depth related diagenesis, can reduce the porosity significantly, which may lead in increase of velocity (Avseth et al., 2005; Bjørlykke and Jahren, 2010). The depth related diagenetic processes may play insignificant role compared to the depositional process related trends in the Blader field. These reservoir formations are not exposed to the temperature or depth, where quartz cementation can significantly reduce the porosity (Avseth, 2010; Bjørlykke, 2010; Johnson and Fisher, 1998).

The reduction of the porosity is influenced by the packing of smaller (clay) grains among the larger (sand) grains (depositional effect) which may deteriorate the sorting (Marion, 1990) or depth related diagenetic effect (cementation) (Marcussen et al., 2010). These effects can be seen in the rock physics analyses (Fig. 6.7). In the Figure 6.7, the data cluster points marked as the well 25/11-13 indicate the two facies, one is the clean sandstone while the other is the shaly sandstone. This variation of the lithology results in the cluster across the different clay trend lines. For further investigation of this well, a log plot is used (Fig. 6.19). The Figure 6.19 illustrates that the two facies may present in the well 25/11-13. The depositional environment of these facies are already discusseded in the chapter 4. Here, two scenarios can be assumed i.e. depositional and depth related diagenetic influence. First in depostional trend scenario, the black box marked in the facies 2, which may shows that the clay content increases (5-10%) in clean sandstone, the Vp values also increase but the porosity decreased (more packing of the sediments) (Bjørlykke, 2010; Marion, 1990; Marion et al., 1992). Furthermore, as the clay content keep increases with depth which lead in decrease of the velocity. It may indicate that the sandstone grains lose contact with the each other, due to the increase in the volume of clay (Marion, 1990; Marion et al., 1992).

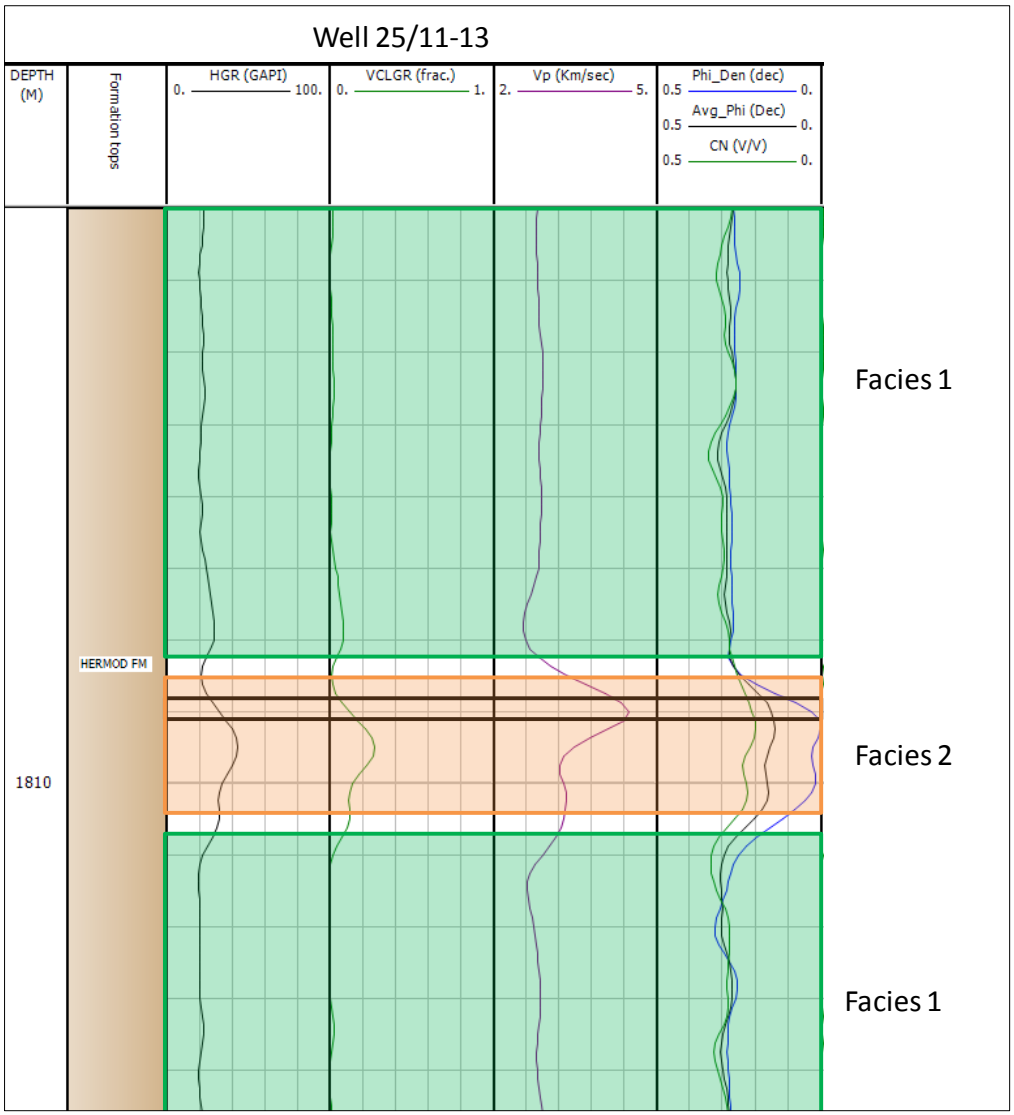

Figure 6.19 Well 25/11-13, high velocity zone marked by the red box.

The other assumption, which can be considered is related to depth-temperature related diagenetic influence. This may be associated to the quartz cementation precipitation. In this shaly interval, the facies 2 (Fig. 6.19) may have the volcanic ash (amorphous silica), which can be the source of the quartz cementation, in the adjacent beds by formation water movement. This may indicate that change in the velocity and porosity is more controlled by depositional influence and as well as depth-temperature related diagenetic influence in this interval. This quartz cementation may reduce the porosity and also increase the velocity (Avseth, 2010; Bjørlykke and Aagaard, 1992; Bjørlykke, 2010; Bjørlykke and Jahren, 2010; Ramm and Bjørlykke, 1994; Thyberg et al., 2000).

But only from the well log analysis it is uncertain about which of the process has lead to this peak in the velocity. Furthermore, the well log interpretation also reveals the presence of the hydrocarbon at top of the formation (Fig. 6.20). The presence of hydrocarbons indicate that this barrier is permeable. But if we assume that this barrier is impermeable (as porosity is very low), then its quite certain that the hydrocarbons migrated up in the formation before the development of impermeable layer. This may increased the possibility of cementation (Rider and Kennedy, 2011).

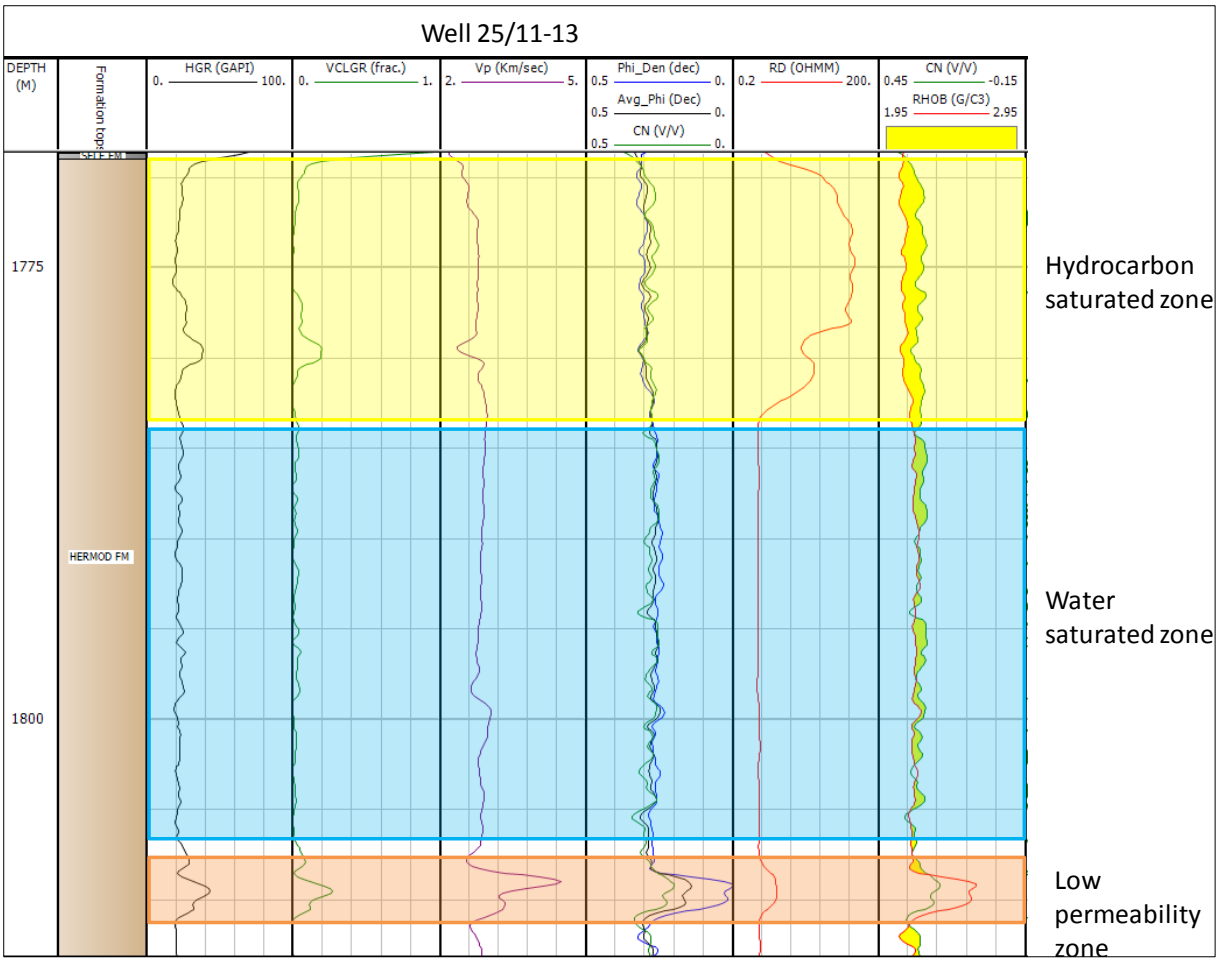

Figure 6.20 Well log plot: hydrocarbon and water saturated zones with low permeability zone at the base.

Many authors like Cornford, 1998; Justwan and Dahl, 2005; Lonergan et al., 1998 and Newman et al., (1993) have established that the source rock of the study area, the Draupne Formation has started expulsion of the hydrocarbons in the Cretaceous till present day. It may indicate that as soon as this Tertiary reservoir formation deposited, the hydrocarbon migration started. As the overburden increases (burial depth and temperature increases), which may lead to the precipitation of the cement (Bjørlykke, 2010; Marcussen et al., 2010). This assumption indicates the depth related diagenetic processes might influence as well. All of these assumptions surely have uncertainty. These uncertainties cannot reduce by the limited data.

In the Figure 6.7, the well 25/11-17 (Balder Formation) shows anomaly on cementation plots. To investigate it further, Vp (km/s), gamma ray (API) and well log plots with temperature are used (Fig. 6.21 25/11-17). Two end facies can be identified on the rock physics by simple cross-plots of gamma ray and velocity (Avseth et al., 2005), as shown in the Figure 6.21. The Facies 1 is clean sandstone intervals with the high velocity (marked by the red color), whereas the Facies 2 is clay intervals, low velocity zone (marked by the green color). The clay intervals may contain the ash layer as the Balder Formation has much more pyroclastic material as compared to the other reservoir formations (Sarg and Skjold, 1982). These volcanic ash materials can be a direct source of the silica, which may precipitate the quartz cement in adjacent sandstone intervals by a movement of the formation water. The

temperature is high enough (77 ^{o}C) to precipitate the quartz cementation as well (Fig. 6.21) (Bjørlykke, 2010, Thyberg et al., 2000). The precipitation of cement can give high peaks in the velocity (Avseth et al., 2005). Moreover, volcanic ash can precipitate the smectite, which may lead to the development of overpressure in the formation. These smectitic clays have very low permeability as compared to the other clays, and it may have retained high porosity as well, due to the ineffective dewatering (Bjørlykke et al., 2010; Mondol et al., 2008; Thyberg et al., 2000). This zone can be marked by the velocity reversals as shown and marked by the green color in the Figure 6.21.

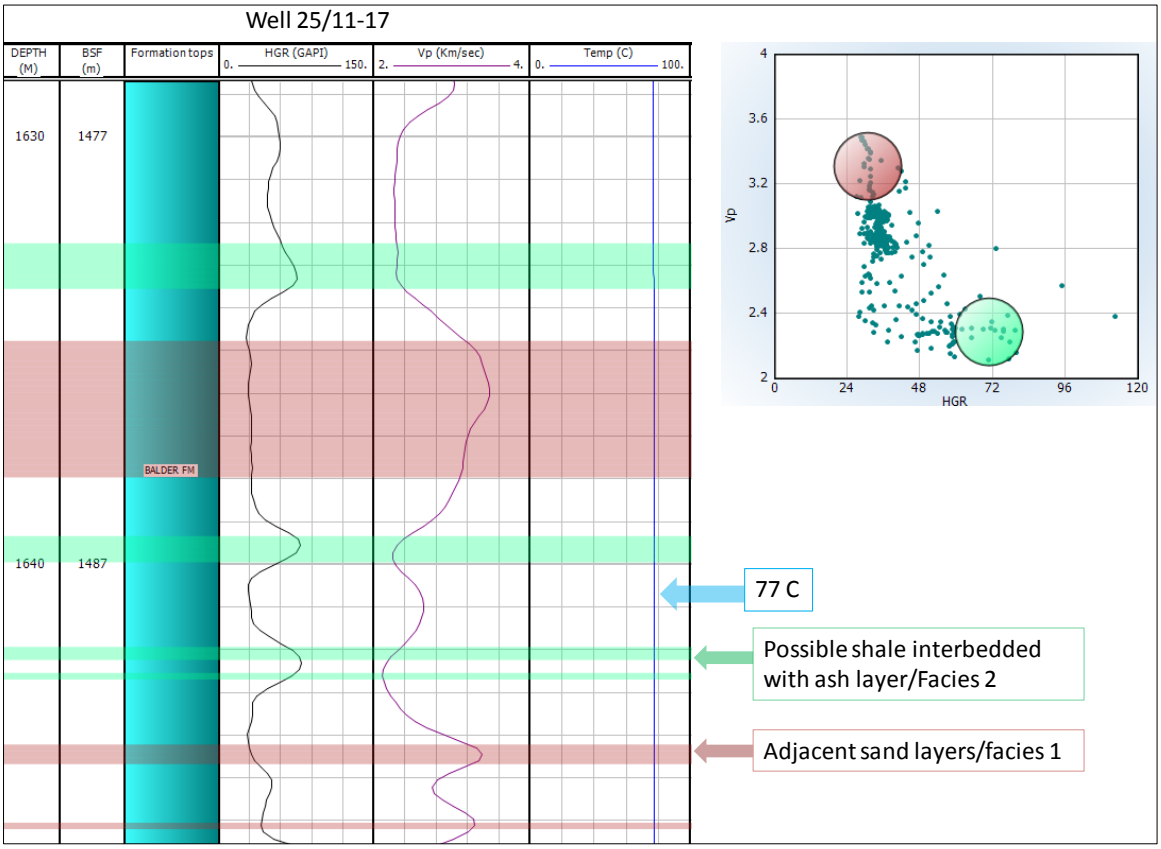

Figure 6.21 Well log plot from the well 25/11-17, assumed two facies in the Balder Formation, plot adopted from Avseth et al., (2005).

The Balder Formation mudstone and volcanic ash also indicate the sediments starvation as these lithology needs the calm environment to deposit. This can be associated with an increase of the sea level (Kjennerud et al., 2001; Norlex, 2013; Thyberg et al., 2000). Moreover, these reservoir formations possess more primary porosity than the secondary porosity (Sarg and Skjold, 1982). The secondary porosity specifically associated with the dissolution of feldspar may not be common in the reservoir formations. As these reservoir formations are the distal deep marine deposit, which may have far less influenced by the meteoric water. This less flushing of the meteoric water will eventually precipitate less kaolinite (Bjørlykke and Jahren, 2010).

6.2.2 Clay effect on the reservoir rocks

In the study area, three main reservoir rocks are present. These reservoir rocks contain the good amount of sands, which are derived from the East Shetland Platform (Jenssen et al., 1993). The thick sandstone intervals may represent the turbidites deposits (Milton and Emery, 2008). The lateral discontinuity of the thick sandstone and the shales bodies, acting as the reservoir and cap/seal rocks respectively, which may give different anomalies. The main focus of the study is to get better understanding of the reservoir sands by using rock physics templates. Han (1986) model, demonstrated the relationship between the porosity and velocity, due to the effect of clay particles. The Han (1986), developed this model by taking the different fractions of the clay volume at the effective stress of 40 MPa. When the points from the reservoir formations plotted with this model, most of the data cluster plunge from the respected curves. This can be interpreted as the overpressure zone, as these data points have retained the porosity in shaly interval (Bjorlykke et al., 2010). The other possible reason for the shifting of the data to the lower side could be due the possible variation of overall effective stress. If we try to estimate the overburden stress by using 'Amoco Compaction Relationship' in Interactive Petrophysic software, then the overburden stress in this area is almost 35-37 MPa. This estimation of the overburden stress may contain error. If it is assumed that difference of stress is somehow accurate, it can be said that if these sediments went under 3-5 MPa of additional stress then these sediments may show higher sonic velocities (Avseth, 2010; Bjorlykke et al., 2010). In this situation, cluster of the data will move up on plot and will follow the clean sandstone curve. It can be said that these intervals may have never underwent stresses of 40 MPa. These assumption may contain significant errors and have to be verified by using other methods. Furthermore, the hydrocarbon saturated points also plotted with the Han (1986) model. None of the hydrocarbon saturated sorted points plunge across their respected line. This could be due to the shifting down of the sonic velocity due to the presence of hydrocarbon. These hydrocarbon saturated intervals have tendency to reduce the sonic velocity (Rider and Kennedy, 2011). Other than that the presence of hydrocarbon also influenced the calculation of porosity. These anomalies surely put significant errors in the analysis. In addition, the calculation of the shale volume, which is used to color-code and sort the data points may have error itself. But all of these anomalies may help us to better understand the reservoir the other way around. The comparison of Han (1986) model and the field data indicates that in reservoir formations, the depth related diagenesis and depositional trends, both control the distribution of the data clusters. The better sorted clean sand mostly match with the clean sandstone lines (Depositional effect, better sorting). In a few intervals, where cementation may have initiated and give kicks in the Vp value (Avseth et al., 2005), causes the data cluster (shaly sand sediments) plunge across the cleaner sandstone trend. The clean sandstone data cluster may fall above the clean sandstone trend line (Depth related diagenetic effect) (Fig. 6.13, data cluster from well 25/11-5) (Avseth et al., 2005; Bjorlykke, 2010; Bjorlykke et al., 2010; Han et al., 1986; Marcussen et al., 2010; Marion et al., 1992).

6.2.3 Rock physics cement model of reservoir rocks

The rock physics cement models and the data points from the field show that most of the reservoir formations intervals are poorly cemented to unconsolidated sand. Only a few well intervals plunge across the cement trend line. These intervals still have high porosity values, which may indicate that the formations have not chemically compacted significantly (Avseth et al., 2005). This show that the Paleocene-Eocene reservoirs only show the poor cementation, when the temperature is high enough to initiate the quartz cementation

(Bjorlykke, 2010). In addition, the volcanic ash is significantly present specifically in the Balder Formation, which may be the source of quartz cementation precipitation at lower temperature (Bjorlykke, 2010). It may be interpreted that the intervals which are adjacent to the volcanic ash layer show peaks in sonic velocity (Avseth, 2010; Bjorlykke, 2010; Bjorlykke and Jahren, 2010; Norlex, 2013). Furthermore, it is quite observable that points which plunge across the contact cement model line still may have quite high porosity. This small amount of cement only increases the stiffness of the sand, without significantly decreasing the porosity (Avseth et al., 2005). The Balder Formation has more clay content than the other reservoir formations. The Balder Formation may contains pyroclastic materials, deposited during the volcanic activity associated with opening of Atlantic Ocean (Briedis et al., 2007). This material can transform into the smectite rich clay (Karlsson et al., 1979; Bjørlykke and Aagaard, 1992). This transformation to the smectite rich clay can decrease the permeability, which may lead to the over pressure development in shaly intervals. This overpressure may retain the porosity, as it can oppose the effective stress. This phenomena may decrease the sonic velcoity, which lead most of the point fall across and below the friable sand line, as it has been observed earlier (Avseth, 2010; Avseth et al., 2000; Bjorlykke, 2010; Bjorlykke et al., 2010; Mondol et al., 2008; Thyberg et al., 2000). The other reason for the main cluster to fall across the friable sand on right side of the rock physics cement models may be due to the depositional influence. This friable sand model represents the right side of the plot as the clean sand, while the left side illustrates that the porosity decreases as the clay content increases between the sand particles. This packing of the clay content in sand particles may reduce the porosity and reduce the sorting, which results in increase of sonic velocity (at certain volume of clay), as the well 25/10-2 showed (Avseth et al., 2010; Dvorkin and Nur, 1996; Marion, 1990; Mukerji and Mavko, 2006). These plots may also indicates that the reservoir formations contained the thick deposits of clean and well sorted sandstone. It also indicates that the sediments were sorted before it deposited as the turbidites in the Balder field area. The distance from the source to the depostional area is 100 km (Avseth et al., 2005; Ostvedt et al., 1990). Its look like in the study area depth-temperature related diagenesis has only a minor effect on the reservoir sandstone as most of these reservoir zones are not buried deep enough (Johnson and Fisher, 1998).

6.2.4 Vp/Vs and acoustic impedance cross-plots

The Vp/Vs ratio and the acoustic impedance analysis of the reservoir formations show very high values of Vp/Vs ratio and low values of the acoustic impedance. Most of the data points fall on the water saturated sandstone line and the contact cement line. The data points saturated with the hydrocarbons did not plunge on the gas saturated line. It may be interpreted here that most of these hydrocarbons intervals may be saturated with oil. Moreover, it may be also assumed that these hydrocarbons saturated intervals may have slight cementation at their grain contacts, which make these sediments stiffer (Avseth et al., 2005). This stiffness give peaks in the Vp values, which may masks the light hydrocarbon effect on the Vp and Vs values to some extent. This masking of the cementation increased the Vp/Vs ratio and brings the cluster of data right across the contact cement line and water saturated sandstone line (Avseth et al., 2005; Avseth et al., 2009; Avseth et al., 2010; Ødegaard and Avest, 2004; Rider and Kennedy, 2011). The shale data points separation is not that much on the plot. The reason which may be interpreted here for not having the separation is uncertainty values of the Vs and estimation of the shale volume itself. Other than that, this rock physics templates account different proportions of the sediments, which results in different trend. The proportion of different sediments and conditions which considered during the development are unknown. So, comparing the field data with the laboratory data will create the uncertainty

itself (Guliyev and Davis, 2006; Feng et al., 2007; Mukerji and Mavko, 2006; Russell and Smith, 2007).

6.2.5 Lambda-Mu-Rho cross-plots

The lambda-Mu-Rho plots used for better understanding of the lithology and the fluid factor of the reservoirs. The lamda-Rho is sensitive to the fluids effect (water-gas), while the Mu-Rho sensitive to the fabric matrix or lithology (Goodway et al., 1997). When these cross-plot are properly color-coded with the vsh and water saturation, the effect of lithology and fluid may be easily marked. In the study area, the main reservoir sections belong to the sandstone lithology, which may be saturated with the gas/oil or water depending upon their startigraphic depth and the location. When these data points are color-coded with shale volume, a clear separation may be seen between the shale and the sandstone lithology. The Mu-Rho (rigidity), which is more sensitive to the lithology brings the sandstone data points up on the cross-plots. The elastic properties of the slightly tight sandstones are higher compared to the porous sandstones. Furthermore, as previously marked during the cementation modeling, a few intervals have slight cementation (Avseth et al., 2005). This depth-temperature related diagenetic influence on the sediments may be easily separated in this plot. As these intervals have higher elastic values. Other than that this slight cementation may increase the overall strength (rigidity) of the rock, which brings these sediments bit up on the plots (Avseth, 2010; Bjørlykke and Jahren, 2010). Furthermore, the Lambda-Rho, is sensitive to the fluids. The sediments intervals which are saturated with the hydrocarbons nearly plunge on the left side of the cross-plots (porous sandstone zone). As the Lambda-Rho shows decrease in incompressiblity, which may indicate that these intervals may conitain the hydrocarbons. The fully water saturated points shift towards the right. The Mu-Rho shifts the sand data points up to separate it from the shale lithology. The rest of the sandstone intervals saturated with the hydrocarbons show a trend towards the top right corner. This may be due to the slight cementation in the sediemnts, which may saturated with the hydrocarbons (Chopra et al., 2003; Contreras and Verdin, 2004; Feng et al., 2007; Goodway et al., 1997; Goodway et al., 2001; Gray and Andersen, 2000; Marcussen et al., 2010; Xu and Bancroft, 1997). The overall effect of the separation between the sandstone/shale lithology and the hydrocarbon/water is not much. This may be due to the derived Vs (shear velocity) values. This derived Vs also leads to some linear trends, which add some uncertainties in the analysis.

Chapter 7: Summary and conclusion

This study focuses on the Balder field, located on north western flank of the Utsira High, the Norwegian North Sea. The Balder field is one of the earliest discovery in the Norwegian part of the North Sea within the post-rift play. Due to the lack of good resolution seismic data, complex stratigraphy and structures, it took more than thirty years to develop the field. The field contains both oil and gas reserves in the thick sandstone deposits, which are enclosed by the stratigraphic and structural traps.

A total of twenty-five well log data consider in this study. Only three wells are dry while six wells show hydrocarbon traces. The remaining sixteen wells have indicated good potential for oil and gas. The data quality of these well logs, in most cases is not good, which put uncertainties in the analyses and outcomes of the study. The three reservoir formations; Balder, Hermod, and Heimdal are recognized as the commercially producible zones. All the three reservoir formations show very good quality sandstones with very high net-to-gross ratio. The main focus of the study is to characterize these three Paleocene to Eocene sandstone reservoirs using petrophysical analysis, compaction study and rock physics diagnostics. However, the petrophysical analysis and compaction study have also been performed to investigate the rock property evaluation of cap and source rocks.

The reservoir intervals of the Paleocene and Eocene sandstones were deposited by the deep marine turbidity currents. These sediments were sourced from the East Shetland Platform. These reservoir formations pinch out in the southeastern wells. The good quality reservoir sandstones with N/G of 90% are present in the northwestern part of the field. The southeastern part of the field contains mud-rich deposits with the N/G of 30%. This may indicate that the southeastern part may be deposited as the distal parts of the turbidite systems, which have less amount of clean sand intervals.

In the petrophysical analysis, basic parameters like porosity, volume of shale and water saturation are calculated. The reservoir formations possess clean sandstone intervals of high porosity saturated with the hydrocarbons. Furthermore, the N/G and pay thickness are estimated on the basis of those parameters. The N/G is as high as 90%. The facies analysis of the reservoir rocks using well log data are also carried out for better understanding of the depositional environments, which may indicate that the clean sandstone reservoirs are of the deep marine turbidite systems. The source, reservoir and cap rocks are identified on the basis of respective well log responses. The well log analyses indicate that the cap rocks are dominated by the shale lithologies which have very less effective porosity. Furthermore, the well log analyses of the source rocks indicate that it may still possess the hydrocarbons, which retard the compaction.

In the compaction study, the transition zones between the mechanical and chemical compactions have been identified using a comparison of compaction trends of the studied well log data and published compaction curves. First, geothermal gradient map of the Balder field is established on the basis of bottom hole temperature. Then this map is utilized further to estimate the depth, where quartz cementation may be initiated. The mechanical and chemical compaction regimes are separated by using the depth-velocity, depth-density and density-velocity cross plots. For better understanding of the transition zone, the data points are also color-coded with temperature. This configurations of the cross plots help to mark the transition zone more accurately. The transition zone varies in different reservoir formation

depending upon the stratigraphic depth and geothermal gradient. The southeastern wells show transition zone in the Balder Formation, while the northwestern wells show transition zone in the Heimdal Formation. This may be due to the shallow basement rocks in the southeastern part as compared to the northwestern part.

The rock physics diagnostics are carried out only to characterize reservoir sands and sandstones. Han (1986) porosity-velocity crossplot of shaley sandstones are used to investigate clay content of the reservoir sands. Dvorkin and Nur (1996) cement models are used to determine the depositional and depth related diagenetic influenced on the reservoir rock properties. These models indicate that the reservoir formation are more influenced by the depositional trends rather than depth related diagenetic effects. The comparison of reservoir sandstones with cement models indicate that the sandstones are slighty cemented, which may give peaks in the sonic velocity. Acoustic impedance and Vp/Vs cross-plot is used to study the fluid as well as the cementation effect on the rock properties. These plots indicate that the reservoir intervals, which are slightly cemented, mask the effect of the hydrocarbons. The Lambda-Mu-Rho crossplots also point out these cemented intervals, which indicate the higher stiffness of the grain frameworks. The hydrocarbon intervals effect on these plots may be masked due to cementation though in small quantities. It may also be masked due to the uncertanity associated with the predicted Vs.

Though several uncertainties mentioned earlier may influence the outcomes of the study but still the findings from integrated approach of petrophysical analysis, compaction study and rock physics diagnostics have significant value to characterize the reservoirs. After critical investigation of results the following conclusions are drawn

- In the petrophysical analyses we observed that the Balder, Hermod and Heimdal formations are the three main reservoirs of the study area. The Balder, Sele and Lista formations are the seals. It is also clear from facies interpretation that the depositional environment of the reservoir formations may be predicted more confidently.
- This study also demonstrates that by using the different cutoff values to estimate porosity, shale volume and water saturation; the N/G with net pay thickness can be estimated more accurately.
- It is clear from petrophysical analyses that all the reservoir formations possess high porosity sandstone intervals with the N/G of 90%. The facies analyses indicate that these formations (Balder, Hermod and Heimdal) have excellent reservoir quality with well sorted and thick sandstone intervals.
- In the compactional study, it is successfully demonstrated that by combining the depth-velocity, depth-density, velocity-density and velocity-porosity cross-plots in combination of geothermal gradient, a more accurate transition zone of mechanical and chemical compactions can be identified..
- This study also demonstrated that by using Marcussen et al., (2010) sand trend line for reservoir zone (sandstone lithology) and Mondol (2007) and Mondol (2009) clay trend lines for cap/source rocks are much better way to conduct the compaction analyses.
- It is clear that the transition zone in the study area heavily depend upon the geothermal gradient. The transition zone varies from formation to formation, depending upon their stratigraphic location/depth and temperature regime. We also observed that none of the reservoir formation is heavily cemented.

- Rock physics diagnostic demonstrated that Han (1986) shaly sand model and Dvorkin and Nur (1996) cement models (Constant, contact and friable cement models), when combine together with carefully sorted well logs, are very useful to study the depositional and depth related diagenetic influence on reservoir rocks.
- The overpressure (under compacted) influenced are also marked on the rock physics templates. The field data compared to the Han 1986 model shows that overpressure may develop in the shale intervals.
- It is also demonstrated that the effect of the hydrocarbons on the well logs masked the actual readings. To overcome this behavior, we suggest that hydrocarbon saturated data should be separated from brine saturated data. We also suggest that fluid replacement modeling may give better results to predict the Tertiary reservoir sandstones of the Balder field.
- In rock physics analyses we observed that reservoir formations are poorly cemented, only few intervals show velocity peaks. It may be due to the contact cementation at grain contacts. We also observed that this small amount of cement can mask the effect of the hydrocarbon and lithology.
- Since we do not have seismic or core data, we are unable to analyze and comment on the sand injection/liquefaction in the Balder field.
- In this study we demonstrated that without cores, seismic or thin section studies, reservoirs can also be characterized by combining multidisciplinary techniques such as petrophysical analysis, compactional study and rock physics diagnostics.

References

Articles

Aase N.E., Bjørkum, P.A., Nadeau, P., (1996) "The Effect of Grain-Coating Microquartz on Preservation of Reservoir Porosity." AAPG Bulletin 80 (10) 1654–1673.

Archie, G.E (1942) "The Electrical Resistivity Log as an Aid in Determning Some Reservoir Characteristics." AIME 146, 54.

Arns Christoph H., Knackstedt Mark A., and Val Pinczewski W. (2002) "Accurate Vp:Vs Relationship for Dry Consolidated Sandstones." The American Geophysical Union.

Asquith G and Krygowski, D (2004) "Porosity Logs, Chapter 4, Basic Well Log Analysis." AAPG Methods in exploration 16, 37-76.

Autric, A., and Dumesnil, P (1985) "Resistivity, Radioactivity, and Sonic Transit Time Logs to Evaluate the Organic Content of Low Permeability Rocks " Log Analyst, 36-45.

Avseth Per, Dvorkin J., Mavko G. and Rykkje J. (2000) "Rock Physics Diagnostics of North Sea Sands: Link between Microstructure and Seismic Properties." . Geophysics, v. 27, p. 2761-2764.

Avseth Per, Mukerji, T., Jorstad, A., Mavko, G. and Veggeland, T (2001) "Seismic Reservoir Mapping from 3-D Avo in a North Sea Turbidite System." Geophysics, Soc. of Expl. Geophys, 1157-1176.

Avseth Per, Mukerji T. and Mavko G. (2005). Quantitative Seismic Interpretation: Applying Rock Physics Tools to Reduce Interpretation Risk. Cambridge, Cambridge University Press.

Avseth Per, Jørstad Arild, Wijngaarden Aart-Jan Van And Mavko Gary (2009) "Rock Physics Estimation of Cement Volume, Sorting, and Net-to-Gross in North Sea Sandstones." The Leading Edge Special Section: Rock physics.

Avseth Per, (2010) Exploration Rock Physics the Link between Geological Processes and Geophysical Observables (Chapter 18), Petroleum Geoscience by Bjørlykke K.: From Sedimentary Environments to Rock Physics." Pp 403-426.

Avseth Per, Mukerji, T., Mavko, G. and Dvorkin Jack (2010) Rock-physics diagnostics of depositional texture, diagenetic alterations, and reservoir heterogeneity in high-porosity siliciclastic sediments and rocks. A review of selected models and suggested work flows ". Geophysics,Vol., 75, NO. 5 P. 75A31–75A47 .

Badley M. E., Price J . D., Dahl C. Rambech and Agdestein T. (1988) "The Structural Evolution of the Northern Viking Graben and Its Bearing Upon Extensional Modes of Basin Formation." Journal of the Geological Society, London 145, 455-472.

Bain, J.S (1993) "Historical Overview of Exploration of Tertiary Plays in the Uk, North Sea." Petroleum Geology of Northwest Europe: Proceedings of the 4th Conference. The Geological Society of London, Parker Jr,, pp. 5-14.

Barnard P.C. And Cooper, B.S. (1981) "Oils and Source Rocks of the North Sea Area. In: Illing, L.V and Hobson, G.D (Eds) Petroleum Geology of the Continental Shelf of North-West Europe,." Heyden, London, 169-175.

Beers, R.F (1945) "Radioactivity and Organic Content of Some Paleozoic Shales." AAPG Bulletin 29, 1-22.

Bergslien, D (2002) "Balder and Jotun-Two Sides of the Same Coin? A Comparison of Two Tertiary Oil Fields in the Norwegian North Sea." Petroleum Geoscience 8, 349-363.

Bergslien, Kyllingstad D. G., Solberg A., Ferguson I. J. and Pepper C. F (2005) ” Jotun Field reservoir geology and development strategy: pioneering play knowledge, multidisciplinary teams and partner co-operation - key to discovery and successful development” Petroleum Geology Conference series Petroleum Geology Conference series 2005, v.6; p 99-110.

Bernabe´ , Y., Fryer D., and Hayes J., (1992) "The Effect of Cement on the Strength of Granular Rocks." Geophysical Research Letters, v. 19, p. 1511– 1514.

Bjørlykke K., Aagaard, P., Dypvik, H., Hastings, D.S., Harper, A.S., (1986) "Diagenesis and Reservoir Properties of Jurassic Sandstones from the Haltenbanken Area, Offshore Mid-Norway." A. M. Spencer, ed., Habitat of hydrocarbons on the Norwegian continental shelf; proceedings of an international conference : London, Graham and Trotman: p. 275– 286.

Bjørlykke, Knut and Aagaard P. (1992) "Clay Minerals in North Sea Sandstones." SEPM Society for Sedimentary Geology, Origin Diagenesis and Petrophysics of Clay Minerals in Sandstones SEPM Special Publication No 47.

Bjorlykke, Knut (1998) "Clay Mineral Diagenesis in Sedimentary Basins; a Key to the Prediction of Rock Properties, Examples from the North Sea Basin." Clay Minerals, v. 33/1, p. 15-34.

Bjørlykke Knut, Jahren Jens, Mondol Nazmul Haque, Marcussen Oyvind, Delphine Croize, Peltonen Christer, and Thyberg Brit, (2009) "Sediment Compaction and Rock Properties." AAPG International Conference and Exhibition, Cape Town, South Africa.

Bjørlykke Knut (2010), Compaction of sedimentary rocks including shales, sandstones and carbonates, Chapter 13, "Petroleum Geoscience by Bjørlykke K.: From Sedimentary Environments to Rock Physics." Pp 329-337.

Bjørlykke Knut (2010b), Heat Transport in Sedimentary Basins, Chapter 9, "Petroleum Geoscience by Bjørlykke K.: From Sedimentary Environments to Rock Physics." Pp 253-257.

Bjørlykke Knut and Jahren Jens (2010), Sandstones and sandstone reservoir, Chapter 4, "Petroleum Geoscience by Bjørlykke K.: From Sedimentary Environments to Rock Physics." pp 113-140

Bjørlykke Knut, Høeg Kaare, Mondol Nazmul Haque (2010), Introduction to Geomechanics: Stress and Strain in Sedimentary Basins, Chapter 11, "Petroleum Geoscience by Bjørlykke K.: From Sedimentary Environments to Rock Physics." Pp 281-298.

Boles, J.R., Franks, S.G, (1979) "Clay Diagenesis in Wilcox Sandstones of Southwest Texas: Implications of Smectite Diagenesis on Sandstone Cementation." Journal of Sedimentary Petrology, 55-70.

Briedis N. A., Bergslien D., Hjellbakk A., R. Hill E., And Moir G. J (2007) "Recognition Criteria, Significance to Field Performance, and Reservoir Modeling of Sand Injections in the Balder Field, North Sea." In: Hurst A. And Cartwright J (Eds.) Sand Injectites: Implications For Hydrocarbon Exploration And Production: Aapg Memoir 87, Pp. 91-102.

Broichhausen H. Æ R. Littke Æ T Hantschel, (2005) "Mudstone Compaction and Its Influence on Overpressure Generation, Elucidated by a 3d Case Study in the North Sea." Springer-Verlag 52056, 4–20.

Brooks J., Cornford C. and Archer R. (1987) "The Role of Hydrocarbon Source Rocks in Petroleum Exploration." Marine Petroleum Source Rocks Geological Society Special Publication; Geological Society, London, Special Publications 26, 17-46.

Bukovics, C., and Ziegler, P. A (1985) "Tectonic Development of the Mid- Norway Continental Margin." Marine and Petroleum Geology, 2, 2–22.

Bungum H., Olesen O., Pascal C., Gibbons S., Lindholm C. And Vestøl O., Norsar, Kjeller (2010) "To What Extent Is the Present Seismicity of Norway Driven by Post-Glacial Rebound?" Journal of the Geological Society, London 167, 373-384.

Carr Matthew B., Hubert Lars, and Dvorkin Jack (2002) "Shear Velocity Prediction in the Norwegian Sea." EAGE 64th Conference and Exhibition Florence, Italy.

Castagna, J. P., Batzle M. L. and Eastwood R. L. (1985). Relationships between Compressional-Wave and Shear-Wave Velocities in Clastic Silicate Rocks. Geophysics, v. 50, p. 571-581.

Castagna, J. P., Batzle M. L. and Kan T. K. (1993). Rock physics - The link between rock properties and AVO response, in offset-dependent reflectivity - Theory and practice of AVO analysis, ed. J. P. Castagna and M. Backus. Investigation in Geophysics, No. 8, SEG, Tulsa, Oklahoma, p. 135-171.

Charlez, P. A. "Rock Mechanics, (1997) Petroleum Applications." 2. Technip, Paris.

Chatellier Jean-Yves, Ferworn Kevin, Larsen Nabila Lazreg, Ko Steve, Flek Pawel, Molgat Marianne, and Anderson Irene (2011) "Overpressure in Shale Gas – When Geochemistry and Engineering Data Meet and Agree." Adapted from oral presentation at AAPG Annual Convention and Exhibition, Houston, Texas, USA.

Chi Xin-Gang And Hua Han, De- (2009) "Lithology and Fl Uid Differentiation Using Rock Physics Template." The Leading Edge, no. University of Houston.

Chopra Satinder, Vladimir Alexeev, And Yong Xu, (2003) Core Laboratories Reservoir Technologies Division. "3d Avo Crossplotting an Effective Visualization Technique." The Leading Edge Interpreter's Corner.

Chuhan, F. A., Kjeldstad A., Bjørlykke K., and Hoeg K. (2002) "Porosity Loss in Sand by Grain Crushing Experimental Evidence and Relevance to Reservoir Quality." Marine and Petroleum Geology, 19, 39-53.

Cluff Suzanne G., Cluff Robert M. (2004) "Petrophysics of the Lance Sandstone Reservoirs in Jonah Field Sublette County, Wyoming." AAPG Studies in Geology 52 and Rocky Mountain Association of Geologists 2004 Guidebook.

Cockings James H., L. Gifford Kessler II, Thomas A. Mazza and Leslie A. Riley (1992) "Bathonian to Mid-Oxfordian Sequence Stratigraphy of the South Viking Graben, North Sea." Geological Society, London, Special Publications 67, 65-105.

Compton S. John (1991) "Origin and Diagenesis of Clay Minerals in the Monterey Formation, Santa Maria Basin Area, California." Clays and Clay Minerals, The Clay Minerals Society, 39, no. No, 5 449-466.

Contreras Arturo and Verdín Carlos Torres (2004) "Ava Sensitivity Analysis and Inversion of 3d Pre -Stack Seismic Data to Delineate a Mixed Carbonate-Siliciclas Tic Reservoir in the Barinas -Apure Basin, Venezuela." The University of Texas at Austin.

Cooper, B. S., Barnard, P. C. And Telnaes, N (1995) "The Kimmeridge Clay Formation of the North Sea." Katz, B. J (ed.) Petroleum Source Rocks. New York: Springer, pp.89-110.

Cornford C., Brooks J. (1989), Chapter: Tectonic Controls on Oil and Gas Occurrences in the North Sea Area: Chapter 34: North Sea and Barents Shelf, Book Extensional Tectonics and Stratigraphy of the North Atlantic Margins, Published by Memoir.

Cornford, C (1990) "Source Rocks and Hydrocarbons of the North Sea, in; Glennie, K.W. (Ed) " Introduction to the Petroleum Geology of the North Sea, 3rd ed., Blackwell, Oxford, 294-361.

Cornford C., (1998) "Source Rocks and Hydrocarbons of the North Sea." Glennie, K. W (ed.) Petroleum Geology of the North Sea; Basic Concepts and Recent Advances. Oxford: Blackwell, pp.376-462.

Crowell Eric, Bennion D. Brant, Shaw David (1995) "Use of Petrophysical Measurements to Determine by-Passed Pay Potential." Reservoir Conformance, Profile Control Water and Gas Shutoff Houston, Texas, USA.

Dahl B., Nysaether E, G. Speers C., and Yukler A. (1987) "Oseberg Area Integrated Basin Modeling, in J. Brooks and K. Glennie, Eds." Petroleum Geology of North West Europe: London, Graham and Trotman, p. 1029–1038.

David C. and Ravalec-Dupin, Le M. (2007) "Rock Physics and Geomechanics in the Study of Reservoirs and Repositories." Geological Society, London, Special Publications 2007, v.284, 1-14.

Dawers N. H., Berge A. M., Häger K.-O., Puigdefabregas C. and Underhill J. R. (1999) "Controls on Late Jurassic, Subtle Sand Distribution in the Tampen Spur Area, Norther North Sea." Petroleum Geology Conference series 5, p827-838.

Dean Lisa (2007) "Reservoir Engineering for Geologists Part 3 – Volumetric Estimation." Reservoir Issue 11.

Dellenbach, J., Espitalie J. and Lebreton F. (1983) "Source Rock Logging." Transactions of the 8th European SPWLA Symposium Paper D.

Dewar Jan (2001) "Rock Physics for the Rest of Us an Informal Discussion." CSEG Recorder, Scott Pickford, a Core Laboratories Company, Calgary.

Dræge Anders (2011) "A Diagenetic Rock Physics Approach for Siliciclastics." The Leading Edge Physics of rocks.

Duindam, P., and Hoorn van, B (1987) "Structural Evolution of the West Shetland Continental Margin." Brooks, J., and Glennie, K., eds., Petroleum geology of northwest Europe: London, Graham and Trotman, p. 765–773.

Downey Marlan (1994) "Hydrocarbon Seal Rocks." AAPG Memoir, 60.

Dvorkin Jack (2007) "Yet Another Vs Equation." SEG/San Antonio, Annual Meeting Yet another Vs equation.

Dvorkin Jack and Nur Amos (1996) "Elasticity of High-Porosity Sandstones Theory for Two North Sea Data Sets." Rock Physics Laboratory, Department of Geophysics, Stanford University, Stanford, California Geophysics, vol. 61, No.5 (September-October 1996) ; P 1363-1370.

Dvorkin Jack snd Nur Amos (2000) "Critical Porosity Models." Department of Geophysics, Stanford University, Stanford, CA 94305-2215.

Dvorkin Jack snd Nur Amos (2001) "Time-Average Equation Revisited." Department Of Geophysics, Stanford University, Stanford.

Dvorkin Jack, Carr Matthew B., and Berge Tim (2002) "Rock Physics Diagnostic in Sand/Shale Sequence." EAGE 64th Conference and Exhibition Florence, Italy, 27.

Dvorkin Jack, Fasnacht Timothy, Uden Richard, Smith Maggie, Derzhi Naum, and Walls Joel (2003) "Rock Physics Diagnostics for Porosity and Lithology Mapping in Ne Gom." Stanford University, Anadarko Petroleum Corporation, and Rock Solid Images, no. SEG.

Dvorkin Jack, Fasnacht Timothy, Uden Richard (2004) "Rock Physics for Fluid and Porosity Mapping in Ne Gom." no. EAGE.

Dypvik Henning (1983) "Clay Mineral Transformations in Tertiary and Mesozoic Sediments from North Sea." The American Association of Petroleutn Geologists Butletin 67, 160-165.

Egbele Emmanuel, Ifeanyi Ezuka and Michael Onyekonwu (2005) "Net-to-Gross Ratios: Implications in Integrated Reservoir Management Studies." Society of Petroleum Engineers.

Ehrenberg, S. N (1990) "Relationship between Diagenesis and Reservoir Quality in Sandstones of the Garn Formation, Haltenbanken, Mid-Norwegian Continental Shelf." AAPG Bulletin v. 74, p. 1538– 1558.

Emery David and Stewart Robert (2006) "Using Vp/Vs to Explore for Sandstone Reservoirs: Well Log and Synthetic Seismograms from the Jeanne D'arc Basin, Offshore Newfoundland." Crewes Research Report Volume 18.

Faleide, J.I., Kyrkjebø, R., Kjennerud, T., Gabrielsen, R.H., Jordt, H., Fanavoll, S. and Bjerk, M.D (2002) "Tectonic Impact on Sedimentary Processes During Cenozoic Evolution of the Northern North Sea and Surrounding Areas." From: DORE, A.G., CARTWRIGHT, J.A., Stoker, M.S., Turner, J.R and White, N. 2002. Exhumation of the North Atlantic Margin: Timing, Mechanisms and Implications for Petroleum Exploration. Geological Society, London, Special Publications, 235–269.

Faleide, J.I., Bjørlykke Knut, Gabrielsen Roy H. (2010), Geology of the Norwegian Continental Shelf, Chapter 22, Petroleum Geoscience by Bjørlykke Knut: From Sedimentary Environments to Rock Physics, pp 467-499.

Fawad, M., Mondol, N.H., Jahren, J. and Bjørlykke, K (2011) "Mechanical Compaction and Ultrasonic Velocity of Sands with Different Texture and Mineralogical Composition, Geophysical Prospecting." v. 59, p. 697-720.

Feng Hong, Brian H Russell and John C Bancroft (2007) "A Comparison of Hydrocarbon Indicators Derived from Avo Analysis." Crewes Research Report Volume 19.

Fertl Walter H. and Chilingar, George V (1988) "Total Organic Carbon Content Determined from Well Logs." SPE formation evaluation.

Fertl, W. H., and Rieke H. H. (1980) "Gamma Ray Spectral Evaluation Techniques Identify Fractured Shale Reservoir and Source Rock Characteristics " Journal of Petroleum Technology 31, 2053-2062.

Fertl, W. H., Chapman, R. E., and Hotz, R. F, (1994) "Studies in Abnormal Pressures." Amsterdam: Elsevier.

Fichler C. And Hospers, J (1990) "Deep Crustal Structure of the Northern North Sea Viking Graben: Results from Deep Reflection Seismic and Gravity Data." Elsevier Science Publishers B.V., no. Amsterdam - Printed in The Netherlands 241-254.

Fitzsimmons R., Veiberg D. And Kenes T. Krå (2005) "Characterization of the Heimdal Sandstones within Alveim, Quads 24 and 25, Norwegian North Sea." Dore ´ , A. G. and Vining, B. A (Eds) Petroleum Geology: North-West Europe And Global Perspectives—Proceedings Of The 6th Petroleum Geology Conference Published by the Geological Society, London, 123-131.

Fjeldskaara W., M. ter Voordeb, Johansenc H., Christiansson P., Faleided J.I., S.A.P.L. Cloetingh (2004) "Numerical Simulation of Rifting in the Northern Viking Graben the Mutual Effect of Modelling Parameters." Tectonophysics 382, 189-212.

Fraser, S. I., Robinson, A. M., Johnson, H. D., Underhill, J. R., Kadolsky, D. G. A., Connell, R., Johannessen, P. And Ravnaas, R (2003) "Upper Jurassic. In: Evans, D., Graham, C., Armour, A. And Bathurst, P (Eds.) " The Millennium Atlas: Petroleum Geology of the Central and Northern North Sea. London: Geological Society, pp. 289-316.

Færseth, R.B (1996) "Interaction of Permo-Triassic and Jurassic Extensional Fault-Blocks During the Development of the Northern North Sea." Journal of the Geological Society of London 153, 931-944.

Gabrielsen Roy H., Kjrkjebø Rune, Faleide Jan Inge, Fjeldskaar Willy and Kjennerud Tomas (2001) "The Cretaceous Post-Rift Basin Cnfiguration of the Northern North Sea." Petroleum Geoscience 7, 137-154.

Gabrielsen R. H. Færseth, R. B., Steel, R. J., Idil, S. And Klovjan, O. S (1990) "Architectural Styles of Basin Fill in the Northern Viking Graben." BLUNDELL, D. J. and GIBBS, A. D (eds) Tectonic Evolution of the North Sea Rifts. Clarendon, Oxford, 158-179.

Gaffney Cline (2010) "Net-What Is It? What Does It Do? How Do We Quantify It? How Do We Use It?" SPE Reservoir Evaluation and Engineering.

Gassmann F., (1951) Uber die elastizitat poroser medien. Vier. Natur Gesellschaft, 96, 1-23.

Giles, M. R., S. L. Indrelid and D. M. D. James (1998) "Compaction the Great Unknown in Basin Modelling." Geological Society, London, Special Publications 141, 15-43.

Goff, J. C. (1983) "Hydrocarbon Generation and Migration from Jurassic Source Rocks in the E Shetland Basin and Viking Graben of the Northern North Sea." J. geol. Soc. London 140, 445-474.

Goodway Bill., Taiwen. Chen. and Downton Jon. (1997) "Improved Avo Fluid Detection and Lithology Discrimination Using Lamepetrophysicalparameters: From P and S Inversions." The Leading Edge, Extended Abstracts, Soc. Expl. Geophysics 67, 128-138.

Goodway Bill (2001) "Avo and Lamé Constants for Rock Parameterization and Fluid Detection." CSEG Recorder, Scott Pickford, a Core Laboratories Company, Calgary, Canada, 39.

Goulty N. R., A. M. Ramdhan and Jones S. J. (2012) "Chemical Compaction of Mudrocks in the Presence of Overpressure." Petroleum Geoscience, v.18; p471-479.

Graue E., Helland-Hansen, W., Johnson, J., Lømo, L., Nøttvedt, A., Rønning, K., Ryseth, A. and Steel, R (1987) "Advance and Retreat of Brent Delta System, Norwegian North Sea." In Brooks, J. and Glennie, K (eds.) Petroleum geology of north west Europe, Graham and Trotman, London, United Kingdom., 915-937.

Gray, F. David and Eric C. Andersen (2000) "Case Histories: Inversion for Rock Properties." EAGE 62nd Conference and Technical Exhibition, Glasgow, Scotland.

Guliyev Eldar and Thomas L. Davis (2006) "Application of Multicomponent Seismic for Vp-Vs Ratio Extraction: Tight Gas Sandstones Example, Rulison Field, Colorado." SEG Annual Meeting.

Guargena Claudia Hegre, G.; Guy B. Smith; Jonathan Wardell; Tor H. Nilsen and Tor M (2007) "Sandstone Injections at Jotun Oil Field, Norwegian North Sea—Modeling Their Possible Effect on Hydrocarbon Recovery." The American Association of Petroleum Geologists AAPG Memoir 87, 81– 89.

Hamada G M (1996) "An Integrated Approach to Determine Shale Volume and Hydrocarbon Potential in Shaly Sand." SCA Conference Paper Number 9641.

Hamar, G.P and Hesjedal, A . (1983) "Lower Cretaceous Stratigraphy and Tectonic of the South-South Eastern Norwegian Offshore." Kaasschieter, J.P.H. and Reijers, T.J.A (eds) ; Petroleum Geology of the Southeastern North Sea and the adjacent onshore area, Geologie en Mijnbouw 62, 135-144.

Han, D., Nur A. and Morgan D. (1986). Effect of porosity and clay content on the wave velocities in sandstones. Geophysics. v. 51(11), p. 2093-2107.

Hanslien, S. " Balder, in A. M. Spencer, E. Holter, C. J. Campbell, S. H. Hanslien, P. H. H. Nelson, E. Nysaether, and E. G. Ormaasen, (1987) Eds., Geology of the Norwegian Oil and Gas Fields: London, Graham and Trotman, P. 193–201.

Haq B. U., Hardenbol, J. And Vail, P. R. (1987) "Chronology of Fluctuating Sea Level since the Triassic." Science, Vol. 235, 1156-1167.

Harland, W, B., Armstrong, R. L., Cox A. V., Craig L. E., Smith A. G. And Smith D.G (1990) "A Geologic Time Scale." Cambridge University Press, Cambridge.

Haynes F.M., Bergslien, D., Burtz, O.M. And Munkholm, M. S (2000) "Applications of Resistivity Modeling in Reservoir Development: Examples from Balder Field." Petrophysics, Vol. 4 (4) , pp.281-293.

Hempton M., Marshall J., Sadler S., Hogg N., Charles R. And Harvey C. (2005) "Turbidite Reservoirs of the Sele Formation, Central North Sea: Geological Challenges for Improving Production." Petroleum Geology Conference series 6, 449-459.

Heritier, F. E., Lossel, P. And Wathne, E (1979) "Frigg Field Large Submarine-Fan Trap in Lower Eocene Rocks of North Sea." AAPG Bulletin 63.

Hinds Gregory S. and Berg Robert R (1990) "Estimating Organic Maturity from Well Logs, Upper Cretaceous Austin Chalk, Texas Gulf Coast." Trans Actions—Gulf Coast Association Of Geological Societies XL.

Hook, J. R (2003) "An Introduction to Porosity." Petrophysics, v. 44, no. 3,, p. 205– 212.

Hospers J. And Ediriweera, K. K (1991) "Depth and Configuration of the Crystalline Basement in the Viking Graben Area, Northern North Sea." Journal of the Geological Society, London 148, pp. 261-265.

Huggett M., J (1992) "Petrography, Mineralogy and Diagenesis of Overpressured Tertiary and Late Cretaceous Mudrocks from the East Shetland Basin." Clay Minerals in the Modern Society. Mineralogical Society, London, United Kingdom 27, 487-506.

Huggett J.M., Gale A.S., And Wray D.S. (2005) "Diagenetic Clinoptilolite and Opal-Ct from the Middle Eocene Wittering Formation, Isle of Wight, U.K." Journal of Sedimentary Research 75, 585-595.

Ingram G.M., Urai J.L and Naylor M.A. (1997) "Sealing Processes and Top Seal Assessment." Hydrocarbon Seals: Imporatance for exploration and Production edited by

P.Møller Pedersen and A.G: Koestler Norwegian Petroleum Society, NPF Special Publication 7,, 165-174.

Isaksen, D. and Tonstad K. (1989) "A Revised Cretaceous and Tertiary Lithological Nomenclature for Norwegian North Sea." Norwegian Petroleum Directorate Bulletin, Vol. 5, ISBN 82-7257-295-8.

Isaksen, G. H., Pottorf R. J., and Jenssen A. I. (1998) "Correlation of Fluid Inclusions and Reservoired Oils to Infer Trap Fill History in the South Viking Graben, North Sea." Petroleum Geoscience,v. 4, p. 41–55.

Isaksen, G. H. And Ledje, K. H. I. (2001) "Source Rock Quality and Hydrocarbon Migration Pathways within the Greater Utsira High Area, Viking Graben, Norwegian North Sea." AAPG Bulletin, Vol.85, pp.861-883.

Jackson a., C.A-L., and Larsen E. (2009) "Temporal and Spatial Development of a Gravity-Driven Normal Fault Array: Middle–Upper Jurassic, South Viking Graben, Northern North Sea." Journal of Structural Geology 31, 388-402.

Jackson Christopher A-L., Kane Karla E., and Larsen Eirik (2010) "Structural Evolution of Minibasins on the Utsira High, Northern North Sea; Implications for Jurassic Sediment Dispersal and Reservoir Distribution " Petroleum Geoscience v. 16 p. 105-120.

Jahren, J (1993) "Microcrystalline Quartz Coatings in Sandstones. A Scanning Electron Microscopy Study." 45th Annual Meeting of the Scandinavian Society for Electron Microscopy, 111-112.

Jahren, J., Ramm, M, (2000) "The Porosity-Preserving Effects of Microcrystalline Quartz Coatings in Arenitic Sandstones; Examples from the Norwegian Continental Shelf. In: Quartz Cementation in Sandstones." Blackwell, Oxford, International, 271-280.

Japsen P., 1999. Overpressured Cenozoic shale mapped from velocity anomalies relative to a baseline for marine shale, North Sea. Petroleum Geoscience, 5 (4), pp. 321-336.

Jenssen, A. I., Bergslien, D., Rye-Larsen, M., And Lindholm, R. M (1993) "Origin of Complex Mound Geometry of Paleocene Submarine-Fan Sandstone Reservoirs, Balder Field, Norway. In: Parker J. R." Petroleum Geology of Northwest Europe: Proceedings of the 4th Conference. The Geological Society of London, pp. 135-143.

Jenssen, T.F., Holm L., Frandsen N. And Michelsen O (1986) "Jurassic-Lower Cretaceous Lithostratigraphic Nomenclature for the Danish Central Trough, Denmarks." Geologiske Undersoegels, Serie A. 12, 65 pp.

Johnson H.D and Fisher M.J, (1998), North Sea Plays: Geological Controls on Hydrocarbon Distribution: Chapter 12, Glennie, K. W (ed.) Petroleum Geology of the North Sea; Basic Concepts and Recent Advances. Oxford: Blackwell, pp 463-549.

Justwan H. And Dahl, B. (2005) "Quantitative Hydrocarbon Potential Mapping and Organofacies Study in the Greater Balder Area, Norwegian North Sea." Petroleum Geology Conference, Vol. 6, pp. 1317-1329.

Justwan H., Meisingset I., Dahl B., Isaksen G.H. (2006) "Geothermal History and Petroleum Generation in the Norwegian South Viking Graben Revealed by Pseudo-3d Basin Modelling." Marine and Petroleum Geology.

Kan T. K., and Sicking, C. J., (1994) "Pre-Drill Geophysical Methods for Geopressure Detection and Evaluation." In studies in abnormal pressures New York: Elsevier.

Karlsson W., Vollset J., Bjørlykke K. And Jdrgensen P (1979) "Changes in Mineralogical Composition of Tertiary Sediments from North Sea Wells." Proc. Int. Clay Conf., Oxford, 281-289.

Katahara Keith, (2006) "Overpressure and Shale Properties: Stress Unloading or Smectite-Illite Transformation." New Orleans 2006 Annual Meeting SEG.

Keer I. Van, Muchez PH. and Viaene W. (1997) "Clay Mineralogical Variations and Evolutions in Sandstone Sequences near Coal Seam and Shales in the Westphalian the Campine Basin (Ne Belgium." Clay Minerals Mineralogical Society, 33, 159-169.

Keym, Matthias, Volker Dieckmann, Brian Horsfield, Michael Erdmann, Roberto Galimberti, Lung-Chuan Kua, Leslie Leith and Olaf Podlaha (2006) "Source Rock Heterogeneity of the Upper Jurassic Draupne Formation, North Viking Graben, and Its Relevance to Petroleum Generation Studies." Organic Geochemistry 37, no. 2 220-243.

Kjennerud T., Faleide J.I., Gabrielsen R.H., Gillmore G.K., Kyrkjebe R., Lippard S.J. and Løseth H. (2001) "Structural Restoration of Cretaceous-Cenozoic (Post-Rift) Palaeobathymetry in the Northern North Sea." Sedimentary Environments Offshore Norway - Palaeozoic to Recent edited by O.J. Martinsen and T. Dreyer. NPF Special Publication, Published by Elsevier Science B.V., Amsterdam 10, 347-364.

Krief M., Garat J., Stellingwerff J., and Ventre J., (1990) "A Petrophysical Interpretation Using the Velocities of P and S Waves (Full-Waveform Sonic) " The Log Analyst 31, 355-369.

Lambeck Kurt, (1995) "Late Devensian and Holocene Shorelines of the British Isles and North Sea from Models of Glacio-Hydro-Isostatic Rebound." Journal of the Geological Society, London, 152, no. Research School of Earth Sciences, The Australian National University, Canberra ACT 0200, Australia 437-448.

Lang H., (1994) "Compaction/Diagenesis of Sediments and Compaction Gradients in Relation to Interval Transit Time." The Log Analyst, 54-59.

Larionov W. W (1969) "Radiometrija Skwaschin." Nedra Verlag, Moscow.

Li Dachang, Dria, and Myra A (1997) "Cutt-Off or Separation? A New Approach to Distinguish Reservoir Rock from Non Reservoir Rock for Reservoir Modeling and Simulation." Society of Petroleum Engineers SPE Rocky Mountain Regional Meeting, Casper, Wyoming, U.S.A, 18-21.

Li Shuling, (2012) Cary Purdy and Shiguo Wu. "Pore Pressure and Fracture Gradient Prediction in Shale Gas Formations: Accounting for Complex Rock Properties and Anisotropies." SPE international, Asia Pacific drilling technology conference and exhibition July 2012,

Lin J.L., and Salisch H.A (1993) "Determination from Well Logs of the Total Organic Carbon in Potential Source Rocks." Society of Petroleum Engineers 23.

Lonergan L., Cartwrigh J., Laver And Staffurth (1998) "Polygonal Faulting in the Tiary of the Central North Sea: Implication for Reservoir Geology." Coward M.P., Daltaban, T.S. and Johnson, H (eds) Structural Geology in Reservoir Characterization, Geological Society, London, Special Publication, 127, 191-207.

Løseth Helge, Lars Wensaas, and Marita Gading (2010) "Deformation Structures in Organic-Rich Shales." The American Association of Petroleum Geologists V. 95 No. 5, 729-747.

Maast Tom Erik, Jahren Jens, and Bjørlykke Knut (2011) "Diagenetic Controls on Reservoir Quality in Middle to Upper Jurassic Sandstones in the South Viking Graben, North Sea." AAPG Bulletin, v. 95, no. 11 The American Association of Petroleum Geologists.

Magoon L. B, and Dow W. G. (1994) "The Petroleum System from Source to Trap." AAPG, 60.

Marcussen Øyvind, Thyberg Brit I., Peltonen Christer, Jahren Jens, Bjørlykke Knut, and Faleide Jan Inge (2009) "Physical Properties of Cenozoic Mudstones from the Northern North Sea: Impact of Clay Mineralogy on Compaction Trends." AAPG Bulletin, 93, 127-150.

Marcussen Øyvind, Maast Tom Erik, Mondol Nazmul H., Jahren Jens, Bjørlykke Knut (2010) "Changes in Physical Properties of a Reservoir Sandstone as a Function of Burial Depth-the Etive Formation, Northern North Sea." Marine and Petroleum Geology 10, 1725–1735.

Marion D (1990) "Acoustical, Mechanical and Transport Properties of Sediments and Granular Materials." Ph.D thesis Stanford University.

Marion D., Nur A., Yin H. and Han D. (1992). Compressional velocity and porosity in sand clay mixtures. Geophysics, v. 57, p. 554-563.

Martinsen Ole J. and Tom Dreyer (2001) "Sedimentary Environments Offshore Norway - Palaeozoic to Recent." Elsevier Science Publishers.

Martinsen O. J. T. Lien and Jackson C. (2005) Cretaceous and Palaeogene turbidite systems in the North Sea and Norwegian Sea Basins: source, staging area and basin physiography controls on reservoir development. Petroleum Geology Conference series 2005, v.6; p1147-1164

McCoy D.D., Grieves W.A. (1997) "Uses of Resistivity Logs to Calculate Water Saturation at Prudhow Bay." Society of Petroleum Engineers.

Meissner F.F (1978) "Petroleum Geology of the Bakken Formation Williston Basin, North Dakota and Montana." Montana Geological Society, Williston Basin Symposium, 207-227.

Miller Susan L. M. (1992) "Well Log Analysis of Vp and Vs in Carbonates." CREWES Research Report 4.

Milton N.J and Emery D. (2008), Outcrop and well data, chapter 4, Sequence startigraphy, 61-79.

Molyneux S.J.M., Cartwright J.A. and Lonergan L, T.H.Huxley, (2002) "Large Scale Deepwater Sediment Remobilisation : Examples from North Sea 3d Seismic and Outcrop." AAPG Annual Meeting Houston, Texas.

Mondol Nazmul Haque, Bjørlykke Knut and Jahren Jens (2008) "Experimental Compaction of Clays: Relationship between Permeability and Petrophysical Properties in Mudstones." Petroleum Geoscience, Vol. 14, 319–337.

Mondol N. H., Bjørlykke K., Jahren J. and Hoeg K (2007) "Experimental Mechanical Compaction of Clay Mineral Aggregates - Changes in Physical Properties of Mudstones During Burial." Marine and Petroleum Geology v. 24, p. 289-311.

Mondol N. H. (2009) "Porosity and Permeability Development in Mechanically Compacted Silt Kaolinite Mixtures. Seg Houston International Exposition and Annual Meeting".

Mudge David C. and Bujak Jonathan P (1996) "Palaeocene Biostratigraphy and Sequence Stratigraphy of the Uk Central North Sea." Marine and Petroleum Geology 13.

Mukerji Tapan and Gary Mavko (2006) "Recent Advances in Rock Physics and Fluid Substitution." CSEG Recorder, Special Edition.

Murphy W. M., Oelkers E. H., and Lichtner P. C. (1989) "Surface Reaction Versus Diffusion Control of Mineral Dissolution and Growth Rates in Geochemical Processes,." in J. Schott and A. C. Lasaga, eds., Kinetic geochemistry: Amsterdam, Elsevier, p. 357– 380.

Murray G.H (1968) "Quantitative Fracture Study - Sanish Pool, Mckenzie County, North Dakota." AAPG Bulletin 57, 57-65.

Myers K.J. and Milton N.J (2008), Concepts and Principles of sequence stratigraphy, chapter 2, Sequence startigraphy, pp 11-44.

Nadin P.A., Kusznir N.J. , Cheadle M.J. (1997) "Early Tertiary Plume Uplift of the North Sea and Faeroe-Shetland Basins." Earth and Planetary Science Letters 48, 109-127.

Newman M.St. J., Reeder, M.L, Woodruff, A.H.W And Hatton (1993) "The Geology of Gryphon Oil Field." Parker, J.R (ed) Petroleum Geology of North West Europe: Proceeding of the 4th Conference, Geological Society; London, 123-133.

Nixon R.p (1973) "Oil Source Beds in Cretaceous Mowry Shale of Nort-Western Interior United States." AAPG Bulletin 57, 136-161.

Nøttvedt A., Gabrielsen R. H., Steel R. J (1995) "Tectonostratigraphy and Sedimentary Architecture of Rift Basins, with Reference to the Northern North Sea." Marine and Petroleum Geology 12, 881–901.

Nøttvedt Arvid, Berge Anker M., Nancye H. Dawers, Færseth Roald B., , Kjell O. Häger, Gunn Mangerud and Cai Puigdefabregas (2000) "Syn-Rift Evolution and Resulting Play Models in the Snorre-H Area, Northern North Sea." Geological Society, London, Special Publications 167, 179-218.

O'Connor S. J., And Walker D. (1993) "Paleocene Reservoirs of the Everest Trend." Petroleum Geology Conference series 4, 145-160.

O'Connor Stephen, Swarbrick Richard, Hoesni Jamaal, Lahann Richard (2011) "Deep Pore Pressure Prediction in Challenging Areas, Malay Basin, Se Asia." Proceedings, Indonesia Petroleum Association, Thirty-Fifth Annual Convention and Exhibition, May 2011.

Odinsen Tore, Christiansson Peter, Gabrielsen Roy H., Faleide Jan Inge and Berge Anker M. (2000) "The Geometries and Deep Structure of the Northern North Sea Rift System." Geological Society, London, Special Publications v.167, p41-57.

Odinsen Tore, Paul Reemst, Peter Van Der Beek, Jan Inge Faleide and Roy H. Gabrielsen (2000) "Permo-Triassic and Jurassic Extension in the Northern North Sea: Results from Tectonostratigraphic Forward Modelling." Geological Society, London, Special Publications v.167, p83-103.

Oelkers E. H., Bjørkum P. A., and Murphy W. M. (1992) "The Mechanism of Porosity Reduction, Stylolite Development and Quartz Cementation in North Sea Sandstones." Y. K. Kharaka and A. S. Maest, eds., Proceedings International Symposium on Water-Rock Interaction, Rotterdam." Balkema 2p., 1183– 1186.

Oelkers E. H., Bjørkum P. A., and Murphy W. M. (1996) "A Petrographic and Computational Investigation of Quartz Cementation and Porosity Reduction in North Sea Sandstones." American Journal of Science v. 296: p. 420– 452.

Okiotor M. E. and Imasuen, O. I (2011) "Facies Characterisation of Well a, Field Y, North-Eastern Niger Delta." Journal of Petroleum Technology and Alternative Fuels, Academic Journals 2 (4) , 45-54.

Omudu L. M. and Ebeniro J.O. (2005) "Cross-Plotting of Rock Properties for Fluid Discrimination Using Well Data in Offshore Niger Delta." Nigerian Journal of Physics, 17.

Ostvedt O. J., Evensen S., Ranaweera H. K. A. (1990) "Sleipner Ost Field, Viking Graben, North Sea, Norway, ." AAPG Special Volumes ; Treatise TR: Structural Traps IV: Tectonic and Nontectonic Fold Traps, 173-196.

Palciauskas V. V (1991) "Primary Migration of Petroleum, in R. K. Merrill, Ed., Source and Migration Processes and Evaluation Techniques." AAPG Treatise of Petroleum Geology, Handbook of Petroleum Geology, 13– 22.

Partington M. A., Mitchener, B. C., Milton, N. J. And Fraser, A. J (1993) "Genetic Sequence Stratigraphy for the North Sea Late Jurassic and Early Cretaceous; Distribution and Prediction of Kimmeridgian-Late Ryazanian Reservoirs in the North Sea and Adjacent Areas." Parker, J. R (ed.) Petroleum Geology of Northwest Europe: Proceedings of the 4th Conference. London: Geological Society, , pp.347-370.

Passey Q.R., Creaney S., Kulla J.B., Moretti F.J., and Stroud J.D. (1990) "A Practical Model for Organic Richness from Porosity and Resistivity Logs." AAPG Bulletin 74 No. 12, 1777-1794.

Pelletier Heath Jay Gunderson, Veritas DGC (2004) "Application of Rock Physics to an Exploration Play: A Case Study from the Brazeau River 3d." CSEG National Convention Great Explorations – Canada and Beyond.

Peltonen Christer, Marcussen Øyvind, Bjørlykke Knut and Jahren Jens (2008) "Mineralogical Control on Mudstone Compaction: A Study of Late Cretaceous to Early Tertiary Mudstones of the Vøring and Møre Basins, Norwegian Sea." Petroleum Geoscience 14, 127-138.

Peltonen Christer, Marcussen Øyvind, Bjørlykke Knut and Jahren Jens (2009) "Clay Mineral Diagenesis and Quartz Cementation in Mudstones: The Effects of Smectite to Illite Reaction on Rock Properties." Marine and Petroleum Geology, 887–898.

Pepper A. S., and Corvi P. J. (1995) "Simple Kinetic Models of Petroleum Formation: Part Iii." Modelling an open system: Marine and Petroleum Geology 12, , p. 417–452.

Peters K. E., and Cassa M. R. (1994) Applied source rock geochemistry, in L. B. Magoon and W. G. Dow, eds., The petroleum system From source to trap: American Association of Petroleum Geologists Memoir 60, Tulsa, Oklahoma, p. 93-120.

Pickett G.R (1963) "Acoustic Character Logs and Their Application in Formation Evaluation." J. Petro Tech., , 659-667.

Platt Nigel H. and Cartwright, Joseph A (1998) "Structure of the East Shetland Platform, Northern North Sea." Petroleum Geoscience 4.

Poupon A., Clavier C., Dumanoir J., Gaymard R. and Misk A. (1970) "Log Analysis of Sand-Shale Sequences a Systematic Approach." SPE, JPT.

Purvis Kevin, (1992) Lower Permian Rotliegend sandstones, southern North Sea: a case study of sandstone diagenesis in evaporite-associated sequences Elsevier Science Publishers B.V. All rights reserved Sedimentary Geology, 77 155-171

Quintero Luis F. and Bassiouni, Zaki (1997) "Gas Zones Detection Using the Dual-Spaced Neutron Tool Responses." SPE Fifth Latin American conference.

Ramm m. and Bjørlykke K. (1994) "Porosity/Depth Trends in Reservoir Sandstones: Assessing the Quantitative Effects of Varying Pore-Pressure, Temperature History and Mineralogy, Norwegian Shelf Data." Clay Minerals in the Modern Society. Mineralogical Society, London, United Kingdom 29, 475-490.

Rattey R. P. And Hayward A. B. (1993) "Sequence Stratigraphy of a Failed Rift System: The Middle Jurassic to Early Cretaceous Basin Evolution of the Central and Northern North Sea." Petroleum Geology Conference series 4, 215-249.

Rawson P. F. and Riley, L. A. (1982) "Latest Jurassic-Early Cretaceous Events and the “Late Cimmerian Unconformity” in North Sea Area." AAPG Bulletin 66, , 2628–2648.

Revil A., Grauls D. and Bre´vart O. (2002) "Mechanical Compaction of Sand/Clay Mixtures." Journal Of Geophysical Research 107, no. 2293.

Rider Malcolm and Kennedy Martin, (2011). “The Geological Interpretation of Well Logs.”

Russell Brian H. and Smith, Tad (2007) "The Relationship between Dry Rock Bulk Modulus and Porosity, an Empirical Study." CREWES Research Report 19.

Sarg J. F., and Skjold L. J (1982) "Stratigraphic Traps in Paleocene Sands in the Balder Area, North Sea." AAPG Memoir, Vol. 32., pp. 197-206.

Sayers Colin M., And Lennert D. Den Boer (2011) "Rock Physics-Based Relations for Density and S-Velocity Versus, P-Velocity in Deepwater Subsalt Gulf of Mexico Shales." The Leading Edge Physics of rocks.

Schlakker Attila, János Csizmeg, György Pogácsás, and Anikó Horti (2012) "Thermal and Maturation History in the Northern Viking Graben (North Sea) " Search and Discovery.

Schmoker J.W (1979) "Determination of Organic Content of Appalachian Devonian Shales from Formation Density Logs." AAPG Bulletin 63, 1285-1298.

Schmoker J.W (1981) "Determination of Organic Matter Content of Appalachian Devonian Shales from Gamma Ray Logs." AAPG Bulletin 67, 2165-2174.

Sheldon Heather A., Wheeler John, Richard H. Worden, And Michael J. Cheadle (2003) "An Analysis of the Roles of Stress, Temperature, and Ph in Chemical Compaction of Sandstones." Journal Of Sedimentary Research, Vol. 73, No. 1, , 64-71.

Shell (1982) "Well Log Interpretation." Chapter 11-13.

Shepherd M. "Rock and Fluid Properties (2009) "Oil field production geology: AAPG Memoir, 91, 65-68.

Srodon J (1999) "Nature of Mixed-Layer Clays and Mechanisms of Their Formation and Alteration." Annual Review of Earth and Planetary Sciences.

Steel R. and Ryseth A. (1990) "The Triassic Early Jurassic Succession in the Northern North Sea: Megasequence Stratigraphy and Intratriassic Tectonics". Geological Society, London, Special Publications 55, 139-168.

Storvoll Vidar And Bjørlykke Knut (2004) "Sonic Velocity and Grain Contact Properties in Reservoir Sandstones." Petroleum Geoscience 2004, v.10; p215-226.

Storvoll Vidar, Bjørlykke Knut, and Mondol Nazmul H. (2005) "Velocity-Depth Trends in Mesozoic and Cenozoic Sediments from the Norwegian Shelf." AAPG Bulletin, v. 89, no. 3 , pp. 359–381.

Soto Rodolfo B, Duarry arteaga, Cinta Martin, Freddy Rodriguez (2010) "The Correct Shale-Volume Characterization Increases Hydrocarbon Reserve: Case Study of Cretaceous Formation, Lake Maracaibo, Venezuela." SPE international Peru.

Soubotcheva Natalia and Stwewart Robert R (2004) "Predicting Porosity Logs from Seismic Attributes Using Geostatistics." Crewes Research Report 16.

Supernaw I.R., Arnold D.M. and A.J (1978) Link "Methods for in-Situ Evaluation of the Source Rock Potential of Earth Formations." United states patent 4, 071, 744.

Swanson V.E (1960) "Oil Yield and Uranium Content of Black Shales." USGS Professional Paper 356, 1-44.

Szarawarska Ewa, Mads Huuse, Andrew Hurst, Wytze de Boer, Liwei Lu, Steven Molyneux and Peter Rawlinsonw (2010) "Three-Dimensional Seismic Characterisation of Large-Scale Sandstone Intrusions in the Lower Palaeogene of the North Sea: Completely Injected Vs. In Situ Remobilised Sandbodies." Journal Compilation Blackwell Publishing Ltd, European Association of Geoscientists and Engineers and International Association of Sedimentologists.

Tanqua Karoo, South Africa." Fine-grained turbidite systems, AAPG Memoir 72/SEPM Special Publication 68,, p. 173–180.

Tatham R.H (1982) "Vp/Vs and Lithology." Geophysics Mar., pp 336-344.

Thomas B. M., Moller-Pedersen P., M. Whitaker F., and Shaw N. D. (1985) "Organic Facies and Hydrocarbon Distributions in the Norwegian North Sea." B. M. Thomas, S. S. Eggen, R. M. Larsen, P. C. Home, and A. G. Dore´ , eds., Petroleum geoIsaksen and Ledje 883 chemistry in exploration of the Norwegian Shelf: London, Norwegian Petroleum Society, Graham and Trotman, p. 3.

Thyberg B. I., Jordt, H., Bjørlykke, K., Faleide, J. I., (2000) "Relationship between Sequence Startigraphy, Mineralogy and Geochemistry in Cenozoic Sediments of Northern North Sea." Geological Society of London, Special Publication 167, 245-272.

Timbrell G. (1993) "Sandstone Architecture of the Balder Formation Depositional System, Uk Quadrant 9 and Adjacent Areas." From Petroleum Geology of Northwest Europe: Proceedings of the 4th Conference (edited by J. R. Parker Published by The Geological Society, London, pp. 107-121., no. Conoco UK Ltd, 116 Park Street, London W1Y 4NN, UK

Torsvik Trond H, Carlos Daniel, Mosar Jon, Cocks L Robin M, Malme Tarjei N. (2002) "Global Reconstructions and North Atlantic Paleogeography 440 Ma to Recent." Batlas—Mid Norway plate reconstruction atlas with global and Atlantic perspectives, 18-39.

Towe K.M (1962) "Clay Mineral Diagenesis as a Possible Source of Silica Cement in Sedimentary Rocks." Journal of Sedimentary Petrology 32, 26-28.

Ulasi Adaeze, Samuel I., Onyekuru O. and Chukwuma Julian Iwuagwu (2012) "Petrophysical Evaluation of Uzek Well Using Well Log and Core Data, Offshore Depobelt, Niger Delta, Nigeria." Pelagia Research Library.

Underhill, J. R (1998) "Jurassic. In: Glennie, K.W." Petroleum Geology of the North Sea; Basic Concepts and Recent Advances, Oxford: Blackwell, pp. 245-292.

Vernik, L., and Nur A., (1992) "Petrophysical Classification of Siliciclastics for Lithology and Porosity Prediction from Seismic Velocities." AAPG Bulletin v. 76: p. 1295- 1309.

Vollset J., and Dore´, A.G (1984) "A Revised Triassic and Jurassic Litho-Stratigraphic Nomenclature of the Norwegian North Sea." Norwegian Petroleum Directorate Bulletin, Vol. 3, ISBN 82-7257-155-2.

Voorde M. Ter, Færseth R. B., Gabrielsen R. H. and S. A. Cloetingh P. L. (2000) "Repeated Lithosphere Extension in the Northern Viking Repeated Lithosphere Extension in the Northern Viking." Geological Society, London, Special Publications 2000 167, 59-81.

Wach Grant D., Theodore C. Lukas, Robert K. Goldhammer, Wickens H. Deville, A. H. Bouma (2000) "Submarine Fan through Slope to Deltaic Transition Basin-Fill Succession, Walderhaug, O (1994a) "Precipitation Rates for Quartz Cement in Sandstones Determined by Fluid-Inclusion Microthermometry and Temperature-History Modeling:." Journal of Sedimentary Research, Section A: Sedimentary Petrology and Processes, v. 64, , p. 324– 333.

Walderhaug, O (1994b) "Temperatures of Quartz Cementation in Jurassic Sandstones from the Norwegian Continental Shelf, Evidence from Fluid Inclusions:." Journal of Sedimentary Research v. 64, p. 311–323.

Walderhaug, O (1996) "Kinetic Modeling of Quartz Cementation and Porosity Loss in Deeply Buried Sandstone Reservoirs:." AAPG Bulletin v. 80,, p. 731–745.

Walderhaug, O (2000) "Modeling Quartz Cementation and Porosity in Middle Jurassic Brent Group Sandstones of the Kvitebjorn Field, Northern North Sea." AAPG Bulletin v. 84, p. 1325–1339.

Walls Joel, Dvorkin Jack, Carr Matt (2004) "Well Logs and Rock Physics in Seismic Reservoir Characterization." Rock Solid Images Offshore Technology Conference.

Wang G., Rossen, R. H., Hjellbakk, A., And Sun, M. C (2003) "Managing a Complex Deepwater Deposit through Advanced Simulation Technologies, Balder Field, Norway." Presented at the SPE Reservoir Simulation Symposium in Houston, Texas, February 3-5. pp. 1–9.

Weaver, C.E (1959) "The Clay Petrology of Sediments. In: Swineford, A (Ed.) , Clays and Clay Minerals." Pergamon Press, Oxford, United Kingdom, 154-187.

Weller, James Marvin (1959) "Compaction of Sediments." AAPG Bulletin February 1959 43, no. 2 273-310.

Wild John and Briedis Nowell (2010) "Structural and Stratigraphic Relationships of the Palaeocene Mounds of the Utsira High." Journal CompilationrBlackwell Publishing Ltd, European Association of Geoscientists and Engineers and International Association of Sedimentologists BasinResearch (2010) 22, 533-547.

Williams, D. M (1990) "The Acoustic Log Hydrocarbon Indicator." Society of Petrophysicists and Well Log Analysts, 31st Logging Symposium, Paper W.

Worthington Paul F., Gaffney, Cline (2011) "The Petrophysics of Problematic Reservoirs." Distinguished Author Series Jpt.

Wyllie, M.R.J., Gregory, A.R and Gardner, G.H.F (1956) "Elastic Wave Velocities in Heterogeneous and Porous Media." Geophysics 121.

Xu, Yong and John C. Bancroft (1997) "Joint Avo Analysis of Pp and Ps Seismic Data." Crewes Research Report 9.

Xu, Yong and John C. Bancroft (1998) "Statistical Vp-Vs Relationships from Well Logs in Blackfoot." Crewes Research Report 10.

Yang Hua, Wenzheng Zhang, Kai Wub, Shanpeng Li, Ping'an Peng, Yan Qin (2010) "Uranium Enrichment in Lacustrine Oil Source Rocks of the Chang 7 Member of the Yanchang Formation, Erdos Basin, China." Journal of Asian Earth Sciences 39, 285-293.

Ziegler, P.A (1982) "Geological Atlas Ofwestern and Central Europe." The Hague, New York, NY: Shell Internationale Petroleum Maatschappij B.V. , no. Distributed by Elsevier Science Pub. Co.

Ziegler, P.A (1988) "Evolution of the Arctic-North Atlantic Rift System." American Association of Petroleum Geologists Memoir 43, 198.

Ziegler, P.A., and Hoorn van, B (1989) "Evolution of North Sea Rift System, in Tankard, A.J., and Balkwill, H.R., Eds., Extensional Tectonics and Stratigraphy of the North Atlantic Margins." American Association of Petroleum Geologists 46, p. 471-500.

Ziegler, P.A (1990) "Geological Atlas of Western and Central Europe (2 Ed.) V." Shell Int. Petrol. Mij. B.V., dist. by Geol. Soc. Publ. House Bath 239, 56.

Ødegaard Erik and Avseth Per, (2004). "Well log and seismic data analysis using rock physics templates." EAGE first break volume 23.

Websites

Glover, Dr. Paul (2005) "Introduction to Petrophysics and Formation Evaluation." Petrophysics MSc Course Notes. Website address

http://www2.ggl.ulaval.ca/personnel/paglover/CD%20Contents/GGL-66565%20Petrophysics%20English/Chapter%201.PDF [Last accessed 20.5.2013]

Norlex, (2013) (Norwegian Interactive Offshore Stratigraphic Lexicon).

Website: http://nhm2.uio.no/norlex/ [Last accessed 20.5.2013]

Website: http://nhm2.uio.no/norges/litho/balder.php

NPD, (Norwegian Petroleum Directorate), (2013).

Website http://www.npd.no/ [Last accessed 20.5.2013]

Bulletins-5:

http://www.npd.no/en/Publications/NPD-bulletins/255-Bulletin-5/ [Last accessed 20.5.2013]

Balder field information, Website address: http://www.npd.no/Global/Engelsk/3-Publications/Facts/Facts2011/Figures/Chapter-10/Balder.pdf." [Last accessed 20.5.2013]

Fact maps, Website address:

http://npdmap1.npd.no/website/NPDGIS/NPDSEARCH/default.htm?NPDID_wellbore=1921 [Last accessed 20.5.2013]

ExxonMobil, (2013).

Website address: http://www.exxonmobil.com/crudeoil/about_crudes_balder.aspx [Last accessed 20.5.2013]

Met, (2013); Meteorologisk institutt.

Website address: http://met.no/English/Climate_in_Norway/ [Last accessed 20.5.2013]

Theweatherprediction, (2013)

Website address: http://www.theweatherprediction.com/habyhints/199/ [Last accessed 20.5.2013]

Appendix I (Petrophysical Analysis)

Correlation of the reservoir rocks (sand and shale units)

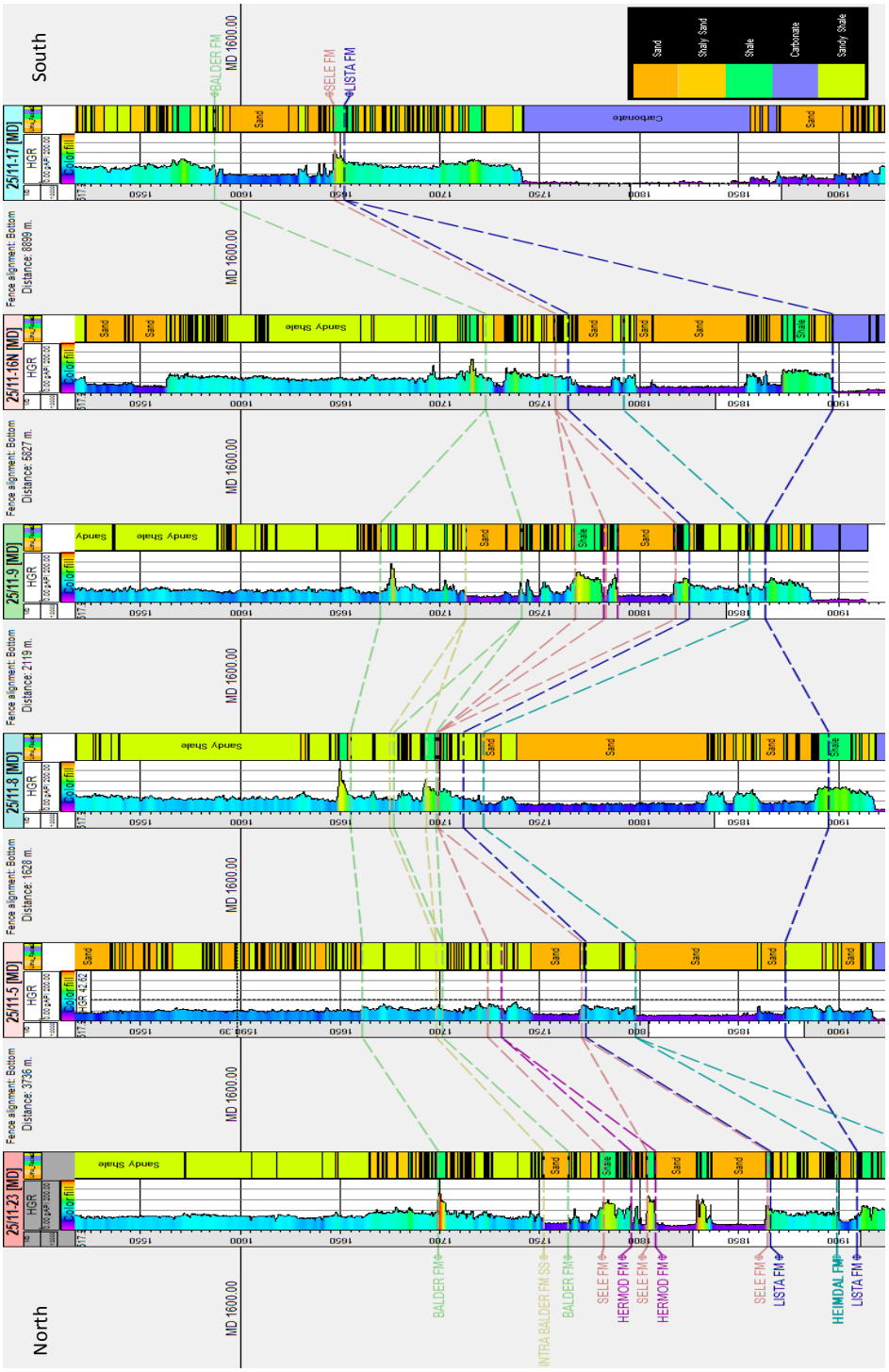

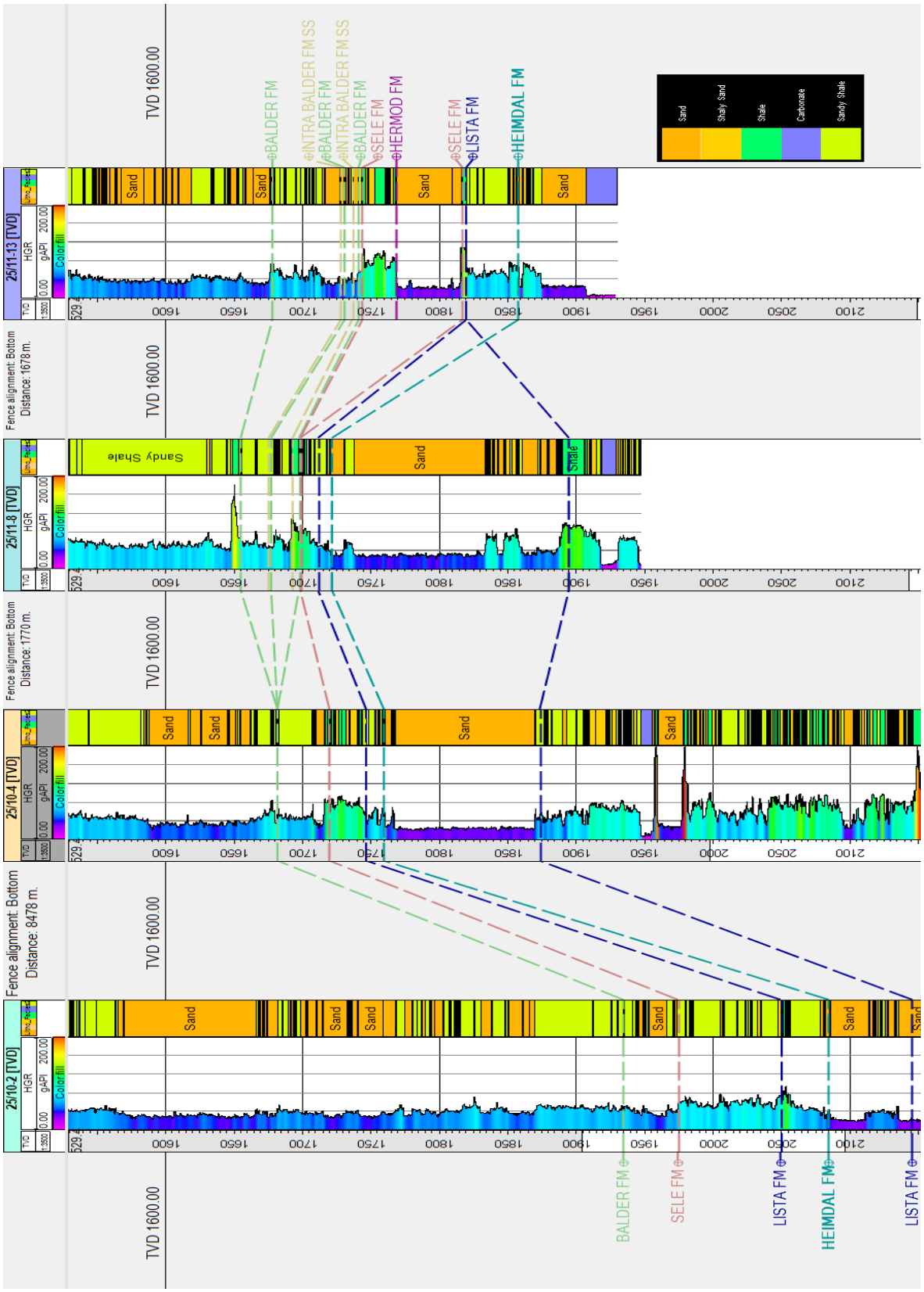
TVD 1600.00
BALDER FM
INTRA BALDER FM SS
BALDER FM
INTRA BALDER FM SS
BALDER FM
SELE FM
HERMOD FM
SELE FM
LISTA FM
HEIMDAL FM
Sand
Shaly Sand
Shale
Carbonate
Sandy Shale
25/11-13 [TVD]
25/11-8 [TVD]
25/10-4 [TVD]
25/10-2 [TVD]
HGR
gAPI
200.00
0.00
Color fill
Fence alignment: Bottom
Distance: 1678 m.
Distance: 1770 m.
Distance: 8478 m.
Sandy Shale
Shale
529
1600
1650
1700
1750
1800
1850
1900
1950
2000
2050
2100
BALDER FM
SELE FM
LISTA FM
HEIMDAL FM
LISTA FM

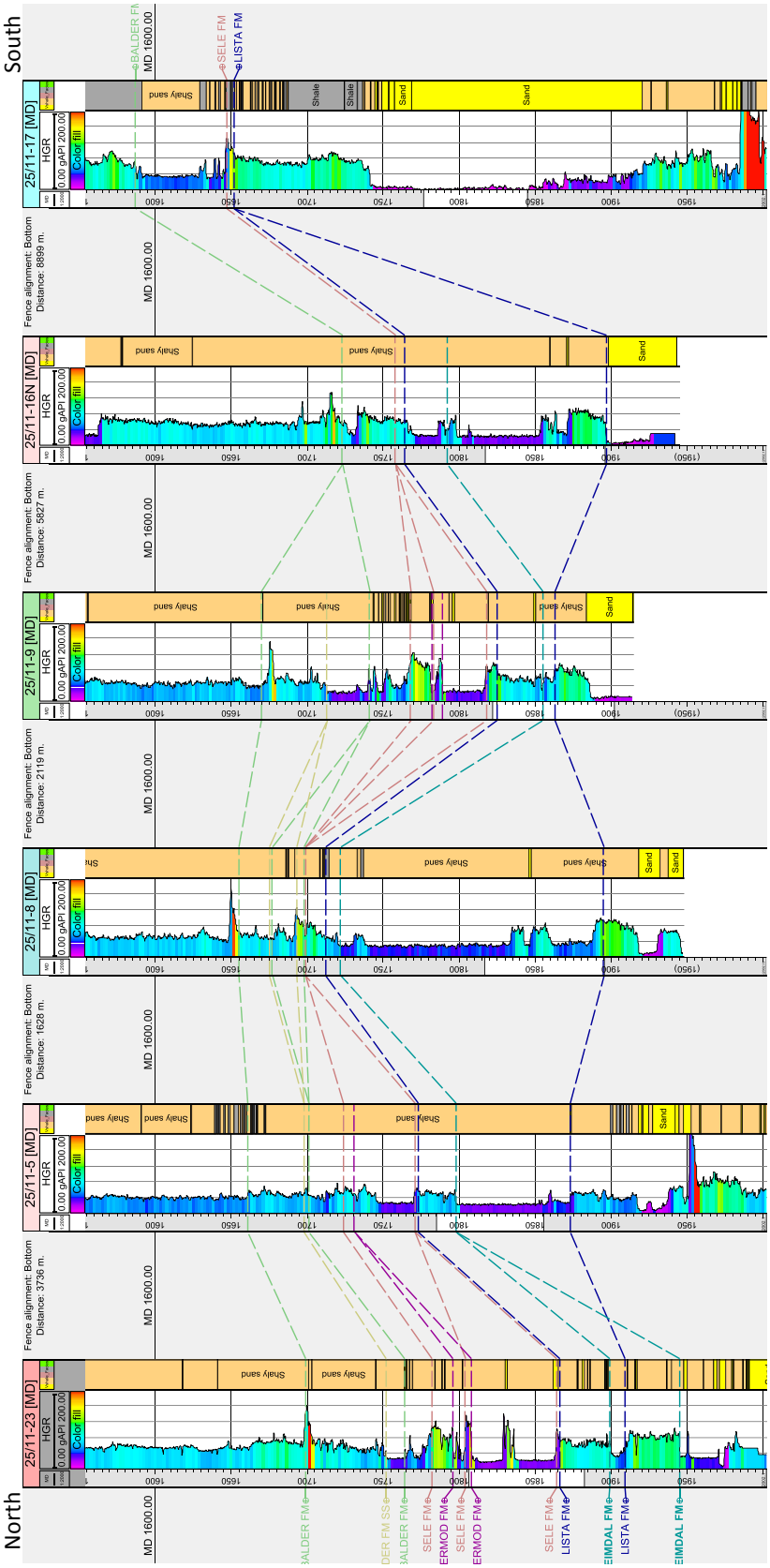
South
North
MD 1600.00
SELE FM
LISTA FM
25/11-17 [MD]
25/11-16N [MD]
25/11-9 [MD]
25/11-8 [MD]
25/11-5 [MD]
25/11-23 [MD]
HGR
Color fill
Shaly sand
Shale
Sand
Fence alignment: Bottom
Distance: 8899 m.
Distance: 5827 m.
Distance: 2119 m.
Distance: 1628 m.
Distance: 3736 m.

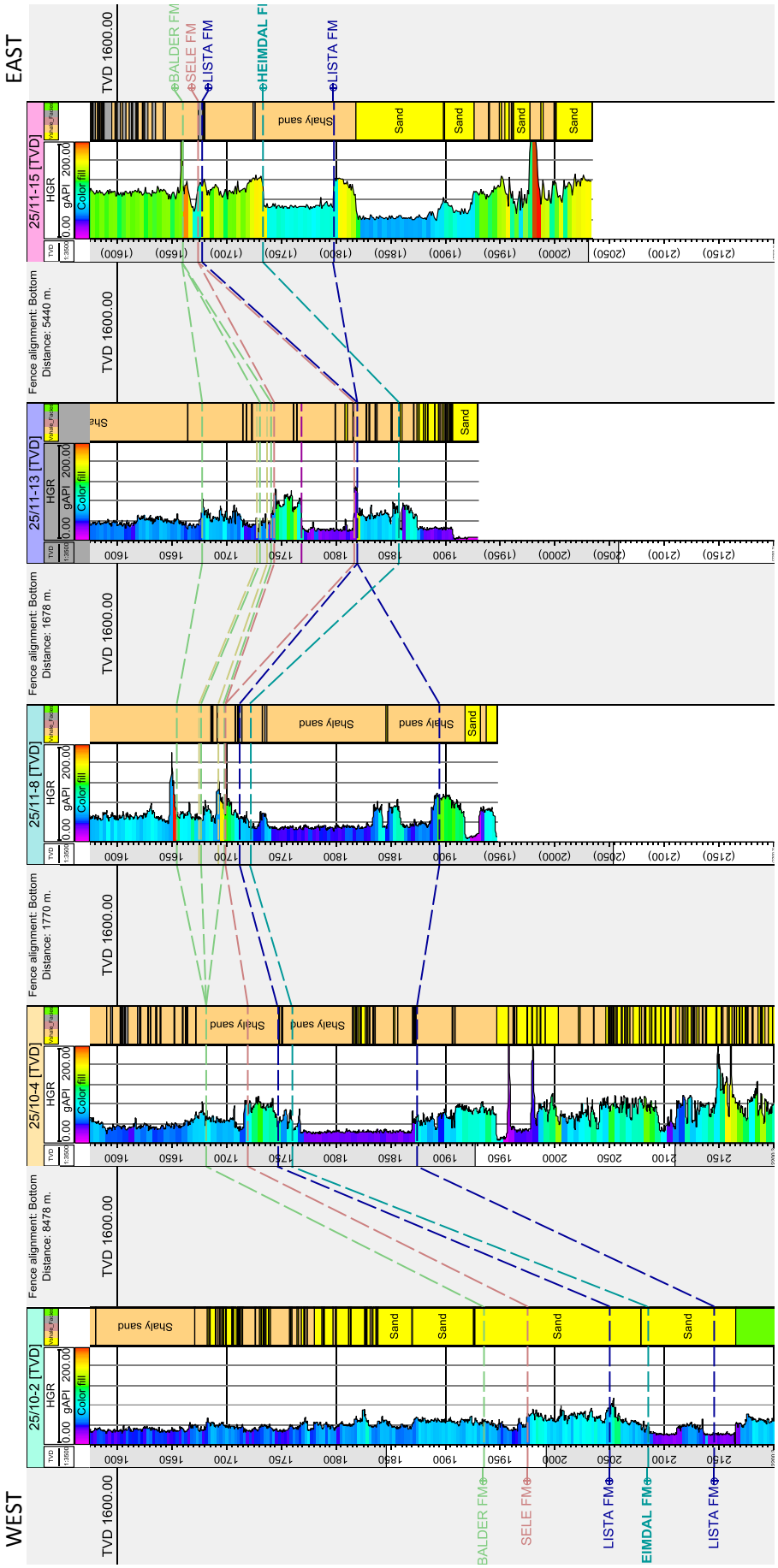
EAST
WEST
TVD 1600.00
BALDER FM
SELE FM
LISTA FM
HEIMDAL FM
25/11-15 [TVD]
25/11-13 [TVD]
25/11-8 [TVD]
25/10-4 [TVD]
25/10-2 [TVD]
HGR
gAPI
Color fill
Shaly sand
Sand
Fence alignment: Bottom
Distance: 5440 m.
Distance: 1678 m.
Distance: 1770 m.
Distance: 8478 m.

Lithology identification

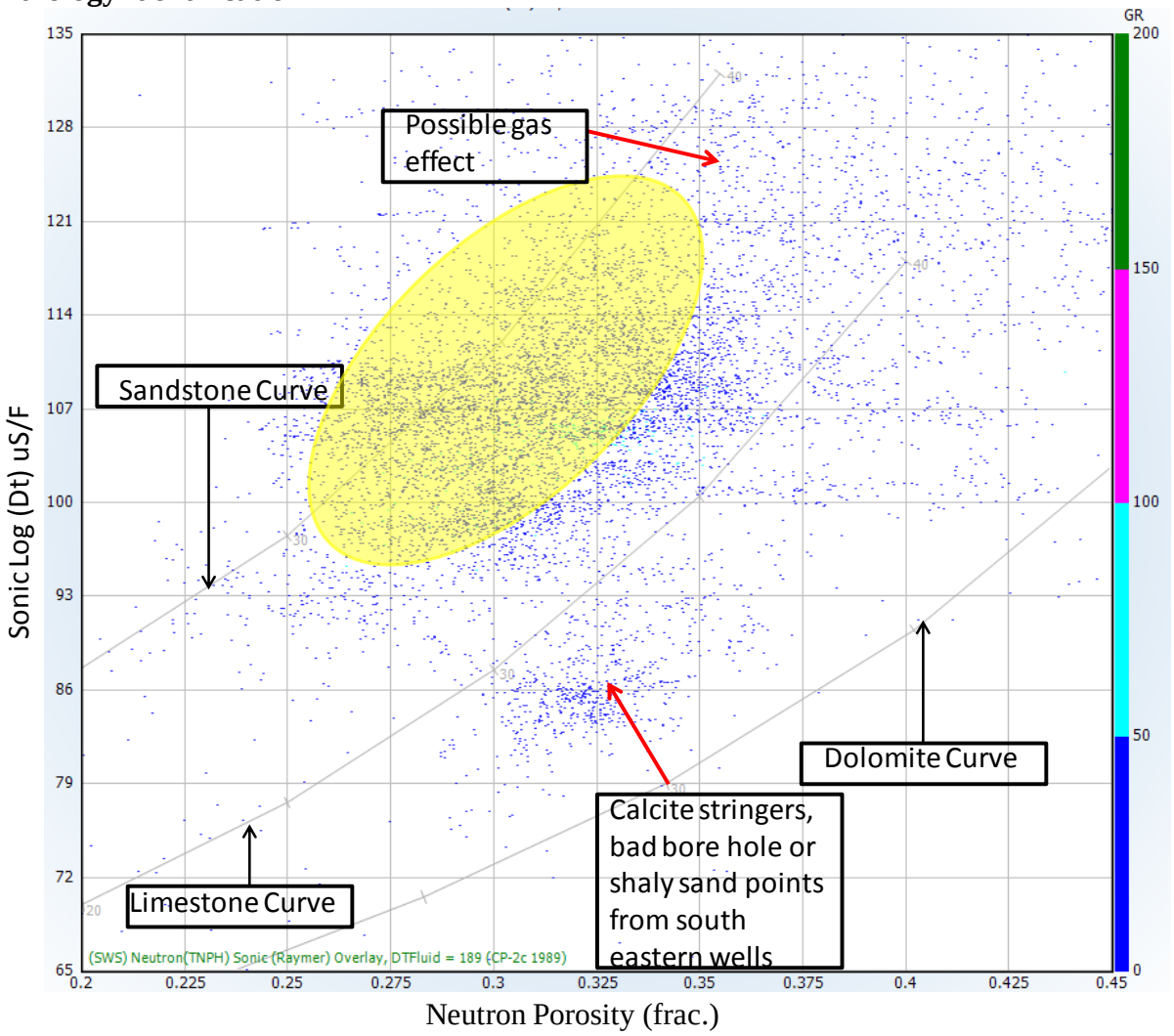

Log Plot of reservoir and cap rock formations

Well 25/10-1

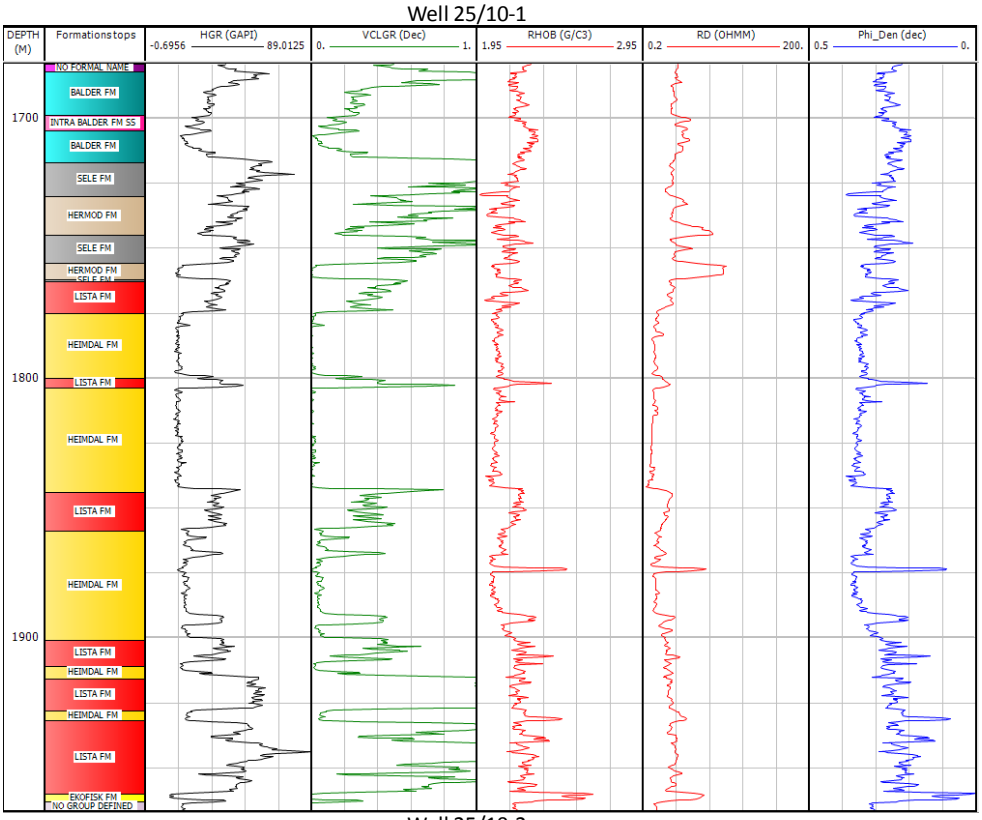

Well 25/10-2

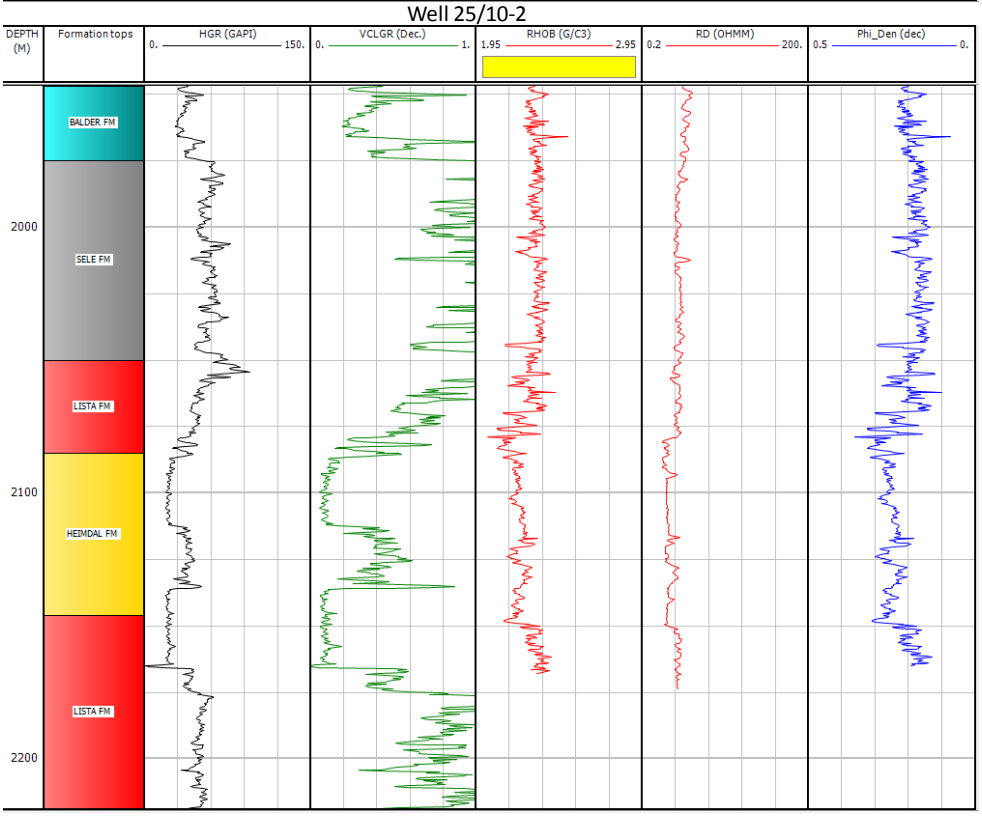

Well 25/10-3

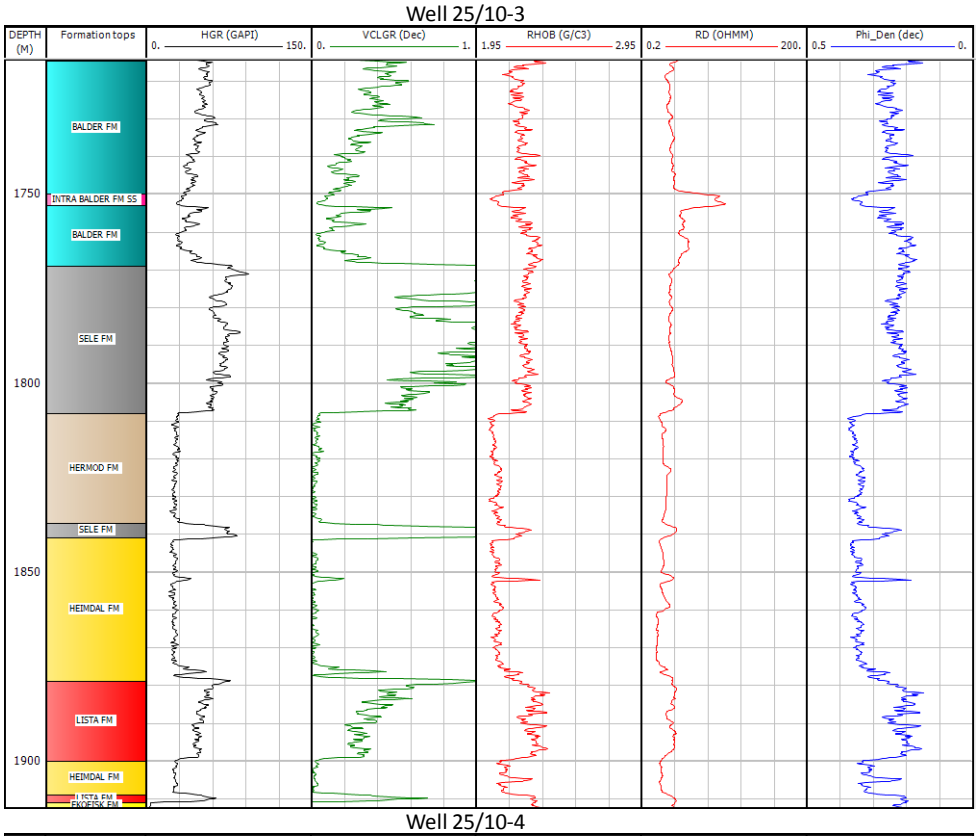

Well 25/10-4

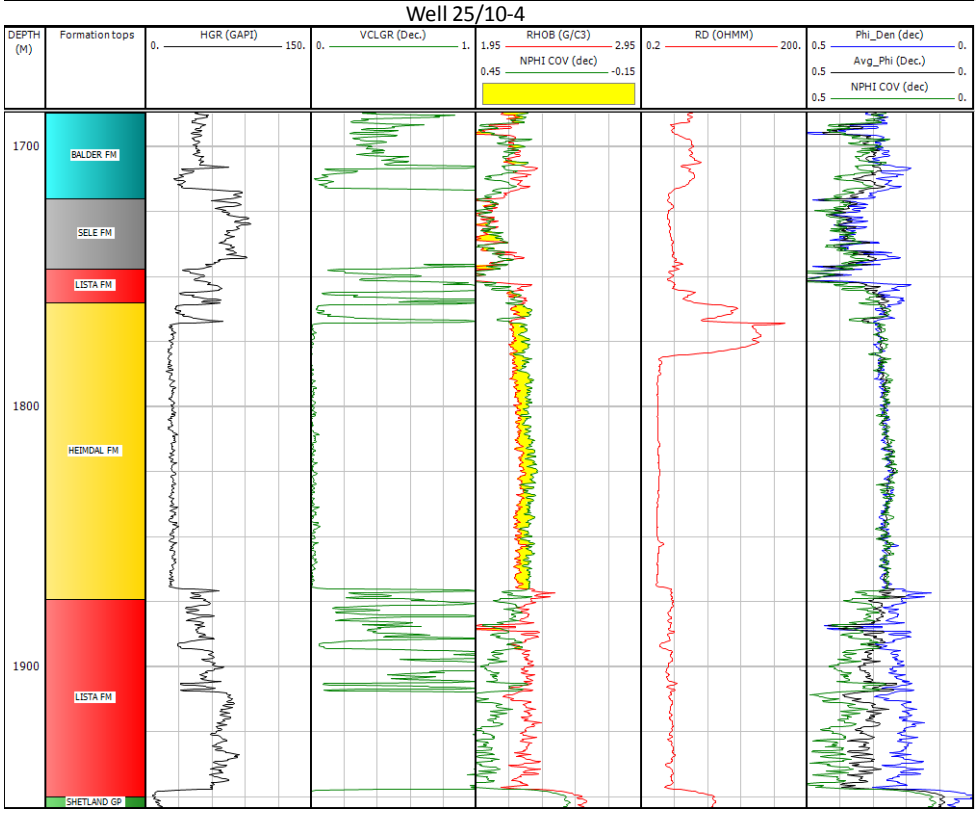

Well 25/10-5

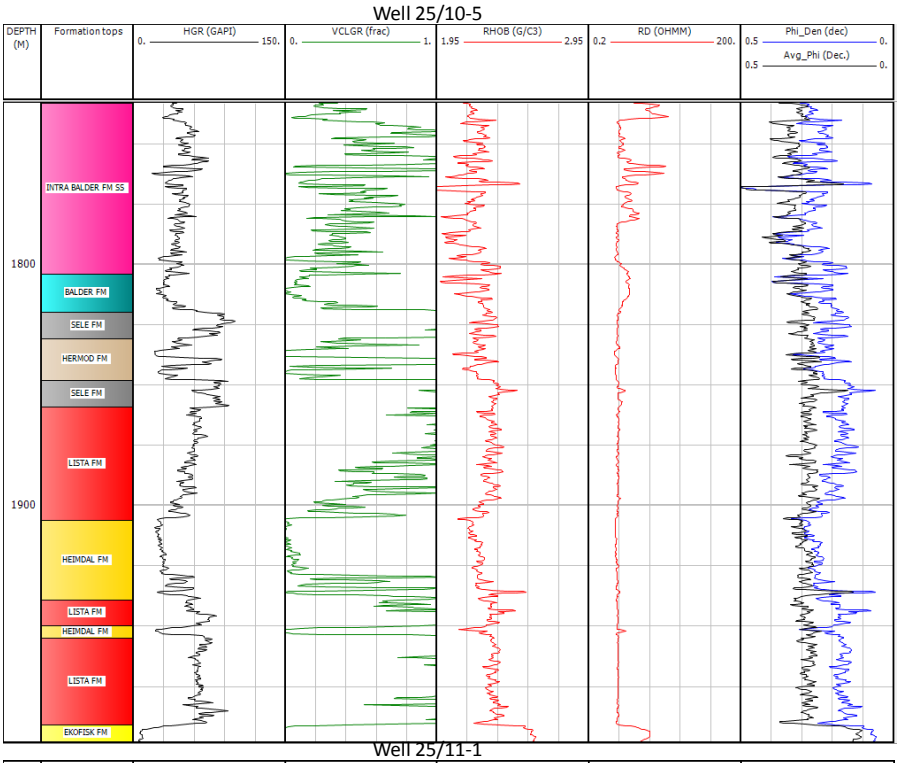

Well 25/11-1

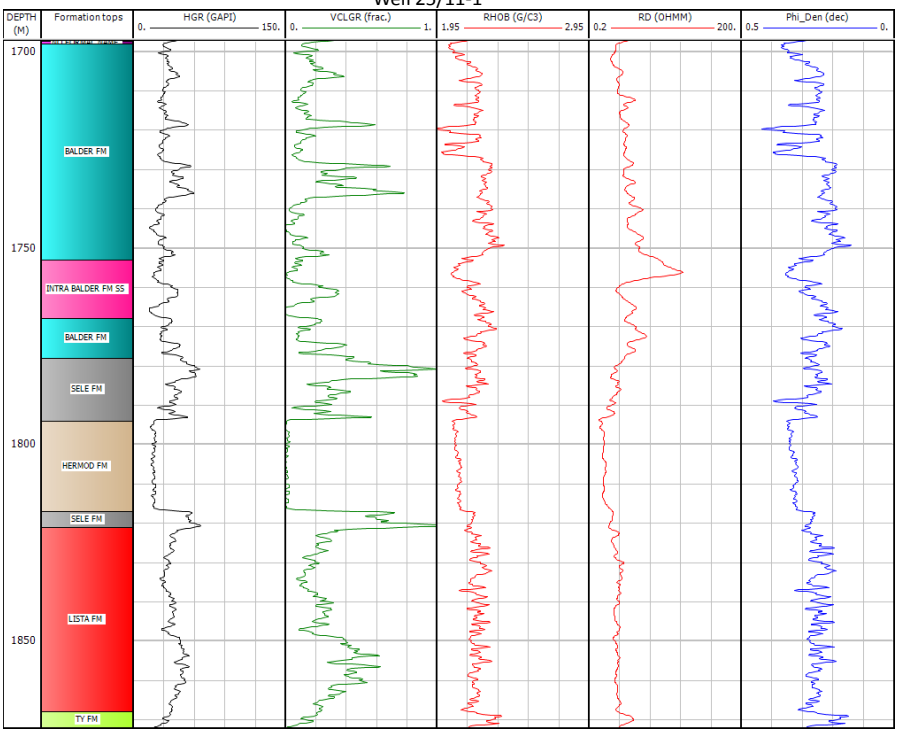

Well 25/11-2

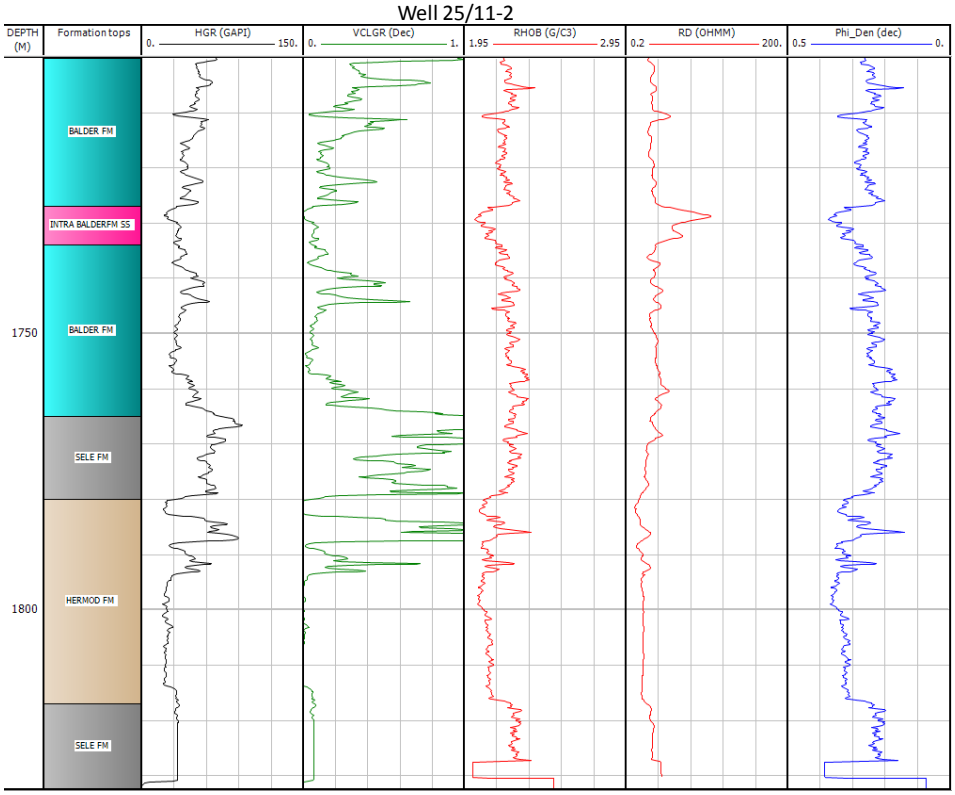

Well 25/11-4

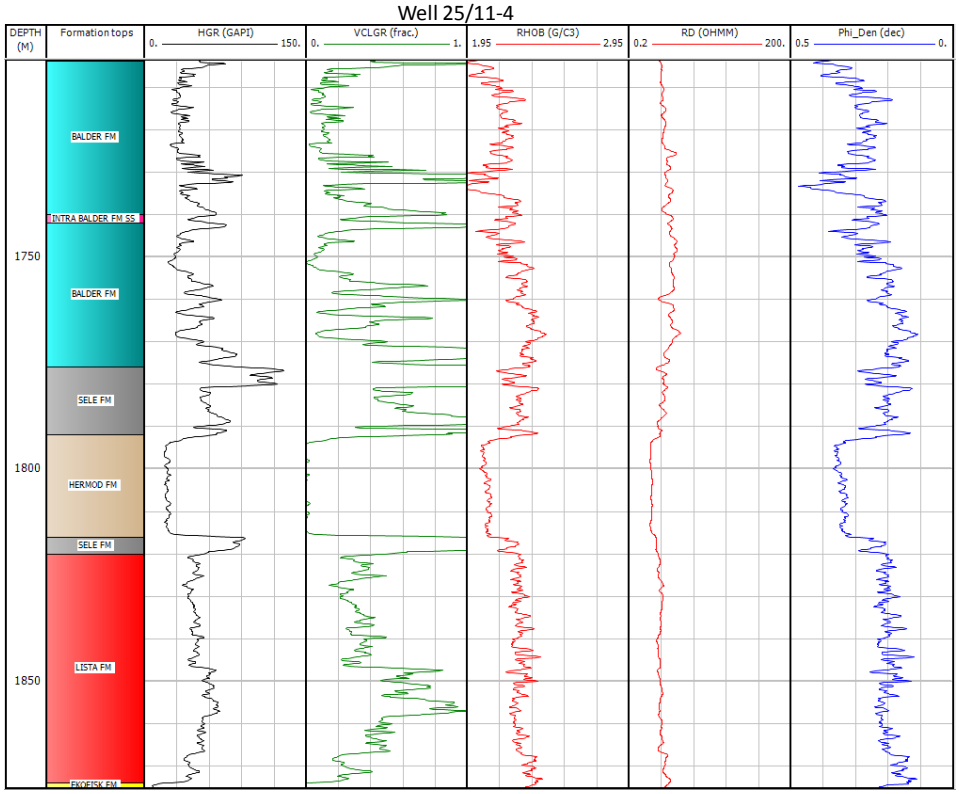

Well 25/11-5

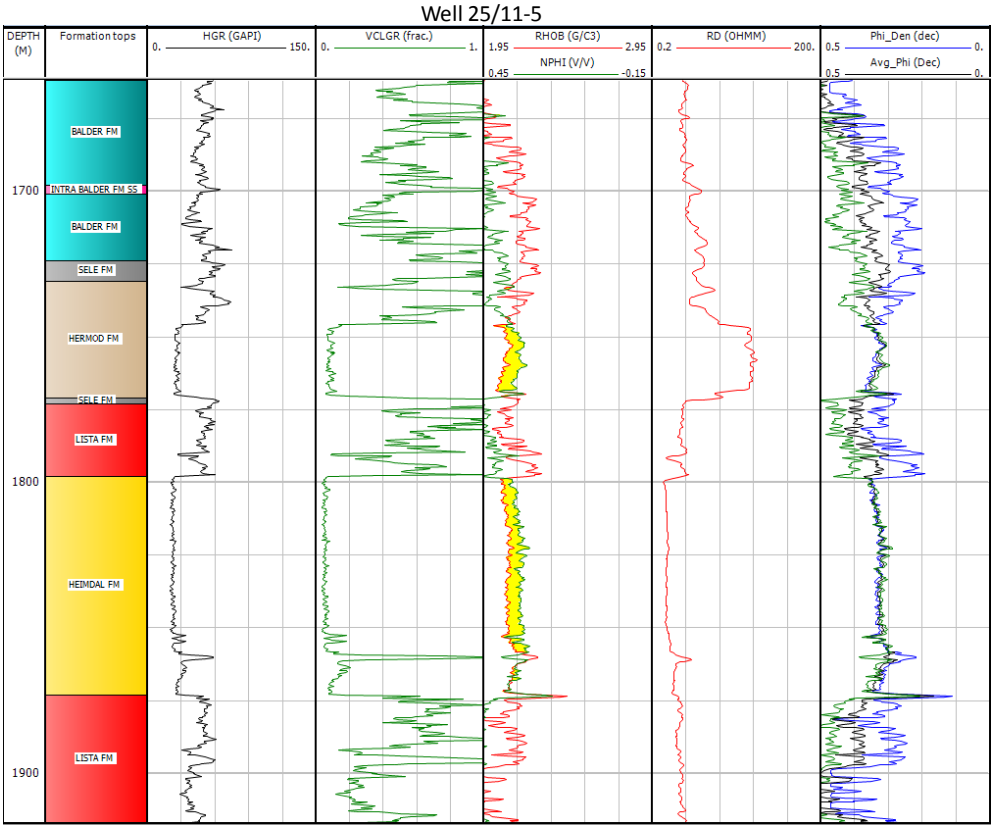

Well 25/11-6

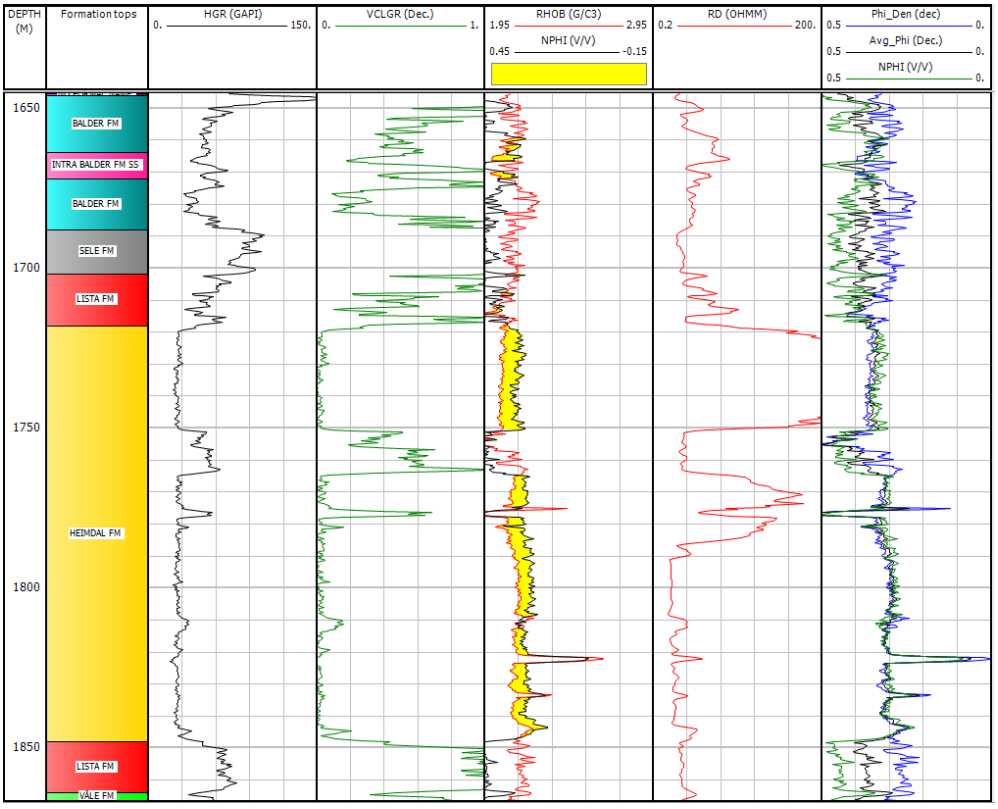

Well 25/11-7

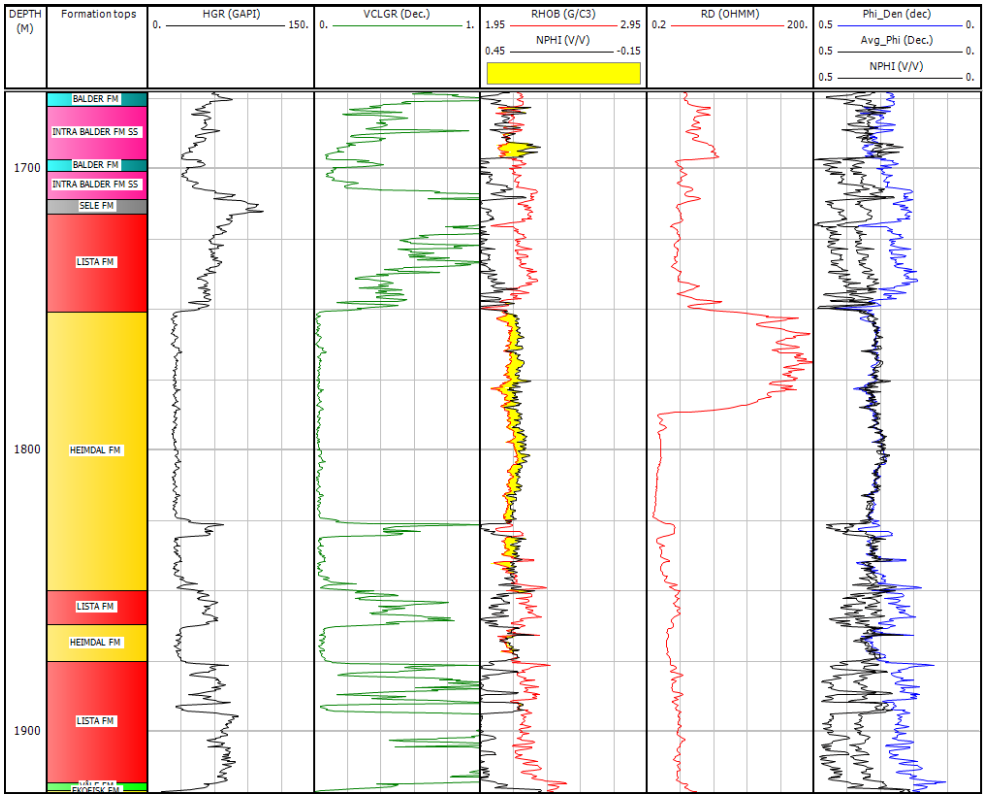

Well 25/11-8

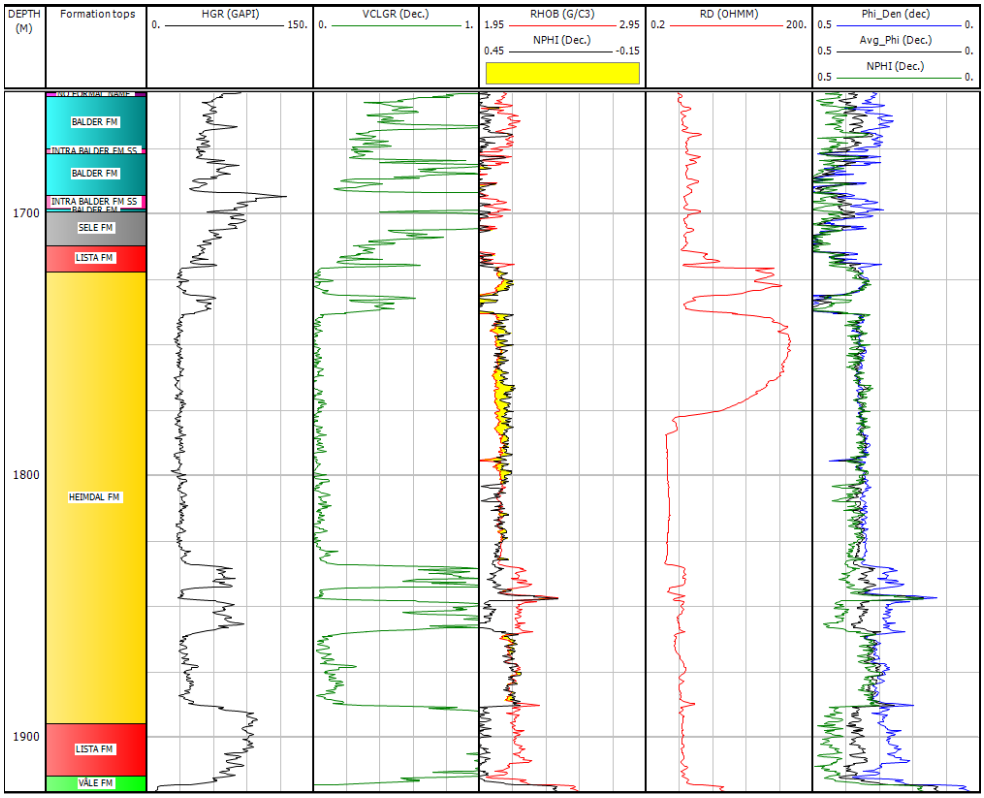

Well 25/11-9

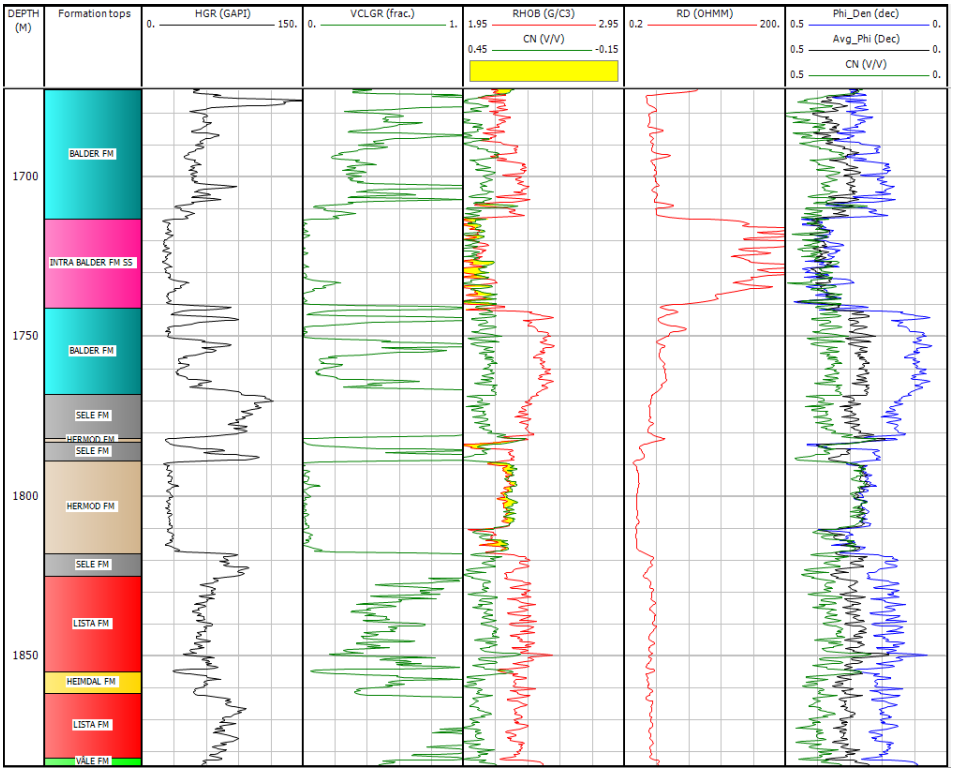

Well 25/11-10

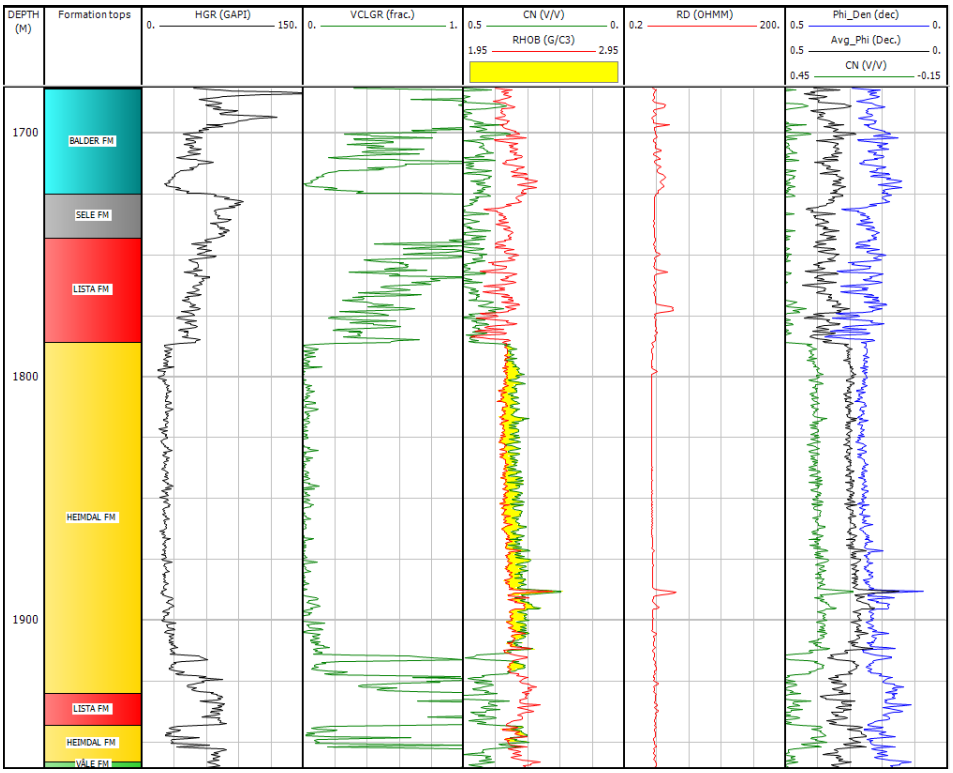

Well 25/11-11

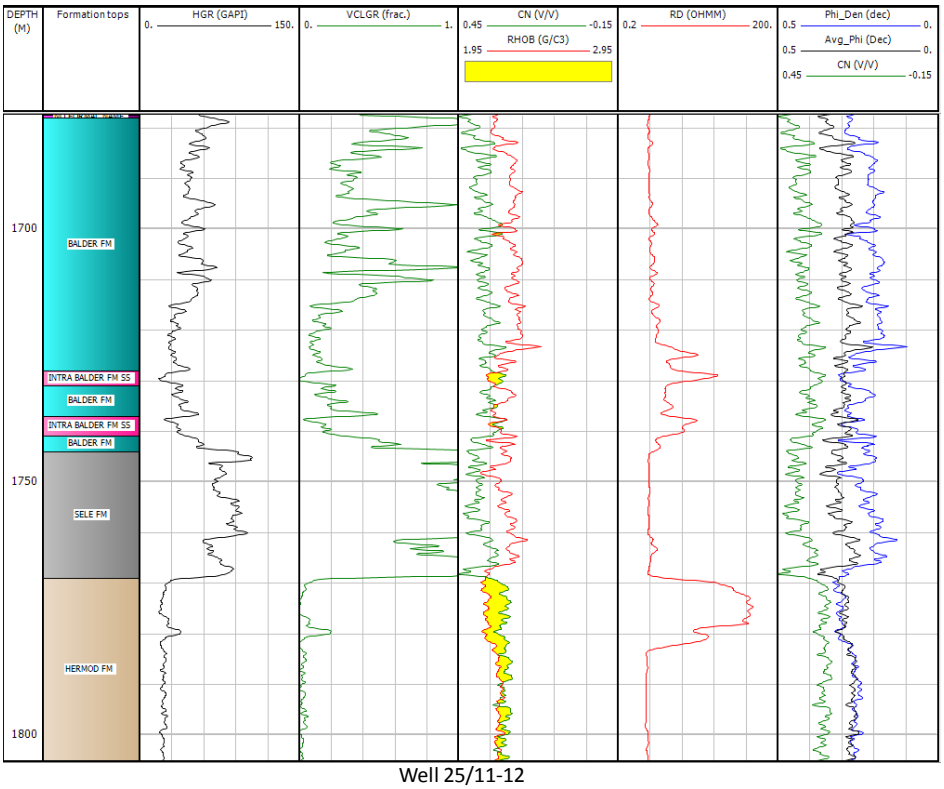

Well 25/11-12

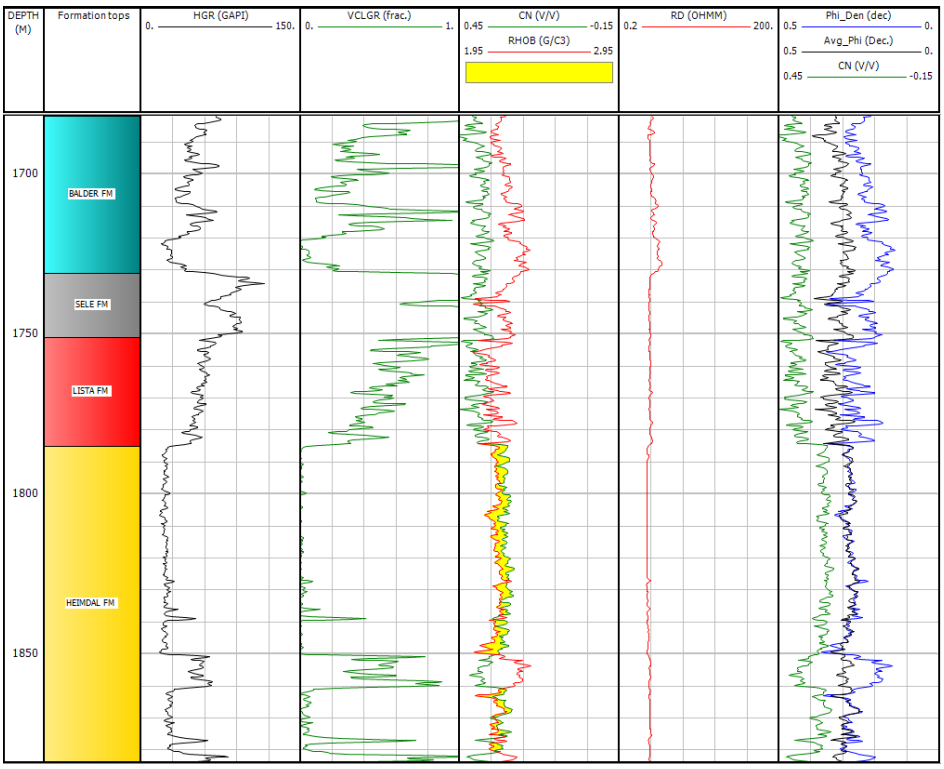

Well 25/11-13

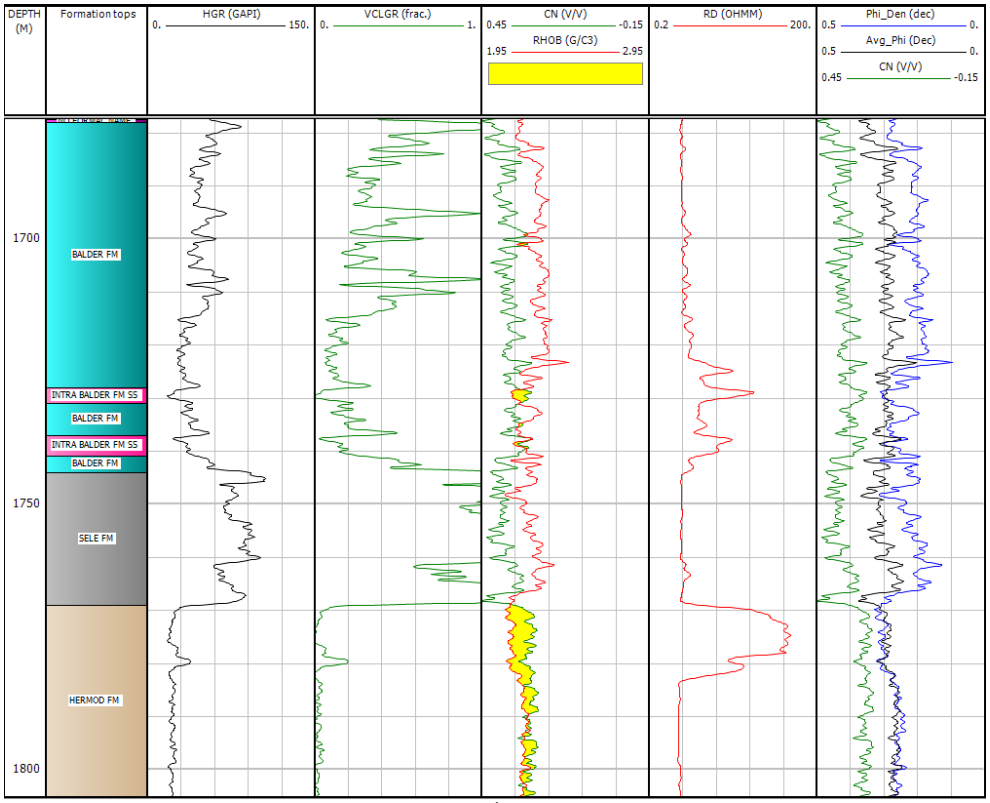

Well 25/11-15

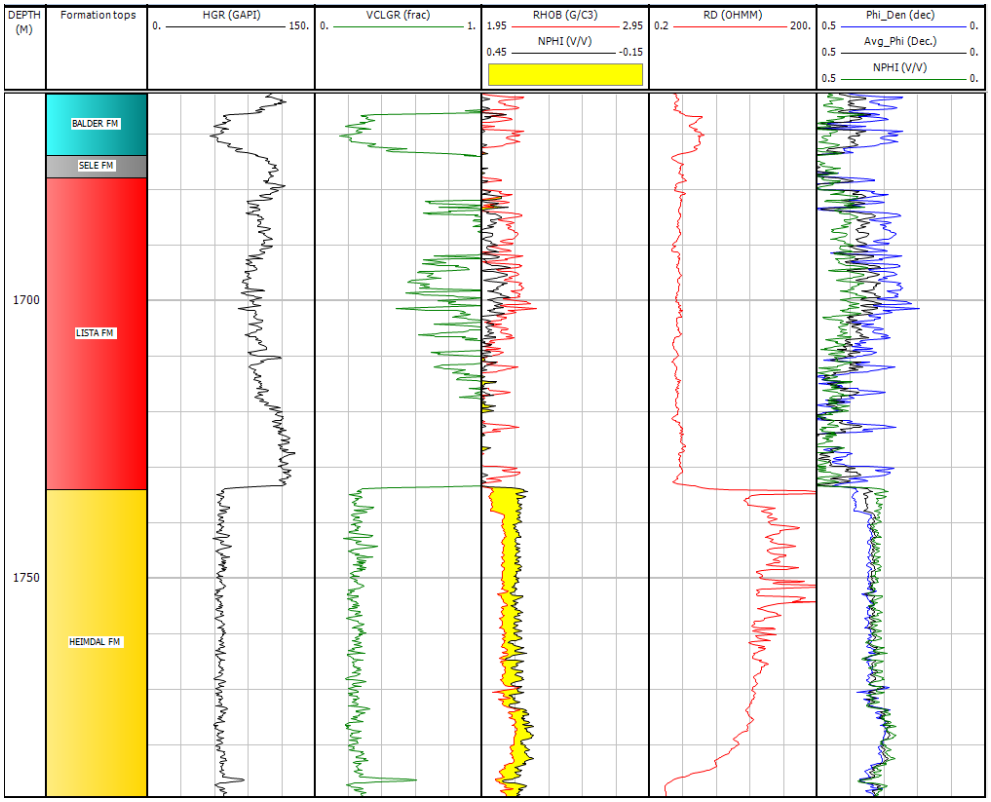

Well 25/11-16

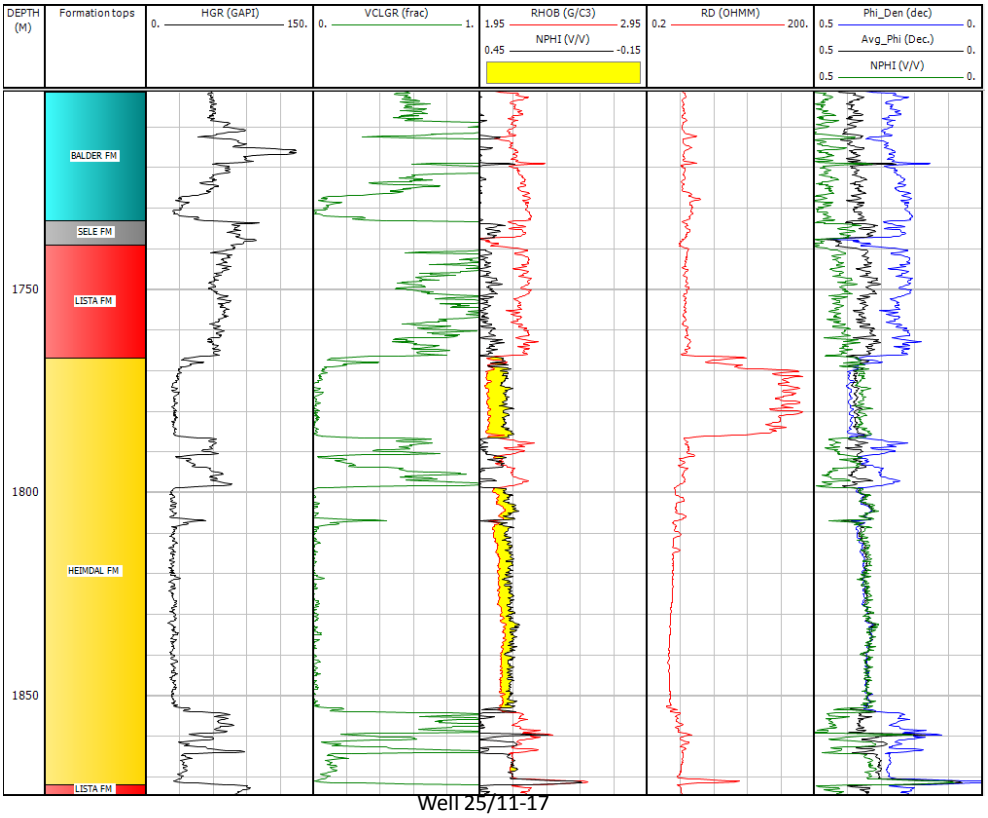

Well 25/11-17

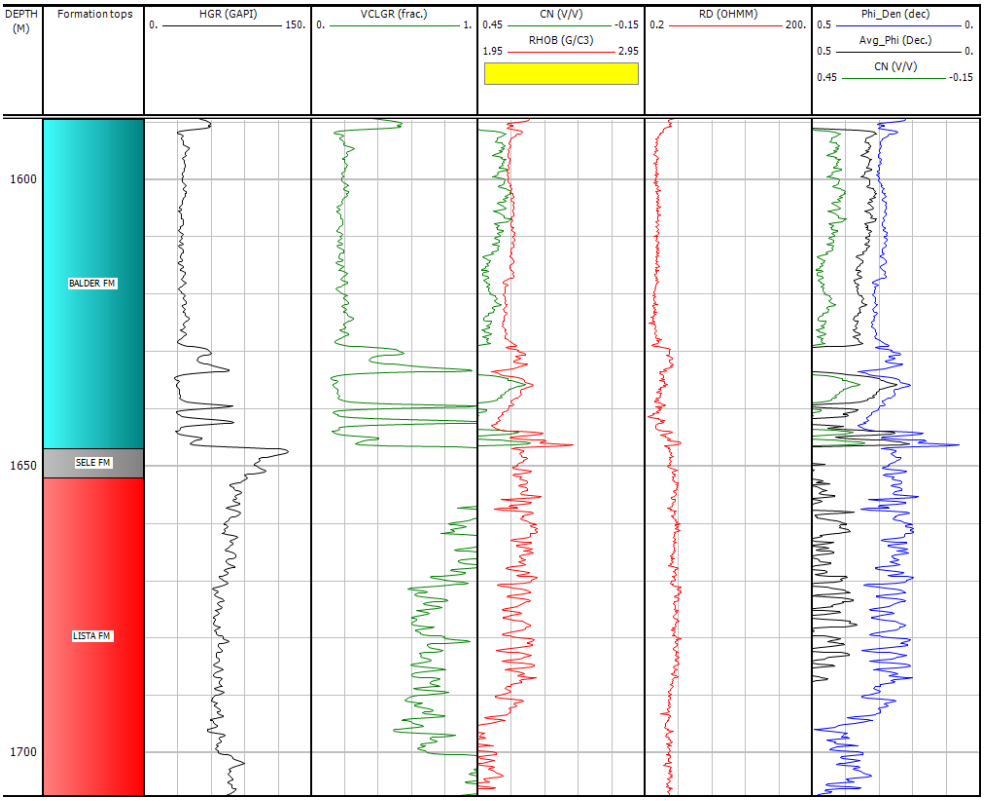

Well 25/11-18

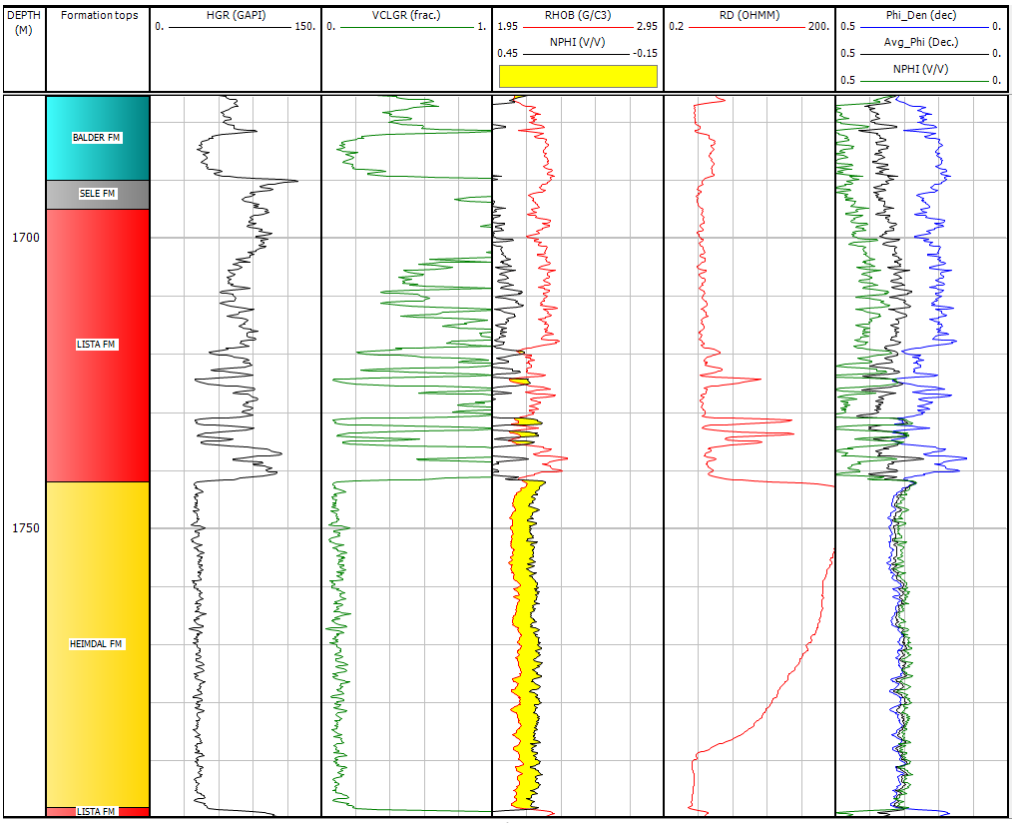

Well 25/11-20

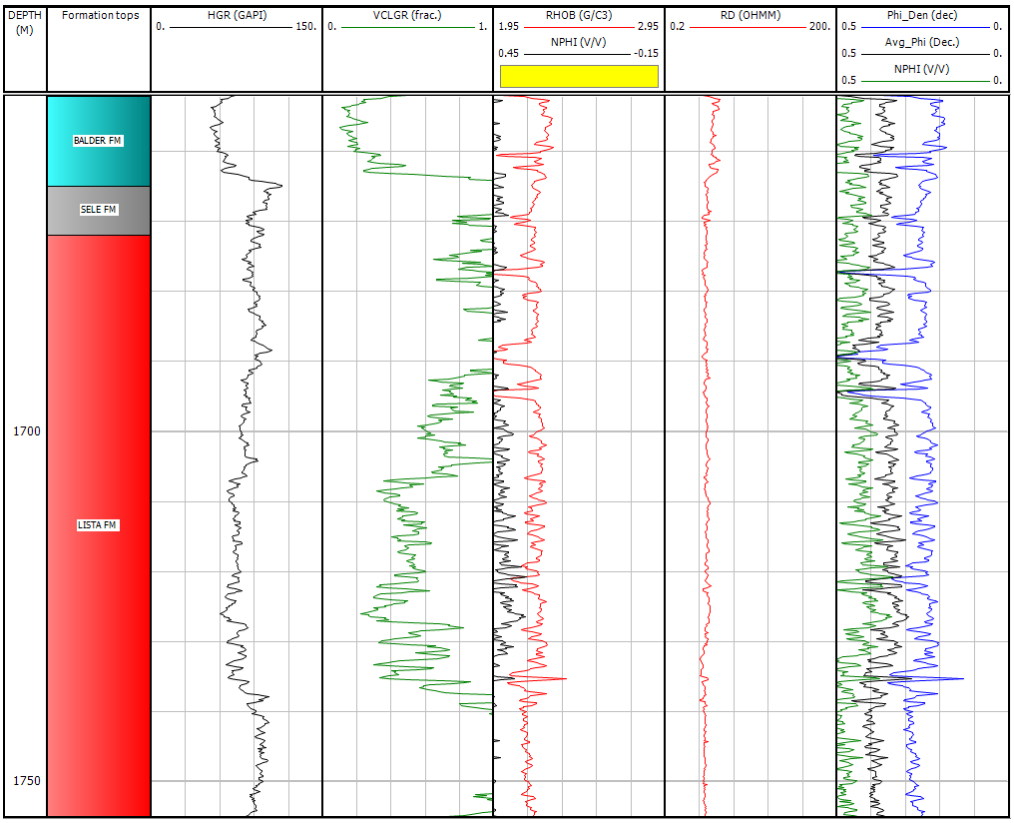

Reservoir Clay volume Histograms

Balder Formation

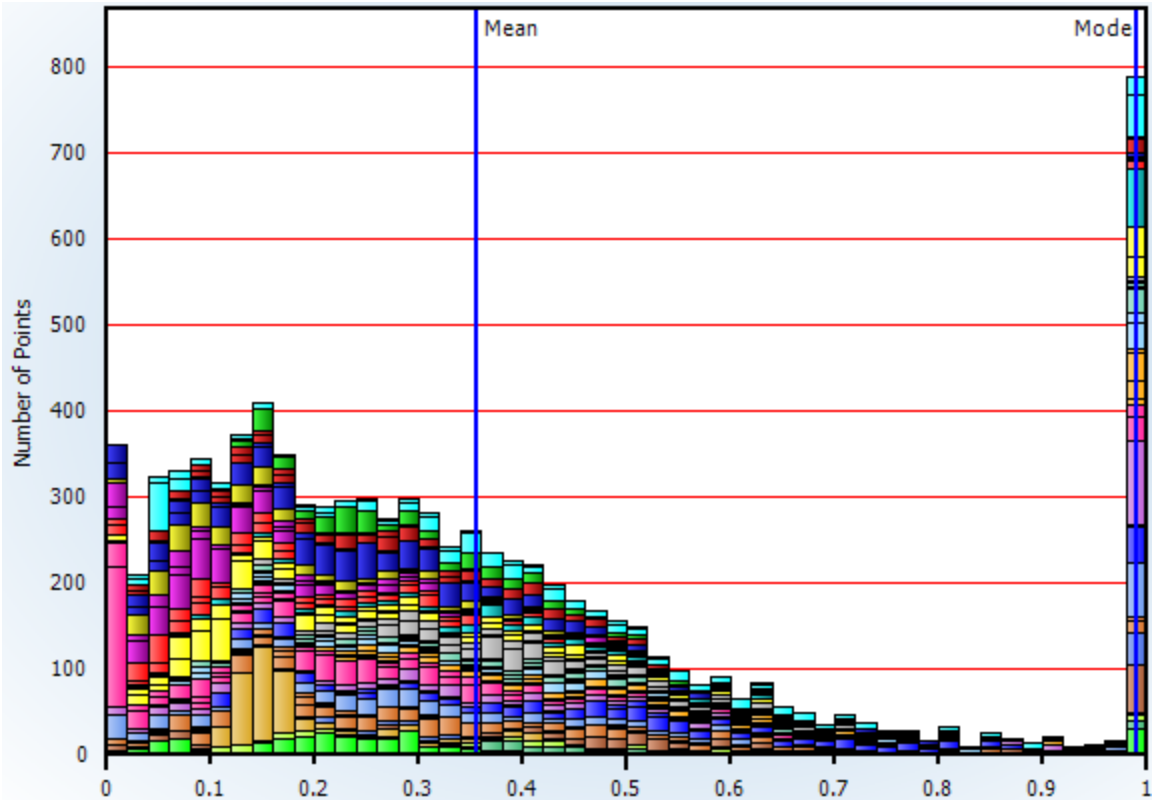

Hermod Fomration

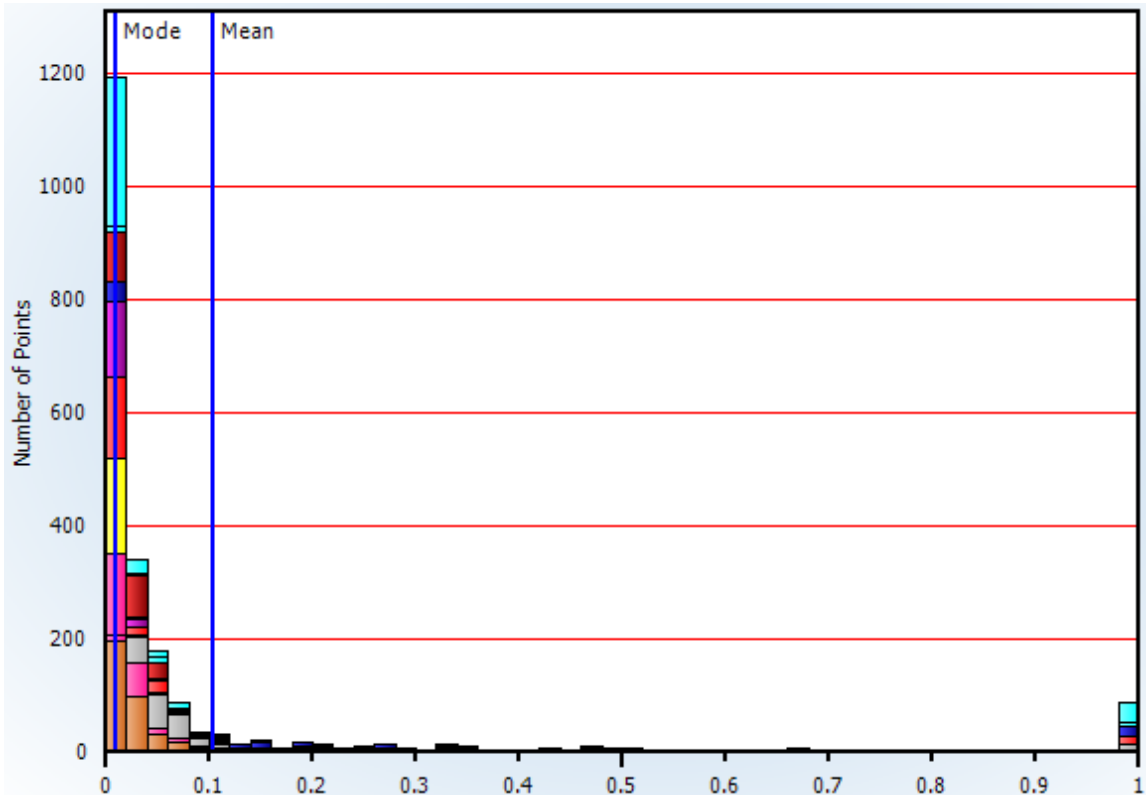

Heimdal Formation

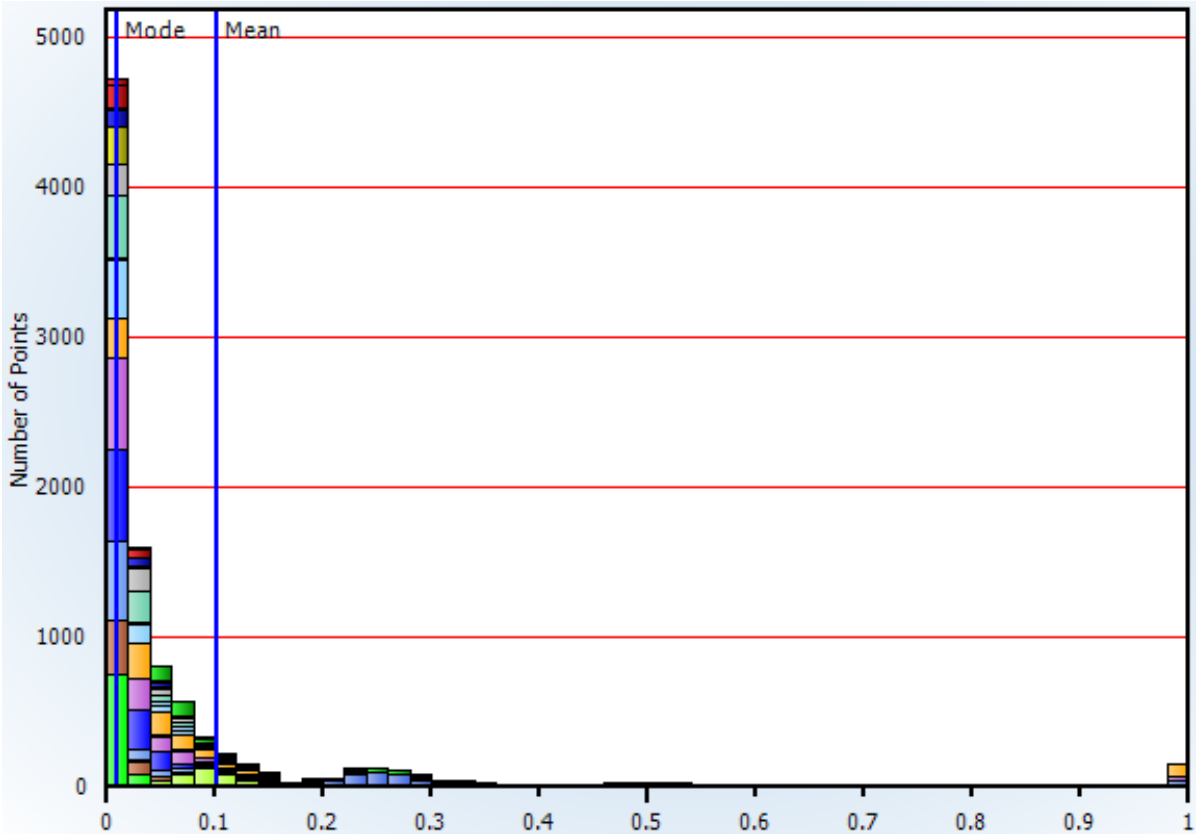

Reservoir Porosity Histograms

Balder Formation¨

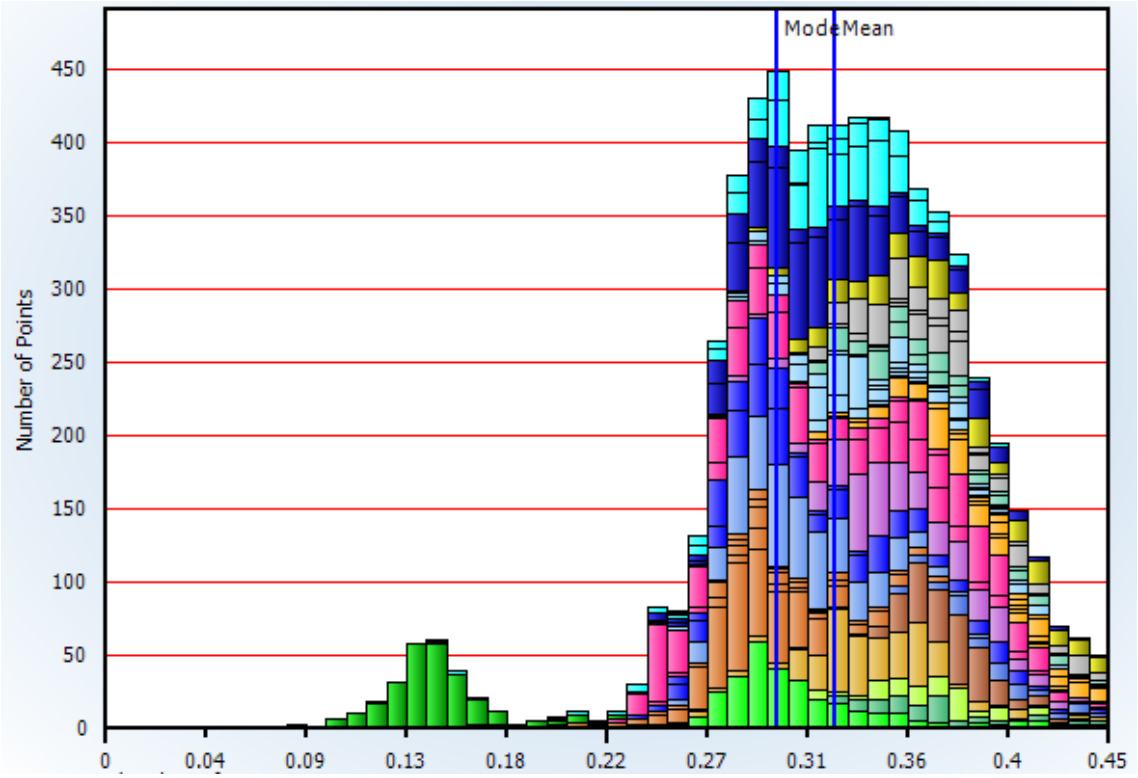

Hermod Formation

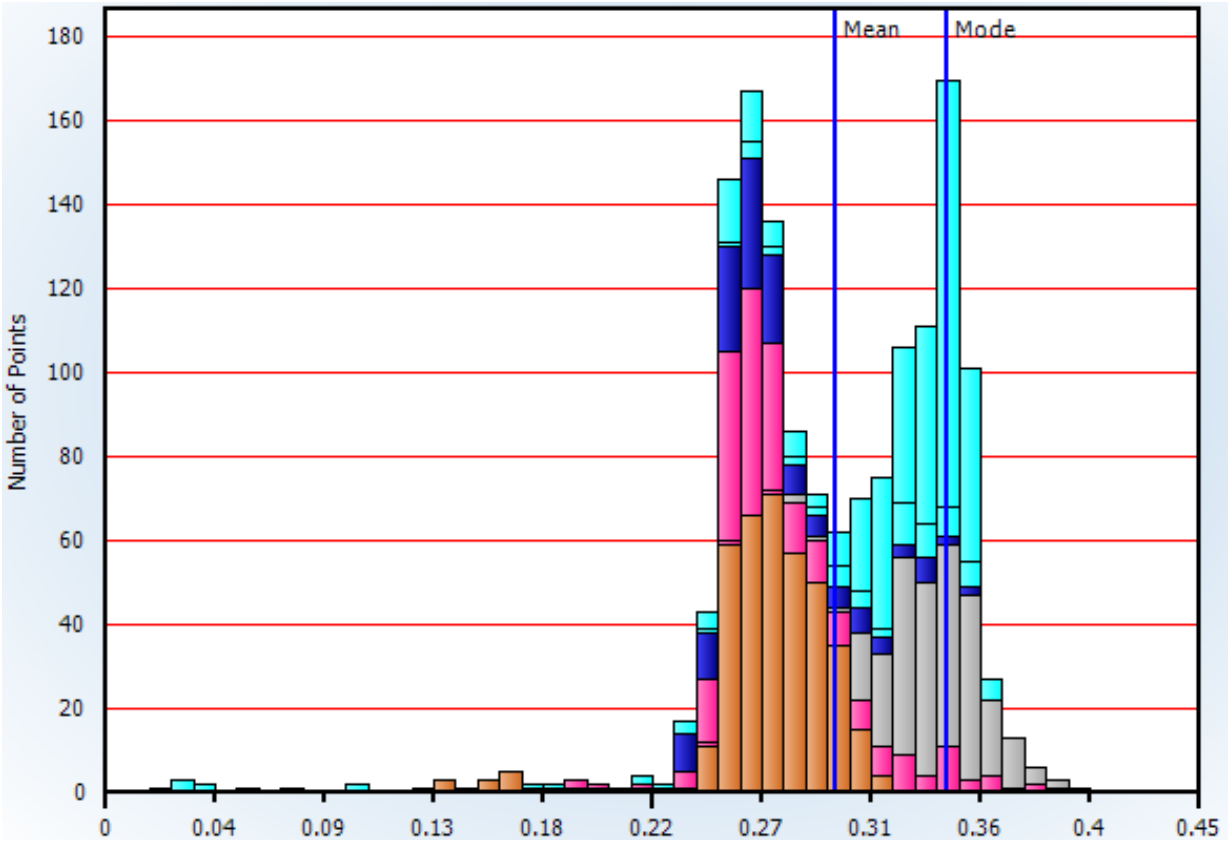

Heimdal Formation

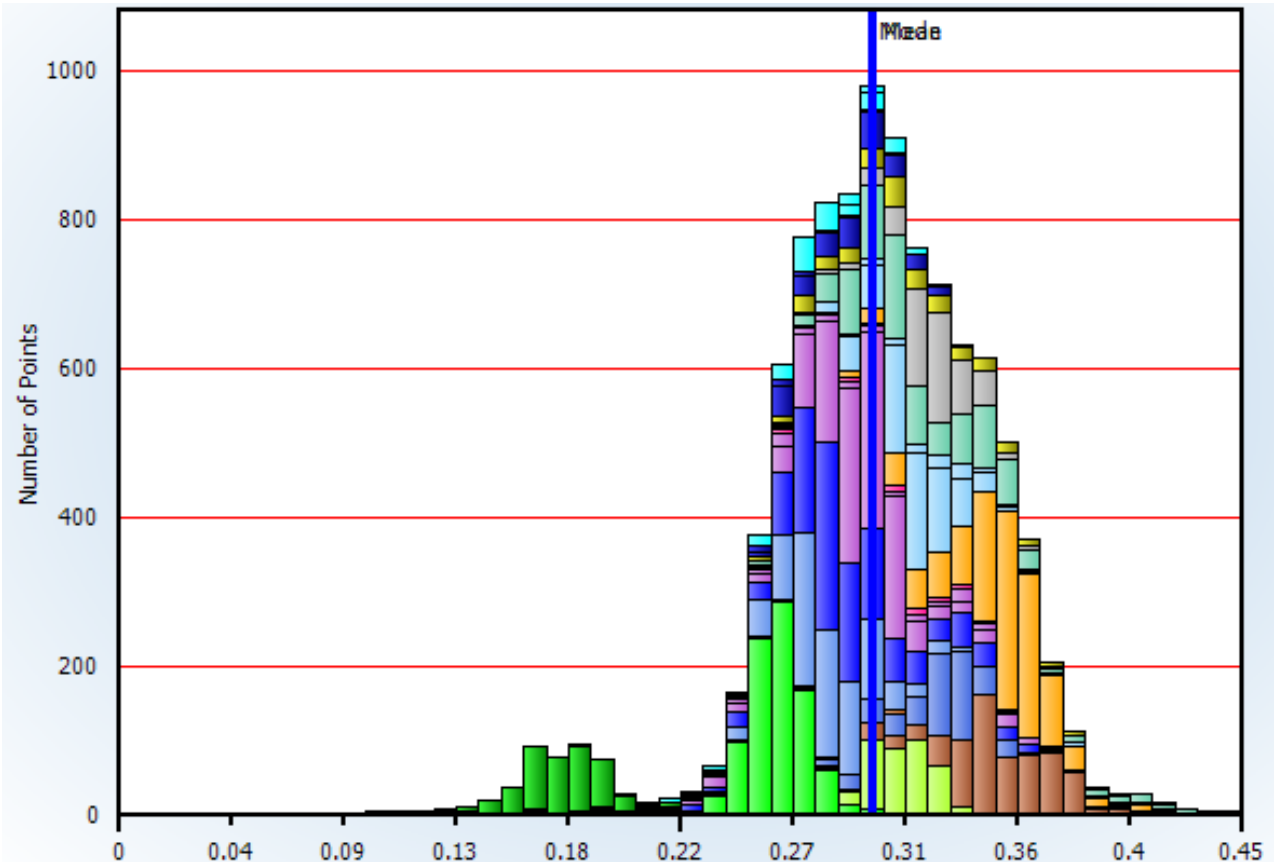

Source rock porosity Histogram

Draupne Formation

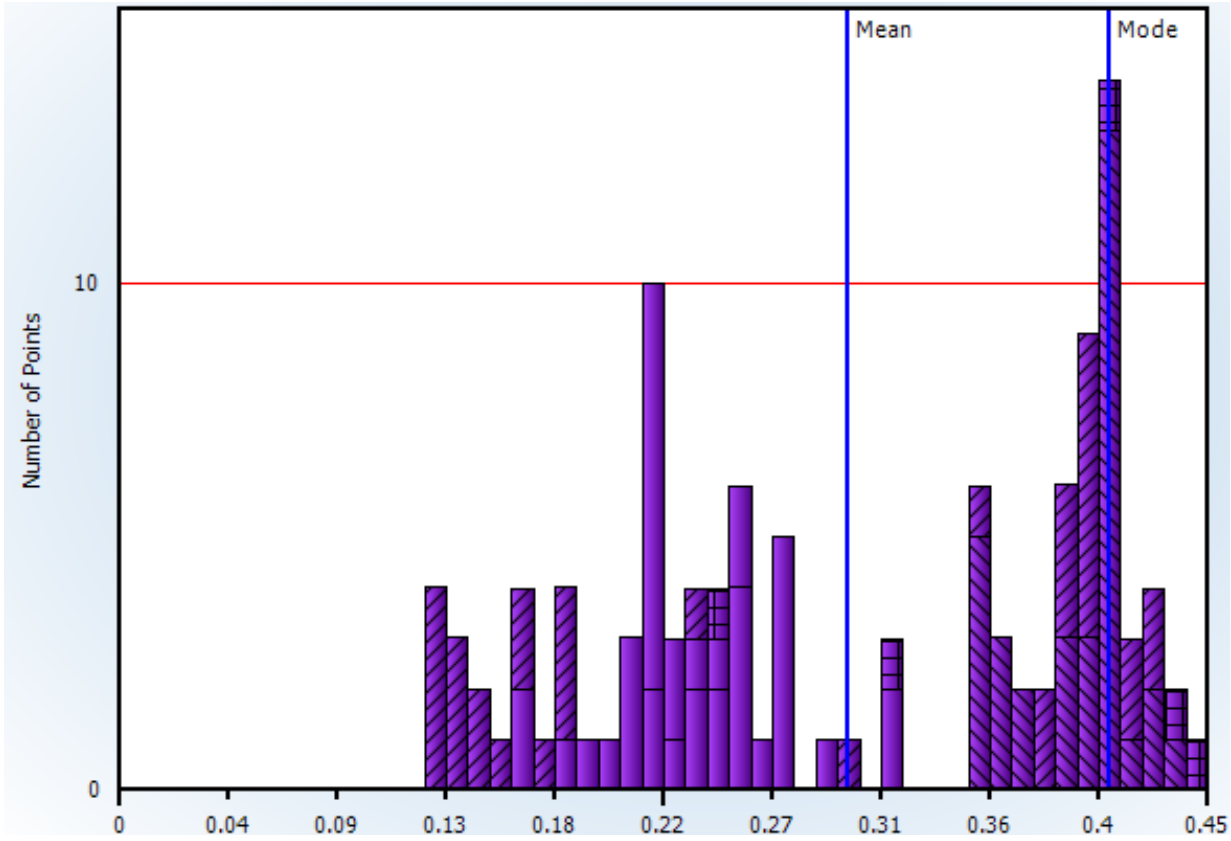

Heather Formation

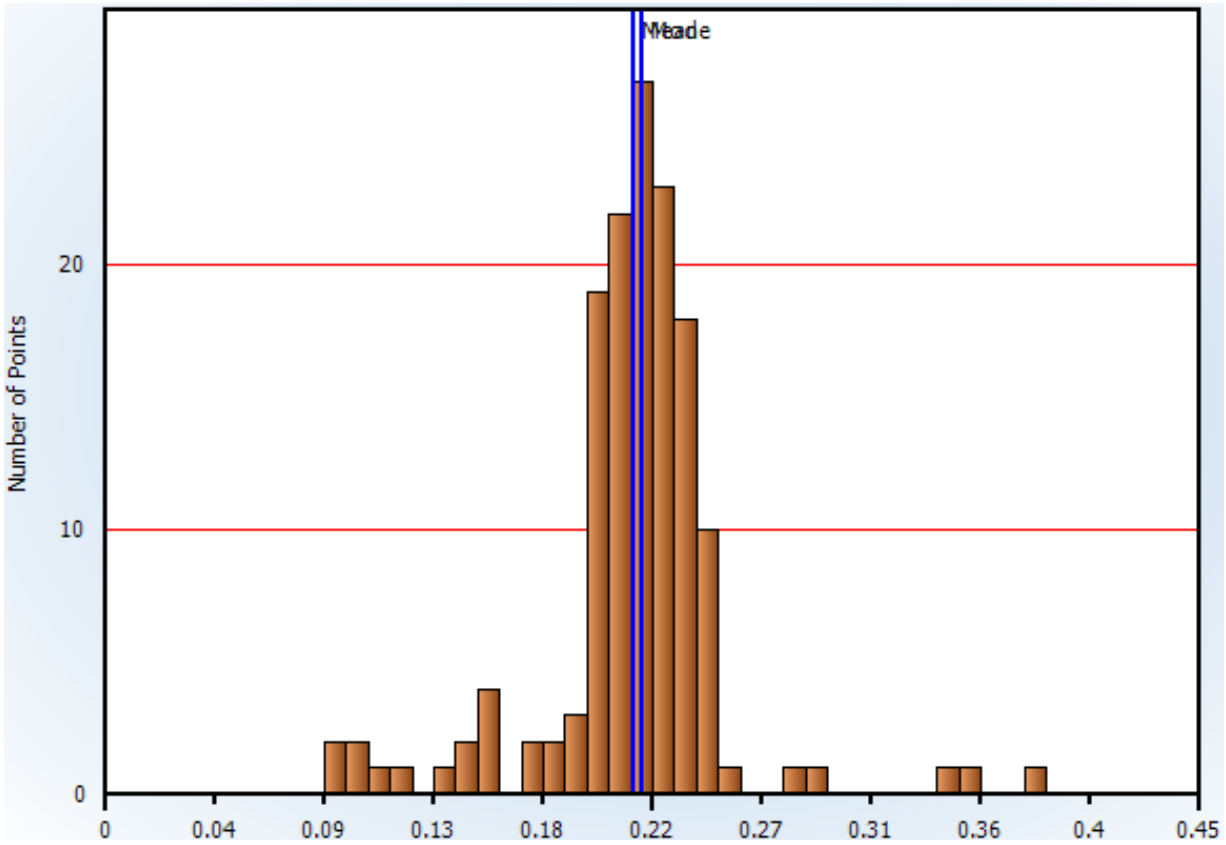

Source rock clay volume Histogram

Draupne Formation

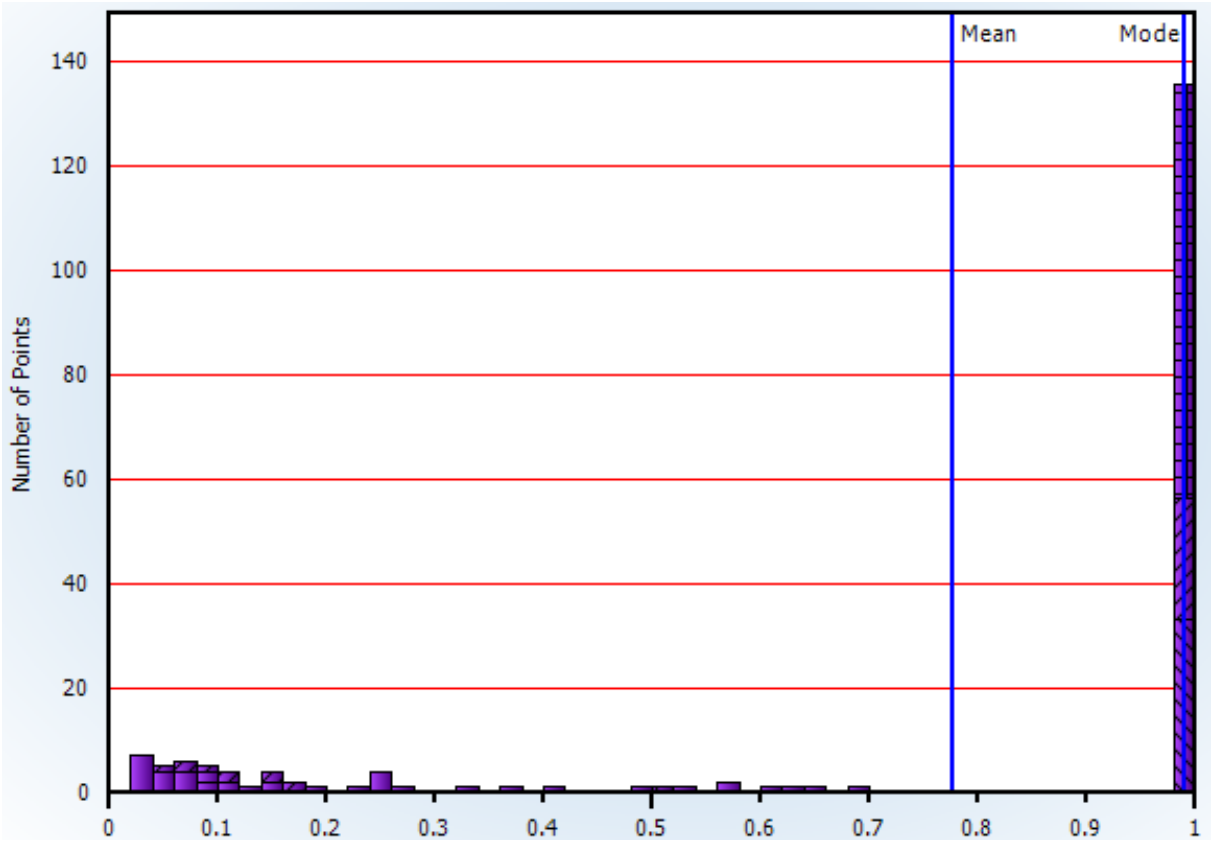

Heather Formation

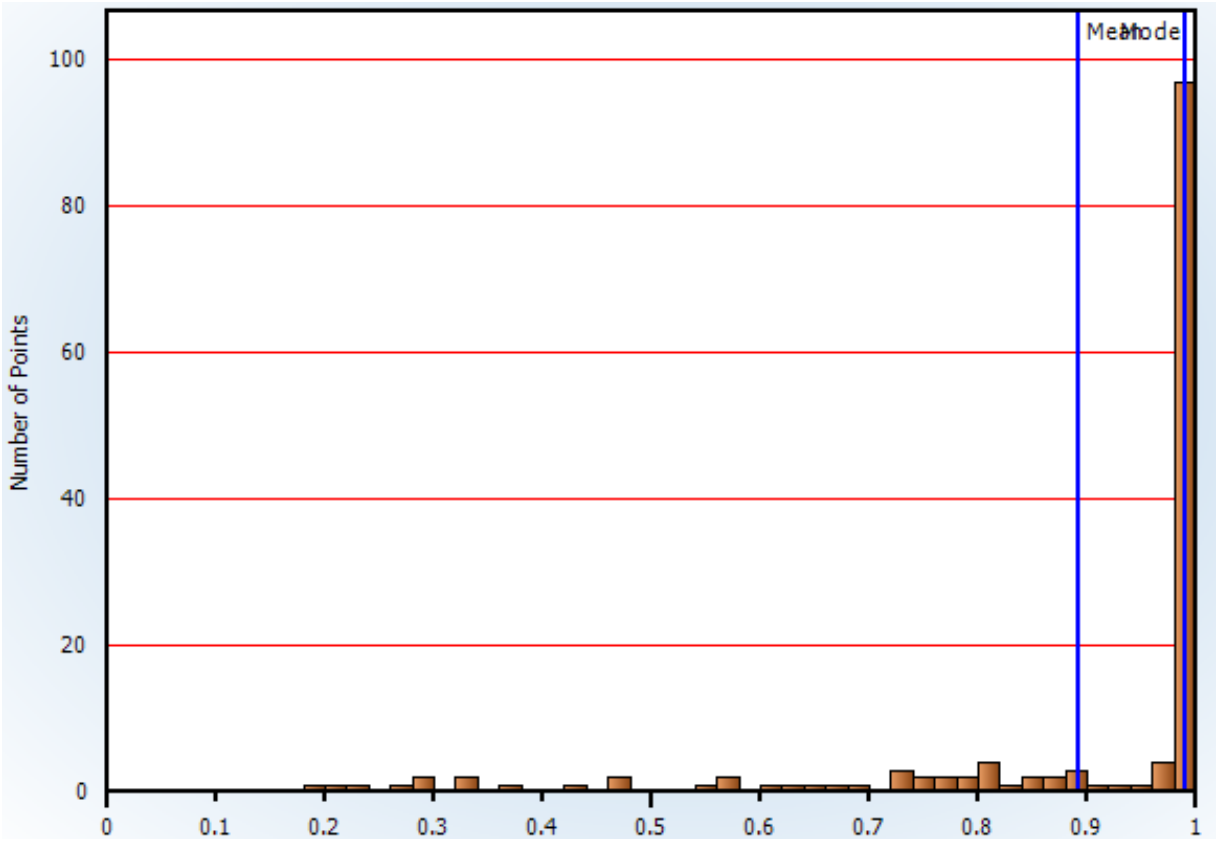

Appendix II (Compaction Analysis)

Transition zone analysis

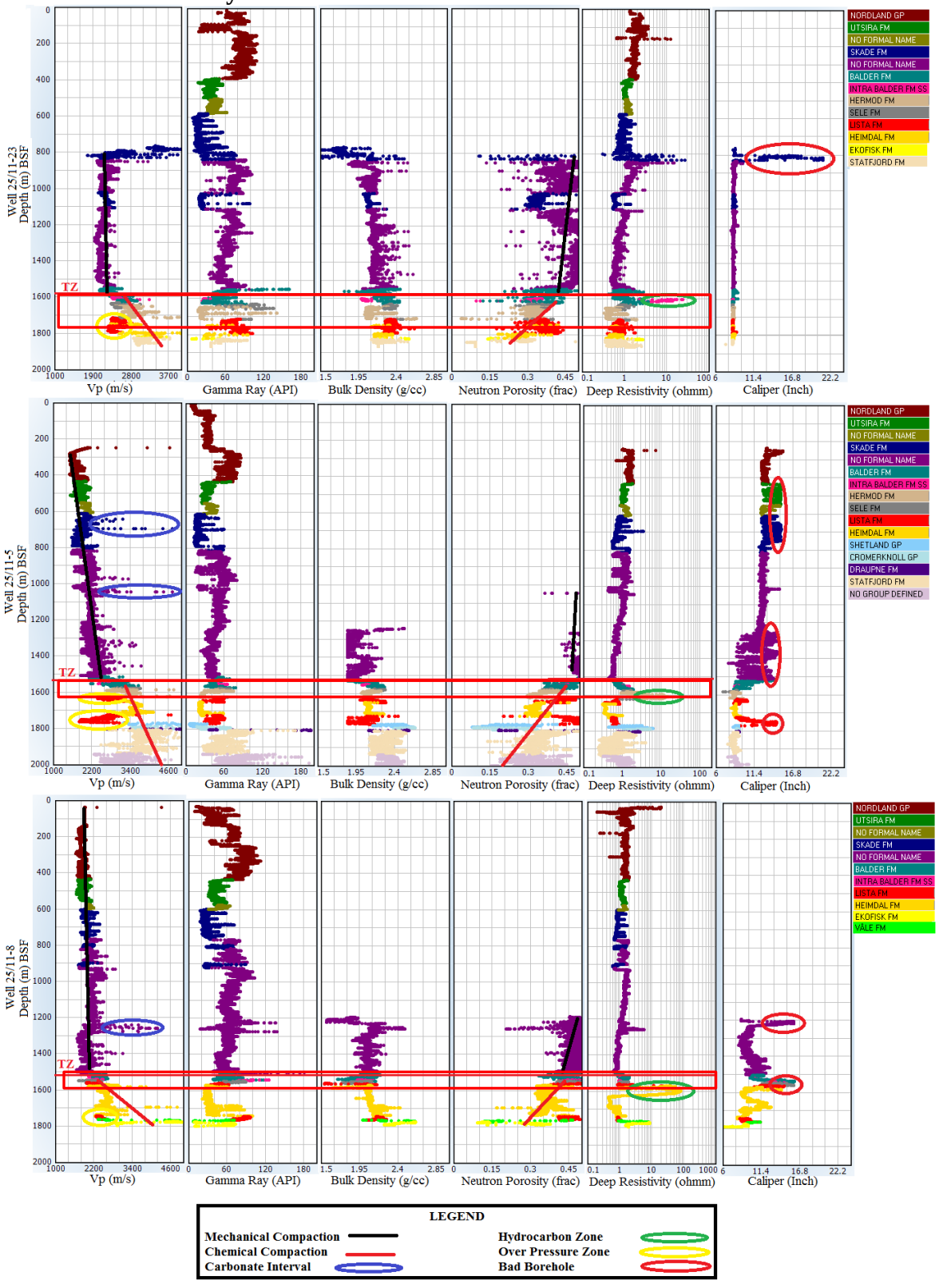

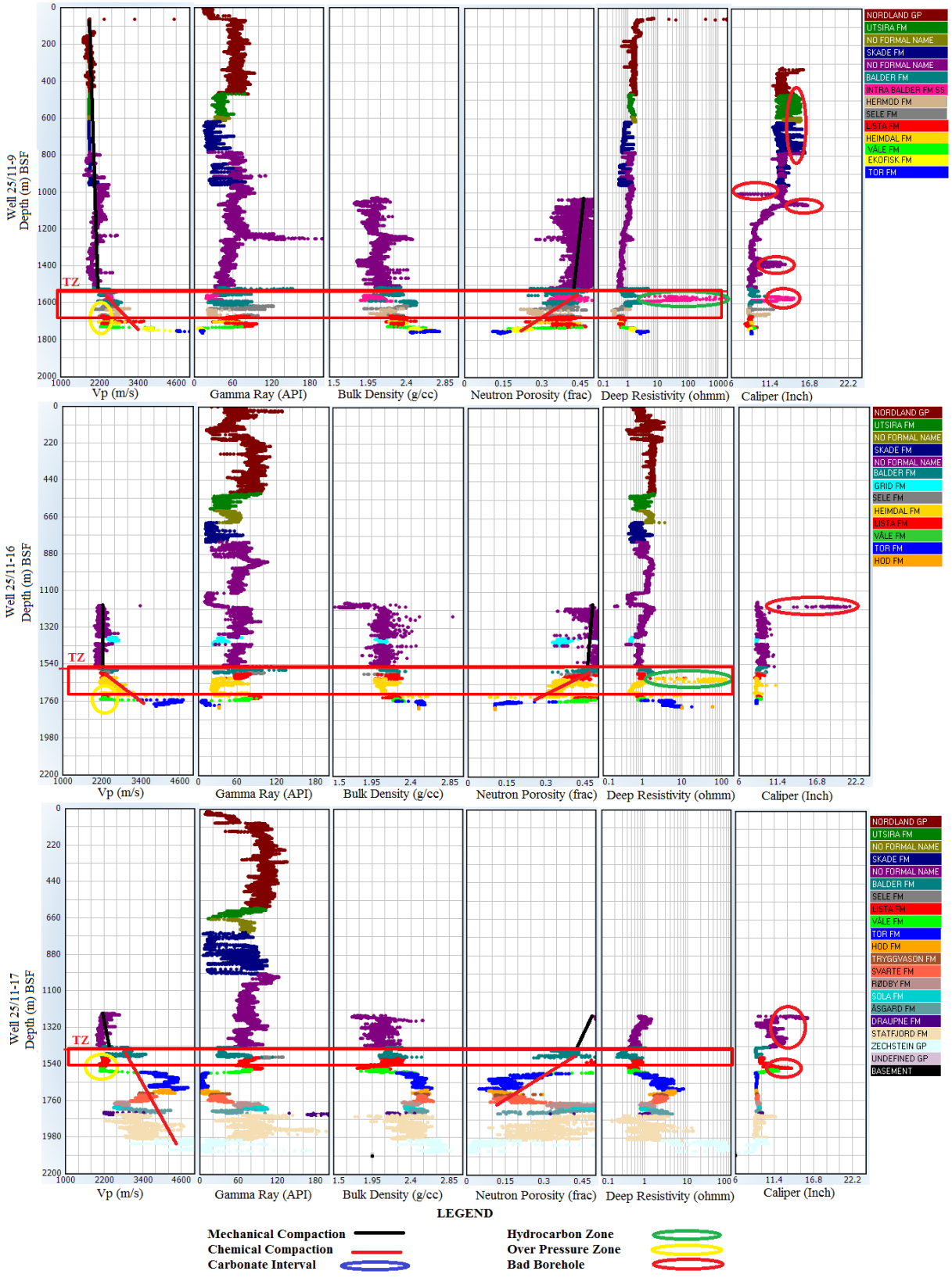
Well 25/11-9
Depth (m) BSF
TZ
Vp (m/s)
Gamma Ray (API)
Bulk Density (g/cc)
Neutron Porosity (frac)
Deep Resistivity (ohmm)
Caliper (Inch)
NORDLAND GP
UTSIRA FM
NO FORMAL NAME
SKADE FM
NO FORMAL NAME
BALDER FM
INTRA BALDER FM SS
HERMOD FM
SELE FM
LISTA FM
HEIMDAL FM
VÅLE FM
EKOFISK FM
TOR FM
Well 25/11-16
Depth (m) BSF
TZ
Vp (m/s)
Gamma Ray (API)
Bulk Density (g/cc)
Neutron Porosity (frac)
Deep Resistivity (ohmm)
Caliper (Inch)
NORDLAND GP
UTSIRA FM
NO FORMAL NAME
SKADE FM
NO FORMAL NAME
BALDER FM
GRID FM
SELE FM
HEIMDAL FM
LISTA FM
VÅLE FM
TOR FM
HOD FM
Well 25/11-17
Depth (m) BSF
TZ
Vp (m/s)
Gamma Ray (API)
Bulk Density (g/cc)
Neutron Porosity (frac)
Deep Resistivity (ohmm)
Caliper (Inch)
NORDLAND GP
UTSIRA FM
NO FORMAL NAME
SKADE FM
NO FORMAL NAME
BALDER FM
SELE FM
LISTA FM
VÅLE FM
TOR FM
HOD FM
TRYGGVASON FM
SVARTE FM
RØDBY FM
SOLA FM
ÅSGARD FM
DRAUPNE FM
STATFJORD FM
ZECHSTEIN GP
UNDEFINED GP
BASEMENT
LEGEND
Mechanical Compaction
Chemical Compaction
Carbonate Interval
Hydrocarbon Zone
Over Pressure Zone
Bad Borehole

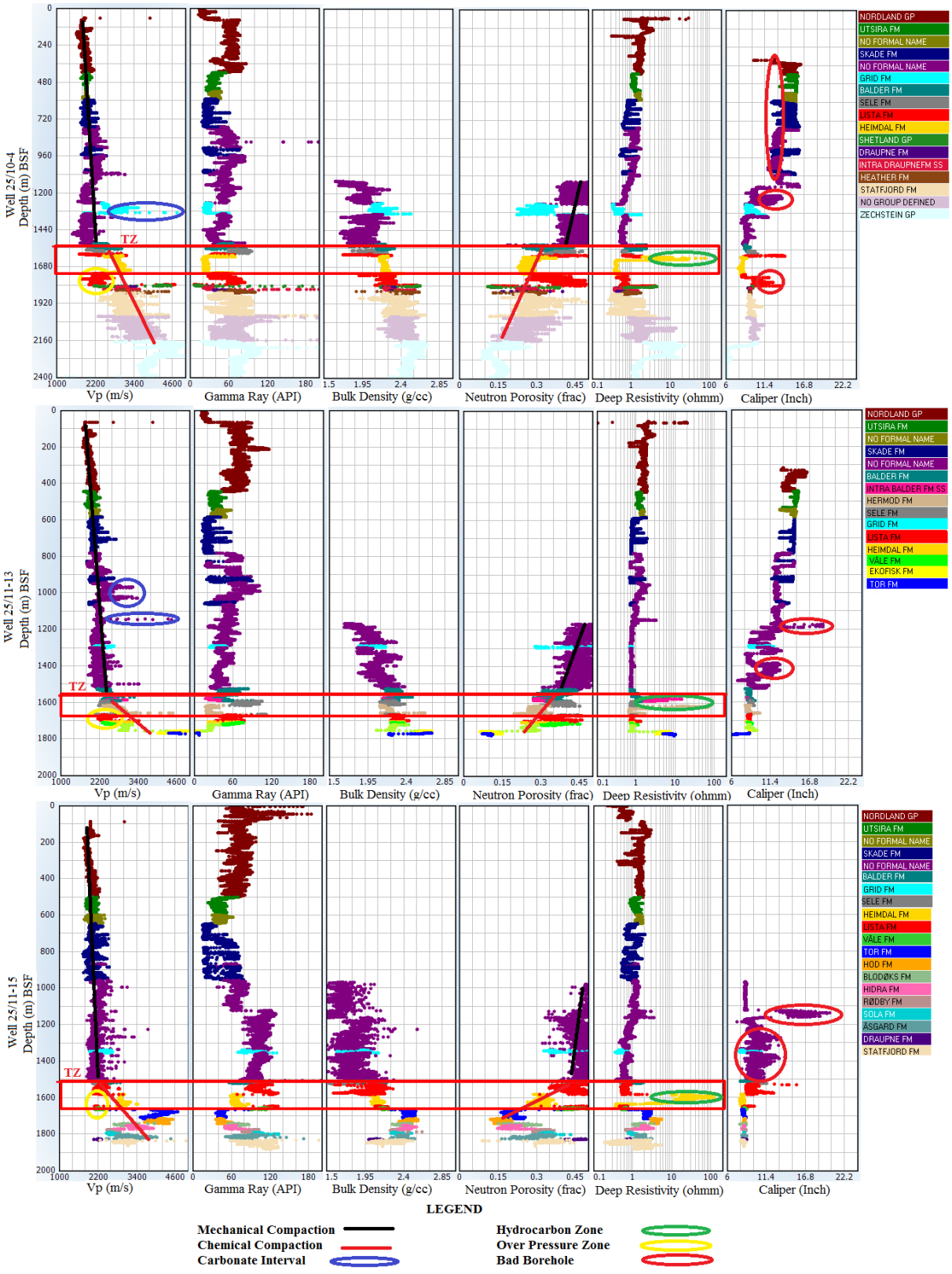
Well 25/10-4
Depth (m) BSF
TZ
Vp (m/s)
Gamma Ray (API)
Bulk Density (g/cc)
Neutron Porosity (frac)
Deep Resistivity (ohmm)
Caliper (Inch)
NORDLAND GP
UTSIRA FM
NO FORMAL NAME
SKADE FM
NO FORMAL NAME
GRID FM
BALDER FM
SELE FM
LISTA FM
HEIMDAL FM
SHETLAND GP
DRAUPNE FM
INTRA DRAUPNEFM SS
HEATHER FM
STATFJORD FM
NO GROUP DEFINED
ZECHSTEIN GP
Well 25/11-13
Depth (m) BSF
TZ
Vp (m/s)
Gamma Ray (API)
Bulk Density (g/cc)
Neutron Porosity (frac)
Deep Resistivity (ohmm)
Caliper (Inch)
NORDLAND GP
UTSIRA FM
NO FORMAL NAME
SKADE FM
NO FORMAL NAME
BALDER FM
INTRA BALDER FM SS
HERMOD FM
SELE FM
GRID FM
LISTA FM
HEIMDAL FM
VÅLE FM
EKOFISK FM
TOR FM
Well 25/11-15
Depth (m) BSF
TZ
Vp (m/s)
Gamma Ray (API)
Bulk Density (g/cc)
Neutron Porosity (frac)
Deep Resistivity (ohmm)
Caliper (Inch)
NORDLAND GP
UTSIRA FM
NO FORMAL NAME
SKADE FM
NO FORMAL NAME
BALDER FM
GRID FM
SELE FM
HEIMDAL FM
LISTA FM
VÅLE FM
TOR FM
HOD FM
BLODØKS FM
HIDRA FM
RØDBY FM
SOLA FM
ÅSGARD FM
DRAUPNE FM
STATFJORD FM
LEGEND
Mechanical Compaction
Chemical Compaction
Carbonate Interval
Hydrocarbon Zone
Over Pressure Zone
Bad Borehole

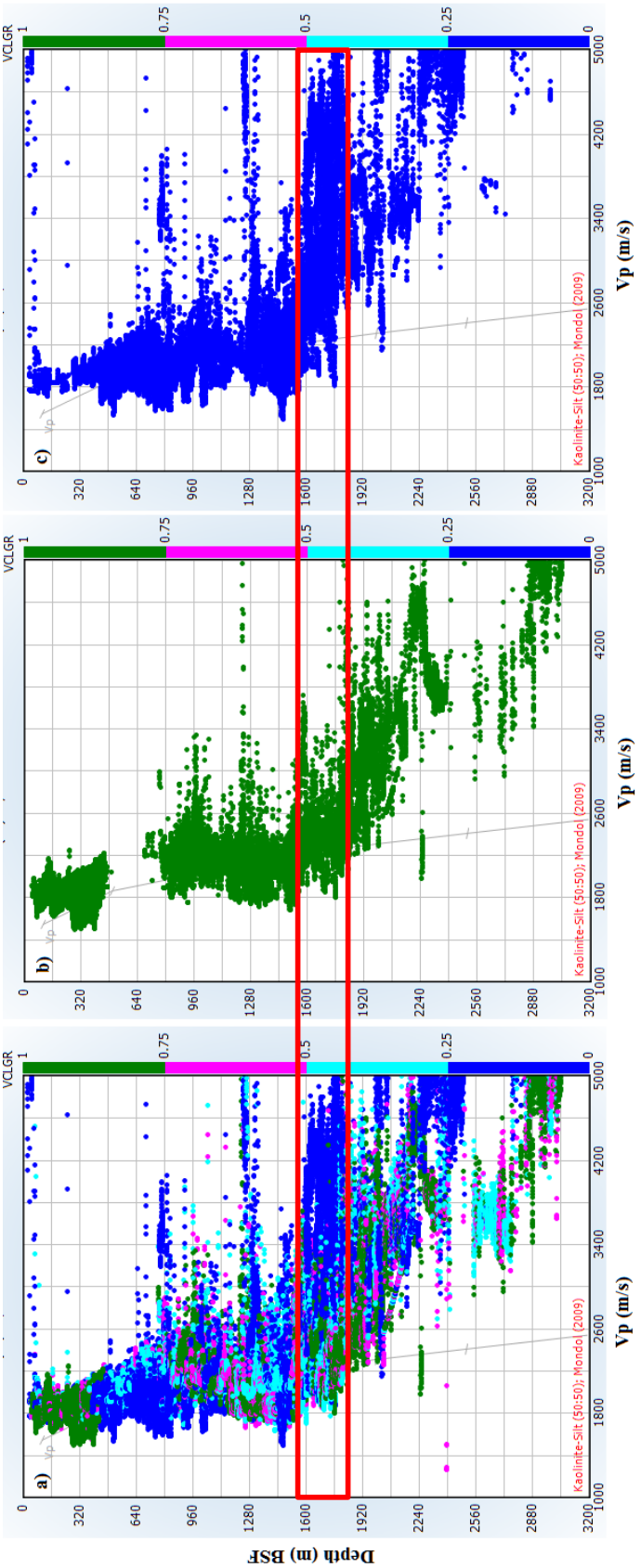
a)
b)
c)
VCLGR
Vp (m/s)
Depth (m) BSF
Kaolinite-Silt (50:50); Mondol (2009)

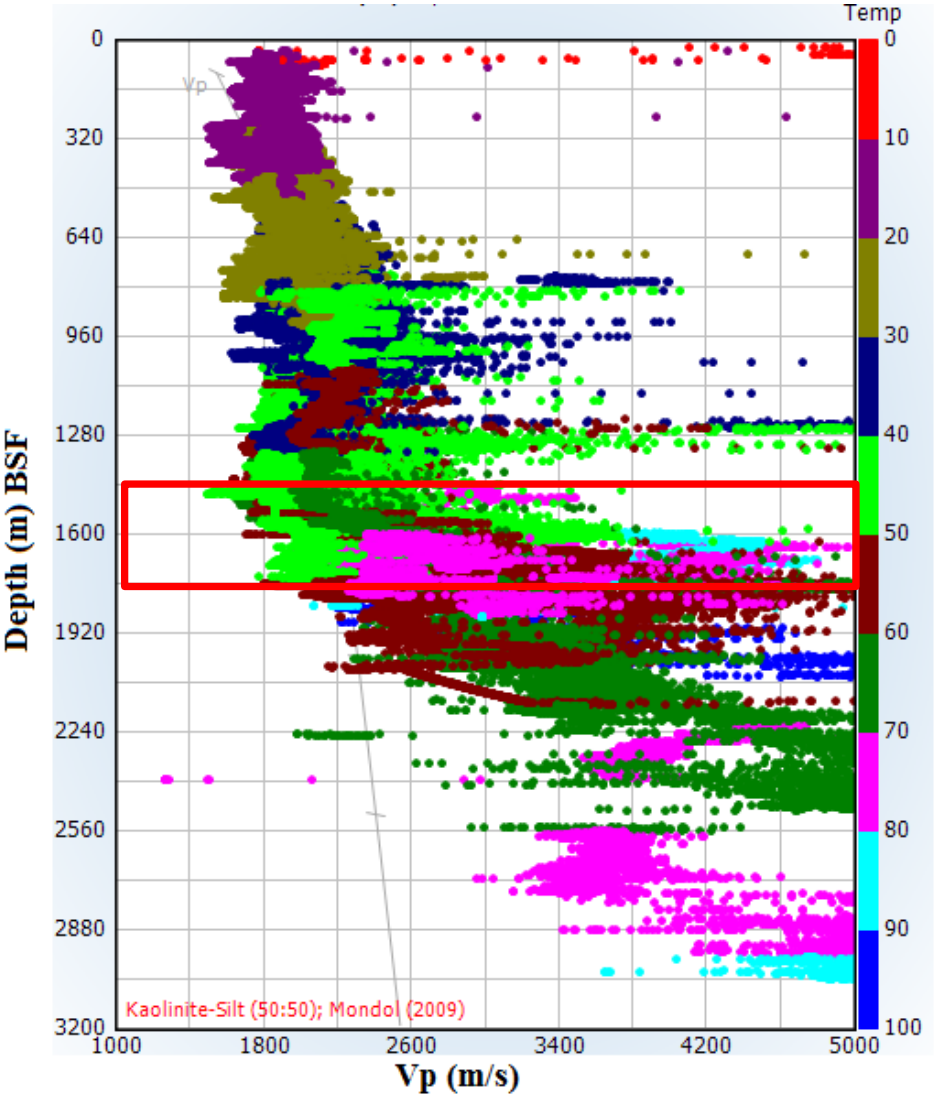
Temp
0
10
20
30
40
50
60
70
80
90
100
Vp
0
320
640
960
1280
1600
1920
2240
2560
2880
3200
Depth (m) BSF
Kaolinite-Silt (50:50); Mondol (2009)
1000
1800
2600
3400
4200
5000
Vp (m/s)

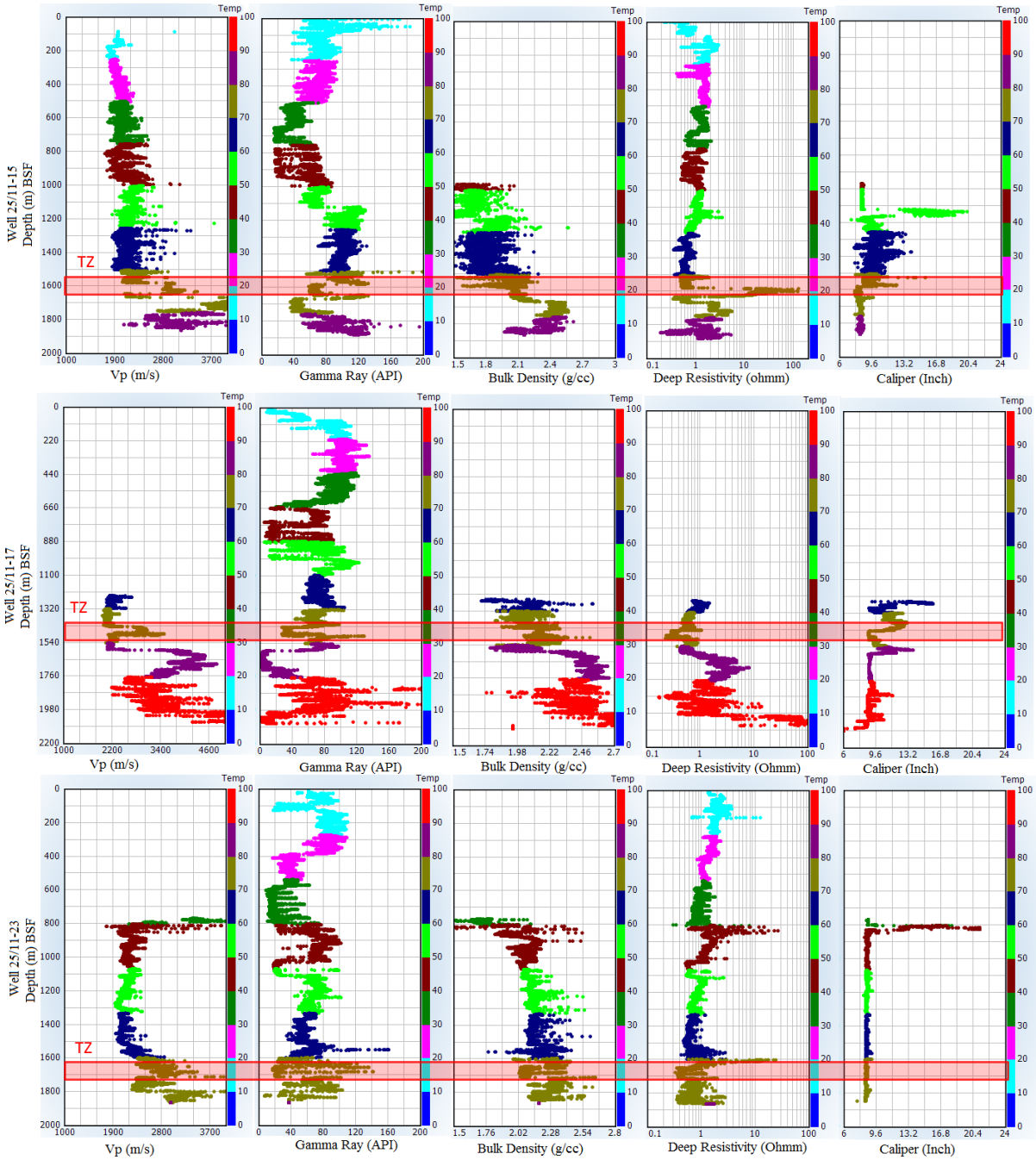
Well 25/11-15
Depth (m) BSF
TZ
Vp (m/s)
Gamma Ray (API)
Bulk Density (g/cc)
Deep Resistivity (ohmm)
Caliper (Inch)
Temp
Well 25/11-17
Depth (m) BSF
TZ
Vp (m/s)
Gamma Ray (API)
Bulk Density (g/cc)
Deep Resistivity (Ohmm)
Caliper (Inch)
Temp
Well 25/11-23
Depth (m) BSF
TZ
Vp (m/s)
Gamma Ray (API)
Bulk Density (g/cc)
Deep Resistivity (Ohmm)
Caliper (Inch)
Temp

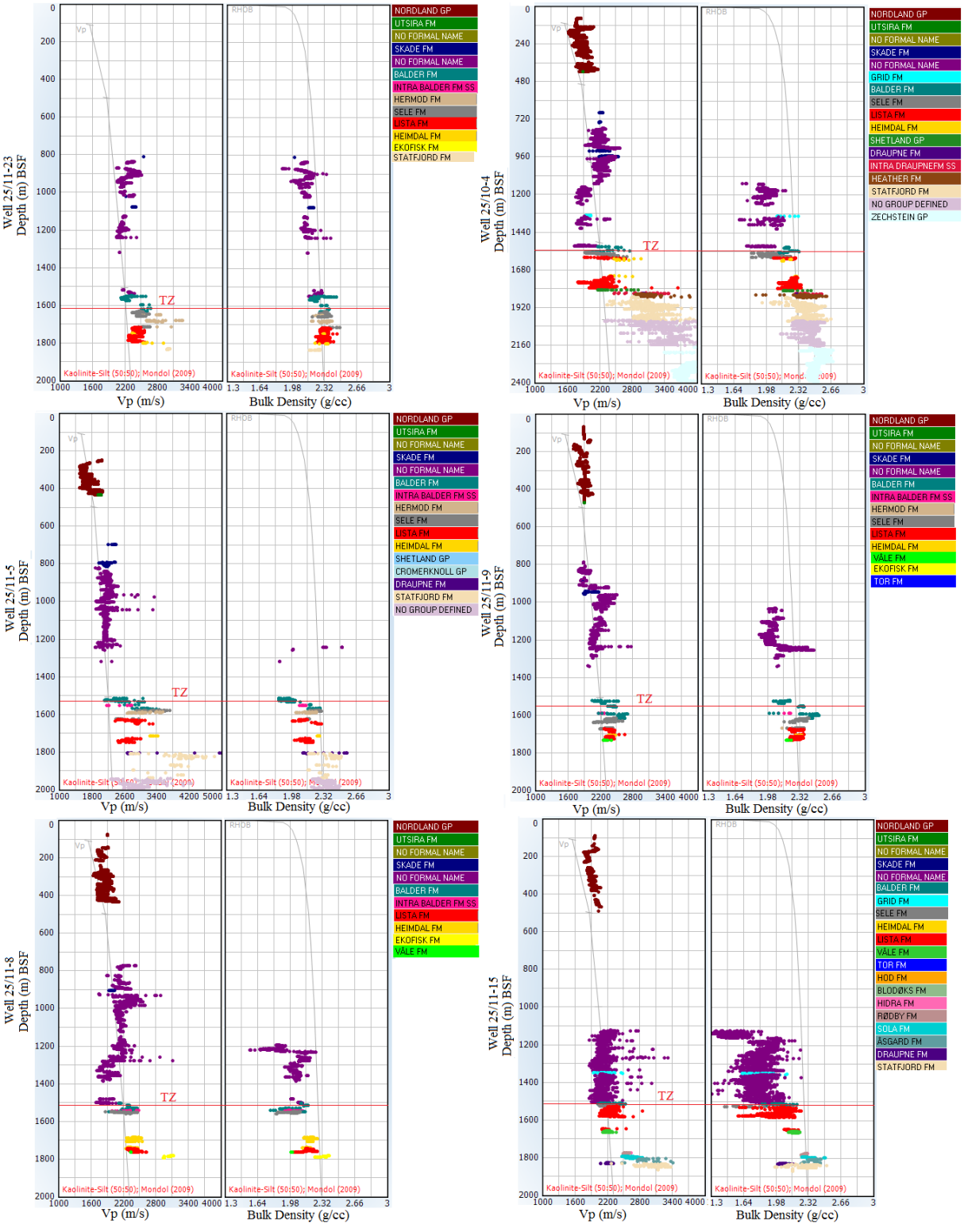
Well 25/11-23
Depth (m) BSF
Well 25/10-4
Depth (m) BSF
Well 25/11-5
Depth (m) BSF
Well 25/11-9
Depth (m) BSF
Well 25/11-8
Depth (m) BSF
Well 25/11-15
Depth (m) BSF
TZ
Vp (m/s)
Bulk Density (g/cc)
Kaolinite-Silt (50:50); Mondol (2009)
NORDLAND GP
UTSIRA FM
NO FORMAL NAME
SKADE FM
BALDER FM
INTRA BALDER FM SS
HERMOD FM
SELE FM
LISTA FM
HEIMDAL FM
EKOFISK FM
STATFJORD FM
GRID FM
SHETLAND GP
DRAUPNE FM
INTRA DRAUPNEFM SS
HEATHER FM
NO GROUP DEFINED
ZECHSTEIN GP
CROMERKNOLL GP
VÅLE FM
TOR FM
HOD FM
BLODØKS FM
HIDRA FM
RØDBY FM
SOLA FM
ÅSGARD FM

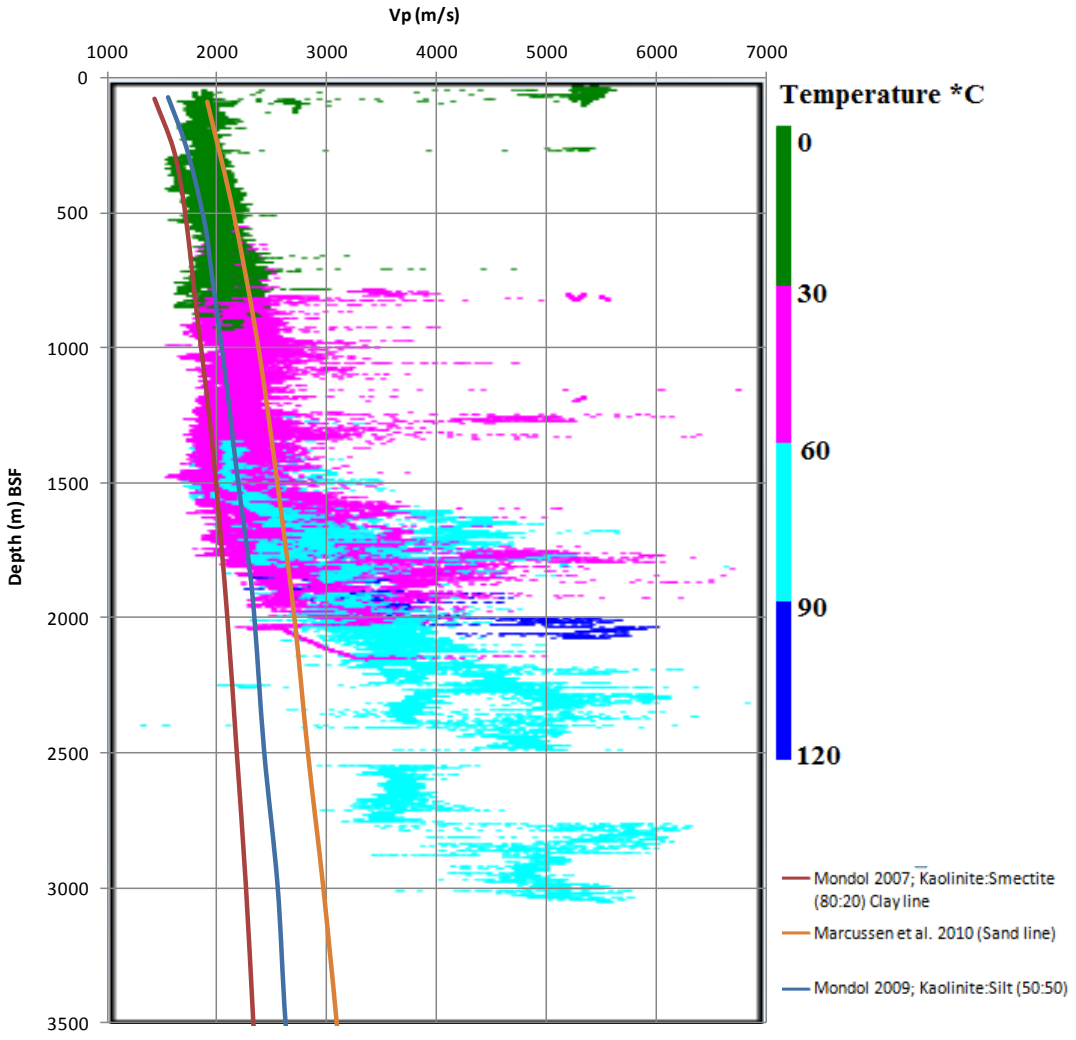
Vp (m/s)
1000
2000
3000
4000
5000
6000
7000
0
500
1000
1500
2000
2500
3000
3500
Depth (m) BSF
Temperature *C
0
30
60
90
120
Mondol 2007; Kaolinite:Smectite (80:20) Clay line
Marcussen et al. 2010 (Sand line)
Mondol 2009; Kaolinite:Silt (50:50)

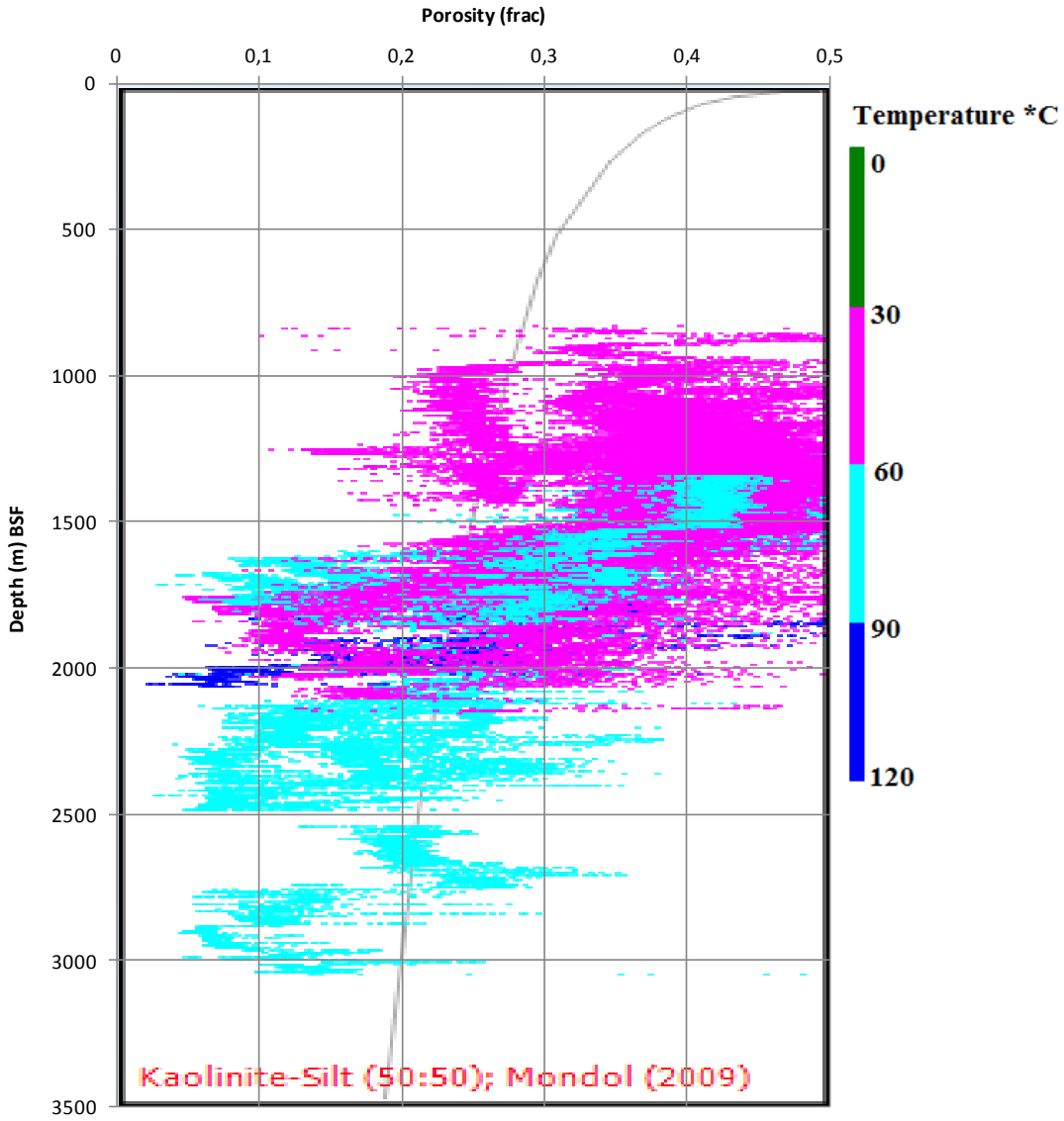
Porosity (frac)
0
0,1
0,2
0,3
0,4
0,5
Depth (m) BSF
0
500
1000
1500
2000
2500
3000
3500
Temperature *C
0
30
60
90
120
Kaolinite-Silt (50:50); Mondol (2009)

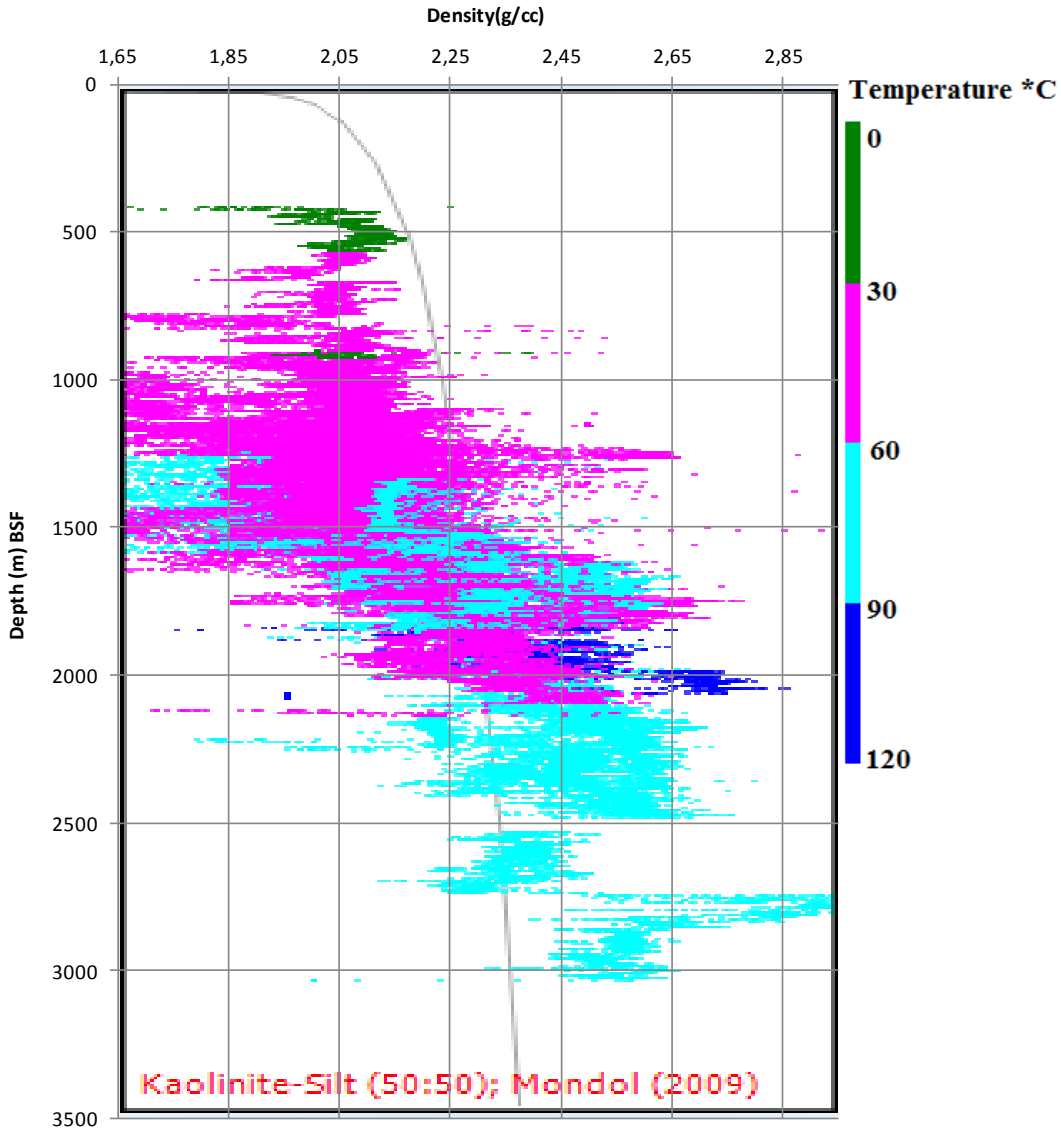
Density(g/cc)
1,65
1,85
2,05
2,25
2,45
2,65
2,85
0
500
1000
1500
2000
2500
3000
3500
Depth (m) BSF
Temperature *C
0
30
60
90
120
Kaolinite-Silt (50:50); Mondol (2009)

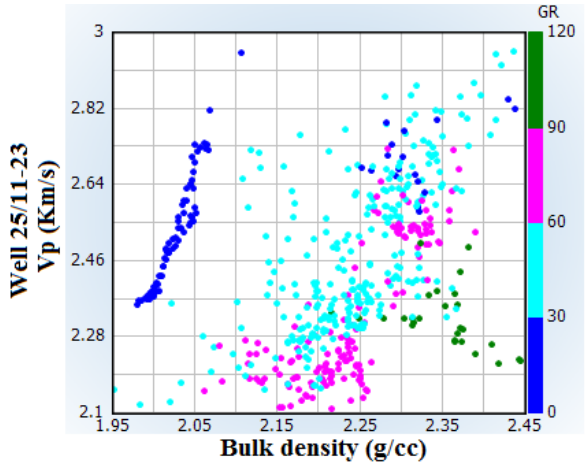
Well 25/11-23
Vp (Km/s)
GR
120
90
60
30
0
3
2.82
2.64
2.46
2.28
2.1
1.95
2.05
2.15
2.25
2.35
2.45
Bulk density (g/cc)

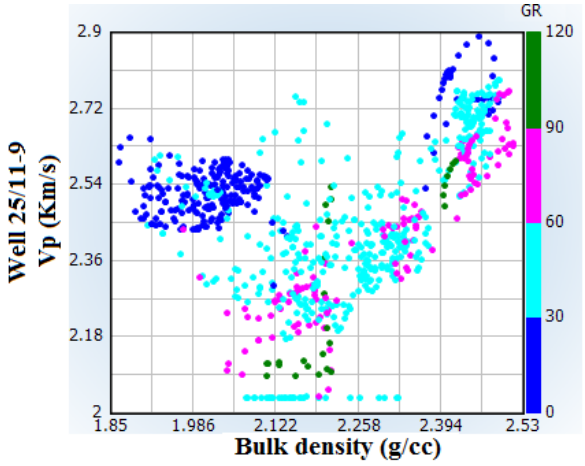
Well 25/11-9
Vp (Km/s)
GR
120
90
60
30
0
2.9
2.72
2.54
2.36
2.18
2
1.85
1.986
2.122
2.258
2.394
2.53
Bulk density (g/cc)

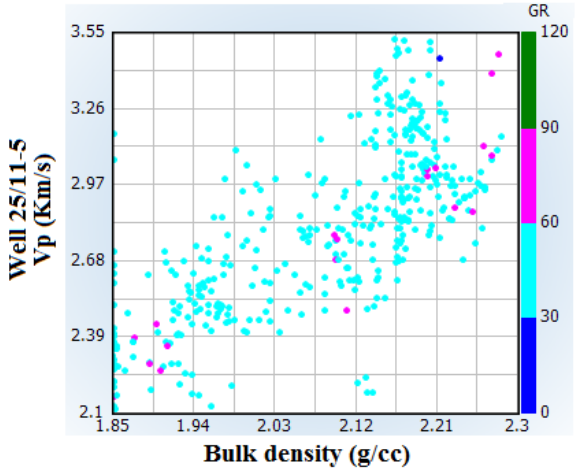
Well 25/11-5
Vp (Km/s)
GR
120
90
60
30
0
3.55
3.26
2.97
2.68
2.39
2.1
1.85
1.94
2.03
2.12
2.21
2.3
Bulk density (g/cc)

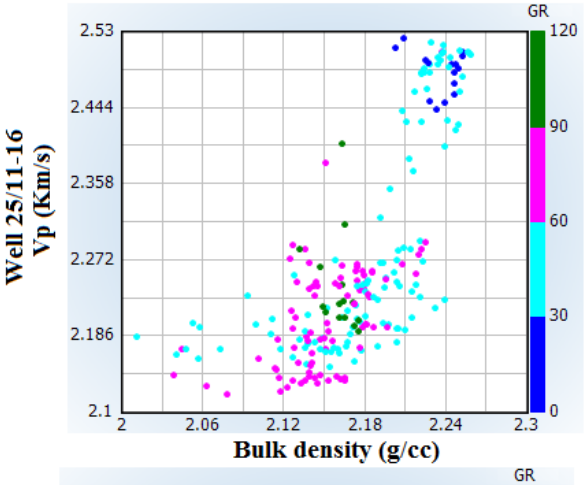
Well 25/11-16
Vp (Km/s)
GR
120
90
60
30
0
2.53
2.444
2.358
2.272
2.186
2.1
2
2.06
2.12
2.18
2.24
2.3
Bulk density (g/cc)

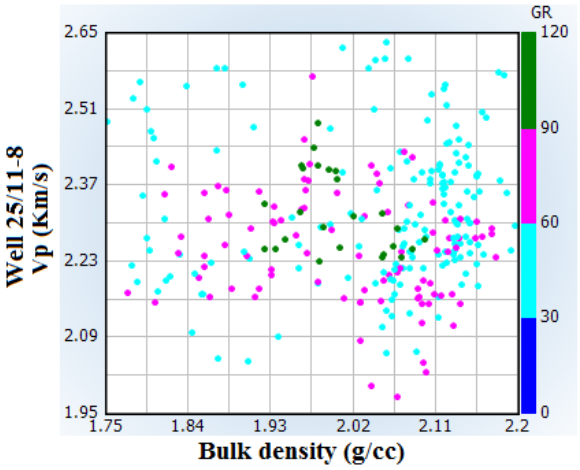
Well 25/11-8
Vp (Km/s)
GR
120
90
60
30
0
2.65
2.51
2.37
2.23
2.09
1.95
1.75
1.84
1.93
2.02
2.11
2.2
Bulk density (g/cc)

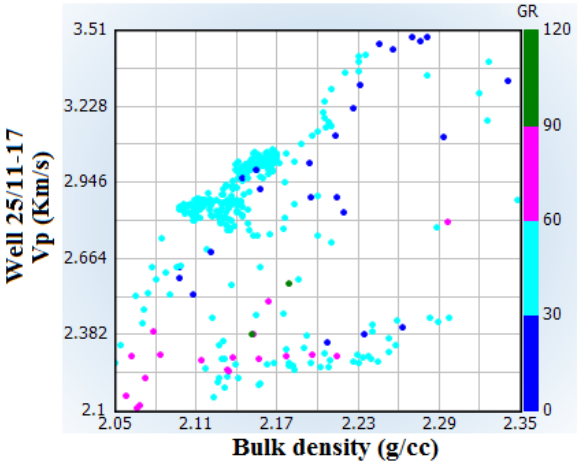
Well 25/11-17
Vp (Km/s)
GR
120
90
60
30
0
3.51
3.228
2.946
2.664
2.382
2.1
2.05
2.11
2.17
2.23
2.29
2.35
Bulk density (g/cc)

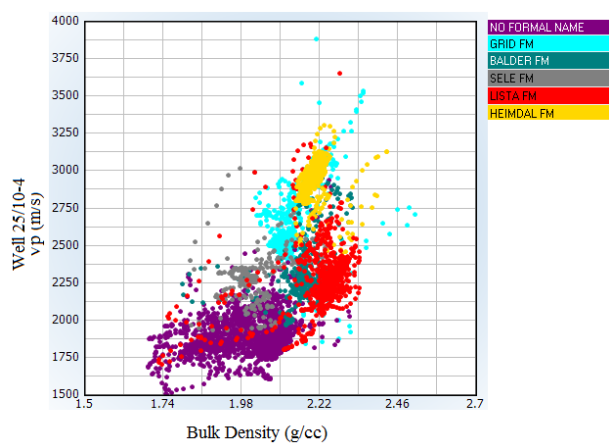
Well 25/10-4
Vp (m/s)
Bulk Density (g/cc)
NO FORMAL NAME
GRID FM
BALDER FM
SELE FM
LISTA FM
HEIMDAL FM

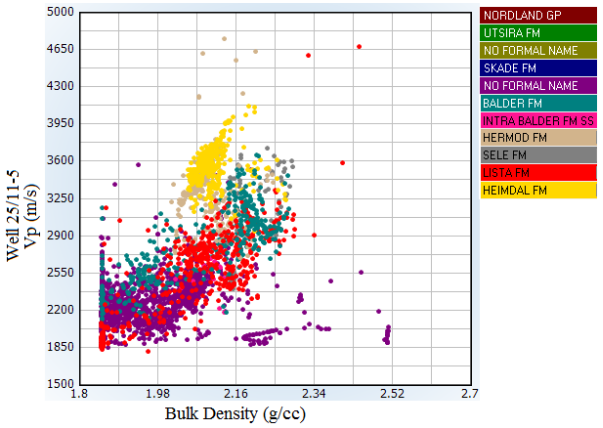
Well 25/11-5
Vp (m/s)
Bulk Density (g/cc)
NORDLAND GP
UTSIRA FM
NO FORMAL NAME
SKADE FM
NO FORMAL NAME
BALDER FM
INTRA BALDER FM SS
HERMOD FM
SELE FM
LISTA FM
HEIMDAL FM

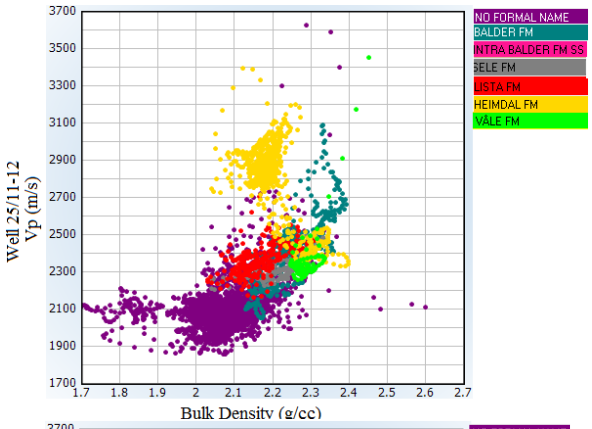
Well 25/11-12
Vp (m/s)
Bulk Density (g/cc)
NO FORMAL NAME
BALDER FM
INTRA BALDER FM SS
SELE FM
LISTA FM
HEIMDAL FM
VÅLE FM

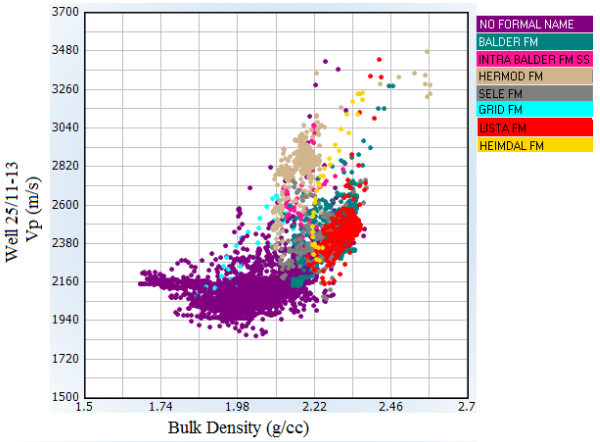
Well 25/11-13
Vp (m/s)
Bulk Density (g/cc)
NO FORMAL NAME
BALDER FM
INTRA BALDER FM SS
HERMOD FM
SELE FM
GRID FM
LISTA FM
HEIMDAL FM

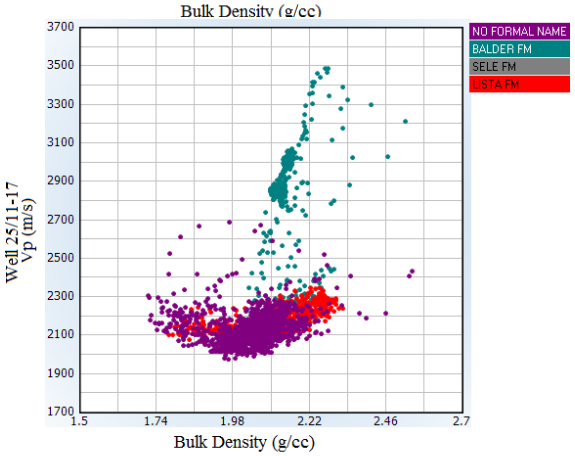
Well 25/11-17
Vp (m/s)
Bulk Density (g/cc)
NO FORMAL NAME
BALDER FM
SELE FM
LISTA FM

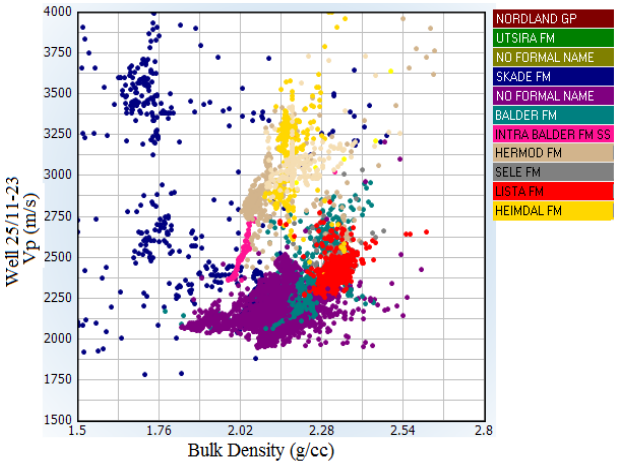
Well 25/11-23
Vp (m/s)
Bulk Density (g/cc)
NORDLAND GP
UTSIRA FM
NO FORMAL NAME
SKADE FM
NO FORMAL NAME
BALDER FM
INTRA BALDER FM SS
HERMOD FM
SELE FM
LISTA FM
HEIMDAL FM

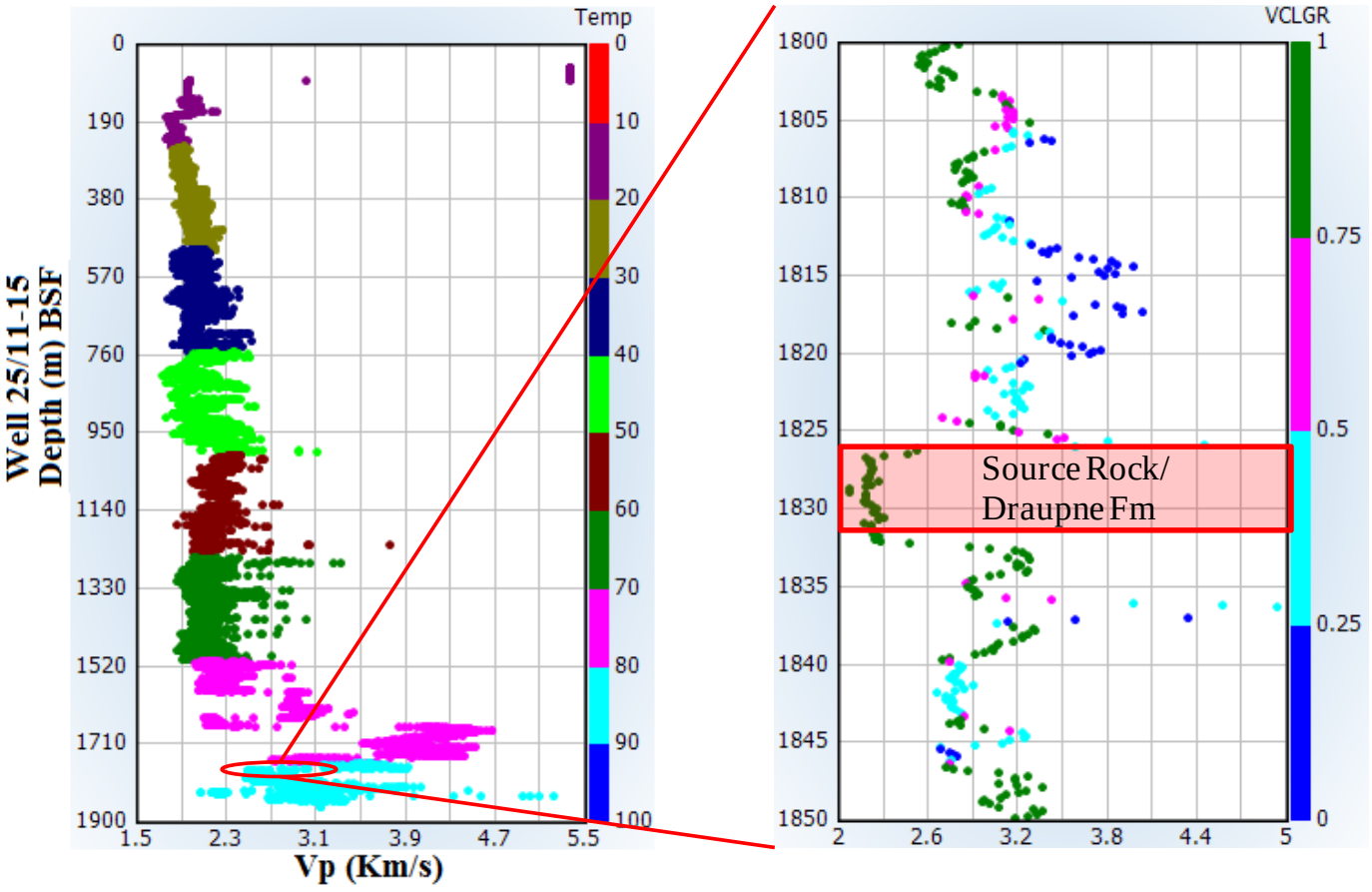
Temp
Well 25/11-15
Depth (m) BSF
0
190
380
570
760
950
1140
1330
1520
1710
1900
1.5
2.3
3.1
3.9
4.7
5.5
Vp (Km/s)
0
10
20
30
40
50
60
70
80
90
100
VCLGR
1800
1805
1810
1815
1820
1825
1830
1835
1840
1845
1850
2
2.6
3.2
3.8
4.4
5
1
0.75
0.5
0.25
0
Source Rock/
Draupne Fm

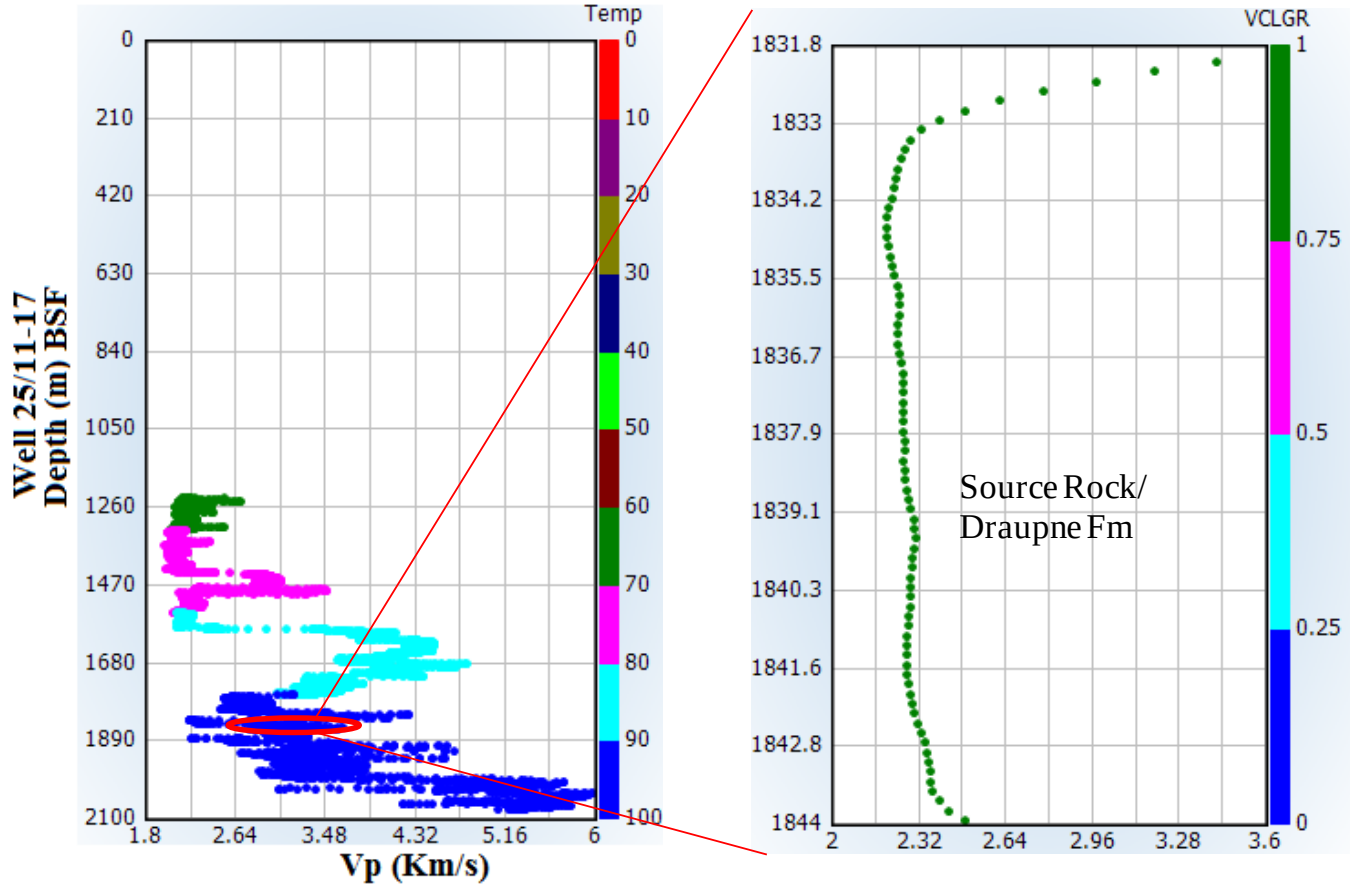
Temp
Well 25/11-17
Depth (m) BSF
0
210
420
630
840
1050
1260
1470
1680
1890
2100
1.8
2.64
3.48
4.32
5.16
6
Vp (Km/s)
0
10
20
30
40
50
60
70
80
90
100
VCLGR
1831.8
1833
1834.2
1835.5
1836.7
1837.9
1839.1
1840.3
1841.6
1842.8
1844
2
2.32
2.64
2.96
3.28
3.6
1
0.75
0.5
0.25
0
Source Rock/
Draupne Fm

Appendix III (Rock physics Analysis)

Lambda-Mu-Rho cross-plot

Balder Formation

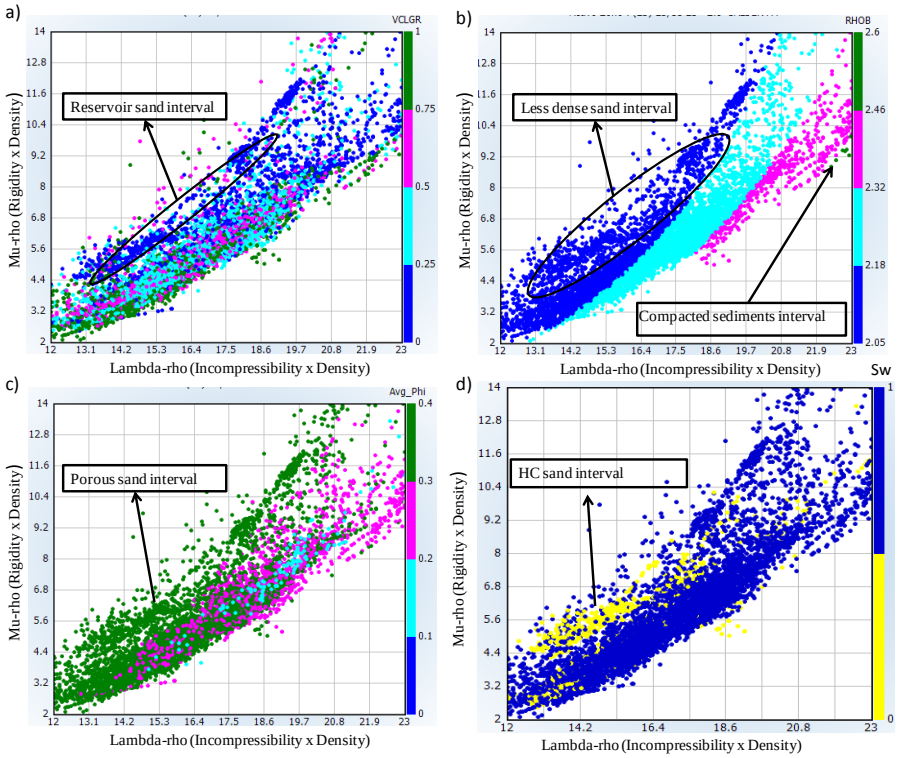

Hermod Formation

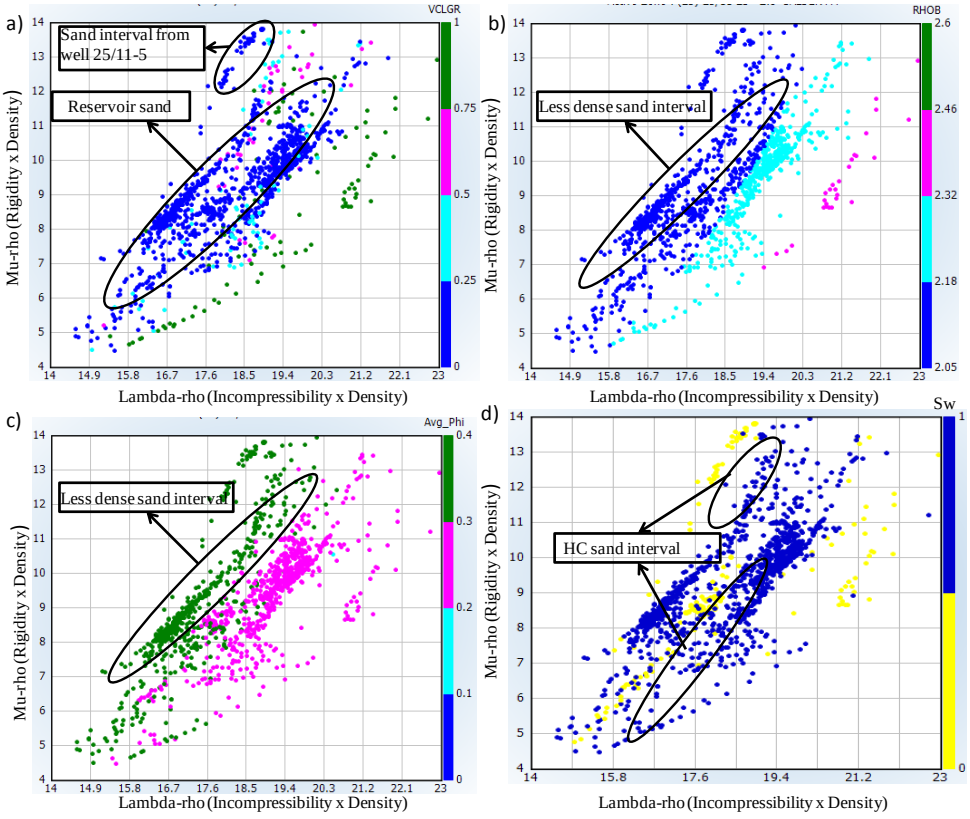

Heimdal Formtion